ULPGC
Universidad de Las Palmas de Gran Canaria
Instituto Universitario de Investigaciones Biomédicas y Sanitarias

DOCTORAL THESIS

Effect of maternal age and metabolic syndrome on preimplantation embryo development

JOAQUÍN LILAO GARZÓN

PhD program:

PhD in Applied Research in Health Sciences

MARCH 2023

LAS PALMAS DE GRAN CANARIA

II

II

II

III

Abbreviations

ARRIVE: Animal Research: Reporting of *In Vivo* Experiments

ART: Assisted Reproduction Technology

AUC: Area Under the Curve

BMI: Body Mass Index

DN: Double Negative (NANOG- GATA6-, N-G6-, or NANOG-GATA4-, N-G4-)

DP: Double Positive (NANOG+GATA6+, N+G6+, or NANOG+GATA4+, N+G4+)

Dpc: Days *post coitum*

Epi: Epiblast

FIGO: International Federation of Gynaecology and Obstetrics

GAD: Glutamic Acid Decarboxylase

GDM: Gestational Diabetes Mellitus

HbA1c: Glycated haemoglobin

HFD: High Fat Diet

ICM: Inner Cell Mass

IDF: International Diabetes Federation

ITT: Insulin Tolerance Test

IVF: *In Vitro* Fertilization

LPS: Lipopolysaccharides

MHFD: Mature High Fat Diet

MINS: Interactive Nuclear Segmentation

MND: Mature Normal Diet

MODY: Maturity-Onset diabetes of the young

ND: Normal Chow Diet

OGTT: Oral Glucose Tolerance Test

OHFD: Old High Fat Diet

OND: Old Normal Diet

PAST: Paleontological Statistics software

PBS: Phosphate-Buffered Saline

PFA: Paraformaldehyde

PrE: Primitive Endoderm

PVP: Polyvinylpyrrolidone

QIF: Quantitative Immunofluorescence Analysis

ROS: Reactive Oxygen Species

T1DM: Type 1 Diabetes Mellitus

T2DM: Type 2 Diabetes Mellitus

TE: Trophectoderm

WHO: World Health Organization

YHFD: Young High Fat Diet

YND: Young Normal Diet

Table of contents

Summary

High and middle-income societies are facing an important decrease in birth rate, as well as an increase in metabolic diseases such as obesity or diabetes, which also have a negative impact on fecundity. Diabetes Mellitus (DM) is characterized by hyperglycaemia due to insufficient insulin secretion or action. Increased maternal age is also behind the decrease in birth rates. The age at first pregnancy in Europe has been delayed to 29.5 years in 2019, with consequences on reproductive capacity and embryo quality.

At the beginning of embryonic development before the embryo implants in the uterus, two sequential cell fate decisions occur. First, totipotent cells in the embryo differentiate into trophectoderm (TE) cells or inner cell mass (ICM) cells. In the second one, the ICM cells that co-express both NANOG and GATA6, make a further decision: they differentiate into Epiblast which will form the embryo proper (Epi, NANOG expressing cells) or into primitive endoderm which will form the yolk sac (PrE, GATA6 expressing cells). I use single cell whole embryo quantitative immunofluorescence (QIF) and 3D neighbourhood data analyses to study this cell fate decision in health and disease.

The aim of this work is to evaluate how diabetes and maternal age disturb female fecundity and early embryo development in mice. To achieve this objective, a high fat diet (HFD) mouse

model for both age and DM was validated through weight monitorization, body composition assessment, and glucose and insulin tolerance tests. Then, its fecundity was assessed by mating and fertilization rates together with the quality their embryos. Finally, the state-of-the-art QIF analysis developed in the laboratory was used to evaluate preimplantation embryo development, focusing on Epi vs PrE cell fate specification.

The results show that diet-induced hyperglycaemia and obesity worsen with age. Embryo quality significantly decreases in association with both maternal age and high-fat diet. QIF embryo analysis shows an increased number of uncommitted cells (NANOG/GATA6 co-expressing cells) together with fewer cells committed to PrE cell fate, indicative of delayed development. I hypothesise that the low fertility observed in older women and women with DM is due to this embryo development delay resulting in low implantation rate or embryo loss.

Resumen

El presente trabajo se centra en el estudio del efecto de la edad y el síndrome metabólico materno en el desarrollo embrionario temprano en un modelo murino.

La prevalencia de la obesidad y la hiperglucemia asociadas al síndrome metabólico están aumentando a nivel global, llegando a considerarse una pandemia. La fertilidad femenina se ve afectada por estas alteraciones, tanto en estados tempranos, dificultando la fecundación y/o la implantación, como en estados más avanzados de la embriogénesis, ya que se asocia con malformaciones cardíacas o del tubo neural y con un incremento en la probabilidad de abortos.

Por otro lado, la edad a la que las mujeres tienen su primer hijo no deja de aumentar, especialmente en países con mayores ingresos. Actualmente, la edad media a la que las mujeres tienen su primer hijo se sitúa en 29.4 años en Europa, llegando a superar los 31 años en España e Italia. Una mayor edad materna se asocia tanto con una mayor dificultad para que se produzca el embarazo como para mantener el mismo.

La diabetes mellitus (DM) en el embarazo se asocia con peores resultados y complicaciones tanto para la madre como para la descendencia. Aunque los estudios clínicos y epidemiológicos resultan de gran importancia tanto para el estudio de estas complicaciones como para la evaluación de la efectividad de

potenciales tratamientos, presentan ciertas limitaciones prácticas y éticas. Los modelos *in vivo* e *in vitro* pueden ayudar a comprender los mecanismos tras estas complicaciones y, a la larga, su prevención y tratamiento.

Durante la elaboración de esta tesis se revisaron en detalle las publicaciones sobre los distintos modelos animales y celulares existentes para el estudio de la diabetes, con especial énfasis en el ambiente intrauterino, para seleccionar aquel modelo que mejor se ajusta a los objetivos a estudiar. El resultado de dicho trabajo se publicó un artículo científico de revisión titulado "*In Vivo and In Vitro Models of Diabetes: A Focus on Pregnancy*" (1).

Se seleccionó un modelo de DM inducida mediante dieta grasa en ratones hembra de distintas edades. En este modelo, la acumulación de grasa conlleva un aumento en la resistencia a la insulina en los tejidos periféricos y un aumento de la glucemia en sangre.

A pesar de la diferencia en la esperanza de vida entre el ratón y el humano, ambos organismos muestran patrones fisiológicos similares, haciendo posible su uso en estudios de envejecimiento. A la hora de evaluar la fertilidad en el modelo de ratón hembra, se tuvo en cuenta que el inicio de la etapa reproductiva se establece a los 45 días de vida y el final en torno

a los 15 meses, (equivalente a los 11.5 y 51 años de las mujeres, respectivamente).

En este trabajo se evalúa si la edad materna y el síndrome metabólico asociado a dieta grasa afectan a la fecundidad en un modelo de ratón de DM tipo 2. A través de una monitorización del peso, caracterización de la composición corporal, metabolismo de la glucosa y diferentes determinaciones físicas y bioquímicas se caracterizó metabólicamente este modelo en distintas edades: hembras jóvenes de 12 semanas, maduras de 9 meses y viejas de 1 año. La alimentación con dieta grasa se asoció, especialmente en animales de mayor edad, con un aumento de la adiposidad, de la intolerancia a la glucosa y de resistencia a la insulina.

Estudios epidemiológicos en humanos han demostrado que la DM y la edad materna avanzada afectan negativamente a la fecundidad, pero no se sabe si este efecto ocurre ya en los primeros momentos del desarrollo embrionario, incluso antes de la implantación en el útero. En humanos, durante los procedimientos de reproducción asistida, la evaluación de la calidad de los embriones de preimplantación obtenidos se realiza atendiendo a sus características morfológicas y clasificándolos en distintas categorías de manera que solo los que presentan mejor aspecto se consideran viables y son trasferidos a la madre para ser llevados a término.

Antes de la implantación, en el desarrollo del embrión se diferencian las primeras células del trofectodermo (TE) que darán lugar a la placenta, del epiblasto (Epi) que formarán el embrión propiamente dicho y del endodermo primitivo (PrE) que darán lugar al primordio de saco vitelino. Para poder analizar este proceso de diferenciación celular, se desarrolló un método que permitiera estudiar los primeros estadíos del desarrollo embrionario mediante inmunofluorescencia cuantitativa en cada una de las células del embrión, prestando especial interés a esta especificación celular que se produce a partir del día 3.5 en desarrollo embrionario de ratón. Más en detalle, durante este desarrollo embrionario, son las células de la masa interna (ICM) del blastocisto las que se diferencian en Epi y PrE. Estos dos destinos celulares se caracterizan por la expresión de los factores de trascripción NANOG y GATA6, respectivamente. El método desarrollado para su análisis fue publicado en el artículo "*The transition from local to global patterns governs the differentiation of mouse blastocysts*" (2). En este trabajo además se estudió la distribución espacio-temporal de NANOG y GATA6 en la ICM del blastocisto de ratón usando un análisis del vecindario celular. El análisis revela un patrón tridimensional que ya se encuentra presente en embriones tempranos donde, células con mayor expresión de NANOG se encuentran rodeadas por aproximadamente nueve células vecinas y células que

expresan GATA6 se agrupan de acuerdo con sus niveles de GATA6. Además, a través del uso de embriones de ratón mutantes se muestra que la agrupación de células GATA6 positivas está regulada por NANOG a través de señalización celular FGF/MAPK. Este estudio cuantitativo sugiere que el vecindario celular tridimensional tiene un papel en la especificación de Epi y PrE, poniendo de manifiesto la importancia del análisis tridimensional a la hora de estudiar la especificación de distintos destinos celulares en el desarrollo embrionario temprano.

En este trabajo, se aparearon ratonas de los distintos grupos de estudio con machos jóvenes y sanos para obtener embriones de preimplantación en estado de blastocisto de día 3.5 tras la fecundación. De manera similar a lo empleado en humanos, se caracterizó su fecundidad mediante parámetros descriptivos y la calidad embrionaria se determinó en base a sus características morfológicas. La fecundidad se vio más afectada por la edad que por la dieta.

Por último, estos embriones se analizaron a nivel celular mediante el protocolo desarrollado de inmunofluorescencia cuantitativa de una sola célula. Los embriones, tanto aquellos procedentes de hembras alimentadas con dieta grasa como de mayor edad mostraron una reducción en la diferenciación celular, indicando un retraso en el desarrollo embrionario.

También se observó un incremento en los niveles de GATA3, que podría actuar inhibiendo la placentación.

Los resultados obtenidos a través de la selección de un modelo de DM tipo 2 inducido por dieta rica en grasa y la metodología desarrollada en el laboratorio de análisis cuantitativo de fluorescencia sostienen que la edad materna avanzada y el síndrome metabólico reducen la fertilidad en las ratonas, mediante mecanismos que están presentes en el momento de la concepción, en estadios muy tempranos del embarazo.

Hypothesis

Maternal age, obesity and diabetes are associated with a reduction in fertility. Older women and women who present metabolic syndrome have more difficulties in successfully getting pregnant and present a higher miscarriage risk, even during fertility treatments.

I hypothesize that these factors (maternal age, obesity, and diabetes) alter embryonic cell fate allocation at early stages of pregnancy, before embryo implantation, and are ultimately responsible for the low fertility rate. In this study, I assess alterations in fecundity and variations at cell fate allocation in preimplantation embryos associated with age and metabolic syndrome through a fat diet induced mouse model for type 2 DM and the development of a state-of-the-art image and data analyses.

Objectives

Main Objective:

The main objective of this research is to assess the effect of maternal age and the metabolic syndrome, including obesity and diabetes, in early mouse preimplantation embryo development.

Specific Objectives:

1. Validation of a high fat diet induced mouse model for obesity and the metabolic syndrome in mouse females at different ages.
    1.1. Establish the mouse model and measure their morphometry during and by the end of the diet.
    1.2. Evaluate the glucose metabolism in the mouse model by the end of the diet.
    1.3. *Post-mortem* characterisation of the mouse model.

2. Assessment of the fecundity of the mouse model at different ages by descriptive methods and embryo quality.

3. Analyses, at single cell level, of the cell fate allocation during epiblast and primitive endoderm specification in the preimplantation embryos from mouse model at different ages.

Introduction

1. Diabetes Mellitus:

Diabetes Mellitus (DM) is a group of metabolic diseases associated with defects in insulin secretion, insulin action or both, that lead to hyperglycaemia (3).

The pancreas is the main actor involved in DM and has two morphological and functional independent components, the exocrine pancreas responsible for digestive enzymes production, and the endocrine pancreas. The endocrine pancreas is organized in islets with five major cell types each one responsible for the secretion of different hormones: α cells (glucagon), β cells (insulin), PP cells (pancreatic polypeptide), δ cells (somatostatin) and ε-cells (ghrelin) (Figure 1 (4)) (4–6). Insulin is a hypoglycaemic hormone that is secreted in response to hyperglycaemia, and it binds to receptors in peripheral tissues such as muscle or adipose tissue, promoting glucose absorption.

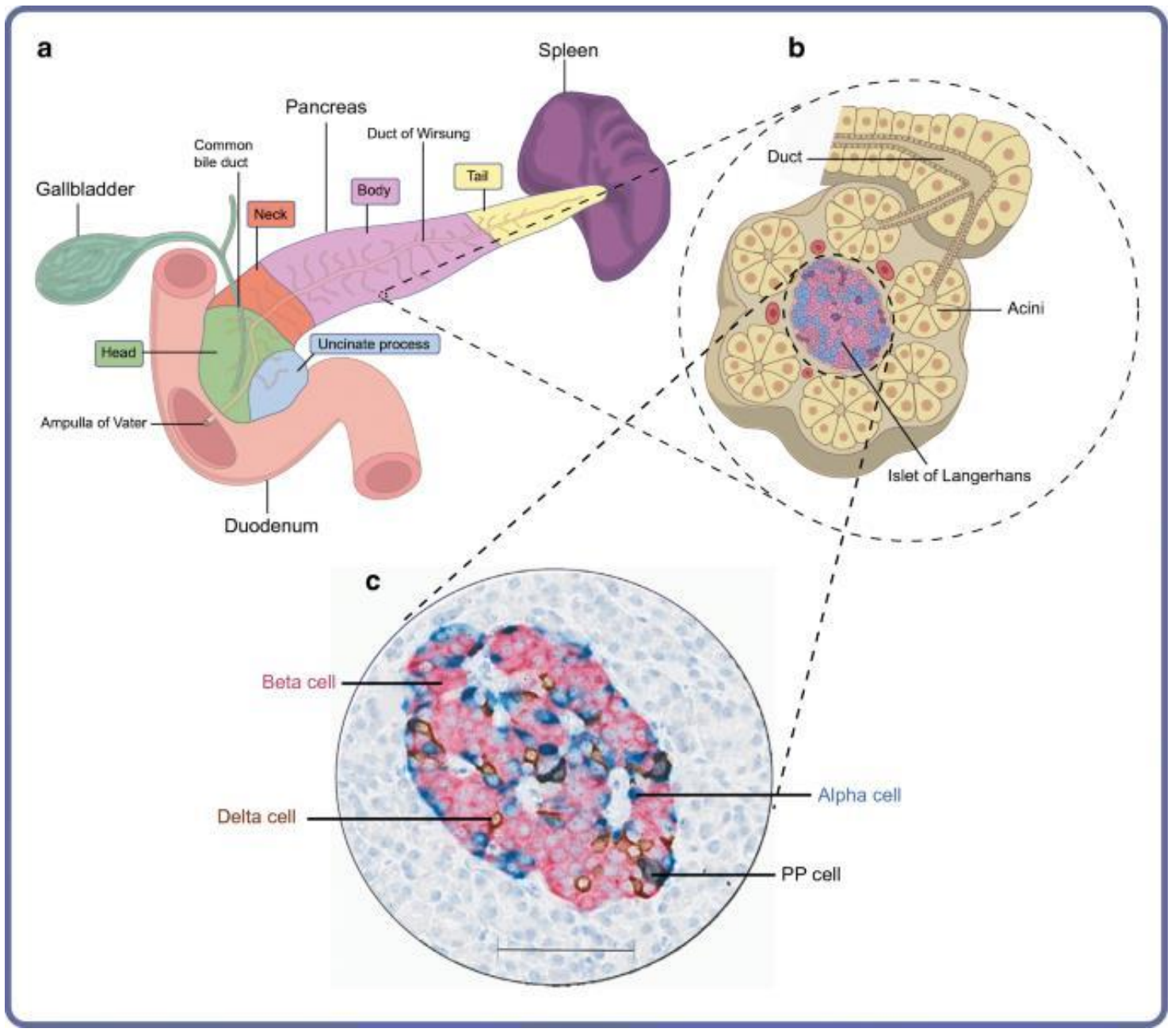

Fig. 1: Anatomical characteristics of the human pancreas. (a) Pancreas and surrounding organs. (b) Cellular organization of endocrine and exocrine pancreas. (c) Pancreatic islet with its cell types. *Taken from Atkinson et al (2020) Diabetologia DOI 10.1007/s00125-020-05203-7 © Springer-Verlag GmbH Germany, part of Springer Nature 2020* (4).

Hyperglycaemia is responsible for damage and dysfunction of several organs including eyes, kidneys, nerves, heart, and blood vessels. The main symptoms of hyperglycaemia are polyuria, polydipsia, weight loss and blurred vision. Besides the symptoms, the diagnosis of DM includes a blood glucose level above 200 mg/dL and glycated haemoglobin (HbA1c or A1c) ≥ 6.5%. Individuals whose glucose levels do not meet the criteria

for diabetes but are too high to be considered normal are considered to suffer prediabetes. Usually, prediabetes is associated with obesity, dyslipidaemia with high triglycerides and/or low HDL cholesterol, and hypertension. It is considered an increased risk for diabetes and cardiovascular disease (3,7).

1.1 Classification of DM:

The current classification of DM according to the American Diabetes Association (ADA) establishes 4 main categories (7):

- Type 1 diabetes (T1DM) is an autoimmune disorder that leads to the destruction of the β-cells, ultimately causing a total insulin deficiency. This disease has a strong genetic influence. T1DM is defined by the presence of one or more of the following autoimmune markers: autoantibodies against islet cells, GAD, insulin, tyrosine phosphatases IA-2 and IA-2β, or ZnT8.
- Type 2 diabetes (T2DM) is the result of a progressive loss of insulin secretion by the β-cells. This loss is induced by peripheral insulin resistance. Although this disease is usually due to environmental causes, other factors have a role in it such as genetic predisposition, age, or ethnicity. Most T2DM patients are overweighted or have a body fat increase in the abdominal region. In these patients, the autoimmune destruction of β cells is infrequent.

- Gestational DM (GDM) occurs when DM is first diagnosed in the second or third trimester of pregnancy. Maternal insulin sensitivity decreases from the second trimester of pregnancy due to the effect of placental hormones (i.e. oestrogen, progesterone, leptin, cortisol, placental lactogen, and placental growth hormone) to increase the glycaemia and facilitate glucose transportation across the placenta (8,9). Under physiological conditions, this hyperglycaemia is compensated by the hypertrophy and hyperplasia of β-cells and the stimulation of insulin secretion. GDM appears upon failure of these compensatory mechanisms (10,11).
- Specific types of DM include those with other aetiology such as monogenic diabetes syndromes, diseases that affect exocrine pancreas or chemical induced diabetes. Maturity-Onset diabetes of the young (MODY) is also included as a specific type of DM and it is characterized by hyperglycaemia at an early age with defects in insulin secretion and no defects in insulin action or obesity (7,12).

1.2 Epidemiology:

DM is one of the fastest growing global health emergencies of this century. Estimating the incidence and prevalence worldwide is not easy due to the lack of data and homogeneity in the criteria for diagnosis depending on the country and the genetic

heterogeneity of different populations. The IDF Diabetes Atlas published in 2021 estimates that 10.5% of the world population (536.6 million) were living with DM in 2021 with 6.7 million of deaths due to DM (Figure 2) (13). Furthermore, the projections foresee that by 2045 the prevalence of DM will be 12.2% (783.2 million). In this context, T1DM represent around 5-10% of DM while over 90% are T2DM. Specific types of DM are less common and only represent 1.5-2% of DM worldwide (13).

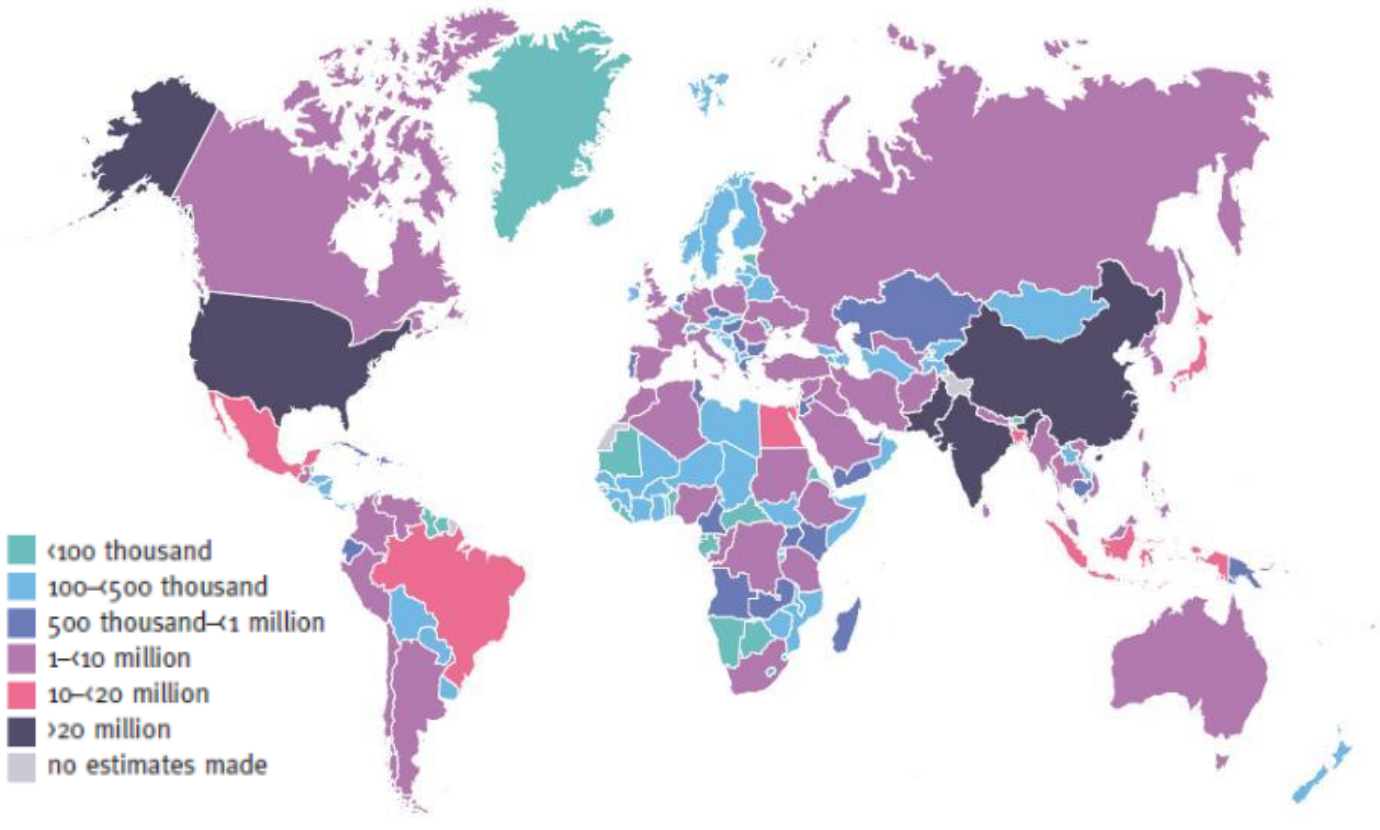

Fig. 2: Estimated total number of adults (20-79 years) with diabetes in 2021. *Taken from the IDF Diabetes Atlas, 10th edition.*

Furthermore, the DM direct economic costs for people or governments have increased 316% in over 15 years and are expected to reach the 1.05 trillion US dollars by 2045. Spain is among the countries with the highest health expenditure due to DM with 15.5 billion US dollars in 2021 (Figure 3) (13).

Rank	Country or territory	Total diabetes-related health expenditure in 2021 (USD billion) in adults (20–79 years)
1	United States of America	379.5
2	China	165.3
3	Brazil	42.9
4	Germany	41.3
5	Japan	35.6
6	United Kingdom	23.4
7	France	22.7
8	Mexico	19.9
9	Spain	15.5
10	Italy	14.7

Fig. 3: The ten countries with the highest total health expenditure (USD) due to diabetes in 2021. *Taken from the IDF Diabetes Atlas, 10th edition.*

1.3 Pregnancy and Diabetes:

Although T1DM is the most frequent form of DM in young people, increasing numbers of children, adolescents, and young adults with T2DM have been reported across the world (14,15). This is important specially in pregnant women that need to cope with two challenging metabolic conditions. The World Health Organization (WHO) and the International Federation of Gynaecology and Obstetrics (FIGO) classify hyperglycaemia during pregnancy in three categories: pre-gestational DM, in women with T1DM or T2DM before pregnancy; GDM, when diagnosed in the second or third trimester of pregnancy; and DM in pregnancy when it is first diagnosed during pregnancy but meets WHO criteria of DM in the non-pregnant state (13,16).

During pregestational DM, when it is not properly controlled, pregnancy enhances medical complications associated to DM for the mother, also increasing preeclampsia risk. In the foetus, not only is there an increased risk for first trimester miscarriage, congenital malformations, intrauterine growth restriction, macrosomia, birth trauma or stillbirth, but also for obesity, glucose intolerance and cardiovascular disease as adults (17–20).

2 Obesity:

Overweight and obesity are defined as abnormal or excessive fat accumulation that present a risk to the overall health. Body mass index (BMI) is used as a metric where normal BMI range between 18.5 to 24.9 kg/m^2, whereas a BMI ≥ 25 kg/m^2 is considered to be overweight, and a BMI ≥ 30 kg/m^2 is classified as obese, with severe obesity defined as a BMI ≥ 40 kg/m^2 (21). In obesity, the excess energy from the diet is transformed into triglycerides and stored as adipose tissue. The stored adipose tissue increases it sizes by both hyperplasia and hypertrophy of adipocytes (22–24).

2.1 Epidemiology:

Nowadays obesity is considered an epidemic driven by the modern lifestyles. Approximately 40% of world population is overweighted and 650 million adults (13%) were obese in 2016 (Figure 4) (25). The increase in obesity is not only observed in adults, but also in children where the prevalence of overweight and obesity has risen from just 4% in 1975 to 18% in 2016 (21,26).

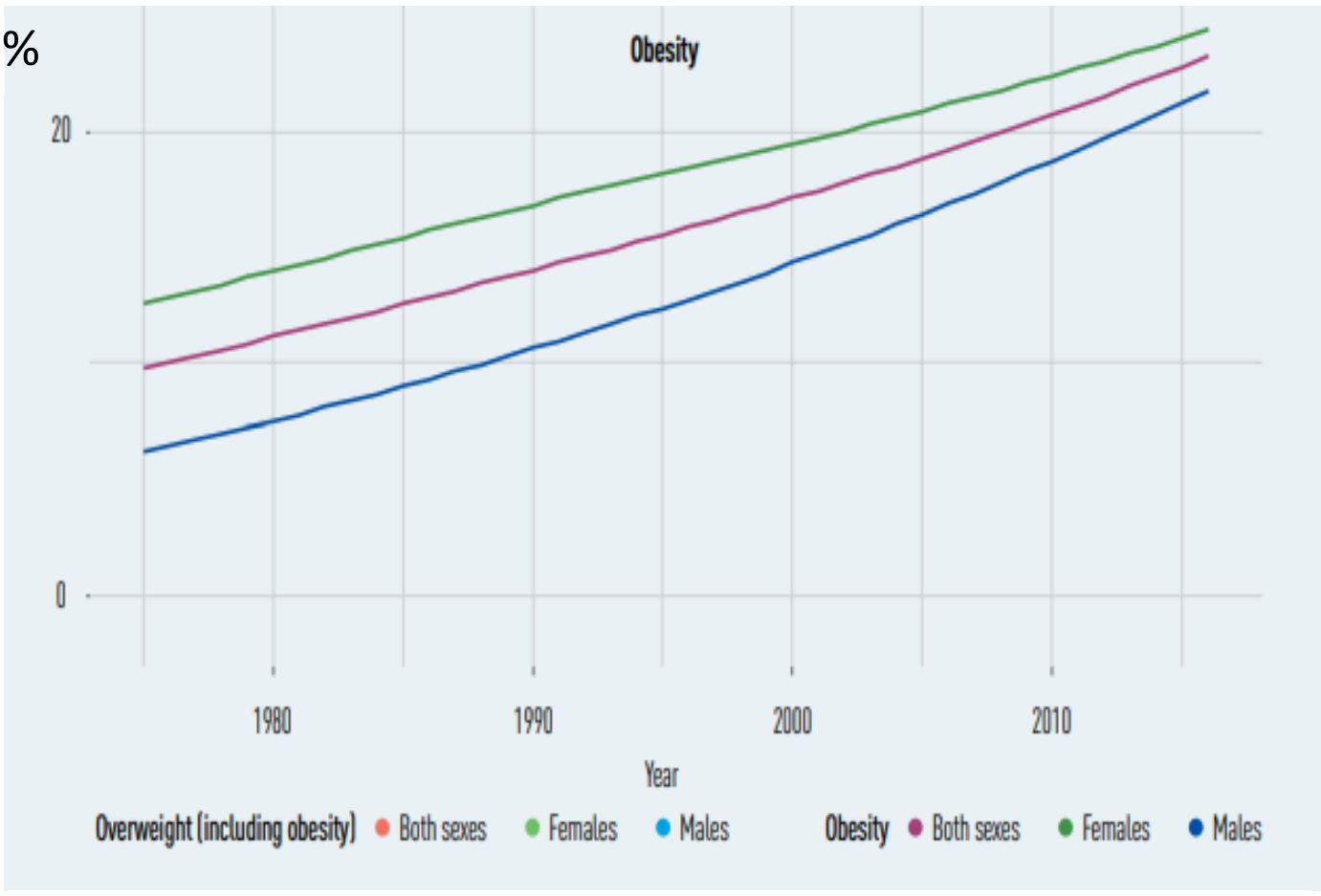

Fig. 4: Prevalence of obesity among adults in the WHO European Region (1975–2016). *Taken from the WHO European Obesity Report, 2022.*

2.2 Obesity and pregnancy:

In the United States of America, almost 56% of women in reproductive age are overweight and 32% are obese with the same tendency observed worldwide (27).

Women with obesity tend to gain more weight during pregnancy, increasing their risk of developing metabolic syndrome during pregnancy or later in life. Their offspring are also at higher risk of obstetric morbidity and mortality, as well as complications later in life, such as T2DM, obesity or cardiovascular disease (28).

Obesity results in a decreased reproductive function in women by different mechanisms. It affects hormone levels, associated with changes in follicular fluid composition that might disrupt oocyte development (24,29–31). Spontaneous abortions and congenital anomalies are more common in women with higher BMI. Obese pregnancies are at higher risk of neural tube and cardiac defects (32), together with higher foetal adiposity (33). At the moment of birth, children from obese women are also at risk for macrosomia.

3 Obesity and Diabetes in Assisted Reproduction Technologies:

Both obesity and DM have negative effects on reproductive health (28,34,35). Obese women often rely on fertility treatments through assisted reproduction technology (ART) to become mothers (36).

Pregestational DM is associated with an increased risk for maternal and foetal morbidity, mortality, and congenital anomalies. Pregnancies achieved through ART have higher risk of preterm delivery and caesarean section. Moreover, both ART and maternal DM are associated with decreased implantation rate (37) and large new-borns for gestational age (38).

Furthermore, a correlation is observed between women with higher BMI requiring higher gonadotropin stimulation doses and

a longer stimulation duration before ART treatment (39). However, the effect of BMI on embryo development is still controversial (40). Poorer quality embryos are associated with poorer fertilization rates leading to fewer successful pregnancies (35,41).

Though ART treatments can be a solution for women living with obesity and/or DM, very little is known about how these factors affect embryo development, especially at early stages of development (40,42,43). Nevertheless, ART treatments are not recommended for women with a BMI above 30-32 kg/m^2 (44).

4 Aging:

Aging constitutes a risk factor in developing age-related diseases that include obesity, T2DM and cancer (45). In 2019, the number of people aged 60 years and older was 1 billion (12%) and projections foresee 2.1 billion by 2050 (46).

4.1 Aging in pregnancy:

Modern lifestyles have resulted in a delay in childbearing women worldwide (47,48). In Europe, age at first pregnancy has been delayed to 29.4 years in 2019 with consequences on reproductive capacity, embryo quality and even offspring's overall health (Figure 5) (49,50).

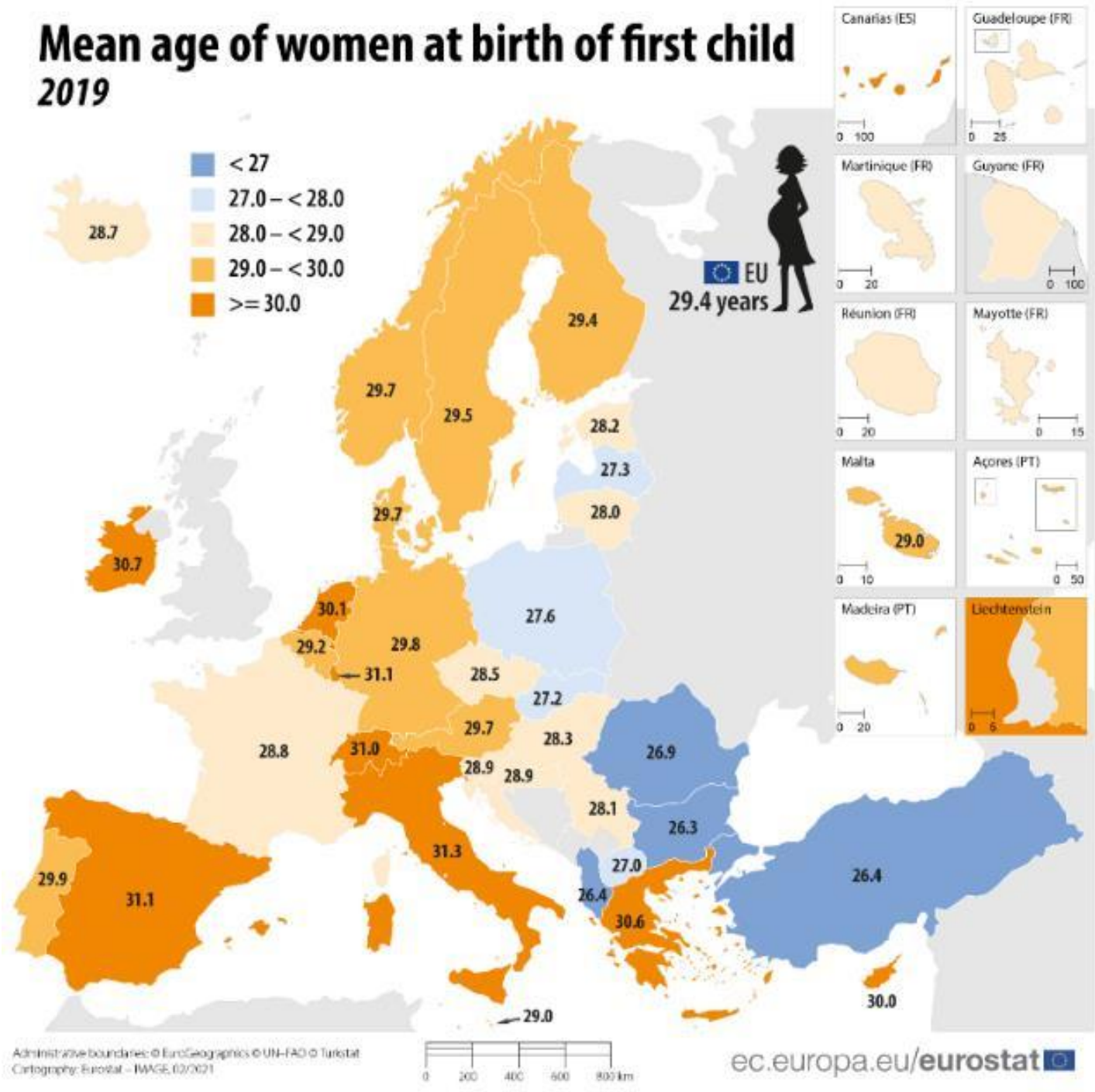

Fig. 5: Mean age of women at birth of first child (2019). *Eurostat.*

Fertility declines with age. The decrease starts around 32 years of age, with an increase in the rate of decline after 37 years. Infertility (failure to conceive after attempting at least twelve months of natural fertilization) or reduced fecundability associated with age is multifactorial. Fecundability is defined as the probability of achieving a pregnancy within one menstrual cycle or the ability to achieve a live birth from one cycle's exposure to the risk of pregnancy (51). A decreased oocyte

number, miscarriage and increased chromosomal abnormalities or endometriosis are some of the factors associated with age and fertility (47,52,53).

Different ART such as social egg donation, embryo freezing, or *in vitro* fertilization (IVF) are the strategies followed by older women with reduced fertility to become pregnant. Maternal age is associated with increased oocyte and embryo aneuploidy, together with reduced success rates in IVF (54). Therefore is especially recommended to perform a preimplantation genetic screening in embryos from older mothers (55).

5 Animal models:

Animal models are a resourceful tool to mimic *in vivo* DM and obesity. In general, models can be grouped as spontaneous or induced. In the spontaneous, mechanisms of disease are supposed to be similar to those in humans (56). Induced models are easier to generate and have the advantage that they phenotypically match hyperglycaemia, obesity, or metabolic syndrome. Among these, there are surgically (57), chemically, toxic or drug (58–60), and diet induced models (61–63).

Despite the differences in lifespan between humans and mice, they show similar patterns in disease pathogenesis and systemic physiology. Usually, female mammals cease to exhibit reproductive cycles by middle age, around 15 months in mouse

or 51 years in humans, while reproductive maturity is reached at 45 days in mice and 11.5 years in humans (64).

Diet-induced models are widely use in T2DM studies, especially in rodents, but also in other species that develop insulin resistance and glucose impairment with high fat diets (1,56,65,66). Furthermore, the use of a mouse model fed with a fat enriched diet allows to combine both obesity and DM in one organism. This allows to better mimic the scenario observed in modern populations where obesity and T2DM coexist in most cases. Moreover, starting the diet at different time points enables to evaluate how obesity and DM affect the model depending on its age.

6 Early preimplantation embryo development:

During preimplantation embryo development, the extraembryonic membranes are the first linages to be specified in the early embryo in which all the cells are totipotent. Prior to implantation, mouse and human embryos proceed through similar morphological changes (67,68). In mouse, the first few days after fertilization (E0.0 to E2.5), cells divide to produce identical and pluripotent blastomeres. At 8-cell stage, cells polarize and compact to form the morula (16-cell stage) (69). In the morula, cells from the outer part differentiate into the trophectoderm (TE) that will form the embryonic placenta (70).

TE cells are characterized by the expression of transcription factors like CDX2 and GATA3 (71–73). Meanwhile, the cells that remain inside are called the inner cell mass (ICM) and these cells co-express the transcription factors NANOG and GATA6 (74–78). At this moment in the development (E3.0, in mouse), cells from the TE pump liquid to form a cavity called blastocoele forming the early blastocyst (67). At E3.5, cells from the ICM asynchronously downregulate either NANOG or GATA6 so those expressing NANOG become the epiblast (Epi, that will form the embryo proper), while those expressing GATA6 form the progenitors for primitive endoderm (PrE, that will mainly become the yolk sac) (79). Later markers for PrE are SOX17, GATA4, and SOX7 (80,81). After the Epi/PrE differentiation, PrE cells are localized between the Epi and the blastocoele, forming an epithelium. Then, the embryo hatches from the *zona pellucida* being ready to implant in the uterus between E4.5 and E5.0 (Figure 6).

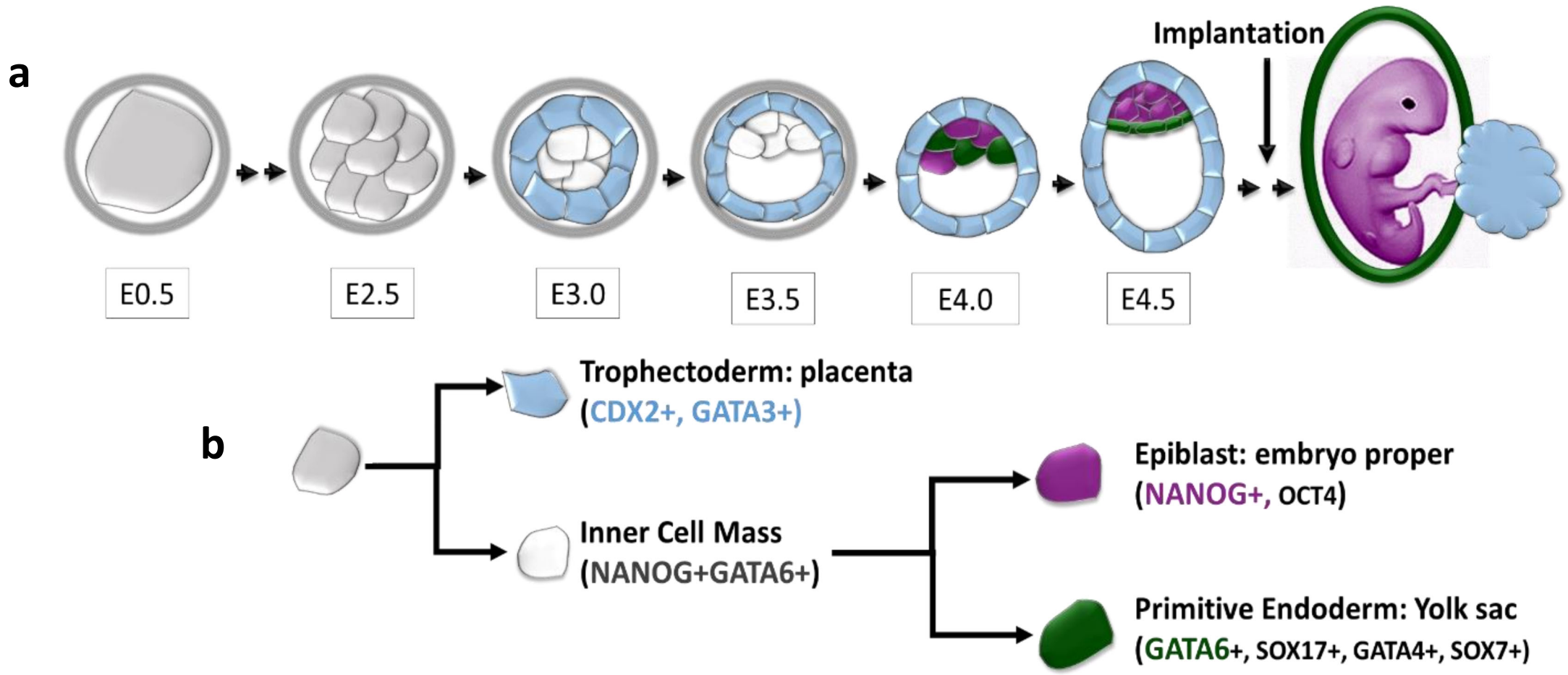

Fig. 6: Key features of the early mouse embryo development. (a) Sequential steps in mouse early embryo development from day 0.5 to implantation. (b) Cell types in mouse early embryo development and principal markers.

Material and Methods

1. Animal Procedures:

C57Bl/6J mice were bred in-house at the Universidad de Las Palmas de Gran Canaria (ULPGC) within the Institute for Biomedical and Healthcare Research (IUIBS) animal facility. All mice were housed with controlled room temperature (20-24ºC) and relative humidity (55-72%). Animals were kept at a 12h light-darkness cycle. All animal studies were conducted following National and European regulations (RD 1201/2005, Law 32/2007, EU Directive 2010/63/EU). These protocols were approved by the Animal Ethics Committee of the ULPGC and were authorised by the competent authority of the Canary Islands Government (reference number: OEBA-ULPGC_10/2019R1).

Female mice were divided into three age groups: young adults at the beginning of their reproductive life (Y: 12 weeks old), mature adults (M: 9 months old) and middle-late age adults, close to their reproductive senescence (O: 1 year old). Animals from different cages but with the same date of birth were grouped together and then randomly assigned to one of two diets following ARRIVE guidelines (82).

High fat diet (HFD) in rodents is an established model for the induction of obesity and the metabolic syndrome (65,66,83). Female mice were divided into two groups and fed a standard

diet (ND) (Envigo, Global Diet 2014) and a HFD (60% energy from fat, D12492; Research Diets, Brogaarden, Lynge, Denmark) for 8 weeks prior to the target age (Figure 7).

Healthy males of up to 6 months of age, from the same colony, were used for breeding purposes.

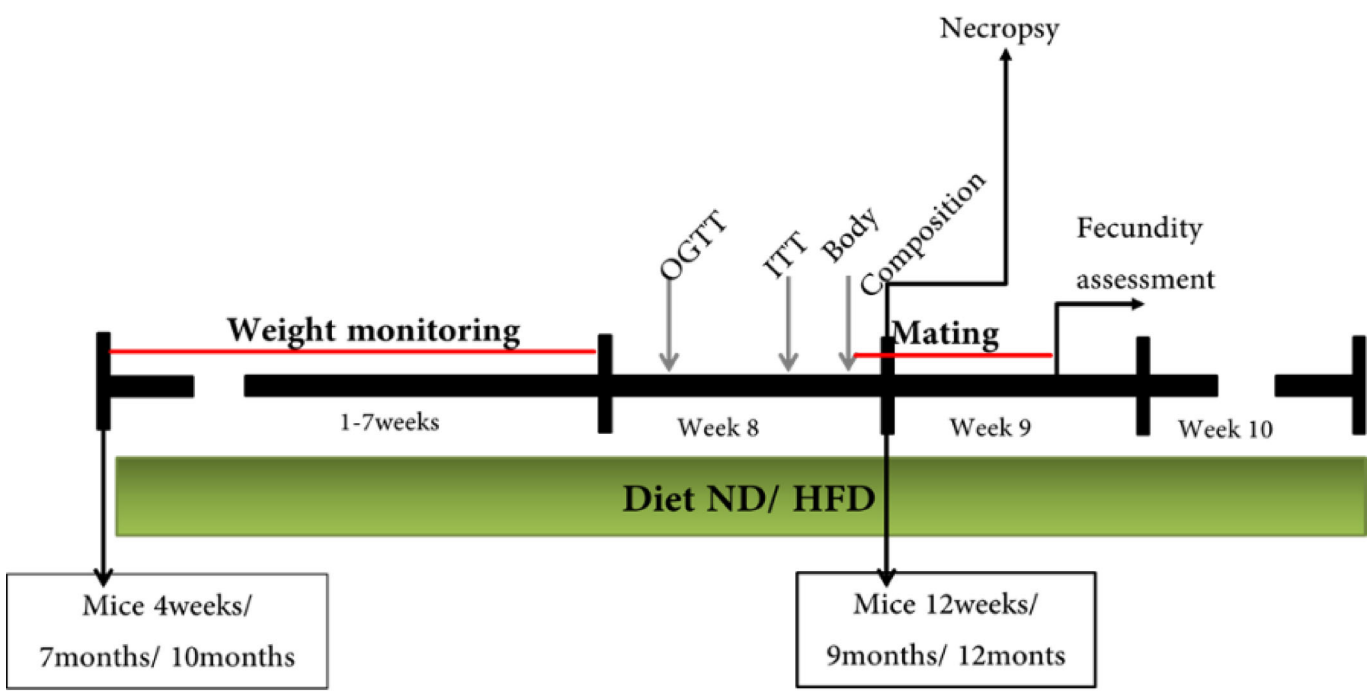

Fig. 7: Experiment design. Female mice of different ages were fed either normal diet (ND) or high fat diet (HFD) and their weight was monitored once a week. On the eighth week, oral glucose tolerance test (OGTT), insulin tolerance test (ITT) and body composition assessment were performed. Then, females were mated with young healthy males for up to 8 days and preimplantation embryos were flushed from the uterus 3.5 days *post coitum*. After the 8 weeks of diet, a necropsy was performed in a few animals.

2. Mouse Model Morphometry:

Body weight was measured weekly (same day and hour) and animals were identified by drawing a permanent line at the base of the tail.

After the 8 weeks of diet, animals were fasted for 6 hours (84) and body composition was measured by Time Domain Nuclear Magnetic Resonance using a Minispec lean fat analyser (Bruker Optics, Inc., The Woodlands, TX). Animals were also weighed at this moment to calculate the percentage of fat and lean mass. Finally, morphometry was performed by measuring head, body and tail length and their body mass index (BMI) was calculated using an standard formula for BMI in mice (85).

3. Mouse Model Glucose Metabolism:

3.1 Oral Glucose Tolerance Test

For the Oral Glucose Tolerance test (OGTT), on the eighth week of diet, mice were fasted for 6h and a 2 g/Kg dose of glucose (G7528, Sigma-Aldrich Chemie GmbH, Steinheim, Germany) in saline solution was administered by oral gavage. Blood was sampled from the tip of the tail every 15 minutes up to 1 hour and glucose concentrations were measured and recorded (Glucomen Areo, Menarini Diagnostics) (86).

3.2 Intraperitoneal Insulin Tolerance Test

The insulin tolerance test (ITT) was performed by intraperitoneal administration of 0.5 U/Kg of insulin (Actrapid, Novo Nordisk, Copenhagen, Denmark), two days after the OGTT. Blood was sampled from the tip of the tail every 15 minutes up to 1 hour and glucose concentrations were measured and recorded (Glucomen Areo, Menarini Diagnostics) (86).

4. Mouse Model *Post-mortem* Analysis:

Animals were killed by isoflurane overdose after 8 weeks of HFD feeding and bled out from the inferior vena cava. Blood was then centrifuged 1500 RPM for 10 minutes and serum preserved at -20°C. Then, different tissues were dissected, weighted, and conserved for further analysis.

4.1 Necropsy

Liver, pancreas, heart, spleen, reproductive system, white and brown fat, kidneys, and gastrocnemius muscles were dissected during the necropsy. The tissues were weighed and preserved in 4% neutral buffered formalin (Applichem-Panreac, Barcelona), processed routinely, and embedded in paraffin-wax. Sections (5 µm-thick) were stained with haematoxylin-eosin. All histological sections were randomly and blindly evaluated by Dr. Oscar Quesada-Canales, a board-certified veterinary pathologist.

4.2 Biochemistry

A full biochemistry panel was performed on 100µl of serum by a microfluidics-based blood chemistry device (PointCare V2 Biochemistry Analyzer, RAL SA, Barcelona). Measured parameters include: albumin, alkaline phosphatase, alanine aminotransferase, amylase, blood urea nitrogen, creatinine, globulin, glucose, phosphorus, total bilirubin, total protein, cholesterol and creatine kinase.

4.3 Islets immunofluorescence

Pancreatic insulin content was evaluated by islets immunofluorescence. After removing the paraffin from the pancreatic sections, samples were permeabilised with 0.05% Triton X-100 for 1h. Pancreas sections were incubated overnight with anti-insulin and anti-Glucagon antibodies (Table 1). Alexa Fluor 488 Tyramide Superboost kit (Invitrogen/Thermo Fisher Scientific, Waltham, MA, USA, B40943) was used to increase insulin fluorescent signal following the manufacturer's instructions.

5. Mouse Model Fecundity Analysis:

Female mice fed for 8 weeks with HFD at different ages were mated to young healthy males no older than 6 months. Animals were mated for up to eight days to allow two consecutive oestrus cycles. Mating was confirmed by the presence of a

vaginal plug. Briefly, each female was located with a lone caged male latter than 6PM and checked for vaginal plug before 8AM for eight days or until the plug was confirmed. Plugged females were identified with a permanent pen at base of the tail as pregnant (E0.5) and regrouped. At day 3.5 *post coitum* (dpc), mice were sacrificed by dislocation of the neck and the abdominal cavity was opened. Once fat and intestines were moved away to clear the area, the uterus formed by two uterine horns connected was dissected out. The two horns were placed in a dish containing PBS and fat and mesometrium membrane were removed under the stereomicroscope. A needle containing M2 medium (Embryomax®; Millipore, Ref. MR-015-D, Burlington, MA, EE. UU) was used to flush both uterine horns and the embryos were collected using a mouth pipette and transferred into a small drop of fresh M2 medium to be fixed afterwards.

The ability to mate and get pregnant and the number of embryos per female were used as fecundity indicators. Mating rate was calculated as the proportion of females with a vaginal plug, as an indirect measure of oestrus cycle. Fertilization rate was calculated as the percentage of females with a plug which had embryos in their uteri.

Following protocols used in assisted reproduction clinics, preimplantation embryo quality was assessed by morphological

features such as size, presence of blastocoel and overall aspect. Embryos were classified into 4 categories (A-D), being A those that present the best features and D the ones poorly developed (87).

6. Preimplantation embryo analysis:

Obtained embryos were prepared for immunofluorescence as previously described (88,89). Preimplantation embryos at 3.5 dpc are surrounded by the *zona pellucida* that was removed using acid Tyrode's to avoid interference with immunostaining (89,90). Embryos were fixed in 4% PFA for 15 minutes and permeabilised using 0.25% Triton X-100 in PBS/PVP for 30minutes at RT and blocked for at least 15 minutes before overnight incubation with primary antibodies (Table 1). Embryos were incubated for 1 hour with appropriate secondary antibodies (Table 2). DAPI (Invitrogen/Thermo Fisher Scientific, Waltham, MA, USA, D1306; 1:1000) was used to stain nuclei.

Table 1: List of Primary antibodies used for immunofluorescence

Antibody	**Host**	**Manufacturer**	**Catalogue Number**	**Dilution**
NANOG	Rat	eBioscience	14–5761	1:200
GATA6	Goat	R&D Systems	AF1700	1:200

GATA4	Rabbit	Santa Cruz	sc-9053	1:200
GATA3	Mouse	eBioscience	MA1-028	1:200
INSULIN	Rabbit	Santa Cruz	sc-9168	1:80
GLUCAGON	Mouse	Sigma-Aldrich	G2654	1:100

Table 2: List of Secondary antibodies used for immunofluorescence

Antibody	**Host**	**Manufacturer**	**Dilution**
Alexa Fluor 488 – conjugated anti-Rat	Donkey	Invitrogen	1:1000
Alexa Fluor 568 – conjugated anti-Goat	Donkey	Invitrogen	1:1000
Alexa Fluor 647 – conjugated anti-Rabbit	Donkey	Invitrogen	1:1000
Alexa Fluor 647 – conjugated anti-Mouse	Donkey	Invitrogen	1:1000

Alexa Fluor 568 – conjugated anti-Mouse	Mouse	Invitrogen	1:1000

7. Microscopy and Image Analysis:

Both Islets of Langerhans and embryos were imaged using an inverted Zeiss LSM Zeiss LSM700 and a Plan-Apochromat 40x/1.3 Oil DIC (UV) VIS-IR M27 objective, with optical section thickness of 1µm. Images were acquired using 512 x 512 pixels (159.73µm x 159.73µm) resolution of and all specimens were stained at the same time (same mixture of antibodies and incubation times) and imaged under the same conditions regarding laser intensity, gain and pinhole. If possible, all specimens from the same experiment were imaged in the same confocal session. Zeiss AIM software (Carl Zeiss Microsystems) and FIJI (91) were used for image acquisition and visualization.

Embryo images were processed and analysed as previously described (2). Briefly, a Matlab-based software called Modular Interactive Nuclear Segmentation (MINS) was used to segment embryo confocal images based on the DAPI nucleus staining (92). MINS detects and segments each nucleus. Then, the fluorescence intensity of each channel in individual cells is

measured and an output of each cell location together with their information is obtained (Figure 8).

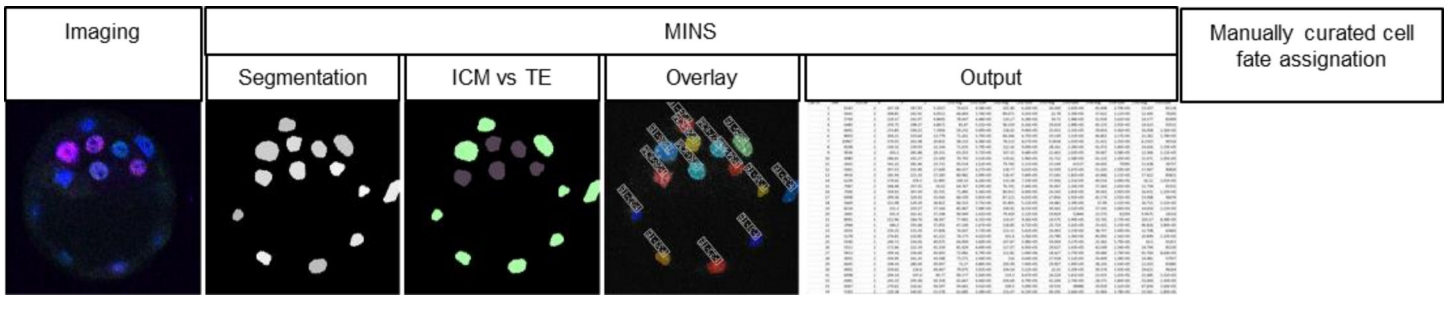

Fig. 8: Image analysis: Pipeline for quantitative characterization of mouse embryos. Imaging with confocal laser scanning fluorescence microscope using sequential scan mode. Segmentation with MINS and automated classification into inner cell mass (ICM) or trophectoderm (TE). Overlay obtained with each cell segmented and identified. Finally, an excel file with location and fluorescence intensity for each cell in the different channels. Image adapted form Fischer et al. 2020.

MINS also automatically classifies cells in the embryo into TE and ICM according to their position. This classification was manually curated in all the embryos to ensure its accuracy. Embryos were classified, according to their total cell number, into early (up to 64 cells), mid (65-90 cells) and late (from 91 cells). Cells were then manually classified into TE and ICM.

The decay in fluorescence along the z axis was corrected (Figure 9) as previously published (93).

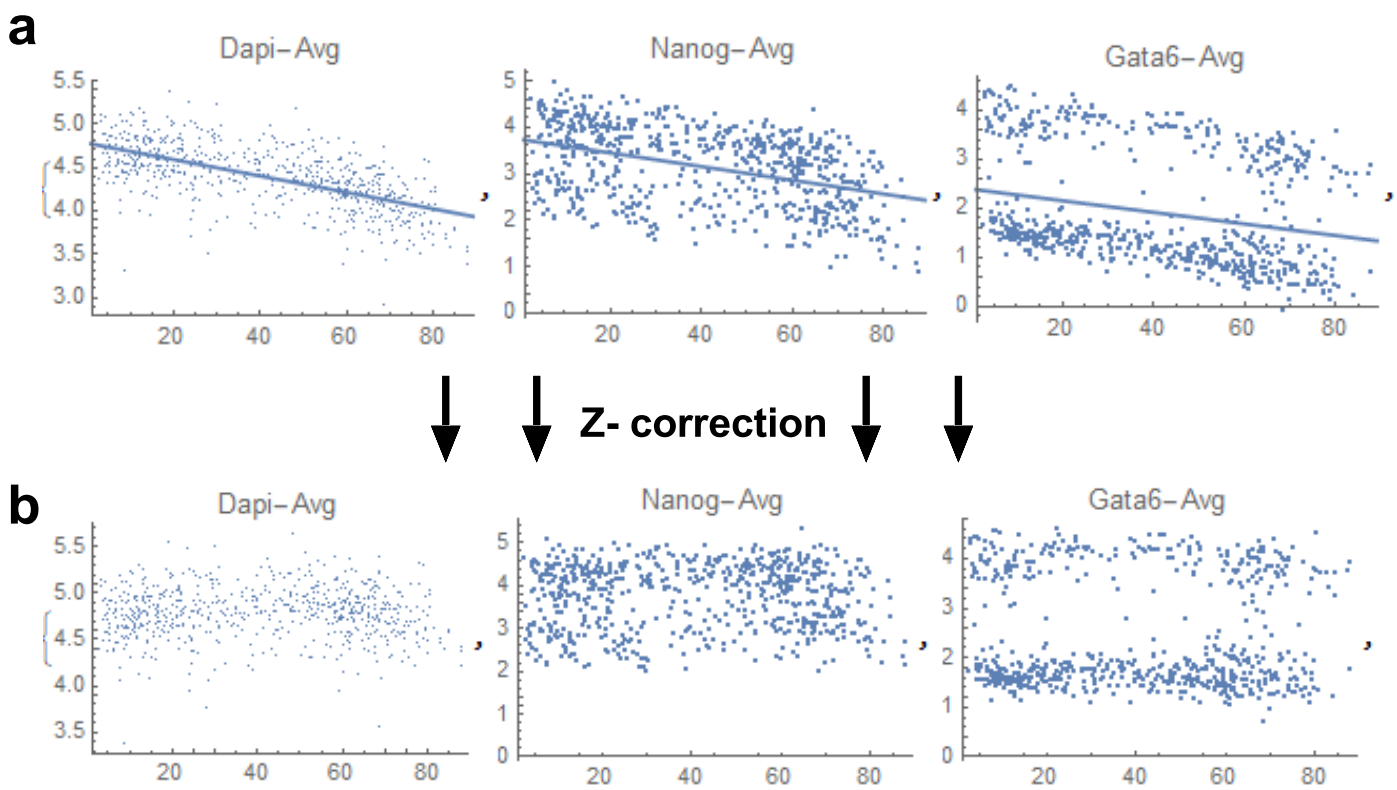

Fig. 9: Image analysis: Correction fluorescence decay in Z-axis. An example of fluorescence decay correction along the Z axis (a) Fluorescence intensity along Z-axis before correction for DAPI, NANOG and GATA6 (b) Fluorescence intensity along Z-axis after correction DAPI, NANOG and GATA6. For these graphs, X- axis show Z position in µm, starting at the cover slip and moving deep into the sample and Y- axis show the average fluorescence levels of the marker in log scale.

A mixture analysis done with the software Paleontological Statistics (PAST) (Figure 10) (94) of NANOG and GATA6 corrected fluorescent levels from ICM cells in late embryos allowed to calculate the threshold level by which a cell was considered to be positive or negative for NANOG or GATA6. This results in each cell being classified as positive or negative: double negative (DN, negative expression for NANOG and GATA6; N-G6-), Epi progenitors (positive for NANOG and negative for GATA6; N+G6-), PrE progenitors (negative for NANOG and positive for GATA6; N-G6+), and double positive (DP) for uncommitted ICM cells

positive for both, NANOG and GATA6; N+G6+). The same classification was based on GATA4 staining instead of GATA6: N-G4- for DN, N+G4+ for DP, N+G4- for Epi and N-G4+ for PrE progenitors.

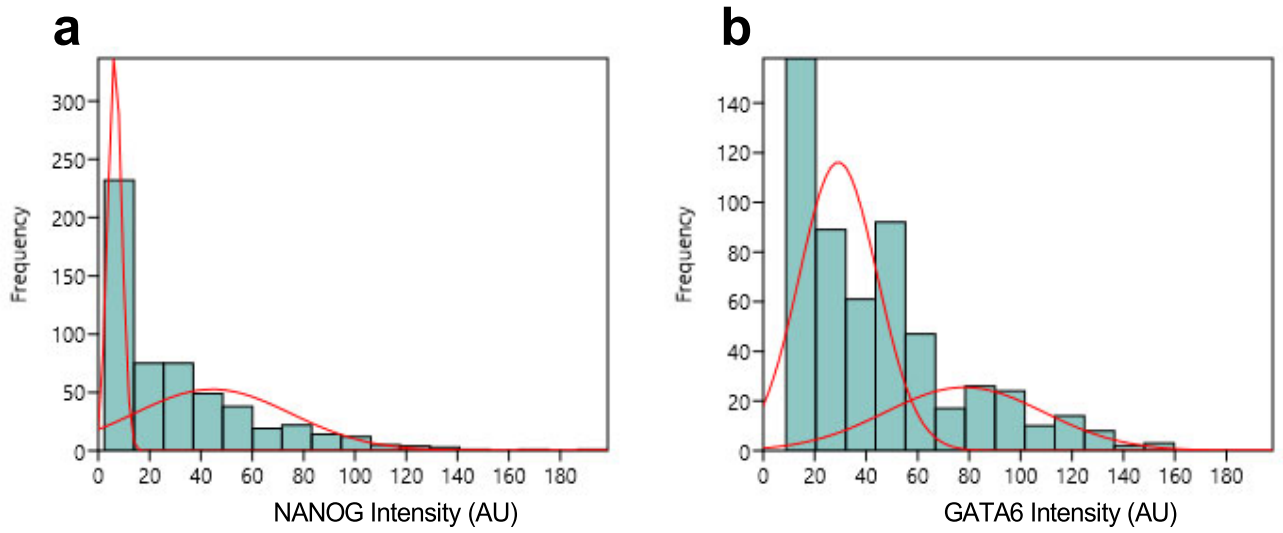

Fig. 10: Image analysis: Mixture analysis performed with PAST (Paleontological Statistics). An example of mixture analysis, for NANOG (a) and GATA6 (b) intensity values are plotted as a histogram, with the distributions displayed in red. The analysis indicates for each value the probability for it belonging to each population, assigning it to the one with highest probability.

Imaging an embryo typically takes 10 to 15 minutes, therefore there was a time limitation to image all the embryos used in this work just in one session. To avoid this problem, a strategy that aligns the thresholds calculated for each session was developed and published as part of the paper (2) "*The transition from local to global patterns governs the differentiation of mouse blastocysts*" included in this thesis. Briefly, thresholds for each dataset were determined using PAST. Then, these thresholds were aligned, correcting NANOG and GATA6 levels accordingly

(Figure 11.a). Once all datasets were aligned, a population analysis was done, whereby the percentage of cells belonging to each of the 4 populations was determined with respect to the total ICM cell number (Figure 11.b). These percentages change over time with more DP cells in earlier stages of development that is reduced in later stages as cells differentiate into Epi or PrE cells and GATA6 or NANOG are downregulated, respectively (79).

Fluorescence decay correction and thresholds alignments calculations were performed using specifically written codes in Mathematica 11.1 (Wolfram Research) (2).

8. Statistics:

Data are presented as mean ± standard error (SEM). ANOVA with Tukey's multiple comparisons test was used for comparisons between groups and Z-test for frequencies, followed by the Bonferroni correction for multiple comparisons. Values of $p<0.05$ were considered statistically significant. Statistical tests were performed using GraphPad Prism version 8.0.0 for Windows, GraphPad Software, San Diego, California USA, www.graphpad.com.

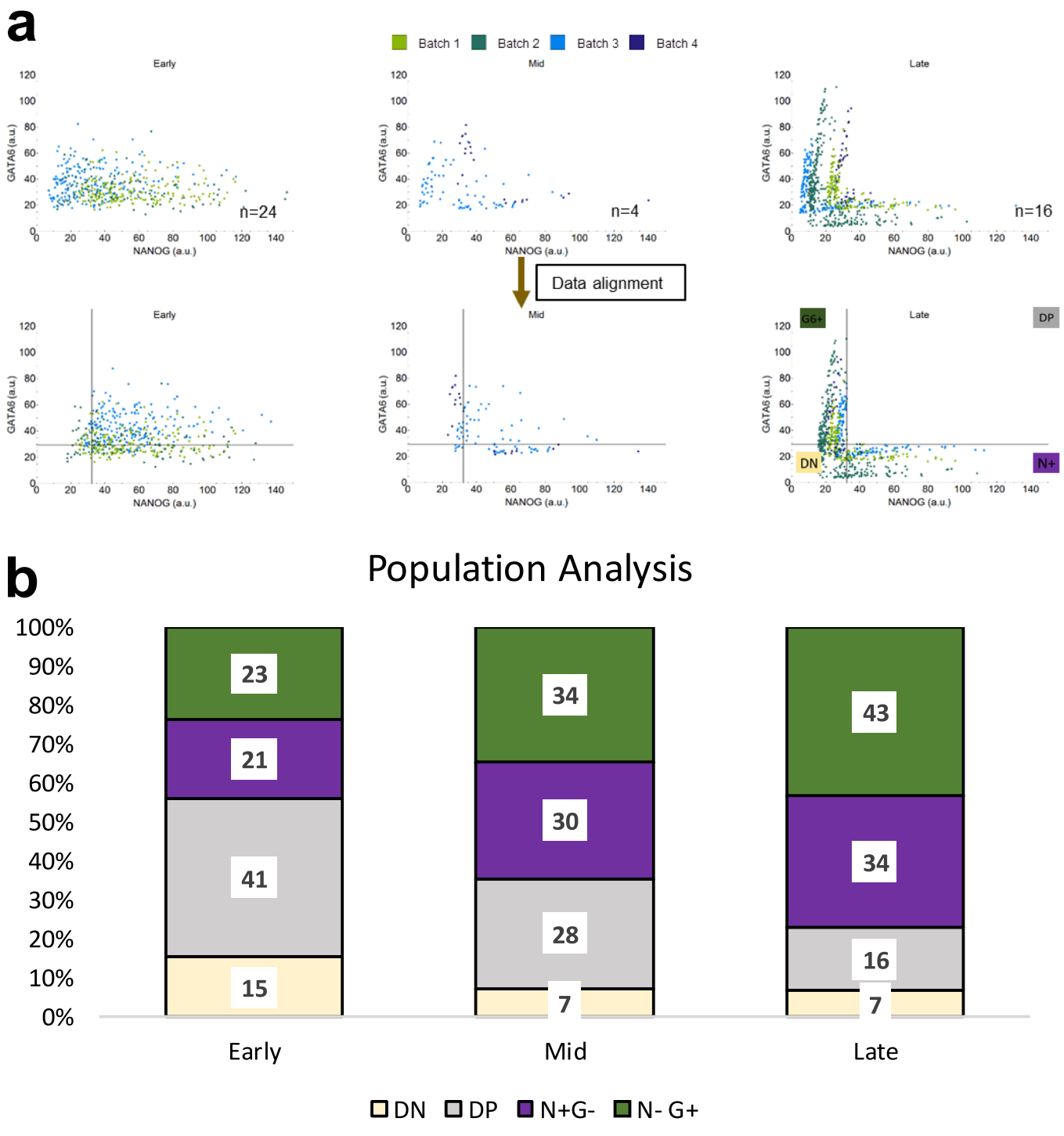

Fig. 11: Image analysis: Representative fluorescence levels alignment and population analysis. Different embryo batches presented different basal levels of fluorescence depending on the immunostaining and the confocal session. (a) Scatter plots in the late stage allows to calculate the thresholds for each data set, align data from different batches and establish a common threshold. These alignment and thresholds can be afterwards extended to earlier stages. Calculated thresholds for NANOG and GATA6 divide cells in four populations: DN (double negative, N-G6-), DP (double positive, N+G6+), Epi (N+G6-) and PrE (N-G6+). (b) These 4 populations are presented in a bar graph as the percentages of each population.

Results

Diet manipulation is a proved useful strategy to induce obesity and mild hyperglycaemia or diabetes in animal models (83). Usually, adult mice are fed during 12 weeks with high fat diet (HFD) to achieve these phenotypic models (61,95). For this work, prepuberal (young, Y), mature (M), and middle-late age (old, O) adult female mice were fed with a HFD for 8 weeks. The model was validated for obesity and mild hyperglycaemia. Normal diet (ND) was used for controls and until reaching the starting experimental age.

1. Mouse Model Validation:

1.1 Morphometry

Mature and old groups fed with HFD showed rapid weight gain that worsened with age. In the young mice, weight was not significantly affected by the HFD nor were their body mass index even after 8 weeks of HFD feeding. In these young animals, the weight increased over time with both diets (ND and HFD) due to physiological growth as they were only 4 weeks old at baseline (Figure 12).

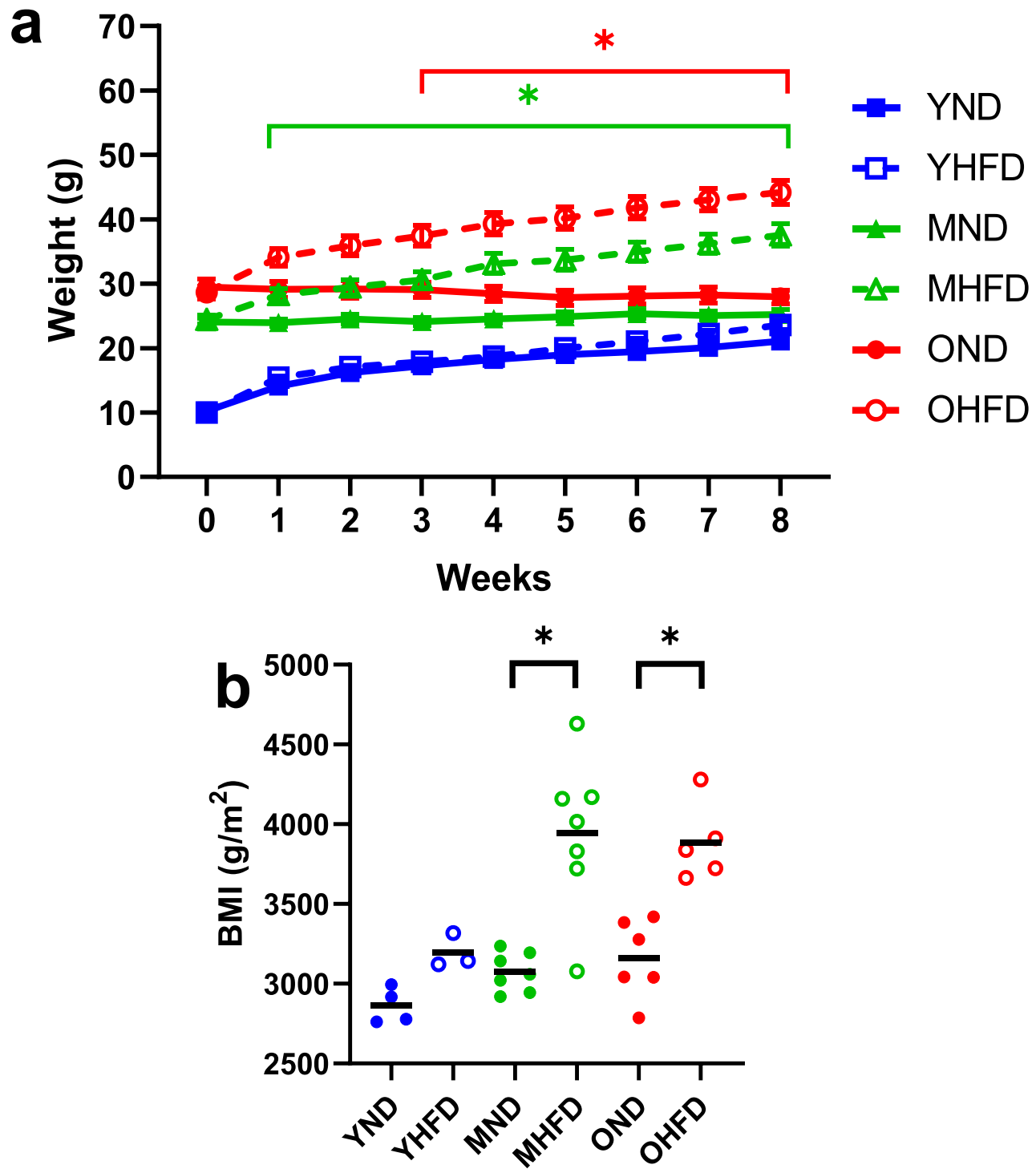

Fig. 12: Effect of 8 weeks of high fat diet (HFD) on weight and BMI. (a) Weekly body weight and (b) body mass index. n= 14 YND, 20 YHFD, 14 MND, 17 MHFD, 9 OND and 21 OHFD. Data are expressed as mean ± SEM, *p<0.05 comparing each HFD group with its ND control or between age-groups. YND= Young (12 weeks) Normal Diet (solid blue), YHFD= Young High Fat Diet (blue circles); MND= Mature (9 months) Normal Diet (solid green), MHFD= Mature High Fat Diet (green circles); OND= Old (1 year) Normal Diet (solid red), OHFD= Old High Fat Diet (red circles).

Nuclear magnetic resonance was used to determine body composition. For all age-groups, HFD was associated with an increased total fat and reduced lean mass. Body composition was similar in mature and old mice while younger groups showed a milder phenotype, independently of the diet. (Figure 13).

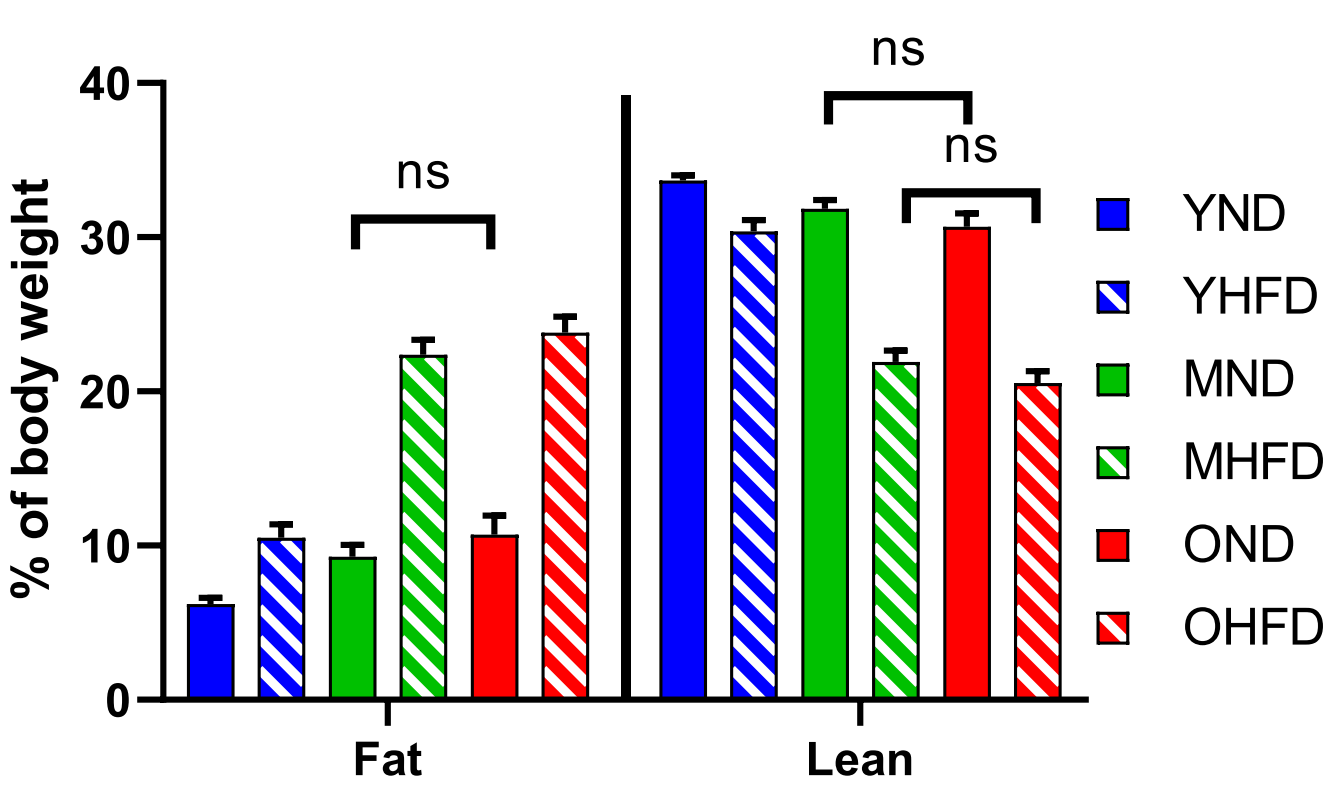

Fig. 13: Effect of 8 weeks of high fat diet (HFD) on body composition. Body composition by nuclear magnetic resonance. n= 14 YND, 20 YHFD, 14 MND, 17 MHFD, 9 OND and 20 OHFD. Data are expressed as mean ± SEM, ns= not significant, otherwise significant *p<0.05 comparing each HFD group with its ND control or between age-groups. YND= Young (12 weeks) Normal Diet (solid blue), YHFD= Young High Fat Diet (patterned blue); MND= Mature (9 months) Normal Diet (solid green), MHFD= Mature High Fat Diet (patterned green); OND= Old (1 year) Normal Diet (solid red), OHFD= Old High Fat Diet (patterned red).

In summary, body weight increments rapidly upon HFD feeding when started during adulthood while in younger animals the

increment happens but does not differ from ND fed animals. HFD affects body composition with an increase in fat at the expense of lean mass even in young animals, where there are no changes in weight.

1.2 Glucose Metabolism

During the last week of diet, OGTTs and ITTs were performed on animals from the different groups to evaluate the effect of both age and HFD on glucose metabolism (Figures 14a, 15a). Area under the curve (AUC) was also calculated for every curve (Figures 14b, 15b).

OGTT performed after 6h of fasting showed higher glucose levels for longer time in mice fed with HFD, and this was especially pronounced in the old animals. Besides, no effect of age was seen as groups fed with ND showed no variation in their levels (Figure 14).

ITT was performed two days after the OGTT, also after 6hours of fasting. HFD was associated with a less prominent glucose-lowering effect of insulin, reflecting increased insulin resistance only in older groups (Figure 15).

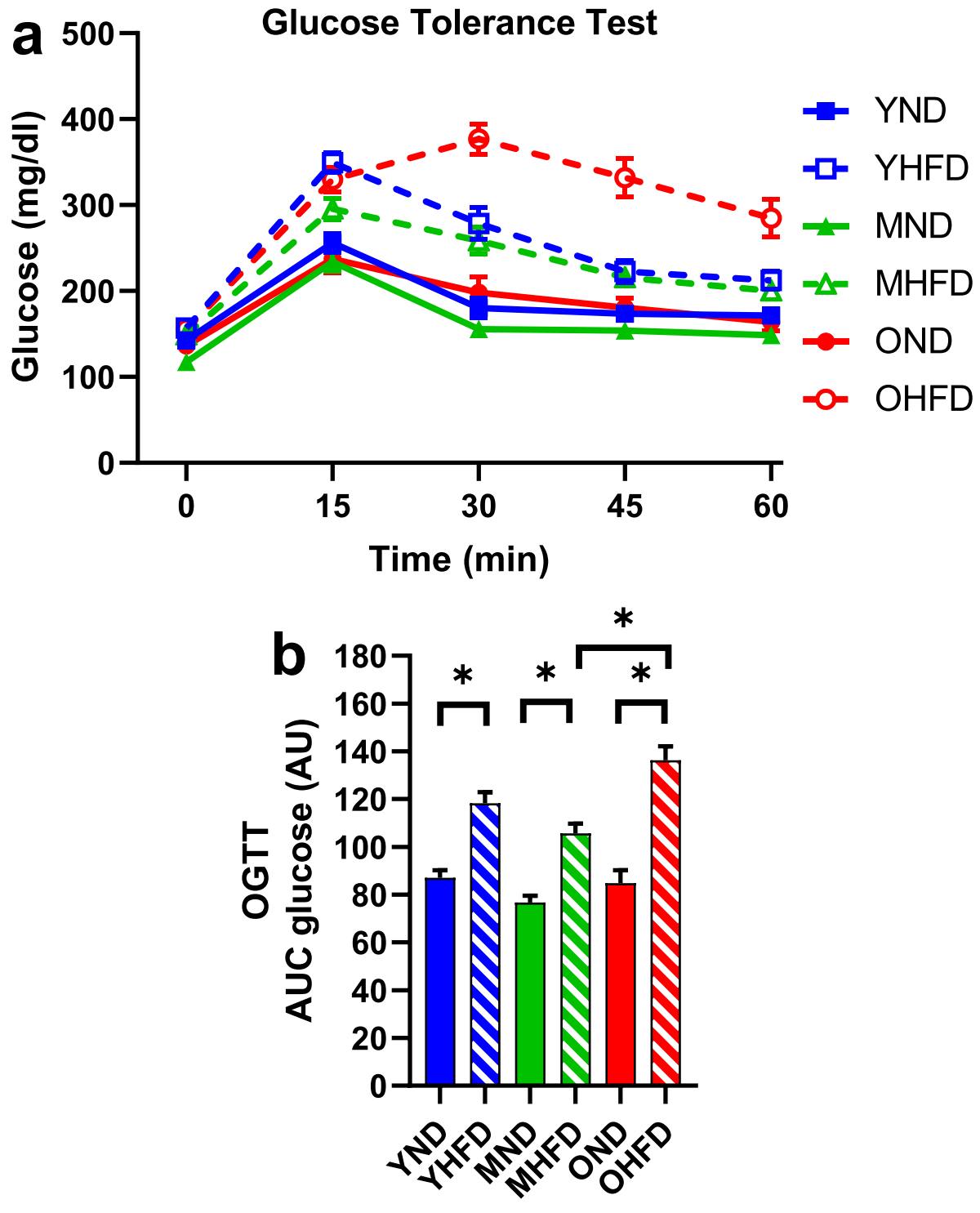

Fig. 14: Oral glucose tolerance test (OGTT)after 8 weeks of high fat diet (HFD). (a) OGTT blood glucose. (b) AUC calculated from OGTT. n=12 YND, 17 YHFD, 14 MND, 17 MHFD, 9 OND and 20 OHFD. Data are expressed as mean ± SEM, *p<0.05 comparing each HFD group with its ND control or between age-groups. YND= Young (12 weeks) Normal Diet (solid blue), YHFD= Young High Fat Diet (patterned blue); MND= Mature (9 months) Normal Diet (solid green), MHFD= Mature High Fat Diet (patterned green); OND= Old (1 year) Normal Diet (solid red), OHFD= Old High Fat Diet (patterned red).

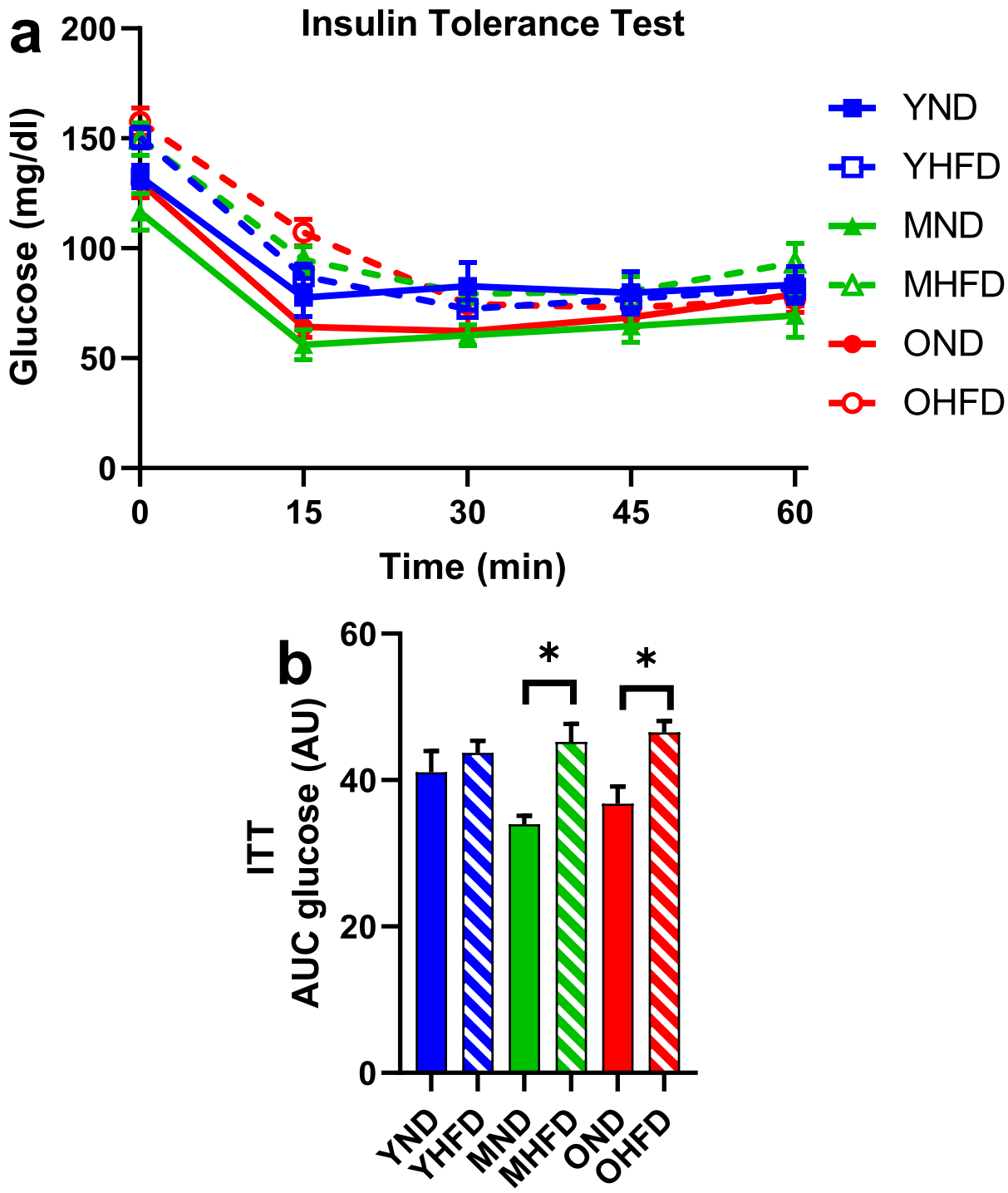

Fig. 15: Insulin tolerance test (ITT) after 8 weeks of high fat diet (HFD). (a) ITT blood glucose. (b) AUC calculated from ITT. n=12 YND, 17 YHFD, 14 MND, 17 MHFD, 9 OND and 20 OHFD. Data are expressed as mean ± SEM, *p<0.05 comparing each HFD group with its ND control or between age-groups. YND= Young (12 weeks) Normal Diet (solid blue), YHFD= Young High Fat Diet (patterned blue); MND= Mature (9 months) Normal Diet (solid green), MHFD= Mature High Fat Diet (patterned green); OND= Old (1 year) Normal Diet (solid red), OHFD= Old High Fat Diet (patterned red).

1.3 Necropsy

During the *post-mortem* evaluation, no evident internal or external gross lesions were identified. Animals fed the HFD showed increased fat mass accumulation, that was more evident in the older groups. The opposite effect was observed in the gastrocnemius muscle mass with decreased muscle mass. Increased weight was also observed in the reproductive system, but this increase was due to fat incremented around the ovaries. Furthermore, HFD seems to have a weight curbing effect on the liver and pancreas (Figure 16).

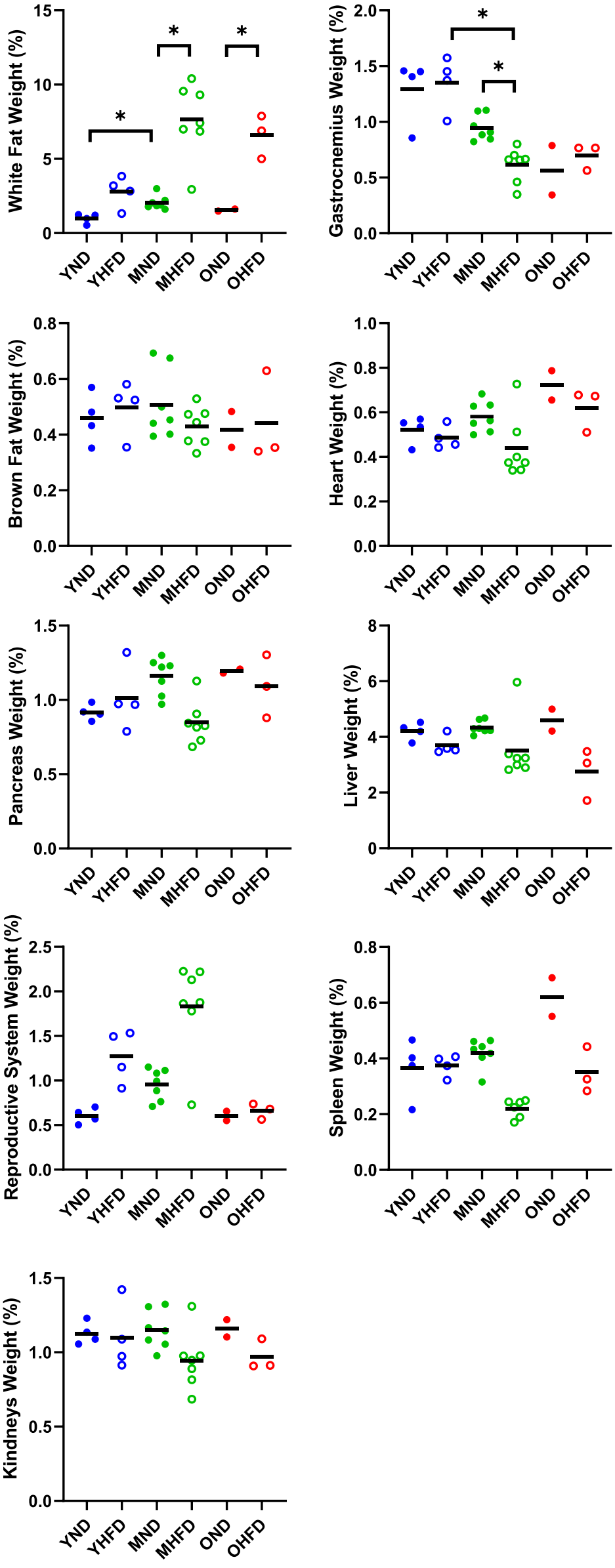
White Fat Weight (%)
15
10
5
0
*
*
*
YND
YHFD
MND
MHFD
OND
OHFD
Gastrocnemius Weight (%)
2.0
1.5
1.0
0.5
0.0
*
*
Brown Fat Weight (%)
0.8
0.6
0.4
0.2
0.0
Heart Weight (%)
1.0
0.8
0.6
0.4
0.2
0.0
Pancreas Weight (%)
1.5
1.0
0.5
0.0
Liver Weight (%)
8
6
4
2
0
Reproductive System Weight (%)
2.5
2.0
1.5
1.0
0.5
0.0
Spleen Weight (%)
0.8
0.6
0.4
0.2
0.0
Kindneys Weight (%)
1.5
1.0
0.5
0.0

Fig. 16: Organ weight after 8 weeks of high fat diet (HFD). Different organs or tissues weighed fresh after their dissection. White fat as the addition of fat from the paragenital fat pads and Gastrocnemius as the addition of the weight of both gastrocnemius muscles from the hind legs. For paired organs result of the addition of both. Data are expressed as median, *p<0.05 either comparing each HFD group with its ND control or between ages; Each point refers to one animal. YND= Young (12 weeks) Normal Diet (solid blue), YHFD= Young High Fat Diet (blue circles); MND= Mature (9 months) Normal Diet (solid green), MHFD= Mature High Fat Diet (green circles); OND= Old (1 year) Normal Diet (solid red), OHFD= Old High Fat Diet (red circles).

1.4 Biochemistry

The full biochemistry panel performed on the different groups showed that animals fed with HFD had higher glucose and total cholesterol blood concentrations than those fed with ND (Figure 17). The recorded glucose concentrations were unusually high, even in the blood from animals fed with the ND when obtained *post-mortem* from the inferior vena cava, in agreement with previous reports (96,97). This phenomenon is linked to the isoflurane used to anesthetize the animals (98). No differences were observed in other measurements (Figure 17).

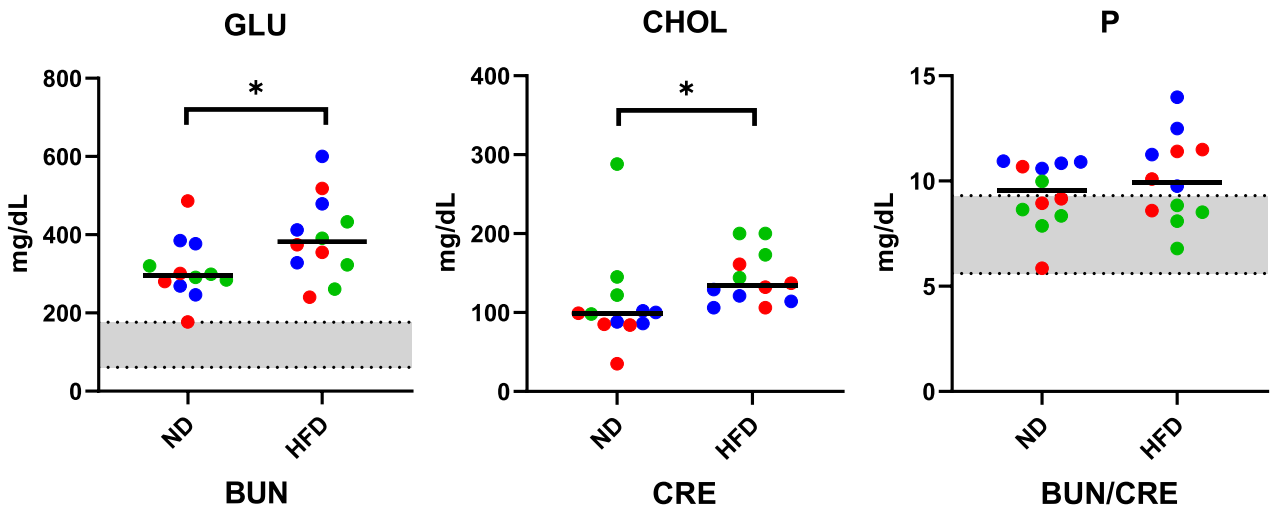
GLU
mg/dL
800
600
400
200
0
*
ND
HFD
BUN
CHOL
mg/dL
400
300
200
100
0
*
ND
HFD
CRE
P
mg/dL
15
10
5
0
ND
HFD
BUN/CRE

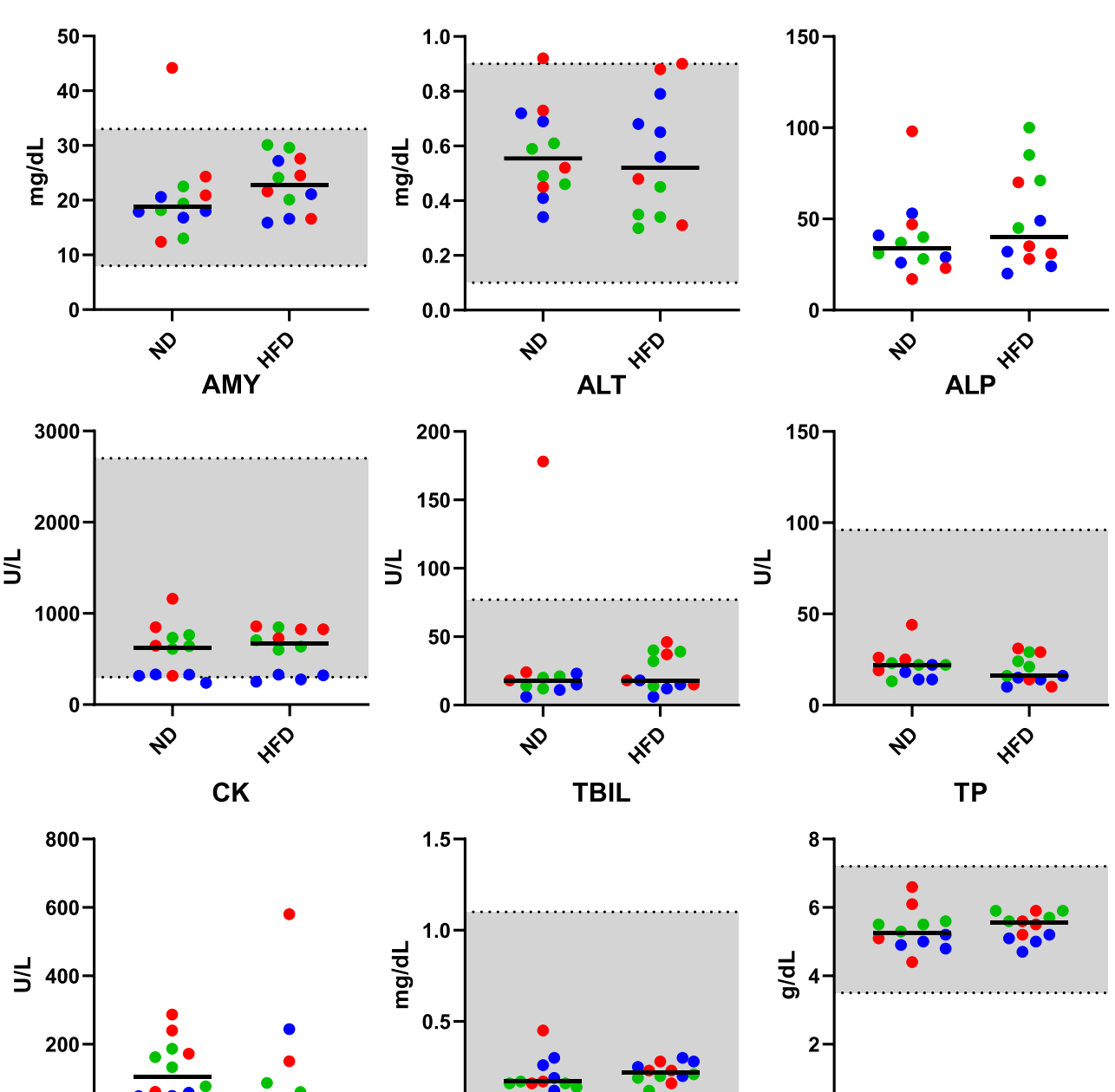
mg/dL
50
40
30
20
10
0
ND
HFD
AMY
mg/dL
1.0
0.8
0.6
0.4
0.2
0.0
ND
HFD
ALT
150
100
50
0
ND
HFD
ALP
U/L
3000
2000
1000
0
ND
HFD
CK
U/L
200
150
100
50
0
ND
HFD
TBIL
U/L
150
100
50
0
ND
HFD
TP
U/L
800
600
400
200
0
ND
HFD
ALB
mg/dL
1.5
1.0
0.5
0.0
ND
HFD
GLO
g/dL
8
6
4
2
0
ND
HFD
ALB/GLO

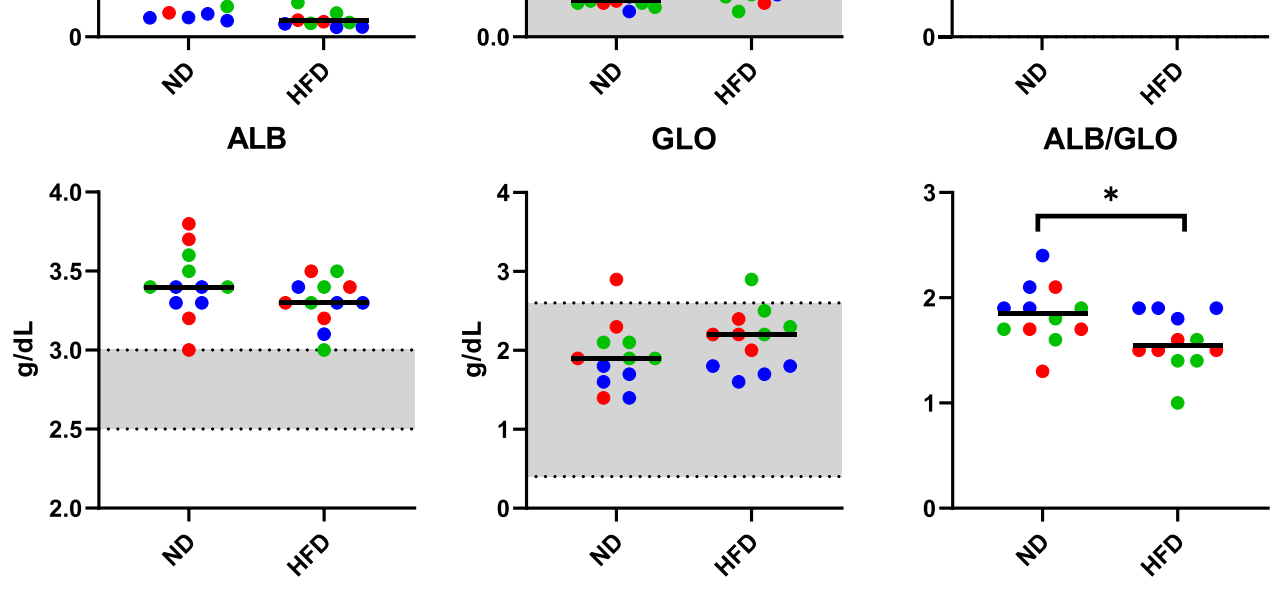
g/dL
4.0
3.5
3.0
2.5
2.0
ND
HFD
g/dL
4
3
2
1
0
ND
HFD
3
2
1
0
*
ND
HFD

Fig. 17: Full panel of biochemistry determinations after 8 weeks of high fat diet (HFD). Panel includes: Glucose (GLU), Cholesterol (CHOL), Blood Urea Nitrogen (BUN), Creatinine (CRE), Albumin (ALB), Globulin (GLO), Total Bilirubin (TBIL), Total Protein (TP), Amylase (AMY), Alanine Aminotransferase (ALT), Alkaline Phosphatase (ALP), Creatine Kinase (CK) and Phosphorus (P). For the biochemistry analysis animals were grouped by diet to increase the statistical power. Data are expressed as median, *p<0.05 comparing each HFD group with the ND control; Each point refers to one animal and grey area to the reference values established by the manufacturer. ND= Normal Diet, HFD= High Fat Diet; Young (12 weeks) in blue, Mature (9 months) in green and Old (1 year) red.

1.5 Histopathology

A histopathological evaluation was performed in the tissue samples from 4 animals per group. Features observed in the different tissues varied in severity and distribution among the studied groups and were examined by an expert pathologist (Table 3).

Liver: All animals, irrespective of age and diet, showed moderate hepatocellular vacuolization-glycogen accumulation. Moderate, diffuse macrovesicular fatty change was detected in both the older groups fed with HFD, but not in the young ones nor the ones fed with ND. Older groups showed evidence of perivascular (periportal and centrilobular) amyloidosis.

The presence of an inflammatory infiltrate (predominantly lymphocytes and rare neutrophils) was evident in older mice, although it was present at younger as well, irrespective of diet.

Only one of the OHFD presented, occasional, and discrete hepatocellular necrosis.

Heart: Multifocal amyloidosis was observed in the heart of older groups, independently of the diet.

Kidney: Young animals showed no obvious lesions and few of the mature animals presented individual cases of medullar mineralization and perivascular infiltration of lymphocytes in the cortex. However, more severe lesions were observed in older females, with interstitial amyloidosis and interstitial lymphocytic nephritis, especially when fed HFD. This latter group also showed lymphocytic infiltration in most of the individuals.

Pancreas: Multifocal perivascular amyloidosis was described in half of the animals in the older groups independently of their diet. And one of them, fed HFD showed a multifocal periductal lymphocytic infiltrate.

Spleen: Multifocal lymphoid hyperplasia and golden-brown pigment-laden macrophages (hemosiderin pigment) appeared only in mature and old animals. Also, all the OHFD group presented severe amyloidosis.

Table 3: Histopathological features found in the respective group and location (number of individuals/total of individuals per group).

Group	YND	YHFD	MND	MHFD	OND	OHFD
Liver	Mild, diffuse hepatocellular vacuolization (glycogen accumulation) (4/4) Randomly, scattered, small aggregates of lymphocytes and rare neutrophils (2/4)	Mild and diffuse hepatocellular vacuolization (glycogen accumulation) (4/4) Minimal perivascular infiltrate of lymphocytes and neutrophils. (1/4) Randomly, scattered small aggregates of lymphocytes and rare neutrophils (3/4)	Moderate, diffuse hepatocellular vacuolization (glycogen accumulation) (4/4) Moderate, diffuse macrovesicular fatty change, (1/4) Mild to moderate perivascular (centrilobular) infiltrate of lymphocytes with fewer neutrophils, (4/4) Randomly, minimal aggregates of lymphocytes, with rare neutrophils, (4/4)	Moderate, diffuse hepatocellular vacuolization (glycogen accumulation) (4/4) Moderate, diffuse macrovesicular fatty change, (2/4) Mild to moderate perivascular (centrilobular) infiltrate of lymphocytes with fewer neutrophils, (4/4) Randomly, minimal aggregates of lymphocytes, with rare neutrophils, (1/4)	Moderate, diffuse hepatocellular vacuolization (glycogen accumulation), (4/4) Mild to moderate perivascular (centrilobular) infiltrate of lymphocytes with fewer neutrophils (2/4) Multifocal, mild-moderate, perivascular (periportal and centrilobular) amyloidosis extending into and expanding	Moderate, diffuse hepatocellular vacuolization (glycogen accumulation) (2/4) Mild, multifocal, macrovesicular fatty change (2/4) Multifocal, mild-moderate, perivascular (periportal and centrilobular) amyloidosis,extending into and expanding adjacent sinusoids (4/4). Mild to moderate perivascular (centrilobular) infiltrate of lymphocytes with fewer neutrophils (4/4) Randomly, minimal aggregates of lymphocytes, with rare neutrophils, (4/4)

					adjacent sinusoids (2/4).	Randomly, ocasional and discrete foci of hepatocellular necrosis with with cellular debris and rare neutrophils (1/4)
Spleen	NPF	npf	Moderate, multifocally disseminated, golden brown pigment-laden macrophages (4/4) Multifocal lymphoid hyperplasia. (4/4)	Moderate, multifocally disseminated, golden brown pigment-laden macrophage (4/4) Multifocal lymphoid hyperplasia (4/4)	Moderate, multifocally disseminated, golden brown pigment-laden macrophage (2/4) Severe amyloidosis (2/4) Multifocal lymphoid hyperplasia (4/4)	Severe amyloidosis (4/4) Multifocal lymphoid hyperplasia (1/4)
Heart	NPF	NPF	Mild, multifocal amyloidosis (1/4)	NPF	Severe, multifocal amyloidosis (1/4), mild, multifocal amyloidosis (1/4)	Severe, multifocal amyloidosis (2/4)
Kidneys	NPF	NPF	Mild-moderate, locally extensive medullary tubular	Mild-moderate, multifocal perivascular	Mild, multifocal, interstitial amyloidosis (1/4) Multifocal,	Mild, multifocal, interstitial amyloidosis (1/4)

			mineralization (1/4)	infiltration of lymphocites in the cortex (1/4)	severe, interstitial lymphocytic nephritis (1/4)	Multifocal, severe, interstitial lymphocytic nephritis (2/4) Mild, multifocal perivascular infiltration of lymphocites in the cortex (3/4)
Pancreas	NPF	NPF	NPF	NPF	Moderate, multifocal, perivascular amyloidosis (1/4)	Moderate, multifocal, perivascular amyloidosis (2/4) Mild, multifocal periductal infiltrate of lymphocytes, (1/4)

Table 3. Pathology evaluation of tissue samples. Only tissues with histopathological features are included in this descriptive table; n=24 (4/group). NPF= Non pathological findings; YND= Young Normal Diet, YHFD= Young High Fat Diet, MND= Mature Normal Diet, MHFD= Mature High Fat Diet, OND= Old Normal Diet, OHFD= Old High Fat Diet.

Qualitative levels of insulin and glucagon, as well as distribution of β and α cells were evaluated by immunofluorescence on pancreatic sections. No qualitative differences were observed in pancreatic insulin or glucagon content comparing age groups or diets (Figure. 18).

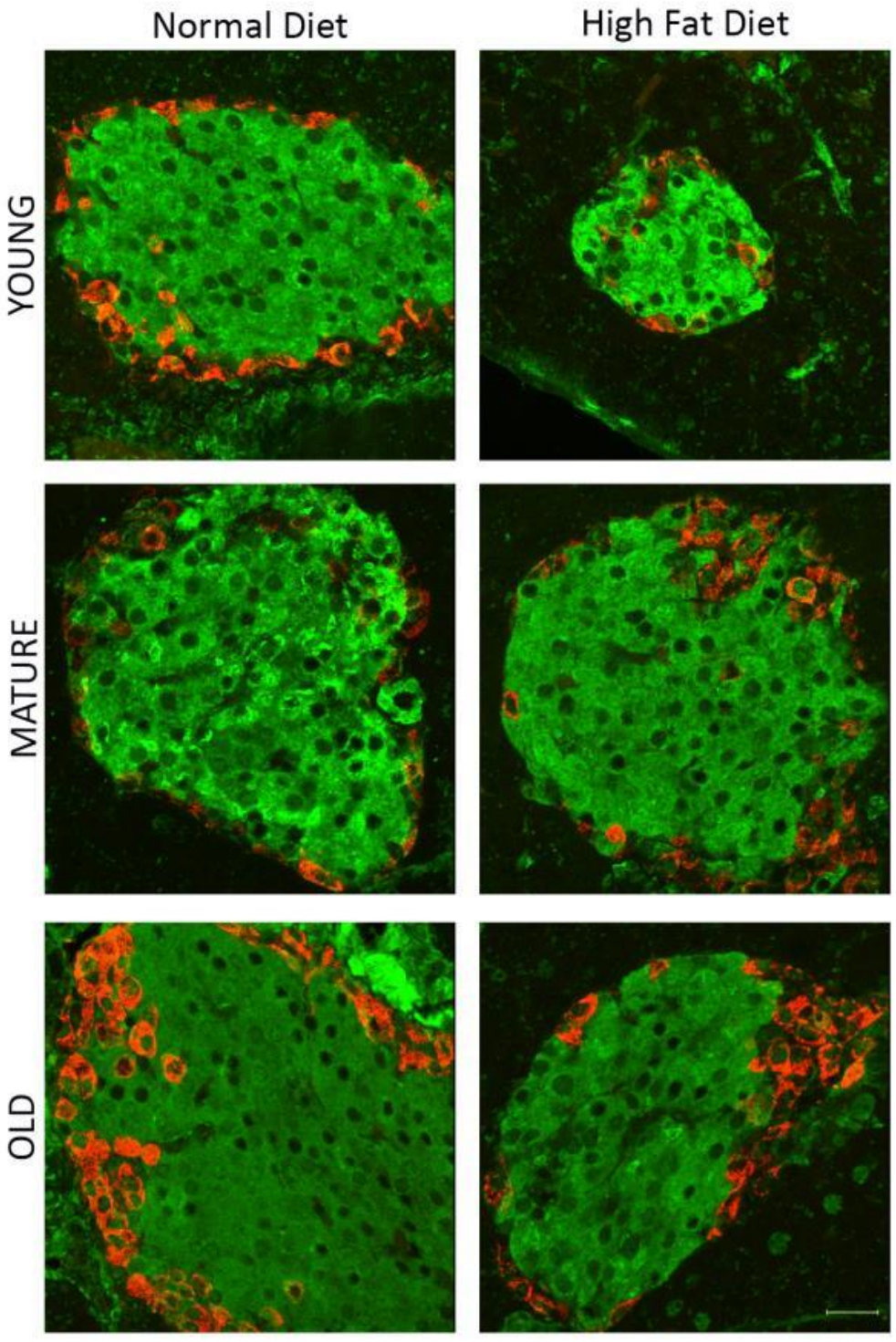

Fig. 18: Qualitative assessment of insulin and glucagon content in pancreatic islets. Pancreas histological sections immunostained for Insulin (green) and Glucagon (red). Representative maximum projection images from Z stacks for each condition are shown. Scale bar: 20 µm.

2. Mouse model fertility assessment:

Female mice fed for 8 weeks with HFD at different ages were mated to young healthy males. Mating and fertilization rates were used as descriptive methods to assess fecundity. Mating rate was calculated as the percentage of females that presented a vaginal plug after eight days of consecutive mating. The fertilization rate was calculated as the percentage of those females from which embryos were recovered 3.5 dpc.

Older animals fed with HFD showed a lower tendency to mate and lower fertilization rates than younger groups. Only one old female fed with ND had embryos and no embryos were obtained from those fed HFD. Old groups (1 year-old) fed both with ND and HFD were not used for further analysis due to their lack of fecundity (Figure 19).

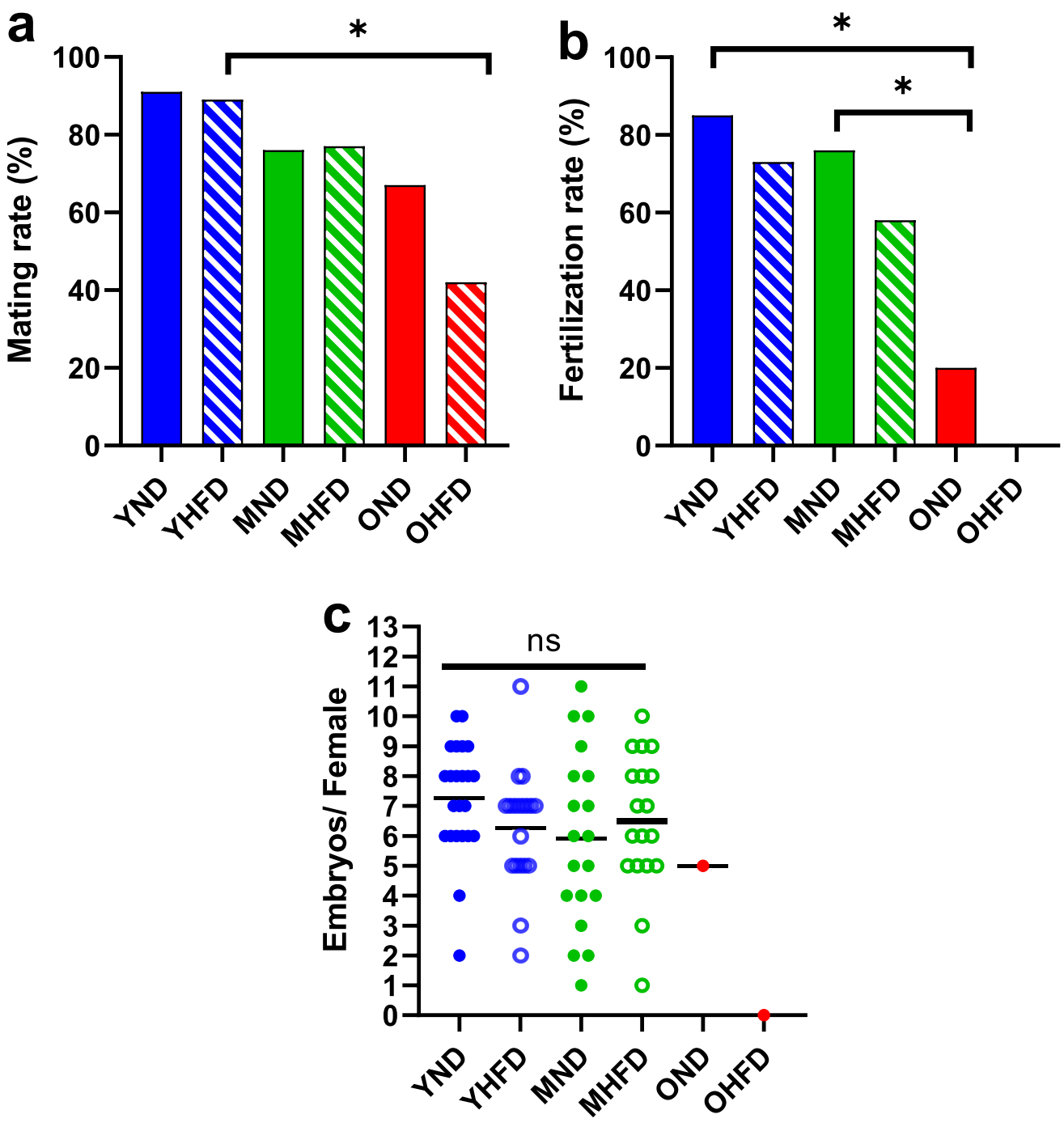

Fig. 19: Effect of 8 weeks of high fat diet on fecundity. (a) Mating rate. n= 33 YND, 38 YHFD, 41 MND, 48 MHFD, 9 OND, 20 OHFD. (b) Fertilization rate. n= 27 YND, 26 YHFD, 25 MND, 31 MHFD, 5 OND and 1 OHFD. (c) Number of embryos obtained per female. Each dot (for ND) and circle (for HFD) indicates one litter. No statistical significance was found in any case *p<0.05 either comparing each HFD group with its ND control or between ages. YND= Young (12 weeks) Normal Diet (solid blue), YHFD= Young High Fat Diet (patterned blue); MND= Mature (9 months) Normal Diet (solid green), MHFD= Mature High Fat Diet (patterned green); OND= Old (1 year) Normal Diet (solid red), OHFD= Old High Fat Diet (patterned red).

Embryos were classified according to their morphological features. The 594 embryos obtained during this work were photographed after being flushed from the uteri and then evaluated at the same time to classify them into four categories according to their size, presence of blastocoele and overall appearance. Young dams fed ND had more embryos with the best features (category A) and fewer with worse features (category D) compared with those fed HFD. No differences were observed between mature females independently of their diet (Figure 20).

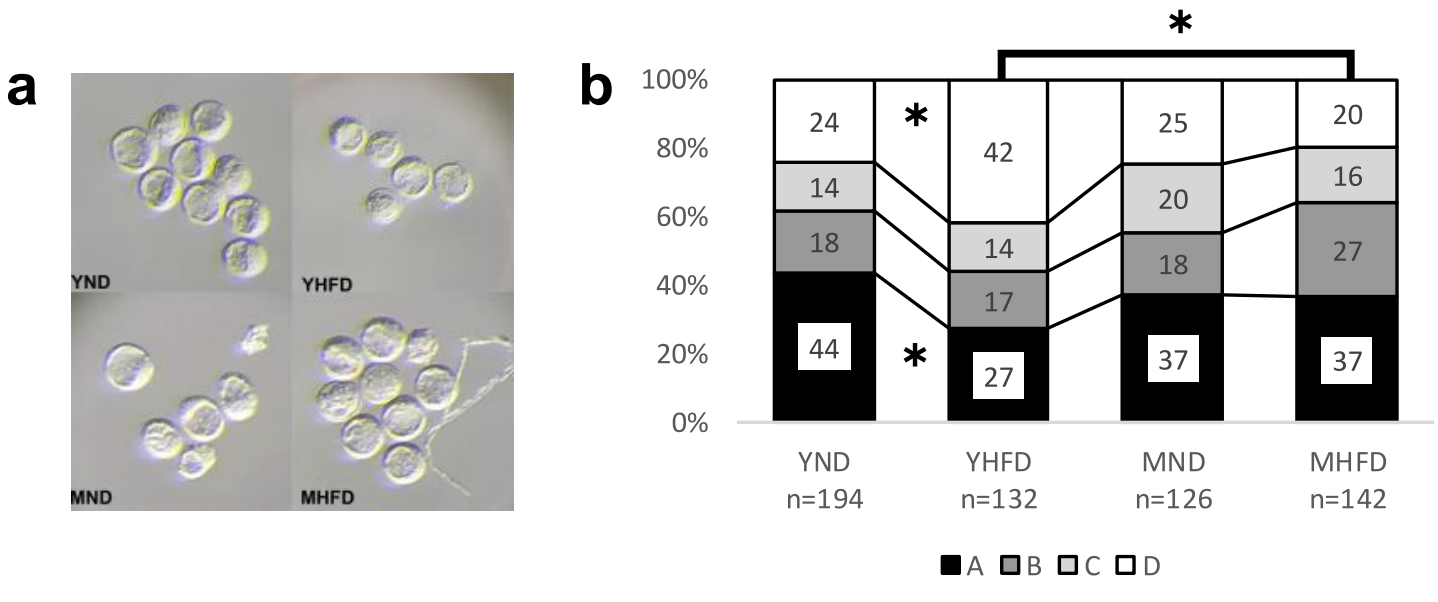

Fig. 20: Preimplantation embryo quality classification according to their morphological features. (a) Representative micrographs of embryos from indicated females. (b) Embryos classified according to their morphological features into four categories (A, B, C, and D, from high to low quality) *p<0.05; YND= Young Normal Diet, YHFD= Young High Fat Diet; MND= Mature (9 months) Normal Diet, MHFD= Mature High Fat Diet

3. Embryo characterization at cellular level:

Embryos were stained for the different markers and imaged. Then, automated image analysis was performed on confocal images and cell fate allocation between TE and ICM cells was manually curated. Subsequently, total cell number together with the classification into TE or ICM cells was done, and the ICM/TE ratio was calculated. An age effect was observed in HFD groups indicating altered patterns in embryo cell fate allocation. (Table 4).

			Total cell number		Total TE number		Total ICM		ICM/TE Ratio	
	Stage	N Embryos	Average	SE	Average	SE	Average	SE	Average	SE
YND	Early	92	54.18	1.06	33.93	0.71	20.25	0.56	0.61	0.02
	Mid	33	72.12	1.07	48.82	1.23	23.30	0.68	0.49	0.03
	Late	2	92.00	1.00	68.50	3.50	23.50	2.50	0.35	0.06
YHFD	Early	64	52.47	1.39	32.45	1.02	20.02	0.61	0.64*	0.02
	Mid	7	71.57	2.22	45.86	3.26	25.71	1.60	0.59	0.07
	Late	1	91.00	NA	65.00	NA	26.00	NA	0.40	NA
MND	Early	17	45.35	3.39	28.47	2.19	16.88	1.51	0.60	0.04
	Mid	4	79.00	3.54	53.00	4.02	26.00	1.08	0.50	0.06
	Late	2	93.00	0.00	67.50	0.50	25.50	0.50	0.38	0.01
MHFD	Early	26	44.84	2.61	29.24	1.63	15.60	1.12	0.53*	0.03
	Mid	23	75.09	1.91	48.04	1.82	27.04	0.76	0.58	0.03
	Late	14	97.86	1.62	69.21	1.97	28.57	1.45	0.42	0.03
*p<0.05 only YHFD vs MHFD										

Table 4: Number of analysed embryos and cells with QIF. Staging criteria: Early (up to 64 cells), Mid (65-90 cells) and Late (from 91 cells). YND= Young Normal Diet, YHFD= Young High Fat Diet, MND= Mature Normal Diet, MHFD= Mature High Fat Diet. TE= trophectoderm cells, ICM= inner cell mass cells.

Immunofluorescence performed on these preimplantation embryos was done with primary antibodies against NANOG, GATA6 or GATA3 to distinguish the three cell fates in the embryo at this stage: Epi, PrE and TE, respectively (Figure 21).

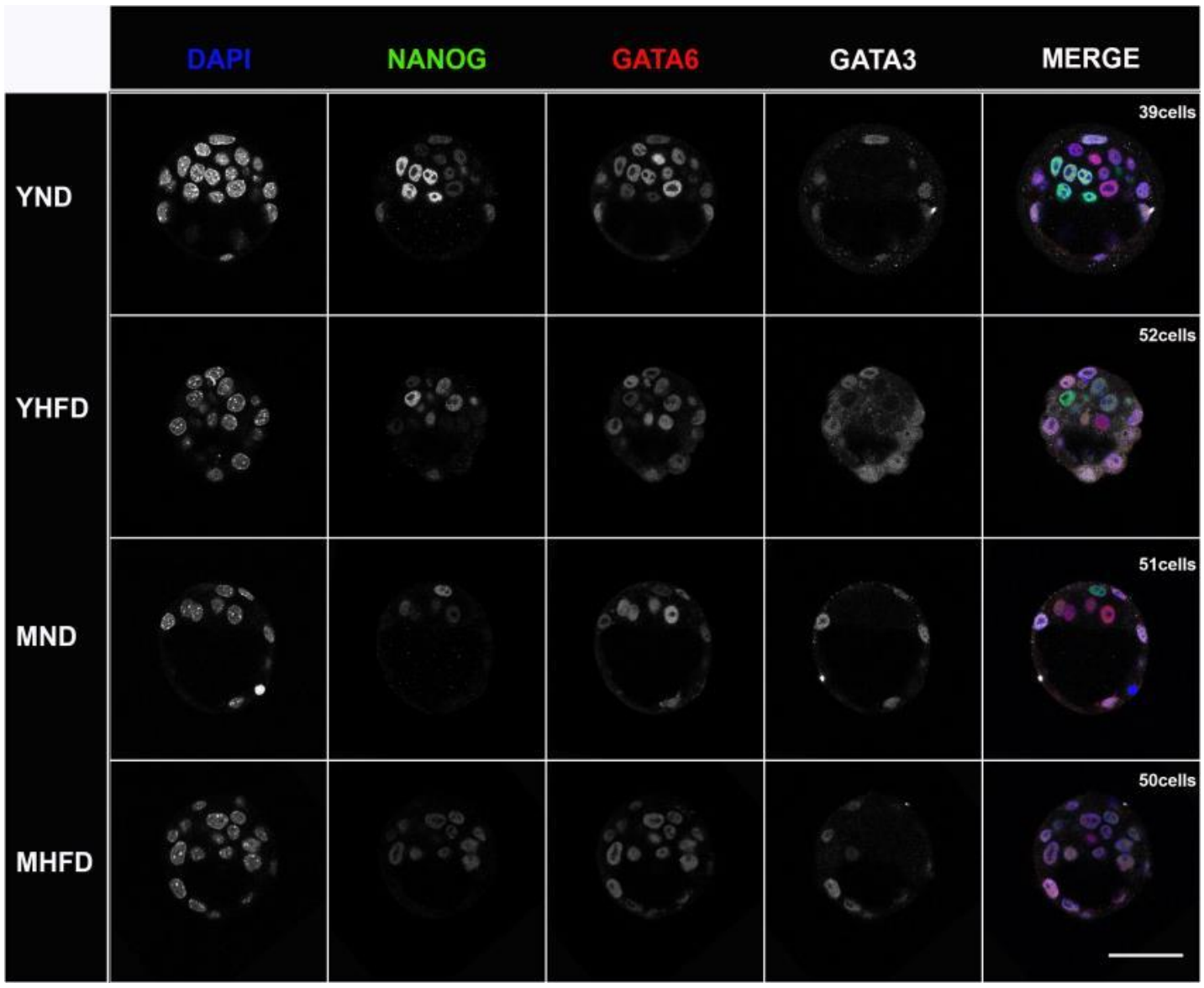

Fig. 21: Representative confocal images of mouse preimplantation embryos. Embryos are immunostained for DAPI (blue), NANOG (green), GATA6 (red) and GATA3 (white) at early stage. Staging criteria: Early (32-64 cells), Mid (65-90 cells) and Late (>90 cells). Young Normal Diet (YND); Young High Fat Diet; Mature Normal Diet (MND); and Mature High Fat Diet (MHFD). All embryos shown were immunostained, imaged and processed together. The first four columns are single confocal z-sections; the last column show the merged confocal images. Scale bar: 50µm.

Cells in the ICM were classified into double positive cells (DP) when co-expressing NANOG and GATA6 (N+G6+), epiblast cells (Epi) when expressing NANOG but not GATA6 (N+G6-), primitive endoderm (PrE) when expressing GATA6 but not NANOG (N-G6+), and double negative (DN) when there was no expression of neither NANOG nor GATA6 (N-G6-). These population analyses are plotted as bar charts where the total amount of cells is represented in these four populations (Figures 22 and 24)

In general, embryos from females fed with HFD had an increased proportion of cells not committed with any cell fate (DP cells) when compared with their controls fed ND. This is especially prominent in mature groups where Epi progenitor proportion is reduced when fed HFD. Regarding different ages, despite no change being observed in the proportion of uncommitted (DP) cells, embryos from mature females showed a defect in cells progressing towards PrE cell fate and an increase in Epi (Figure 22).

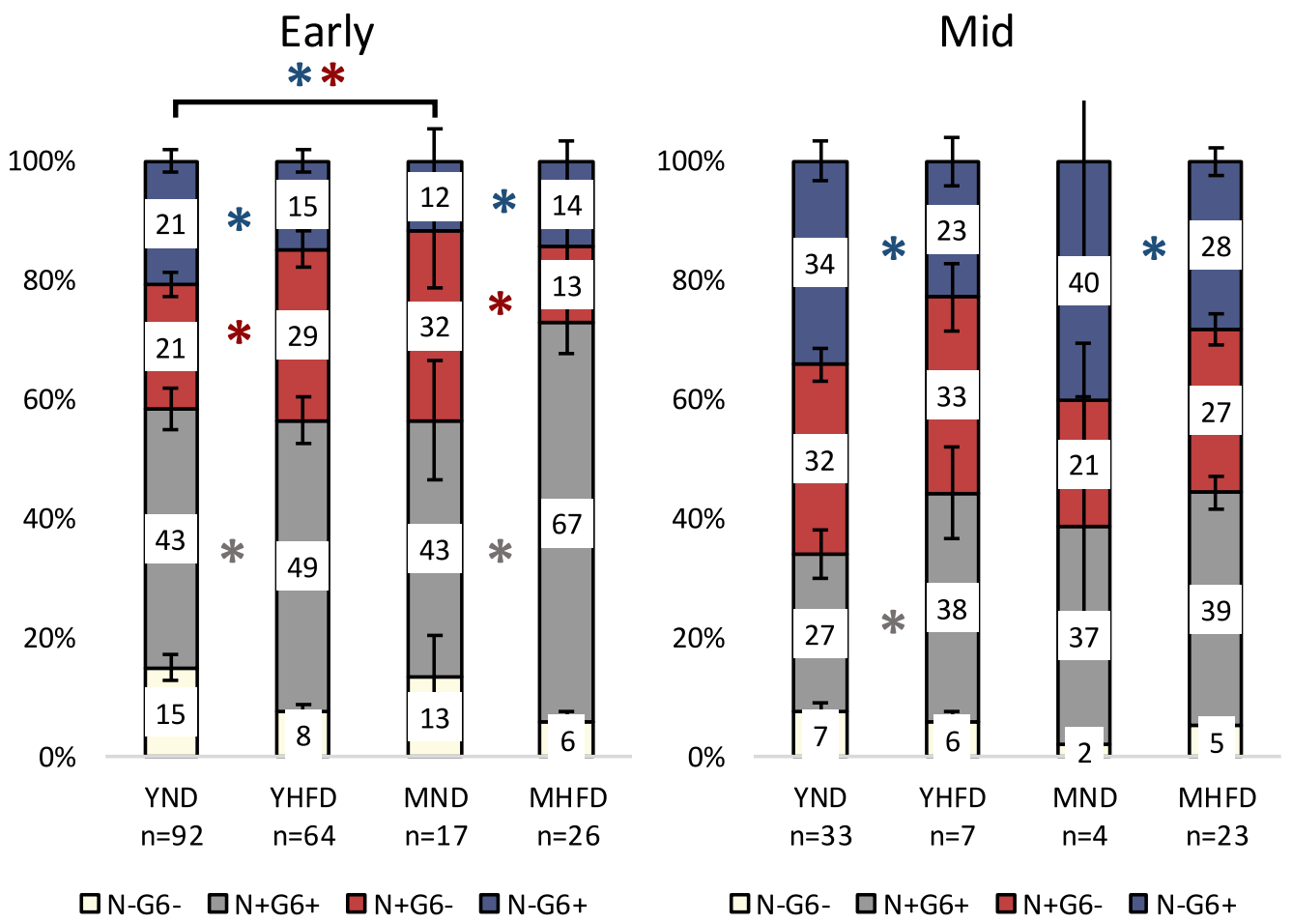

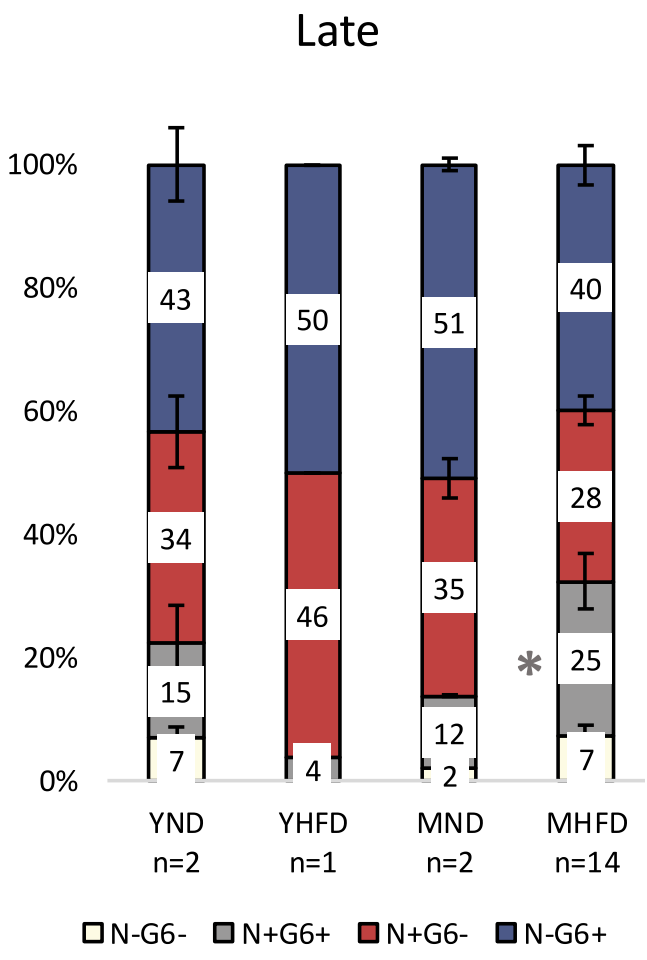

Fig. 22: Variations in embryo developmental stage assessed by single cell quantitative immunofluorescence analysis of NANOG and GATA6. Population analyses as the percentage of the total number of cells in the ICM in (a) early embryos, (b) mid embryos and (c) late embryos. Data are expressed as mean ± SEM, *p<0.05 comparing each HFD group with its ND control or between age-groups. PrE cells in blue, Epi cells in red, DP cells in grey and DN cells in white; YND= Young Normal Diet, YHFD= Young High Fat Diet; MND= Mature Normal Diet, MHFD= Mature High Fat Diet.

Expression levels of the different markers were quantified based on their fluorescence intensity in each individual cell and plotted as violin plots (Figures 23 and 25). Although the population analysis showed more Epi progenitors in young HFD embryos, NANOG levels were significantly lower both in DP cells and in Epi progenitors. The same effect was observed in mature dams, regardless of the diet: NANOG levels were significantly lower in DP cells. Epi progenitors showed higher levels of NANOG in mature only on HFD (Figure 23 a, b).

GATA6 levels were significantly lower in HFD embryos independently of the age in DP cells. MND embryos showed higher levels of GATA6 than YND embryos (Figure 23 c, d).

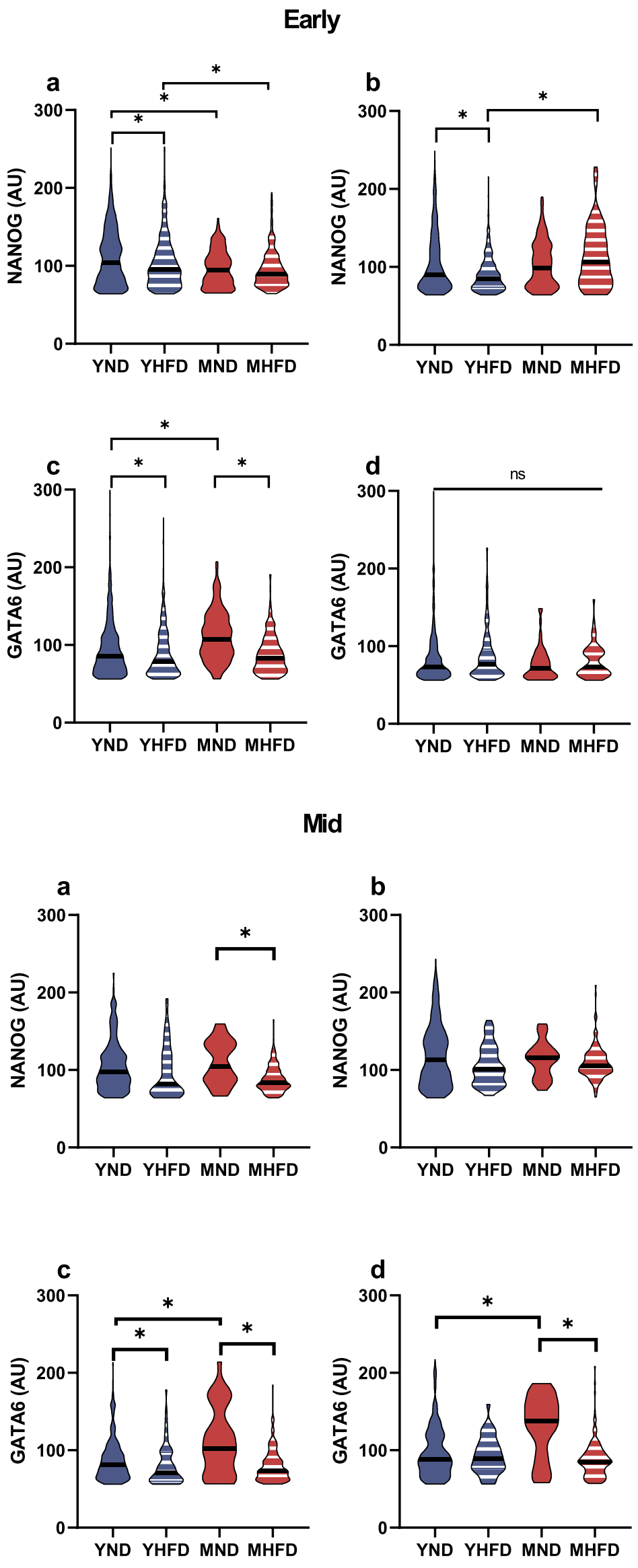
Early
a
b
c
d
NANOG (AU)
GATA6 (AU)
300
200
100
0
YND YHFD MND MHFD
*
ns
Mid
a
b
c
d
NANOG (AU)
GATA6 (AU)
300
200
100
0
YND YHFD MND MHFD
*

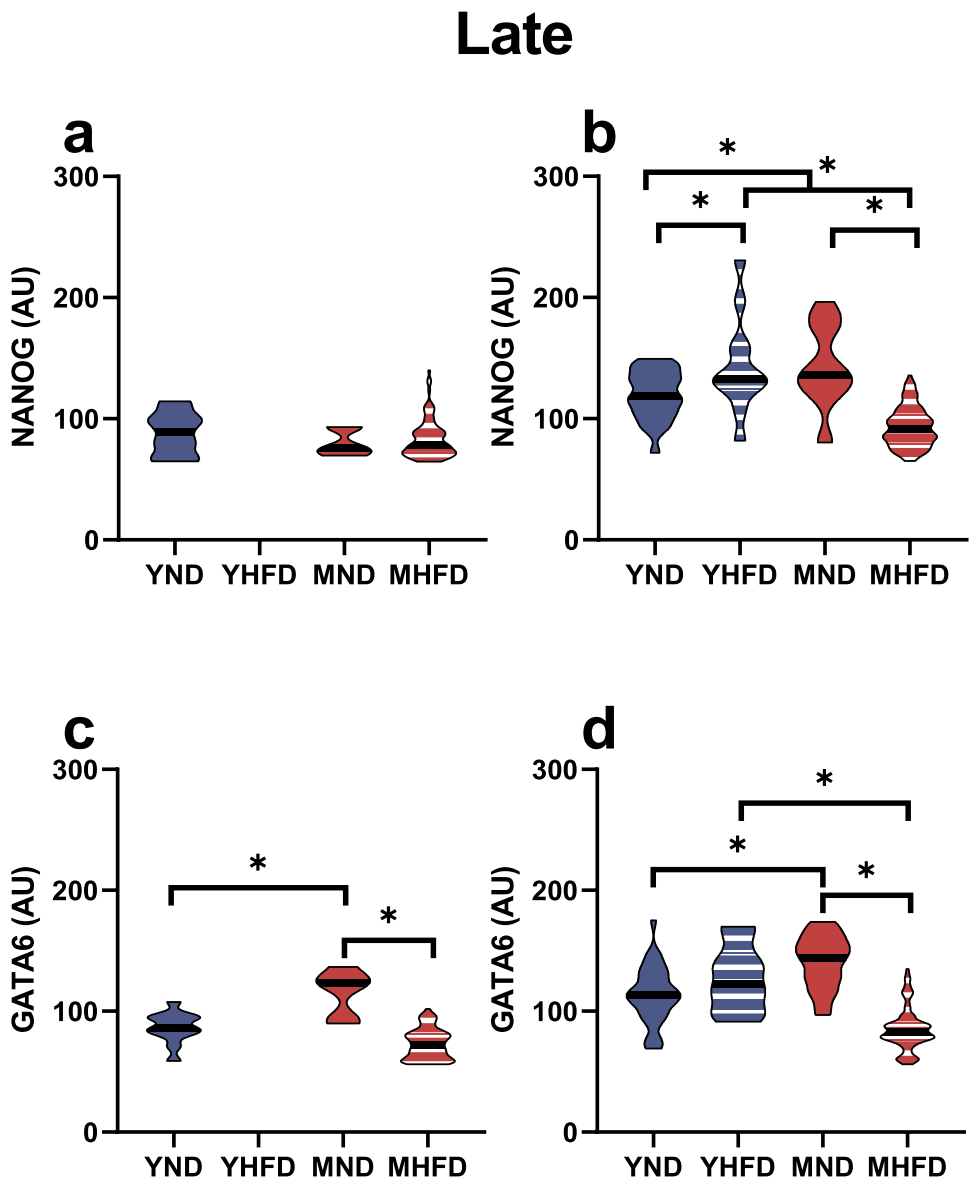

Fig. 23: Variations in fate marker levels assessed by single cell quantitative immunofluorescence analysis of NANOG and GATA6. Violin plots showing NANOG expression levels (AU) in single DP cells (a) and in Epi progenitors (b). Violin plots showing GATA6 levels (AU) in single DP cells (c) and in PrE progenitors (d). Data are expressed as mean ± SEM, *p<0.05 comparing each HFD group with its ND control or between age-groups. Results showed for the three different stages: Early, Mid and Late; YHFD= Young High Fat Diet (patterned blue); YND= Young Normal Diet, YHFD= Young High Fat Diet; MND= Mature Normal Diet, MHFD= Mature High Fat Diet.

During early embryo development, different PrE markers follow one another in time. The first one that appears is GATA6, followed by SOX17, GATA4 and SOX7 (99). After staining some embryos with a more developmentally advanced PrE marker such as GATA4, equivalent results were obtained for the population (Figure 24) and expression level analyses (Figure 25). As GATA4 is a late marker of PrE, very few cells co-expressing NANOG and GATA4 were observed (80). Hence, the levels of GATA4 in N+G4+ cells were not measured (Figure 25).

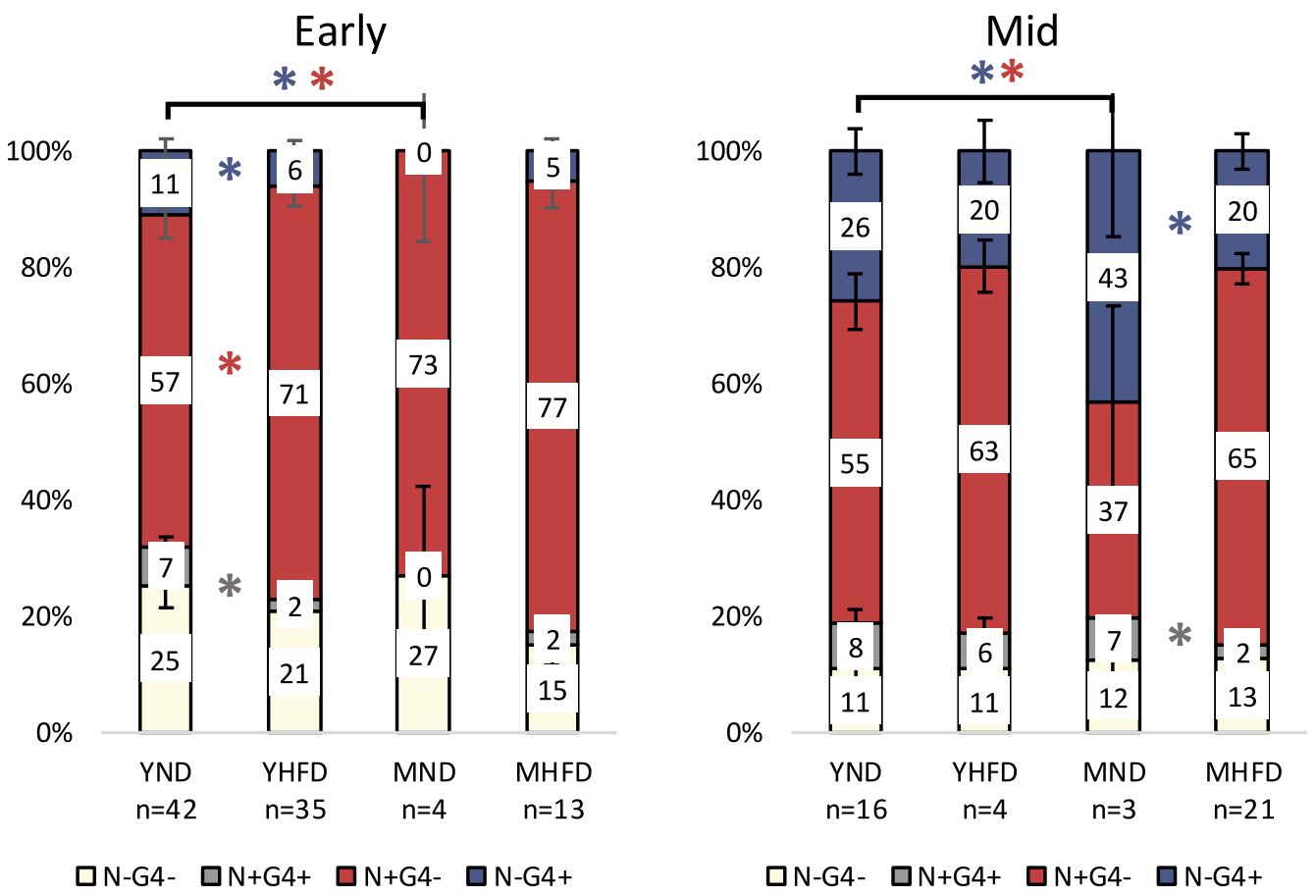

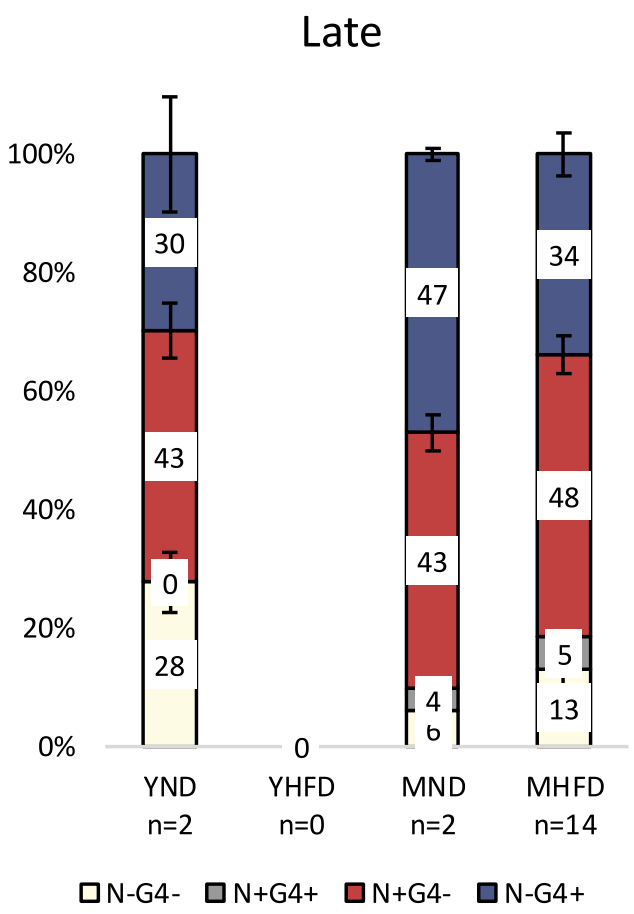

Fig. 24: Variations in embryo developmental stage assessed by single cell quantitative immunofluorescence analysis of NANOG and GATA4. Population analyses as the percentage of the total number of cells in the ICM in (a) early embryos, (b) mid embryos and (c) late embryos. Data are expressed as mean ± SEM, *p<0.05 comparing each HFD group with its ND control or between age-groups. PrE cells in blue, Epi cells in red, DP cells in grey and DN cells in white; YND= Young Normal Diet, YHFD= Young High Fat Diet; MND= Mature Normal Diet, MHFD= Mature High Fat Diet.

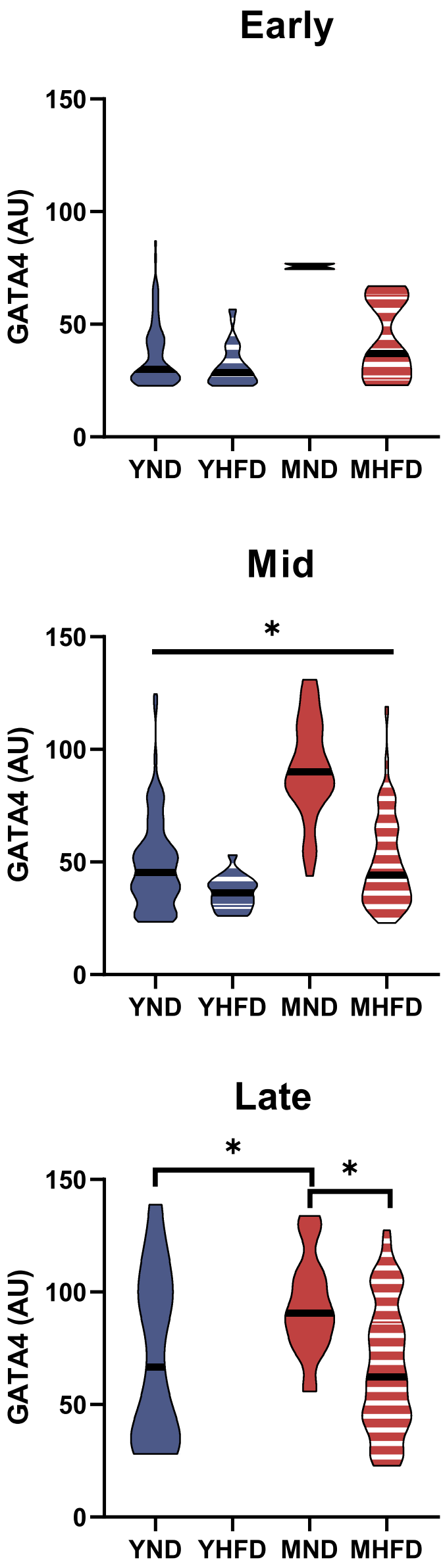
Early
150
100
50
0
GATA4 (AU)
YND YHFD MND MHFD
Mid
*
150
100
50
0
GATA4 (AU)
YND YHFD MND MHFD
Late
*
*
150
100
50
0
GATA4 (AU)
YND YHFD MND MHFD

Fig. 25: Variations in fate marker levels assessed by single cell quantitative immunofluorescence analysis of GATA4. Violin plots showing GATA4 levels (AU) in single PrE. Data are expressed as mean ± SEM, *p<0.05 comparing each HFD group with its ND control or between age-groups. Results showed for the three different stages: Early, Mid and Late; YND= Young Normal Diet, YHFD= Young High Fat Diet; MND= Mature Normal Diet, MHFD= Mature High Fat Diet.

In summary, the higher number of uncommitted cells that co-express NANOG and GATA6 together with fewer cells fully committed to a cell fate (especially to PrE), and cell fate marker levels measured indicate that preimplantation embryos developed in a metabolic syndrome environment (that includes obesity and hyperglycaemia) or from mature mothers are delayed in their normal development when compared with their healthier controls.

To investigate TE cell fate, embryos were immunostained for GATA3 that was almost ubiquitously expressed (Figure 26b). For young animals, GATA3 levels were significantly higher in embryos from mothers were fed HFD. The embryos from mature ones had a slightly reduction in the HFD group. Embryos from mature animals fed with ND, also showed higher levels of GATA3 than those from young controls (Figure 26a).

a

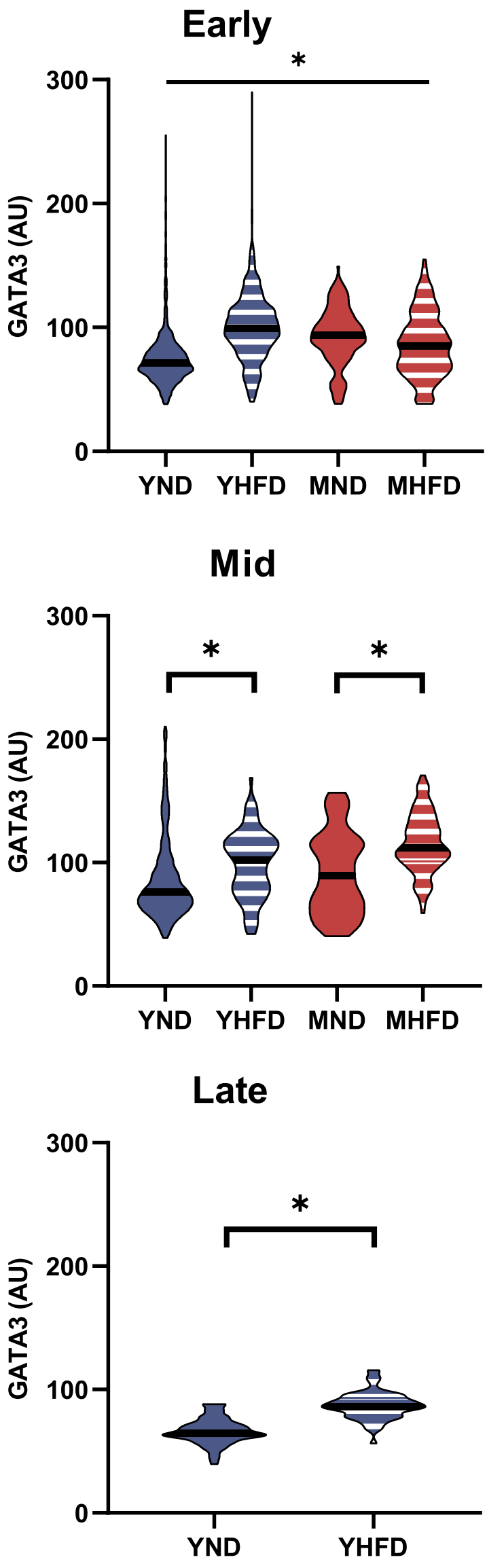
Early
*
300
200
100
0
GATA3 (AU)
YND
YHFD
MND
MHFD
Mid
*
*
300
200
100
0
GATA3 (AU)
YND
YHFD
MND
MHFD
Late
*
300
200
100
0
GATA3 (AU)
YND
YHFD

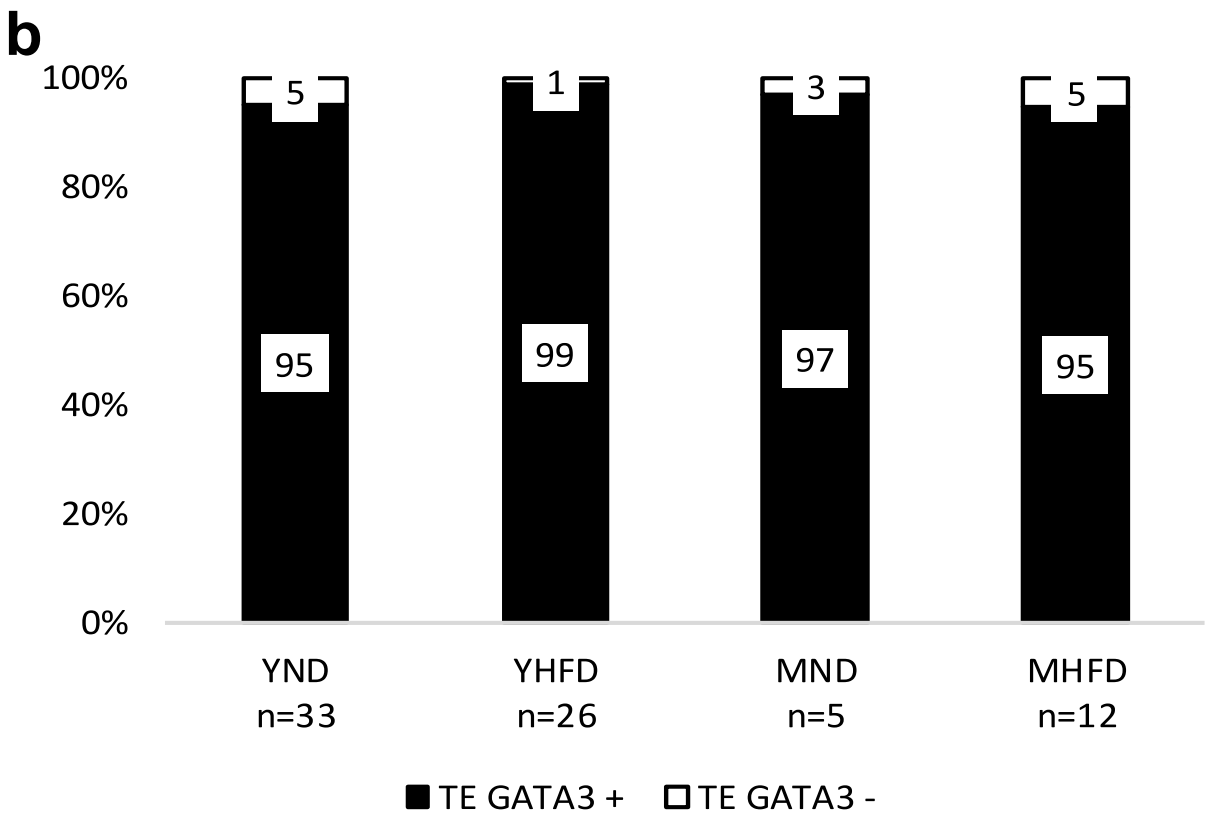

Fig. 26: Variations in GATA3 levels in the trophectoderm (TE) assessed by quantitative immunofluorescence analysis. (a) Population analysis as the percentage of the total number of cells in the TE. (b) Violin plots showing GATA3 expression levels (AU) in different stages. *p<0.05 either comparing each HFD group with its ND control or between ages. YND= Young Normal Diet, YHFD= Young High Fat Diet; MND= Mature Normal Diet, MHFD= Mature High Fat Diet.

Discussion

In this thesis, I assessed the impact of maternal age and HFD feeding on early preimplantation embryo development, specifically Epi versus PrE cell fate decision through state-of-the-art single cell quantitative confocal image and data analyses.

As in humans, HFD feeding in mice led to an increase in body fat, glucose intolerance and insulin resistance. This is the first study to report a delay in early preimplantation embryo development, based on the single cell analysis of the expression levels of markers for Epi versus PrE cell fate specification, associated with maternal age and HFD feeding. In this study, alterations in GATA3 levels, showing an effect of maternal age and HFD feeding in TE differentiation were also described. The relevance of this work is that it allows us to describe embryo development disorders that could be responsible for embryo loss in the first few days after fertilization, inducing the low fertility described in older and overweight or obese women (100).

First, this study confirmed that 8 weeks of HFD feeding during adulthood induced overweight and obesity in female mice as shown in previous studies (101,102). Interestingly, this effect is not observed when diet started before puberty. In fact, despite having similar weight and BMI by the end of the experiment, these young animals fed with HFD showed almost twice as much fat mass as their control group and a reduction in lean mass,

revealing a differential effect of diet composition on their metabolism.

The OGTT revealed that HFD feeding induces glucose impairment as all the groups fed with HFD, even young animals, showed more difficulties to lower the blood glucose levels than their controls. The ITT revealed some degree of insulin resistance that was evident in the older groups, but also a tendency towards insulin resistance in young animals when fed HFD. However, age itself did not have a direct effect on glucose intolerance, in agreement with a previous study (102).

When the effects of childhood obesity in adulthood are assessed, body weight and BMI alone are used as indicators (103). Here, I demonstrate that in female mice, 8 weeks of HFD did not affect body weight and BMI when started before puberty. However, other parameters that influence overall health such as body composition and glucose metabolism were deeply affected. Hence, some of these other parameters (like body composition) should be studied along body weight and BMI before assuming a normal metabolic status in the clinical scenario.

Furthermore, with the results obtained here, an eight weeks HFD feeding in C57Bl6 female mice is validated as a prediabetic mouse model with distinct levels of obesity and hyperglycaemia

based on their age; young adults, mature adults, and middle-late age adults. This mouse model allowed us to analyse how maternal age and changes in diet may affect fecundity.

Selected maternal ages were based on previously published studies. Usually, mice are divided into mature adults (3-6 months), middle aged (10-15 months) and old (18-24 months) and some authors even expand mouse lifespan up to 36 months (64,104,105). In this context, the reproductive senescence is established between 10 to 15 months in female mice. Nevertheless, other authors establish the irregular fertility that precedes reproductive senescence at approximately 8 months of age (106) in line with the lower fertility observed in mature groups (9 months old) in the present research.

Infertility is defined in humans as the failure to conceive naturally after attempting at least for twelve months and it is a rising problem in our society. Many factors such as psychological stress, smoking, drugs, or diet, as well as variations in body weight have a significant effect on fertility. The excess fat accumulation that defines overweight (BMI>25 Kg/m^2) and obesity (BMI>30 Kg/m^2) in women tends to be associated with numerous reproductive disorders such as infertility, polycystic ovary syndrome, higher rate of miscarriage, as well as pregnancy complications (GDM, pre-eclampsia, and macrosomia). Furthermore, worse outcomes following fertility treatments are

also associated with overweight and obese women compared to women with normal BMI. In these situations, the response to ovulation induction is poorer, and obese women require higher doses of gonadotropins and longer treatment courses for follicular development and ovulatory cycles (39). Regarding blastocyst quality, high BMI is not necessarily associated with low embryo quality, but a reduction in the implantation rate is observed (40,42,107).

T2DM is usually happening together with obesity. However, in the absence of obesity, T2DM is also associated with diminished fertility and frequent need for ART (108). Implantation rate is also reduced in women with T2DM, regardless of BMI, as shown by recent research developed by the Danish registry of ART (107). Here, no significant differences in mating or fertilization rates were observed. However, young females fed HFD showed a reduced embryo quality. Surprisingly, no diet effect was observed in embryos from mature females suggesting that age itself has a bigger impact than obesity on embryo quality.

During mammalian preimplantation development, two sequential cell fate decisions occur. At first, TE (precursor of the placenta) and ICM cells arise from the blastomeres. Later, the ICM cells located inside the embryo make a further decision and differentiate either into Epi or PrE (109). Over the years, some studies had suggested that inflammation and oxidative stress

can critically affect these cellular events having an impact on embryo quality (110). Furthermore, preimplantation embryos cultured in the presence of lipopolysaccharides (LPS) have lower proportion of SOX17 expressing cells, suggesting that the oxidative stress induced by lipopolysaccharides may be impairing PrE specification and normal embryonic. Moreover, the culture with drugs that are used to treat DM and correct the oxidative stress, such as barbering or metformin, reverted these PrE development impairments (110). Hence, I propose that abnormal redox levels, as those observed in DM or caused by LPS, can be linked to embryonic preimplantation abnormalities.

For this study I used GATA3 as TE marker. This transcription factor is highly expressed in the invasive murine trophoblast giant cells of the blastocyst, responsible of embryo implantation (73). The knockdown of GATA3 enhances placental cell invasion upon contact with the endometrium (111). Therefore, the high levels of GATA3 associated both with maternal age and HFD feeding observed during this research might be responsible for impaired placentation. Similarly, embryos that have been treated with lipopolysaccharides showed an increased expression CDX2, another TE marker (110), supporting the impaired placentation hypothesis to further explain the decreased fertility.

This research has some limitations. For example, it would have been interesting to measure caspase-3 activity or reactive oxygen species (ROS) in the embryos from mature and from HFD fed females to assess if oxidative stress is the main cellular mechanism affected by HFD and age. However, it has been shown in previous studies that oxidative stress is strongly correlated with the prevalence of T2DM, obesity and aging. The mechanisms behind this hypothesis are numerous and include the high ROS production caused by hyperglycaemia and oxidation of fatty acids or the decrease in antioxidant capacity (112–115).

In summary, the research undertaken during this thesis demonstrated that only 8 weeks of HFD (60% fat content) feeding are enough to model obesity and the metabolic syndrome in female C57BL/6 mice. Moreover, at young ages altered corporal composition and glucose metabolism are masked by the absence of weight change. Regarding fertility assessment, age seems to be the most prominent factor determining reduced fecundity, but both HFD feeding and age are associated with a delay in normal preimplantation embryo development that could be an explanation for the lower implantation rates observed in women with overweight or type 2 diabetes (42,107).

Conclusions

1. An induced prediabetic mouse model is validated with an age-dependent degree of obesity and hyperglycaemia. In this model, young animals' body composition and glucose alteration are masked by normal weight.

2. Despite that no differences were found in mating and fertilization rates, embryo quality decreased by high fat diet. Even in control groups, one year old females showed no fecundity.

3. The higher number of uncommitted cells and the fewer proportion of cells committed to primitive endoderm fate, and cell fate marker levels indicate that preimplantation embryos developed under an obese environment or from mature females are delayed in their normal development.

References

1. Lilao-Garzón J, Valverde-Tercedor C, Muñoz-Descalzo S, Brito-Casillas Y, Wägner AM. In Vivo and In Vitro Models of Diabetes: A Focus on Pregnancy. In: Advances in experimental medicine and biology [Internet]. Adv Exp Med Biol; 2020 [cited 2020 Jun 8]. Available from: http://link.springer.com/10.1007/5584_2020_536

2. Fischer SC, Corujo-Simon E, Lilao-Garzon J, Stelzer EHK, Muñoz-Descalzo S. The transition from local to global patterns governs the differentiation of mouse blastocysts. PLoS One [Internet]. 2020 May 1 [cited 2021 Apr 12];15(5). Available from: https://pubmed.ncbi.nlm.nih.gov/32413083/

3. American Diabetes Association. Diagnosis and classification of diabetes mellitus, ADA Clinical Practice Recommendations. Diabetes Care. 2013;36 Suppl 1:S67-74.

4. Atkinson MA, Campbell-Thompson M, Kusmartseva I, Kaestner KH. Organisation of the human pancreas in health and in diabetes. Diabetologia [Internet]. 2020 Oct 1 [cited 2022 Dec 7];63(10):1966–73. Available from: https://link.springer.com/article/10.1007/s00125-020-05203-7

5. Thorel F, Népote V, Avril I, Kohno K, Desgraz R, Chera S, et al. Conversion of adult pancreatic alpha-cells to beta-cells after extreme beta-cell loss. Nature [Internet]. 2010 Apr 22 [cited 2022 Nov 3];464(7292):1149–54. Available from: https://pubmed.ncbi.nlm.nih.gov/20364121/

6. Chera S, Baronnier D, Ghila L, Cigliola V, Jensen JN, Gu G, et al. Diabetes recovery by age-dependent conversion of pancreatic δ-cells into insulin producers. Nature [Internet]. 2014 Oct 23 [cited 2022 Nov 3];514(7523):503–7. Available from: https://pubmed.ncbi.nlm.nih.gov/25141178/

7. 2. Classification and diagnosis of diabetes: Standards of medical care in diabetesd2019. Diabetes Care. 2019 Jan 1;42:S13–28.

8. Leturque A, Ferre P, Burnol AF, Kande J, Maulard P, Girard J. Glucose utilization rates and insulin sensitivity in vivo in tissues of virgin and pregnant rats. Diabetes [Internet]. 1986 [cited 2022 Nov 3];35(2):172–7. Available from: https://pubmed.ncbi.nlm.nih.gov/3510923/

9. Buchanan TA, Metzger BE, Freinkel N, Bergman RN. Insulin sensitivity and B-cell responsiveness to glucose during late pregnancy in lean and moderately obese women with

normal glucose tolerance or mild gestational diabetes. Am J Obstet Gynecol [Internet]. 1990 [cited 2022 Nov 3];162(4):1008–14. Available from: https://pubmed.ncbi.nlm.nih.gov/2183610/

10. Yamashita H, Shao J, Friedman JE. Physiologic and molecular alterations in carbohydrate metabolism during pregnancy and gestational diabetes mellitus. Clin Obstet Gynecol [Internet]. 2000 Mar [cited 2022 Nov 3];43(1):87–98. Available from: https://pubmed.ncbi.nlm.nih.gov/10694991/

11. Di Cianni G, Miccoli R, Volpe L, Lencioni C, Del Prato S. Intermediate metabolism in normal pregnancy and in gestational diabetes. Diabetes Metab Res Rev [Internet]. 2003 Jul [cited 2022 Nov 3];19(4):259–70. Available from: https://pubmed.ncbi.nlm.nih.gov/12879403/

12. Froguel P, Velho G. Molecular Genetics of Maturity-onset Diabetes of the Young. Trends Endocrinol Metab [Internet]. 1999 May 1 [cited 2022 Nov 3];10(4):142–6. Available from: https://pubmed.ncbi.nlm.nih.gov/10322408/

13. Webber S. International Diabetes Federation. IDF Diabetes Atlas [Internet]. 10th ed. Vol. 102, Diabetes

Research and Clinical Practice. Brussels, Belgium; 2021. 147–148 p. Available from: https://www.diabetesatlas.org

14. Mayer-Davis EJ, Lawrence JM, Dabelea D, Divers J, Isom S, Dolan L, et al. Incidence Trends of Type 1 and Type 2 Diabetes among Youths, 2002-2012. N Engl J Med [Internet]. 2017 Apr 13 [cited 2022 Nov 3];376(15):1419–29. Available from: https://pubmed.ncbi.nlm.nih.gov/28402773/

15. 6th edition | IDF Diabetes Atlas [Internet]. [cited 2022 Nov 3]. Available from: https://diabetesatlas.org/atlas/sixth-edition/

16. Guariguata L, Linnenkamp U, Beagley J, Whiting DR, Cho NH. Global estimates of the prevalence of hyperglycaemia in pregnancy. Diabetes Res Clin Pract. 2014 Feb 1;103(2):176–85.

17. Eriksson UJ. Congenital anomalies in diabetic pregnancy. Semin Fetal Neonatal Med [Internet]. 2009 Apr [cited 2022 Nov 3];14(2):85–93. Available from: https://pubmed.ncbi.nlm.nih.gov/19131288/

18. Sheffield JS, Butler-Koster EL, Casey BM, McIntire DD, Leveno KJ. Maternal diabetes mellitus and infant

malformations. Obstet Gynecol. 2002;100(5):925–30.

19. Jovanovic R, Jovanovic L. Obstetric management when normoglycemia is maintained in diabetic pregnant women with vascular compromise. Am J Obstet Gynecol [Internet]. 1984 Jul 15 [cited 2022 Nov 3];149(6):617–23. Available from: https://pubmed.ncbi.nlm.nih.gov/6742044/

20. Feig DS, Razzaq A, Sykora K, Hux JE, Anderson GM. Trends in deliveries, prenatal care, and obstetrical complications in women with pregestational diabetes: a population-based study in Ontario, Canada, 1996-2001. Diabetes Care [Internet]. 2006 [cited 2022 Nov 3];29(2):232–5. Available from: https://pubmed.ncbi.nlm.nih.gov/16443865/

21. Obesity and overweight [Internet]. [cited 2022 Oct 28]. Available from: https://www.who.int/en/news-room/fact-sheets/detail/obesity-and-overweight

22. Jo J, Gavrilova O, Pack S, Jou W, Mullen S, Sumner AE, et al. Hypertrophy and/or Hyperplasia: Dynamics of Adipose Tissue Growth. PLoS Comput Biol [Internet]. 2009 [cited 2022 Oct 28];5(3):1000324. Available from: /pmc/articles/PMC2653640/

23. Chooi YC, Ding C, Magkos F. The epidemiology of obesity.

Metabolism [Internet]. 2019 Mar 1 [cited 2022 Oct 28];92:6–10. Available from: https://pubmed.ncbi.nlm.nih.gov/30253139/

24. Wang N, Luo LL, Xu JJ, Xu MY, Zhang XM, Zhou XL, et al. Obesity accelerates ovarian follicle development and follicle loss in rats. Metabolism [Internet]. 2014 Jan [cited 2022 Nov 3];63(1):94–103. Available from: https://pubmed.ncbi.nlm.nih.gov/24135502/

25. WHO EUROPEAN REGIONAL OBESITY REPORT 2022. 2022 [cited 2022 Nov 4]; Available from: http://apps.who.int/bookorders.

26. Ladabaum U, Mannalithara A, Myer PA, Singh G. Obesity, Abdominal Obesity, Physical Activity, and Caloric Intake in U.S. Adults: 1988-2010. Am J Med [Internet]. 2014 [cited 2022 Nov 3];127(8):717. Available from: /pmc/articles/PMC4524881/

27. Flegal KM, Carroll D, Kit BK, Ogden CL. Prevalence of obesity and trends in the distribution of body mass index among US adults, 1999-2010. JAMA [Internet]. 2012 Feb 1 [cited 2022 Nov 3];307(5):491–7. Available from: https://pubmed.ncbi.nlm.nih.gov/22253363/

28. Catalano PM, Shankar K. State of the Art Review: Obesity

and pregnancy: mechanisms of short term and long term adverse consequences for mother and child. BMJ [Internet]. 2017 [cited 2022 Oct 28];356. Available from: /pmc/articles/PMC6888512/

29. Gonzalez MB, Robker RL, Rose RD. Obesity and oocyte quality: significant implications for ART and emerging mechanistic insights. Biol Reprod [Internet]. 2022 Feb 1 [cited 2022 May 23];106(2):338–50. Available from: https://pubmed.ncbi.nlm.nih.gov/34918035/

30. Pohlmeier WE, Xie F, Kurz SG, Lu N, Wood JR. Progressive obesity alters the steroidogenic response to ovulatory stimulation and increases the abundance of mRNAs stored in the ovulated oocyte. Mol Reprod Dev [Internet]. 2014 [cited 2022 Nov 3];81(8):735–47. Available from: https://pubmed.ncbi.nlm.nih.gov/24824196/

31. Rich-Edwards JW, Goldman MB, Willett WC, Hunter DJ, Stampfer MJ, Colditz GA, et al. Adolescent body mass index and infertility caused by ovulatory disorder. Am J Obstet Gynecol [Internet]. 1994 [cited 2022 Nov 3];171(1):171–7. Available from: https://pubmed.ncbi.nlm.nih.gov/8030695/

32. Mitanchez D, Chavatte-Palmer P. Review shows that

maternal obesity induces serious adverse neonatal effects and is associated with childhood obesity in their offspring. Vol. 107, Acta Paediatrica, International Journal of Paediatrics. Blackwell Publishing Ltd; 2018. p. 1156–65.

33. Waters TP, Huston-Presley L, Catalano PM. Neonatal body composition according to the revised institute of medicine recommendations for maternal weight gain. J Clin Endocrinol Metab [Internet]. 2012 Oct [cited 2022 Oct 28];97(10):3648–54. Available from: https://pubmed.ncbi.nlm.nih.gov/22821895/

34. Pridjian G. Pregestational diabetes. Obstet Gynecol Clin North Am. 2010;37(2):143–58.

35. Zaadstra BM, Seidell JC, Van Noord PAH, Te Velde ER, Habbema JDF, Vrieswijk B, et al. Fat and female fecundity: prospective study of effect of body fat distribution on conception rates. BMJ [Internet]. 1993 [cited 2022 Nov 3];306(6876):484–7. Available from: https://pubmed.ncbi.nlm.nih.gov/8448457/

36. Schieve LA, Cohen B, Nannini A, Ferre C, Reynolds MA, Zhang Z, et al. A population-based study of maternal and perinatal outcomes associated with assisted reproductive technology in Massachusetts. Matern Child Health J

[Internet]. 2007 Nov [cited 2022 Nov 3];11(6):517–25. Available from: https://pubmed.ncbi.nlm.nih.gov/17345154/

37. Larsen MD, Jensen DM, Fedder J, Jølving LR, Nørgård BM. Live-born children after assisted reproduction in women with type 1 diabetes and type 2 diabetes: a nationwide cohort study. Diabetologia [Internet]. 2020 Sep 1 [cited 2022 Sep 30];63(9):1736–44. Available from: https://link.springer.com/article/10.1007/s00125-020-05193-6

38. Maresh MJA, Holmes VA, Patterson CC, Young IS, Pearson DWM, Walker JD, et al. Glycemic targets in the second and third trimester of pregnancy for women with type 1 diabetes. Diabetes Care [Internet]. 2015 Jan 1 [cited 2022 Nov 3];38(1):34–42. Available from: https://pubmed.ncbi.nlm.nih.gov/25368104/

39. Ozekinci M, Seven A, Olgan S, Sakinci M, Keskin U, Akar ME, et al. Does obesity have detrimental effects on IVF treatment outcomes? BMC Womens Health [Internet]. 2015 Aug 19 [cited 2022 Oct 9];15(1). Available from: https://pubmed.ncbi.nlm.nih.gov/26285703/

40. Qi L, Liu YP, Wang SM, Shi H, Chen XL, Wang NN, et al.

Abnormal BMI in Male and/or Female Partners Are Deleterious for Embryonic Development and Pregnancy Outcome During ART Process: A Retrospective Study. Front Endocrinol (Lausanne). 2022 Apr;13:517.

41. Crosignani PG, Ragni G, Parazzini F, Wyssling H, Lombroso G, Perotti L. Anthropometric indicators and response to gonadotrophin for ovulation induction. Hum Reprod [Internet]. 1994 [cited 2022 Nov 3];9(3):420–3. Available from: https://pubmed.ncbi.nlm.nih.gov/8006129/

42. Bellver J, Ayllón Y, Ferrando M, Melo M, Goyri E, Pellicer A, et al. Female obesity impairs in vitro fertilization outcome without affecting embryo quality. Fertil Steril. 2010 Jan;93(2):447–54.

43. Rbmonline-, Vol. Effect of increased body mass index on oocyte and embryo quality in IVF patients. 2007;(5). Available from: http://www.rbmojournal.com/article/S1472-6483(10)60385-9/pdf

44. Nutrition and reproduction in women The ESHRE Capri Workshop Group 1. 2006 [cited 2023 Feb 13]; Available from: https://academic.oup.com/humupd/article/12/3/193/55

4114

45. Spinelli R, Parrillo L, Longo M, Florese P, Desiderio A, Zatterale F, et al. Molecular basis of ageing in chronic metabolic diseases. Journal of Endocrinological Investigation. Springer; 2020.

46. Ageing and health [Internet]. [cited 2022 Oct 31]. Available from: https://www.who.int/news-room/fact-sheets/detail/ageing-and-health

47. Crawford NM, Steiner AZ. Age-related Infertility. Obstet Gynecol Clin North Am. 2015 Mar 1;42(1):15–25.

48. Kahveci B, Melekoglu R, Evruke IC, Cetin C. The effect of advanced maternal age on perinatal outcomes in nulliparous singleton pregnancies. BMC Pregnancy Childbirth. 2018 Aug 22;18(1).

49. Women in the EU are having their first child later - Products Eurostat News - Eurostat [Internet]. [cited 2022 Mar 24]. Available from: https://ec.europa.eu/eurostat/web/products-eurostat-news/-/ddn-20210224-1

50. Myrskylä M, Fenelon A. Maternal Age and Offspring Adult Health: Evidence From the Health and Retirement Study.

Demography [Internet]. 2012;49(4):1231–57. Available from: file:///C:/Users/Silvia/AppData/Local/Mendeley Ltd./Mendeley Desktop/Downloaded/Myrskylä, Fenelon - 2012 - Maternal Age and Offspring Adult Health Evidence From the Health and Retirement Study.pdf

51. Limiñana-Gras RM. Health and Gender Perspective in Infertility. Psychol Gend Heal Concept Appl Glob Concerns. 2017 Jan 4;363–400.

52. Rothman KJ, Wise LA, Sørensen HT, Riis AH, Mikkelsen EM, Hatch EE. Volitional Determinants and Age-related Decline in Fecundability: A General Population Prospective Cohort Study in Denmark. Fertil Steril [Internet]. 2013 Jun [cited 2022 Oct 31];99(7):1958. Available from: /pmc/articles/PMC3672329/

53. Faddy MJ, Gosden RG, Gougeon A, Richardson SJ, Nelson JF. Accelerated disappearance of ovarian follicles in mid-life: implications for forecasting menopause. Hum Reprod [Internet]. 1992 Nov 1 [cited 2022 Nov 3];7(10):1342–6. Available from: https://academic.oup.com/humrep/article/7/10/1342/664511

54. Rubio C, Bellver J, Rodrigo L, Castillón G, Guillén A, Vidal

C, et al. In vitro fertilization with preimplantation genetic diagnosis for aneuploidies in advanced maternal age: a randomized, controlled study. Fertil Steril [Internet]. 2017 May;107(5):1122–9. Available from: https://www.sciencedirect.com/science/article/pii/S0015028217302546?via%3Dihub

55. Seshadri S, Morris G, Serhal P, Saab W. Assisted conception in women of advanced maternal age. Best Pract Res Clin Obstet Gynaecol [Internet]. 2021 Jan 1 [cited 2022 Oct 31];70:10–20. Available from: https://pubmed.ncbi.nlm.nih.gov/32921559/

56. Brito-Casillas Y, Melián C, Wägner AM. Study of the pathogenesis and treatment of diabetes mellitus through animal models. Endocrinol y Nutr [Internet]. 2016;63(7):345–53. Available from: http://linkinghub.elsevier.com/retrieve/pii/S1575092216300481

57. Markowitz J, Soskin S. PANCREATIC DIABETES AND PREGNANCY. Am J Physiol Content. 1927 Feb 1;79(3):553–8.

58. Aerts L, Vercruysse L, Van Assche FA. The endocrine pancreas in virgin and pregnant offspring of diabetic

pregnant rats. Diabetes Res Clin Pract [Internet]. 1997 Oct [cited 2019 Nov 5];38(1):9–19. Available from: http://www.ncbi.nlm.nih.gov/pubmed/9347241

59. Kiss ACI, Woodside B, Felício LF, Anselmo-Franci J, Damasceno DC. Impact of maternal mild hyperglycemia on maternal care and offspring development and behavior of Wistar rats. Physiol Behav. 2012;107(3):292–300.

60. Liao Z, Wang J, Tan H, Wei L. Cinnamon extracts exert intrapancreatic cytoprotection against streptozotocin in vivo. Gene. 2017 Sep 5;627:519–23.

61. Surwit RS, Kuhn CM, Cochrane C, McCubbin JA, Feinglos MN. Diet-induced type II diabetes in C57BL/6J mice. Diabetes. 1988;37(9):1163–7.

62. Warr CG, Shaw KH, Azim A, Piper MDW, Parsons LM. Using Mouse and Drosophila Models to Investigate the Mechanistic Links between Diet, Obesity, Type II Diabetes, and Cancer. Int J Mol Sci [Internet]. 2018 Dec 18 [cited 2019 Nov 5];19(12). Available from: http://www.ncbi.nlm.nih.gov/pubmed/30567377

63. Brito-Casillas Y, López-Ríos L, Wiebe JC, Muñoz-Mediavilla C, Nóvoa-Mogollón FJ, Ojeda A, et al. Uromastyx

acanthinura as a natural treatment in a mouse model of type 2 diabetes. Endocrinol y Nutr [Internet]. 2016 Jan;63(1):13–8. Available from: http://www.ncbi.nlm.nih.gov/pubmed/26598444

64. Dutta S, Sengupta P. Men and mice: Relating their ages. Life Sci. 2016 May 1;152:244–8.

65. Igosheva N, Abramov AY, Poston L, Eckert JJ, Fleming TP, Duchen MR, et al. Maternal Diet-Induced Obesity Alters Mitochondrial Activity and Redox Status in Mouse Oocytes and Zygotes. Sorensen TIA, editor. PLoS One [Internet]. 2010 Apr;5(4):e10074–e10074. Available from: http://dx.plos.org/10.1371/journal.pone.0010074

66. Chen T, Hill JT, Moore TM, Cheung ECK, Olsen ZE, Piorczynski TB, et al. Lack of skeletal muscle liver kinase B1 alters gene expression, mitochondrial content, inflammation and oxidative stress without affecting high-fat diet-induced obesity or insulin resistance. Biochim Biophys Acta - Mol Basis Dis [Internet]. 2020 Apr [cited 2020 Apr 30];165805. Available from: https://linkinghub.elsevier.com/retrieve/pii/S0925443920301502

67. Lokken AA, Ralston A. The Genetic Regulation of Cell Fate

During Preimplantation Mouse Development [Internet]. 1st ed. Vol. 120, Current Topics in Developmental Biology. Elsevier Inc.; 2016. 173–202 p. Available from: http://dx.doi.org/10.1016/bs.ctdb.2016.04.006

68. Rossant J, Tam PPL. Cell Stem Cell Perspective New Insights into Early Human Development: Lessons for Stem Cell Derivation and Differentiation. Stem Cell [Internet]. 2017 [cited 2022 Oct 31];20:18–28. Available from: http://dx.doi.org/10.1016/j.stem.2016.12.004

69. Hyafil F, Morello D, Babinet C, Jacob F. A cell surface glycoprotein involved in the compaction of embryonal carcinoma cells and cleavage stage embryos. Cell. 1980;21(3):927–34.

70. Lehtonen E, Snow MHL. Early development in the mouse: Would it be affected by microgravity? Adv Sp Res. 1989;9(11):201–8.

71. Strumpf D. Cdx2 is required for correct cell fate specification and differentiation of trophectoderm in the mouse blastocyst. Development [Internet]. 2005;132(9):2093–102. Available from: http://dev.biologists.org/cgi/doi/10.1242/dev.01801

72. Beck F, Erler T, Russell A, James R. Expression of Cdx-2 in

the mouse embryo and placenta: possible role in patterning of the extra-embryonic membranes. Dev Dyn [Internet]. 1995 [cited 2022 Nov 4];204(3):219–27. Available from: https://pubmed.ncbi.nlm.nih.gov/8573715/

73. Home P, Ray S, Dutta D, Bronshteyn I, Larson M, Paul S. GATA3 is selectively expressed in the trophectoderm of peri-implantation embryo and directly regulates Cdx2 gene expression. J Biol Chem [Internet]. 2009 Oct;284(42):28729–37. Available from: http://www.ncbi.nlm.nih.gov/pubmed/19700764

74. Fleming TP. A quantitative analysis of cell allocation to trophectoderm and inner cell mass in the mouse blastocyst. Dev Biol. 1987 Feb 1;119(2):520–31.

75. Yamanaka Y, Ralston A, Stephenson RO, Rossant J. Cell and molecular regulation of the mouse blastocyst. Dev Dyn [Internet]. 2006;235(9):2301–14. Available from: file:///C:/Users/Silvia/AppData/Local/Mendeley Ltd./Mendeley Desktop/Downloaded/Yamanaka et al. - 2006 - Cell and molecular regulation of the mouse blastocyst.pdf

76. Lavial F, Bessonnard S, Ohnishi Y, Tsumura A,

Chandrashekran A, Fenwick MA, et al. Bmi1 facilitates primitive endoderm formation by stabilizing Gata6 during early mouse development. Genes Dev [Internet]. 2012;26(13):1445–58. Available from: file:///C:/Users/Silvia/AppData/Local/Mendeley Ltd./Mendeley Desktop/Downloaded/Lavial et al. - 2012 - Bmi1 facilitates primitive endoderm formation by stabilizing Gata6 during early mouse development.pdf

77. Chambers I, Colby D, Robertson M, Nichols J, Lee S, Tweedie S, et al. Functional expression cloning of Nanog, a pluripotency sustaining factor in embryonic stem cells. Cell [Internet]. 2003;113(5):643–55. Available from: file:///C:/Users/Silvia/AppData/Local/Mendeley Ltd./Mendeley Desktop/Downloaded/Chambers et al. - 2003 - Functional expression cloning of Nanog, a pluripotency sustaining factor in embryonic stem cells.pdf

78. Plusa B, Piliszek A, Frankenberg S, Artus J, Hadjantonakis AK. Distinct sequential cell behaviours direct primitive endoderm formation in the mouse blastocyst. Development [Internet]. 2008 Sep 15 [cited 2022 Oct 31];135(18):3081–91. Available from: https://journals.biologists.com/dev/article/135/18/3081/64789/Distinct-sequential-cell-behaviours-direct

79. Saiz N, Williams KM, Seshan VE, Hadjantonakis A-K. Asynchronous fate decisions by single cells collectively ensure consistent lineage composition in the mouse blastocyst. Nat Commun [Internet]. 2016;7:13463. Available from: http://www.nature.com/doifinder/10.1038/ncomms13463

80. Plusa B, Piliszek A, Frankenberg S, Artus J, Hadjantonakis A-K. Distinct sequential cell behaviours direct primitive endoderm formation in the mouse blastocyst. Development [Internet]. 2008;135(18):3081–91. Available from: http://dev.biologists.org/cgi/doi/10.1242/dev.021519

81. Chazaud C, Yamanaka Y, Pawson T, Rossant J. Early Lineage Segregation between Epiblast and Primitive Endoderm in Mouse Blastocysts through the Grb2-MAPK Pathway. Dev Cell [Internet]. 2006;10(5):615–24. Available from: file:///C:/Users/Silvia/AppData/Local/Mendeley Ltd./Mendeley Desktop/Downloaded/Chazaud et al. - 2006 - Early Lineage Segregation between Epiblast and Primitive Endoderm in Mouse Blastocysts through the Grb2-MAPK Pat.pdf

82. Percie Du Sert N, Hurst V, Ahluwalia A, Alam S, Avey MT, Baker M, et al. The ARRIVE guidelines 2.0: Updated guidelines for reporting animal research. BMC Vet Res [Internet]. 2020 Jul 14 [cited 2022 Sep 6];16(1):1–7. Available from: https://bmcvetres.biomedcentral.com/articles/10.1186/s12917-020-02451-y

83. Lilao-Garzón J, Valverde-Tercedor C, Muñoz-Descalzo S, Brito-Casillas Y, Wägner AM. In Vivo and In Vitro Models of Diabetes: A Focus on Pregnancy. In: Advances in experimental medicine and biology. Adv Exp Med Biol; 2020.

84. Andrikopoulos S, Blair AR, Deluca N, Fam BC, Proietto J. Evaluating the glucose tolerance test in mice. Am J Physiol - Endocrinol Metab. 2008 Dec;295(6).

85. Gargiulo S, Gramanzini M, Megna R, Greco A, Albanese S, Manfredi C, et al. Evaluation of growth patterns and body composition in c57bl/6j mice using dual energy x-ray absorptiometry. Biomed Res Int. 2014;2014.

86. Brito-Casillas Y, Melián C, Wägner AM. Study of the pathogenesis and treatment of diabetes mellitus through animal models. Endocrinol y Nutr [Internet]. 2016

Aug;63(7):345–53. Available from: http://www.ncbi.nlm.nih.gov/pubmed/27246633

87. Gardner DK, Balaban B. Assessment of human embryo development using morphological criteria in an era of time-lapse, algorithms and “OMICS”: is looking good still important? Mol Hum Reprod [Internet]. 2016 Oct 1 [cited 2022 Mar 22];22(10):704–18. Available from: https://pubmed.ncbi.nlm.nih.gov/27578774/

88. Nichols J, Silva J, Roode M, Smith A. Suppression of Erk signalling promotes ground state pluripotency in the mouse embryo. Development. 2009;136(19):3215–22.

89. Nichols J, Smith A. Naive and Primed Pluripotent States. Cell Stem Cell [Internet]. 2009;4(6):487–92. Available from: http://dx.doi.org/10.1016/j.stem.2009.05.015

90. Na J, Lykke-Andersen K, Torres Padilla ME, Zernicka-Goetz M. Dishevelled proteins regulate cell adhesion in mouse blastocyst and serve to monitor changes in Wnt signaling. Dev Biol [Internet]. 2007;302(1):40–9. Available from: file:///C:/Users/Silvia/AppData/Local/Mendeley Ltd./Mendeley Desktop/Downloaded/Na et al. - 2007 - Dishevelled proteins regulate cell adhesion in mouse blastocyst and serve to monitor changes in Wnt

signaling.pdf

91. Schindelin J, Arganda-Carreras I, Frise E, Kaynig V, Longair M, Pietzsch T, et al. Fiji: an open-source platform for biological-image analysis. Nat Methods 2012 97 [Internet]. 2012 Jun 28 [cited 2023 Jan 31];9(7):676–82. Available from: https://www.nature.com/articles/nmeth.2019

92. Lou X, Kang M, Xenopoulos P, Muñoz-Descalzo S, Hadjantonakis AK. A rapid and efficient 2D/3D nuclear segmentation method for analysis of early mouse embryo and stem cell image data. Stem Cell Reports. 2014 Mar 11;2(3):382–97.

93. Saiz N, Mora-Bitrià L, Rahman S, George H, Herder JP, García-Ojalvo J, et al. Growth-factor-mediated coupling between lineage size and cell fate choice underlies robustness of mammalian development. Elife [Internet]. 2020 Jul 1 [cited 2022 Sep 15];9:1–38. Available from: https://pubmed.ncbi.nlm.nih.gov/32720894/

94. Hammer DAT, Ryan PD, Hammer Ø, Harper DAT. Past: Paleontological Statistics Software Package for Education and Data Analysis. Palaeontol Electron [Internet]. 2001 [cited 2023 Jan 31];4(1):178. Available from:

http://palaeo-electronica.orghttp//palaeo-electronica.org/2001_1/past/issue1_01.htm.

95. Korou L-MA, Doulamis IP, Tzanetakou IP, Mikhailidis DP, Perrea DN. The effect of biological age on the metabolic responsiveness of mice fed a high-fat diet. [cited 2019 Jun 20]; Available from: https://journals.sagepub.com/doi/pdf/10.1177/0023677213480768

96. Yu Q, Li J, Dai C ling, Li H, Iqbal K, Liu F, et al. Anesthesia with sevoflurane or isoflurane induces severe hypoglycemia in neonatal mice. PLoS One [Internet]. 2020 [cited 2022 May 23];15(4):e0231090. Available from: https://journals.plos.org/plosone/article?id=10.1371/journal.pone.0231090

97. Chan YK, Davis PF, Poppitt SD, Sun X, Greenhill NS, Krishnamurthi R, et al. Influence of tail versus cardiac sampling on blood glucose and lipid profiles in mice. Lab Anim. 2012;46:142–7.

98. Horber FF, Krayer S, Miles J, Cryer P, Rehder K, Haymond MW. Isoflurane and whole body leucine, glucose, and fatty acid metabolism in dogs. Anesthesiology [Internet]. 1990 [cited 2022 May 23];73(1):82–92. Available from:

https://pubmed.ncbi.nlm.nih.gov/2360744/

99. Artus J, Piliszek A, Hadjantonakis AK. The primitive endoderm lineage of the mouse blastocyst: Sequential transcription factor activation and regulation of differentiation by Sox17. Dev Biol [Internet]. 2011;350(2):393–404. Available from: http://dx.doi.org/10.1016/j.ydbio.2010.12.007

100. Silvestris E, de Pergola G, Rosania R, Loverro G. Obesity as disruptor of the female fertility. 2018 Mar 9 [cited 2022 Mar 31];16(1):1–13. Available from: https://doi.org/10.1186/s12958-018-0336-z

101. Picklo MJ, Idso J, Seeger DR, Aukema HM, Murphy EJ. Comparative effects of high oleic acid vs high mixed saturated fatty acid obesogenic diets upon PUFA metabolism in mice. Prostaglandins, Leukot Essent Fat Acids. 2017 Apr 1;119:25–37.

102. Soleimanzad H, Montaner M, Ternier G, Lemitre M, Silvestre JS, Kassis N, et al. Obesity in Midlife Hampers Resting and Sensory-Evoked Cerebral Blood Flow in Mice. Obesity [Internet]. 2021 Jan 1 [cited 2022 Mar 11];29(1):150–8. Available from: https://onlinelibrary.wiley.com/doi/full/10.1002/oby.23

051

103. Bentham J, Di Cesare M, Bilano V, Bixby H, Zhou B, Stevens GA, et al. Worldwide trends in body-mass index, underweight, overweight, and obesity from 1975 to 2016: a pooled analysis of 2416 population-based measurement studies in 128·9 million children, adolescents, and adults. Lancet. 2017 Dec 16;390(10113):2627–42.

104. Life span as a biomarker [Internet]. [cited 2022 Mar 31]. Available from: https://www.jax.org/research-and-faculty/research-labs/the-harrison-lab/gerontology/life-span-as-a-biomarker

105. Chaix A, Deota S, Bhardwaj R, Lin T, Panda S. Sex- and age-dependent outcomes of 9-hour time-restricted feeding of a Western high-fat high-sucrose diet in C57BL/6J mice. Cell Rep. 2021 Aug 17;36(7):109543.

106. Brinton RD. Minireview: Translational animal models of human menopause: Challenges and emerging opportunities. Endocrinology [Internet]. 2012;153(8):3571–8. Available from: file:///C:/Users/Silvia/AppData/Local/Mendeley Ltd./Mendeley Desktop/Downloaded/Brinton - 2012 - Minireview Translational animal models of human

menopause Challenges and emerging opportunities.pdf

107. Larsen MD, Jensen DM, Fedder J, Jølving LR, Nørgård BM. Live-born children after assisted reproduction in women with type 1 diabetes and type 2 diabetes: a nationwide cohort study. Diabetologia [Internet]. 2020 Jun 16 [cited 2020 Jun 23];1–9. Available from: http://link.springer.com/10.1007/s00125-020-05193-6

108. Mattsson K, Nilsson-Condori E, Elmerstig E, Vassard D, Schmidt L, Ziebe S, et al. Fertility outcomes in women with pre-existing type 2 diabetes—a prospective cohort study. Fertil Steril [Internet]. 2021 Aug 1 [cited 2022 Oct 9];116(2):505–13. Available from: http://www.fertstert.org/article/S0015028221001278/fulltext

109. Rossant J. Genetic Control of Early Cell Lineages in the Mammalian Embryo. https://doi.org/101146/annurev-genet-120116-024544 [Internet]. 2018 Nov 26 [cited 2022 Mar 22];52:185–201. Available from: https://www.annualreviews.org/doi/abs/10.1146/annurev-genet-120116-024544

110. Miao X, Cui W. Berberine alleviates LPS-induced apoptosis, oxidation, and skewed lineages during mouse

preimplantation development. Biol Reprod [Internet]. 2022 Jan 12 [cited 2022 Apr 4]; Available from: https://pubmed.ncbi.nlm.nih.gov/35024788/

111. Chiu YH, Chen H. GATA3 inhibits GCM1 activity and trophoblast cell invasion. Sci Rep [Internet]. 2016 Feb 22 [cited 2022 Mar 30];6. Available from: https://pubmed.ncbi.nlm.nih.gov/26899996/

112. Davalli P, Mitic T, Caporali A, Lauriola A, D'Arca D. ROS, Cell Senescence, and Novel Molecular Mechanisms in Aging and Age-Related Diseases. Oxid Med Cell Longev [Internet]. 2016 [cited 2022 Apr 5];2016. Available from: https://pubmed.ncbi.nlm.nih.gov/27247702/

113. Fernández-Sánchez A, Madrigal-Santillán E, Bautista M, Esquivel-Soto J, Morales-González Á, Esquivel-Chirino C, et al. Inflammation, oxidative stress, and obesity. Int J Mol Sci [Internet]. 2011 May [cited 2022 Apr 5];12(5):3117–32. Available from: https://pubmed.ncbi.nlm.nih.gov/21686173/

114. Jawerbaum A, White V. Animal models in diabetes and pregnancy. Endocr Rev [Internet]. 2010 Oct [cited 2019 Nov 1];31(5):680–701. Available from: http://www.ncbi.nlm.nih.gov/pubmed/20534704

115. Rehman K, Akash MSH. Mechanism of Generation of Oxidative Stress and Pathophysiology of Type 2 Diabetes Mellitus: How Are They Interlinked? J Cell Biochem [Internet]. 2017 Nov 1 [cited 2022 Apr 5];118(11):3577–85. Available from: https://pubmed.ncbi.nlm.nih.gov/28460155/

Annex 1: Publications

1. In Vivo and In Vitro Models of Diabetes: A Focus on Pregnancy

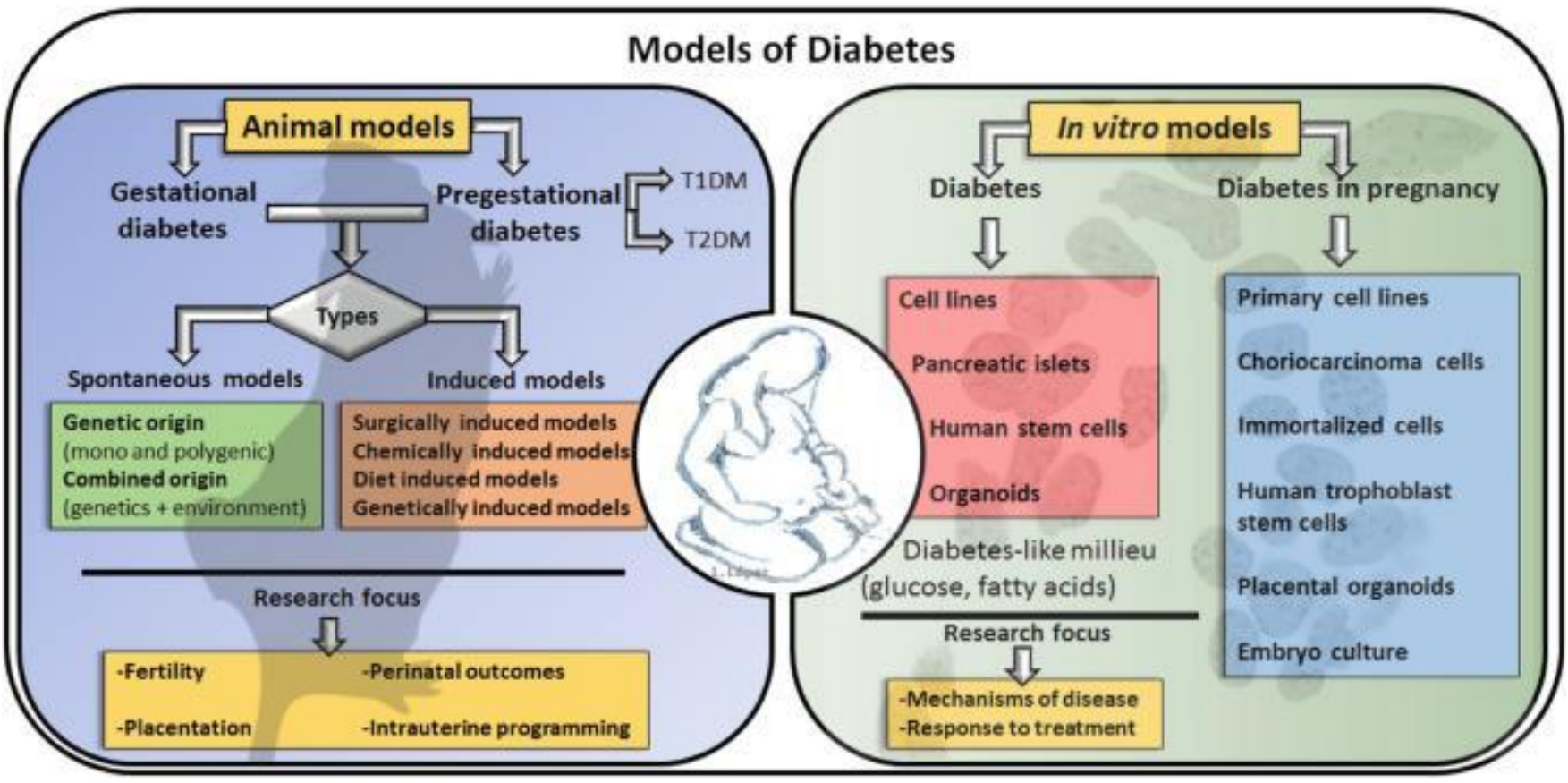

Adv Exp Med Biol - Advances in Internal Medicine
https://doi.org/10.1007/5584_2020_536

In Vivo and *In Vitro* Models of Diabetes: A Focus on Pregnancy

Joaquín Lilao-Garzón, Carmen Valverde-Tercedor, Silvia Muñoz-Descalzo, Yeray Brito-Casillas, and Ana M. Wägner

Abstract

Diabetes in pregnancy is associated with an increased risk of poor outcomes, both for the mother and her offspring. Although clinical and epidemiological studies are invaluable to assess these outcomes and the effectiveness of potential treatments, there are certain ethical and practical limitations to what can be assessed in human studies.

Thus, both *in vivo* and *in vitro* models can aid us in the understanding of the mechanisms behind these complications and, in the long run, towards their prevention and treatment. This review summarizes the existing animal and cell models used to mimic diabetes, with a specific focus on the intrauterine environment.

Keywords

Animal model · Embryo culture · Fertility · Gestation · Gestational diabetes · *In vitro* model · Intrauterine programing · Organoids · Pregestational diabetes · Streptozotocin

J. Lilao-Garzón, C. Valverde-Tercedor, S. Muñoz-Descalzo, and Y. Brito-Casillas (✉)
Instituto Universitario de Investigaciones Biomédicas y Sanitarias (IUIBS), Universidad de Las Palmas de Gran Canaria (ULPGC), Las Palmas de Gran Canaria, Islas Canarias, Spain
e-mail: yeray.brito@ulpgc.es

A. M. Wägner
Instituto Universitario de Investigaciones Biomédicas y Sanitarias (IUIBS), Universidad de Las Palmas de Gran Canaria (ULPGC), Las Palmas de Gran Canaria, Islas Canarias, Spain

Servicio de Endocrinología y Nutrición, Complejo Hospitalario Universitario Insular Materno-Infantil de Gran Canaria, Las Palmas de Gran Canaria, Spain

Diabetes Mellitus (DM) is a group of metabolic diseases associated with defects in insulin secretion, insulin action or both, inducing chronic hyperglycaemia, which leads to organ damage (American Diabetes Association 2013).

According to the current classification of DM, type 1 diabetes (T1DM) is an autoimmune disorder leading to the destruction of β-cells, ultimately causing total insulin deficiency. Type 2 diabetes (T2DM), produced by progressive loss of insulin secretion by the β-cells, is usually associated with peripheral insulin resistance and obesity (American Diabetes Association 2019). Other specific types of diabetes include monogenic DM, pancreatic diseases and drug-induced DM (American Diabetes Association 2019). Monogenic DM include Maturity-onset diabetes of the young (MODY) and neonatal diabetes, caused by a single mutation that leads to deficient insulin secretion (Vaxillaire and Froguel 2006).

DM first diagnosed in the second or third trimester of pregnancy is defined as Gestational Diabetes (GDM) (American Diabetes Association 2019). From the second trimester, maternal insulin sensitivity decreases due to the effect of

placental hormones (i.e. oestrogen, progesterone, leptin, cortisol, placental lactogen, and growth hormone), which facilitate glucose transport across the placenta to the growing foetus (Plows et al. 2018a). In physiological conditions, these glycaemic changes are compensated by pancreatic β-cells hypertrophy and hyperplasia, and the secretion of glucose-stimulated insulin. However, upon failure of these compensatory mechanisms, hyperglycaemia is triggered and GDM occurs (Barbe et al. 2019; Plows et al. 2018b).

DM in pregnancy can be present before conception (pregestational diabetes) or develop during pregnancy (GDM). Moreover, mild hyperglycaemia, not fulfilling the criteria for DM diagnosis, may be present before pregnancy, too. When working with DM models, it is important to define the type of DM targeted in each study, since model choice and appropriateness will depend on this. Indeed, model characterisation is also challenging, and may lead to discrepancies in the nomenclature used (e.g. GDM vs mild DM).

1 Animal Models of Diabetes

Animal models are a valuable tool to study DM, although none is comprehensive enough to fully reproduce any form of the disease. The most extensively used species are mice (Hanafusa et al. 1994) and rats (Phillips et al. 1996), but also rabbits (Mage et al. 2019), cats (Pérez-López et al. 2019), dogs (Moshref et al. 2019) or bigger animals like sheep (Dickinson et al. 1990) and pigs (Ezekwe et al. 1984) are used.

These animal models can be classified according to whether their diabetes is spontaneous or induced (Brito-Casillas et al. 2016). The mechanisms of disease in spontaneous DM models are presumed to be similar to human DM, especially in polygenic models. The latter include Non-Obese-Diabetic mouse (NOD) (Hanafusa et al. 1994), the BioBreeding Diabetes-Prone rat (BB) (Jacob et al. 1992a) and the Zucker fatty rat (Phillips et al. 1996). Spontaneous mouse models for monogenic DM include ob/ob, Lep^{ob} (Kaufmann et al. 1981) and $Lepr^{db}$ (Huang et al. 2009). Other models, such as diabetic cats and dogs, combine genetic alterations with environmental factors (Moshref et al. 2019).

Induced models are easier to generate and have the advantage that they phenotypically match hyperglycaemia, obesity or the metabolic syndrome. However, it is necessary to be cautious when generating them, to ensure that they represent the targeted disease phenotype. There are surgically induced models (SIM); chemically, toxic or drug induced models (CIM); and diet induced models (DIM). In the SIM, a part or all of the pancreas is surgically removed. In CIM several drugs with affinity and toxicity for the β-cells are used, though streptozotocin (STZ) and alloxan are most commonly employed. On the other hand, DIM are widely used in T2DM studies, especially in rodents, but also in other species that develop insulin resistance and glucose impairment upon high fat diets (Brito-Casillas et al. 2016). A combination of these methods can also be used in order to mimic different types of DM.

1.1 Animal Models of Gestational and Pregestational Diabetes

1.1.1 Surgically Induced Models (SIM)

The first models developed for GDM were based on partial pancreatectomy in dogs, during different stages of pregnancy (Pasek and Gannon 2013; Markowitz and Soskin 1927; Carlson and Drennan 1911). Due to ethical, economic and practical reasons, rodents are the most currently used species to develop SIMs (Sharma et al. 1999; Jawerbaum et al. 1993). They allow for the study of both utero-placental defects and foetal alterations, as well as differences in intrauterine metabolic patterns (Jawerbaum et al. 1993). One of the biggest disadvantages of these models is their lack of specificity since both the endocrine and exocrine tissues are removed, resulting in other, non-DM related symptoms (Pasek and Gannon 2013). Furthermore, the diabetic phenotype is caused by the lack of endocrine pancreas. Therefore, these models only mimic certain aspects of GDM, caused by insulin

deficiency, but do not account for insulin resistance.

1.1.2 Chemically, Toxic or Drug Induced Models (CIM)

CIM are mainly generated in rodents and are commonly used to develop T1DM. Since this approach allows to control the time-point of the induction of DM, authors use this strategy to develop models of GDM (Türk et al. 2018). Induction is usually done in early pregnancy, before the embryonic pancreas develops (Martin et al. 1995; Sugimura et al. 2009), in order to avoid foetal β-cell destruction by the chemical agent utilized (Pasek and Gannon 2013; López-Soldado and Herrera 2003; Aerts et al. 1997).

As described for SIM, this strategy induces DM within days, with mild to severe hyperglycaemia, depending on the doses and the regime applied (López-Soldado and Herrera 2003; Lee et al. 2019). Due to the fast induction, STZ is commonly used to study a variety of pregnancy-related DM complications, such as preimplantation embryo defects, congenital malformations, utero-placental defects, foetal alterations or offspring defects (Jawerbaum and White 2010).

The main disadvantage of CIM models is the variability in the response to the drug. Even within the same species, many variables (strain, age, sex. . .) can change the outcome. This has led to a lack of consensus in the scientific community for a dosing strategy to generate the DM models (Pasek and Gannon 2013). Table 1 summarises the different STZ regimes used in studies published between 2012 and 2018. Indeed, even with the same regime, the type of DM obtained is classified differently.

1.1.3 Diet Induced Models (DIM)

Dietary modification is another strategy to generate DM. Different approaches are used, such as continuous glucose infusions (Gauguier et al. 1990) or a diet enriched in fat (High Fat Diet, HFD) that will induce obesity, a known risk factor for DM. These approaches are mostly used to generate T2DM (Surwit et al. 1988), but also GDM models (Holemans et al. 2004). Although diet alteration is one of the most complete strategies to mimic DM, there are some factors that need to be taken into account, since they may have an impact on the response to the diet. These include dietary fat origin and animal housing and number, as density and hierarchical behaviours can affect feeding (Feige et al. 2008). Combination of HFD with high fructose diet (HFHF) has been used to mimic fast food diets that usually combine fat enriched food with carbonated beverages enriched in sugars (Lozano et al. 2016). HFHF fed rats develop not only T2DM but also associated complications like hepatic fibrosis, inflammation and oxidative stress (Lozano et al. 2016).

The main advantages of this strategy are that it can be used to study both pre-existing DM during pregnancy and GDM, both in maternal and embryonic scenarios. Another advantage is that it provides an alternative to study DM in animals where genetic modification is not possible either due to the lack of genetic engineering availability or because of long generation times. The main disadvantages are that it does not consider genetic variability and other possible collateral disorders, such as obesity and hypertension, often associated to T2DM but not necessarily present in GDM (Feige et al. 2008).

1.1.4 Genetic Models

Genetic models have an important role in understanding the general influence of DM on health. However, as their diabetic phenotype is usually severe already before pregnancy, it has been difficult to generate specific models of GDM using this approach (Pasek and Gannon 2013).

The NOD mouse (Hanafusa et al. 1994; Pearson et al. 2016) and BB rat (Jacob et al. 1992b) that develop spontaneous DM, similar to human T1DM, are the main genetic models for this disease. Both have been used as models to study diabetes complications before and during pregnancy, such as intrauterine growth restriction, neural tube defects, premature birth or macrosomia (Moley et al. 1991; Burke et al. 2007; Eriksson et al. 1989).

Several polygenic strategies have been found to study T2DM, such as inbred mouse models

Table 1 Examples of streptozotocin regimes to generate diabetic mouse models

STZ dose (mg/Kg)	Number of IP injections	Mouse Strain	Type of DM induced according to the reference	Developmental Stage	References
50	1	ICR	DM induced on neonatal mice	Neonate	Kataoka et al. (2013)
50	5	C57BL/6	T1DM	Adult	Chaudhry et al. (2013)
50	5	C57BL/6	Hyperglycemia defined by non-fasting BG >300 mg/dL	Adult	Kim et al. (2016a)
50	5	C57BL/6	Defined as subdiabetogenic doses of STZ	Adult	Kurlawalla-Martinez et al. (2005)
150	1	C57BL/6	Combined with HFD to model T2DM	Adult	Song et al. (2008)
180	1	C57BL/6	T1DM effect on preimplantation embryos	Adult	Brown et al. (2018)
60	1	C57BL/6	DM induction on neonates	E16.0-E18.0	Yang et al. (2013)
35	5	ICR	T1DM triggered by gradual insulitis	Adult	Priel et al. (2007)
240	1	Kunming mice	T1DM defined by fasting BG >11.1 mmol/L	Adult	Liao et al. (2017)
100	2	C57BL/6 and ICR	Defined as mild DM	Adult	Shimizu et al. (2012)
100 + 80	1 + 1	C57BL/6	Combination with genetic and HFD model for T2DM	Adult	Chen et al. (2015)
75	3	Kunming mice	DM characterized by BG >16 mmol/L	Adult	Wang et al. (2018)
190	1	C57BL/6	Pregestational DM defined by non-fasting BG >13.3 mmol/L	Immature (20–24 days)	Chang et al. (2005)
230	1	CD1	Pregestational DM defined by non-fasting BG >17.0 mmol/L	Adult	Ge et al. (2014)
50	5	C57BL/6	Pregestational T1DM defined by fasting BG >11 mmol/L	Adult	Dowling et al. (2014)
75	3				

STZ streptozotocin, *BG* blood glucose, *DM* Diabetes mellitus, *HFD* high fat diet, *IP* intraperitoneal, *T1DM* type 1 diabetes mellitus, *T2DM* type 2 diabetes mellitus

like the TALLYHO/Jng (Dontas et al. 2012) and the New Zealand Obese mouse (Herberg and Coleman 1977), or the sand rat (*Psammomys obesus*). In laboratory conditions, these animals develop T2DM within weeks (Kaiser et al. 2005).

The mutant mouse for the leptin receptor *db/db* is a classic monogenic model to study T2DM. Lack of leptin receptor causes an increase in appetite, obesity and insulin resistance. This model has specific characteristics to be considered: the homozygous *db/db* females are sterile, and heterozygous animals do not show a specific phenotype until pregnancy, when they develop insulin resistance and GDM (Yamashita et al. 2001, 2003).

Something similar happens in mutant mice for the prolactin receptor (*PrlR*), responsible for increasing the proliferation of β-cells during pregnancy, in response to prolactin. This β-cell increment is a compensatory strategy to counterbalance insulin resistance in pregnancy. The complete lack of this receptor renders females infertile but, in the heterozygous state, pregnancy is possible and is followed by moderate glucose intolerance, similar to GDM (Huang et al. 2009).

The main advantages of genetic models are the wide range of studied phenotypes and the possibility of generating new ones through genetic engineering. The main disadvantage is their monogenic character, and the limited number of

species where genetic modifications are possible. In spontaneous genetic models, the main limitation is long generation time, as in bigger animals like sheep or pigs, where gestation lasts between 152 and 114 days (Pasek and Gannon 2013).

1.2 Animal Studies on Gestational and Pregestational Diabetes

1.2.1 Fertility

Ovulation is the point in time when female fertility can be first affected by DM. Animal models used to study ovulation in DM are usually models with mild hyperglycaemia. Hence, the oestrus cycle still occurs, and neither oocyte maturation nor fertilization are affected (Novaro et al. 1998). Folliculogenesis, oogenesis, and preimplantation embryogenesis are impaired in mouse models with severe hyperglycaemia, independently of the induction strategy (Lee et al. 2019).

Preimplantation embryos from diabetic BB rats show difficulties to reach the expanded blastocyst state and around 30% are abnormal (Vercheval et al. 1990). In fact, experiments on cultured embryos from CIM diabetic mice, show that even brief exposure to maternal hyperglycaemia can negatively affect embryonic development (Wang and Moley 2010). This was also confirmed by one-cell stage embryo transfer from diabetic mice to non-diabetic mice (Wyman et al. 2008).

The observed damage in preimplantation embryos has been related to a decrease in the expression of glucose transporters like *GLUT1* in the embryo caused by maternal hyperglycaemia. Indeed, a decrease in these transporters can lead to apoptosis in early embryos (Wang and Moley 2010; Chi et al. 2000).

Implantation is the next developmental step that can be affected in DM to cause impaired fertility. Different studies, both with NOD and STZ treated mice, show more resorption sites in these models than in non-diabetic or prediabetic animals (Brown et al. 2018; Burke et al. 2007). These resorption sites represent places in the uterus where implantation is initiated, but the embryo fails to develop.

The reason behind these implantation defects is unknown. However, one possibility is that hyperglycaemia induces inflammatory cytokines in the female reproductive tract, leading to DNA damage that results in suboptimal embryos, which start implantation but whose development does not progress and are therefore reabsorbed (Brown et al. 2018).

1.2.2 Placentation

STZ administration in mice or rats is the main strategy to develop *in vivo* DM for placenta studies. These models show not only structural, functional and developmental abnormalities (Capobianco et al. 2005; Acar et al. 2008; Suwaki et al. 2007; Favaro et al. 2013), but also abnormal gene expression (Yu et al. 2008). An upregulation in placental nutrient transporters, such as GLUT1 for glucose or *SystemA* for amino acids, has been observed in T1DM and GDM models, which may result in an increased flux of nutrients to the foetus (Jansson et al. 1999, 2006).

Oxidative stress seems to have an important role in the aberrant placenta observed in diabetic pregnancies. The diabetic placenta shows a limited ability to respond to oxidative stress as well as an enhanced production of mitochondrial ROS (Lappas et al. 2011). It has been proposed that this stress is caused by extracellular matrix metalloproteinases, since there is a correlation between blood glucose concentrations and the placental expression of these proteinases (Ding et al. 2018).

Furthermore, during diabetic pregnancy, nutrient transporters increase and promote a more nutritious foetal environment causing macrosomia. However, there are also placental disorders related to reduced blood flow and increased placental glucose consumption, that lead to intrauterine growth restriction (see Fig. 1) (Zamudio et al. 2010; Illsley and Baumann 1866).

1.2.3 Perinatal Outcomes

Human epidemiological studies show negative effects of maternal DM on their offspring.

Maternal DM can cause macrosomia at birth that, in turn, increases the risk of shoulder dystocia, insulin resistance, caesarean section delivery, and neonatal hypoglycaemia (Araujo Júnior et al. 2017; Schwartz et al. 1994; Esakoff et al. 2009). Such disorders cause high neonatal morbidity and mortality.

Most of the research on this matter is done through human epidemiology. However, some studies in rodents are available. To evaluate the intrauterine environment effect on foetuses, CIMs are mainly used (Gonzalez and Jawerbaum 2006; Martínez et al. 2008), but also inbred genetic models like BB rats. In the latter, the diabetic environment during organogenesis decreases embryonic survival and growth rates, and can alter skeletal and internal organ development (Eriksson et al. 1989).

An interesting strategy to study the intrauterine environment in these genetic models while avoiding the embryonic genetic background is to transfer the embryos, one-cell mouse zygotes or blastocysts, from healthy to diabetic females. Also, embryo transfer from diabetic to healthy females is being used to study more acute, short-term effects on the embryos (Wyman et al. 2008; Rousseau-Ralliard et al. 2019).

1.2.4 Intrauterine Programming

High glucose levels during pregnancy promote malformations and inadequate organization of the hypothalamus. These changes affect food intake and energy balance increasing offspring's susceptibility to body weight dysregulation (Šeda et al. 2018). In the long term, babies from diabetic mothers show an increased risk of obesity, T2DM and cardiovascular disease (Plows et al. 2018b).

On the other hand, several studies show lower body weight in offspring from rats where GDM is chemically induced by STZ. Furthermore, other authors show that in male offspring from diabetic mothers, the weight of the reproductive organs is significantly lower. It is suggested that this reduction is due to a decrease in testosterone levels (Türk et al. 2018; Amorim et al. 2011). Finally, low body weight can persist into adulthood (Van Assche et al. 2001), which in rats is explained by deficiencies in milk production and quality during lactation (Lau et al. 1993). However, a direct toxic effect of STZ on the offspring cannot be ruled out. Indeed, there is discrepancy between these findings and what is found in human studies, where macrosomia is the predominant complication of GDM (see Fig. 1).

Animal models are a valuable tool to study the mechanisms behind these effects. A recent report shows how the oxidative stress present in the maternal diabetic environment programmes adult hypertension in the offspring by hyperphosphorylation of the renal dopamin1 (D1) receptor. In this case, hypertension is caused by dysfunction of the D1 receptor that is responsible for ≈60% of sodium excretion during increased sodium intake (Luo et al. 2018).

Finally, *Socs2* null mutant mice have been recently proposed as a model for GDM associated to aging, as older pregnant females show lower birth and higher mortality rates, associated with a high frequency of foetal macrosomia (Brito-Casillas 2019).

2 *In Vitro* Models

In vitro models are complementary to *in vivo* models. They do not represent complex physiological systems as faithfully as *in vivo* models do. However, they allow researchers to study numerous and precise experimental conditions simultaneously, investing fewer resources than with animal studies. They have certain advantages, as they can be used in parallel to test the reproducibility of results, be genetically modified by transfection to investigate the role of several genes and be used to screen for drugs. Furthermore, the use of *in vitro* models allows to reduce the number of animals used in research, in compliance with the 3 R's principles. These *in vitro* models include cell-lines, islets, human stem cells and organoids. Their specific advantages and disadvantages are summarized in Table 2.

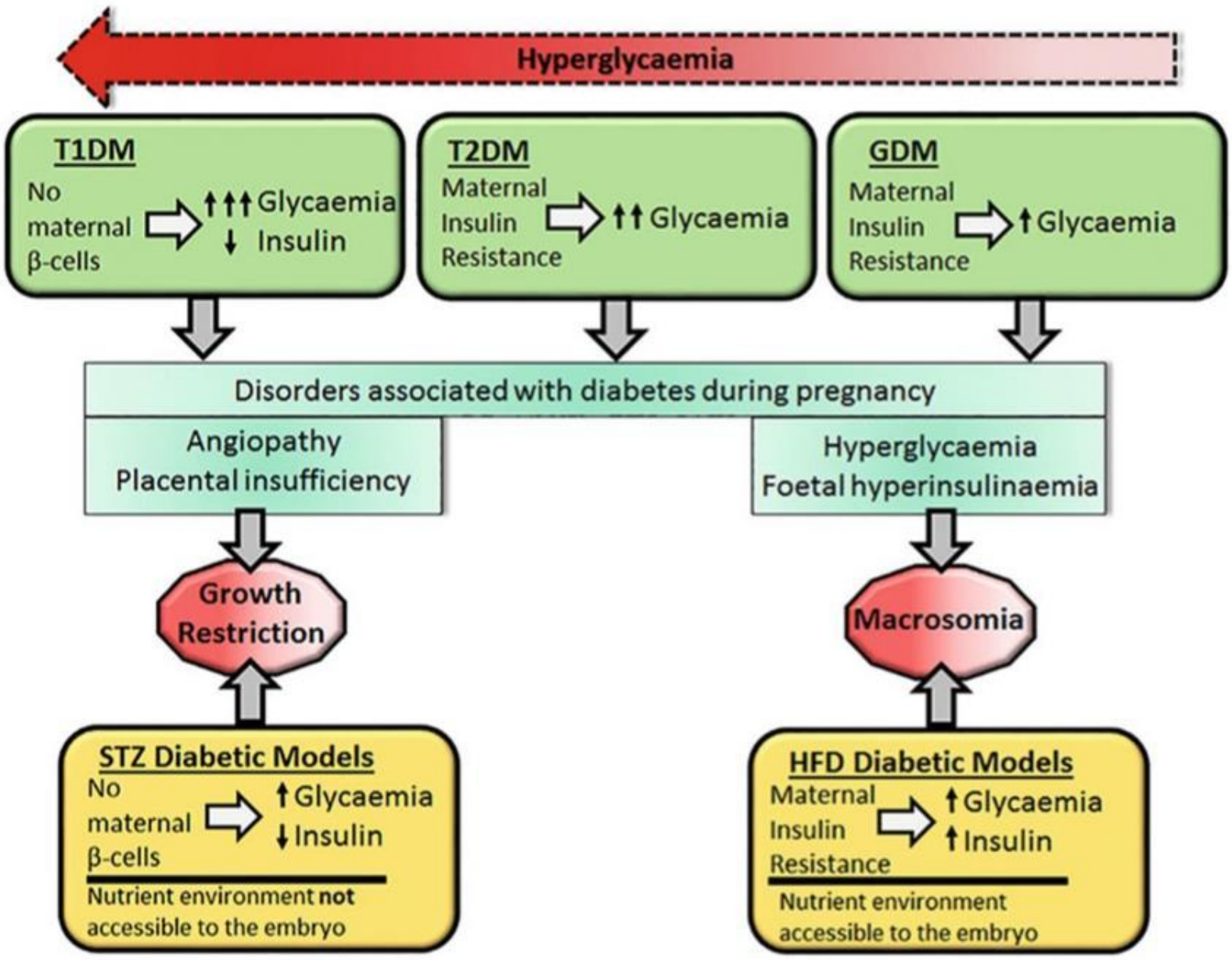

Fig. 1 Overview of the mechanisms involved in diabetes and its complications during pregnancy and the animal models used to mimic them. Both type 2 and gestational diabetes are associated with insulin resistance and mild-to-moderate hyperglycaemia, whereas type 1 diabetes is associated with insulin deficiency and more severe hyperglycaemia. The most frequent complications of diabetes in pregnancy are associated with hyperglycaemia itself, compensated by the foetus with an increased insulin secretion that leads to macrosomia. Vascular complications, on the other hand, are associated with placental insufficiency, and induce complications such as preeclampsia and intrauterine growth restriction. Animal models do not always truthfully reflect the human disease. *T1DM* Type 1 Diabetes Mellitus, *T2DM* Type 2 Diabetes Mellitus, *GDM* Gestational diabetes Mellitus, *STZ* Streptozotocin, *HFD*: High Fat Diet

2.1 *In Vitro* Models of Diabetes

2.1.1 Cell Models of Diabetes

Until recently, rodents have been the main source of β-cell lines. The latter are obtained from radiation induced insulinoma, such as RIN cell lines (Chick et al. 1977); virally induced insulinoma, like the cell line In-111 (Uchida et al. 1979); oncogenic transfection of primary β-cells using the simian-vacuolating virus 40 (SV40) antigen oncogene from the insulin gene promoter, like MIN-6 (Miyazaki et al. 1990); and electrofusion of primary pancreatic β-cells. The latter technique was used to generate the BRIN-BD11 cell line from the RINm5F clone (McClenaghan et al. 1996). This cell line is widely used in β-cell biology and drug target research since it behaves like β-cells, with an almost normal response to glucose and to other modulators of insulin secretion. A high number of researchers use INS-1 cells, obtained from rat insulinoma, which proliferate easily and fast in culture, though their response to glucose is lower than that of primary islets (Chick et al. 1977; Asfari et al. 1992).

While rodent cell lines allow great advances in β-cell research, the use of a stable human cell line

Table 2 Advantages and disadvantages of *in vitro* models for human diabetes research

In vitro models of diabetes	Advantages	Disadvantages
Murine β-cell lines	Easy to culture Many types of cells are available Good option to test drugs and study cell physiology	Differences from human make difficult to choose the most appropriate murine β-cell line No vascularization and cell to cell interaction
Human β-cell lines	Easy to culture Stable human cell line allows progress in human diabetes research and in clinical applicability	It is not easy to produce stable human cell lines, and there are only few of them Most human cell lines have some genetic defects, grow slowly or have a low response to glucose No vascularization and cell to cell interaction
Murine pancreatic islets	Can be isolated in less time and with less cost than human islets Short generational times Easy to be genetically modified	There are differences in islet architecture, vascularization and blood flow from human islets
Human pancreatic islets	Maintain the islet structure and all cell types Used to study the biology of the human pancreas	Limited donor supply Do not allow long functional studies Heterogeneity in their characteristics: size, genetics...
Human stem cells	A renewable source of β-cells Can be genetically modified Allow longer studies than pancreatic islets	To obtain them, a long and expensive process is needed
Organoid cultures	Resemble the diseased organ architecture better than traditional 2D cultures	Do not have vascularization

would have more direct clinical applicability. However, their generation is not straight forward. Most of them have genetic defects, grow slowly or have an insufficient response to glucose (Green et al. 2015). Nevertheless, there are also well characterized cell lines, such as NAKT-15, created by transfection of human islet cells with SV40 T-antigen, that restore normoglycemia in diabetic mice (Narushima et al. 2005). The 1.1 B4 cell line, produced by electrofusion of isolated cadaveric human β-cells with immortal PANC-1 epithelial cells, expresses most of the genes and proteins related with insulin production. Furthermore it shows similar characteristics to isolated human β-cell lines, although insulin content is lower than in rodent cells. 1.1 B4 cells are used to study human β-cell biology and function (Ota et al. 2013; Krause et al. 2014; Elumalai et al. 2017) and have been used to demonstrate glucotoxic effects on gene expression and insulin secretion (Vasu et al. 2013).

Another, well characterized cell line is EndoC-βH1, considered a stable human β-cell line with many applications (Scharfmann et al. 2016). These cells are responsive to glucose at a physiological range. They were immortalized with transgenes to generate the cell lines EndoC-βH2 and EndoC-βH3 which are very similar to primary β-cells (Scharfmann et al. 2014; Benazra et al. 2015). The EndoC-βH1 cell line is widely used to study human β-cell physiology and to screen and identify glucose-lowering drugs (Grieco et al. 2014; Andersson et al. 2015; Gurgul-Convey et al. 2015; Krishnan et al. 2015; Tsonkova et al. 2018).

2.1.2 Pancreatic Islets

The endocrine pancreas is organized in islets with five major cell types, each one responsible for the secretion of different hormones: α-cells (glucagon), β-cells (insulin), PP-cells (pancreatic polypeptide), δ-cells (somatostatin) and ε-cells (ghrelin) (Zhou and Melton 2018).

The advantages of using whole pancreatic islets are that they maintain their tridimensional structure and contain all cell types and, thus, would be expected to reproduce what happens *in vivo* more faithfully. Pancreatic islets have

been used to study the biology of the pancreas, test drugs and study potentially preventive interventions. However, due to the vascular damage after their isolation, they cannot be used in long studies (Schmied et al. 2000).

Rodent islets predominantly employed in DM research are currently being replaced by human islets. Thanks to the increased availability of the latter, several advances have been accomplished: knowledge of the islet structure, gene expression, insulin secretion, cell proliferation and their response to stress situations (Hart and Powers 2019). Indeed, comparisons between islets from healthy donors and those with DM give information on differential β-cell identity, gene expression, etc., that can be useful to elucidate mechanisms of disease (Marchetti et al. 2019).

However, universally accepted criteria to define human islet quality are not yet available. Some authors use islet insulin production to measure quality (Hart and Powers 2019) and propose a list of features which should be reported on each human islet preparation. This list includes information about the origin/source, isolation centre, estimated purity and viability, total culture time, functional measurement, and description of islet use.

The organization of networks and consortia, such as the Islet Cell Resource Center Consortium (ICRCC), have increased human pancreatic islet availability (Kaddis et al. 2009; Niland et al. 2010).

2.1.3 Human Stem Cells

Human pluripotent stem cells (hPSCs), human embryonic stem cells (hESCs) and human induced pluripotent stem cells (hiPSCs) have been differentiated into pancreatic β-like cells. To this end, it is necessary to collect fibroblasts or peripheral blood mononuclear cells (PBMCs) from patients and then reprogramme them into hiPSCs (Amirruddin et al. 2019).

Human pluripotent stem cells have some advantages for human DM research, as they are a renewable source of β-cells, and can be modified genetically (Balboa et al. 2019). Hence, these cells represent a new model to study pathogenic mechanisms and test drugs (Amirruddin et al. 2019).

Moreover, they can be used as part of newer technologies like organ-on-a-chip devices, single cell RNA-sequencing, development of hypoimmunogenic cells and promotion of vascularization of the β-like cells (Amirruddin et al. 2019).

On the other hand, they also present some disadvantages, since long and cumbersome procedures are necessary to obtain them. However, recent progress has been made in the protocols to differentiate hPSCs into pancreatic β-like cells.

Many authors have developed protocols leading to insulin producing, β-like cells. Sometimes these cells are polyhormonal β-like cells, which do not express key β cell transcription factors (Bruin et al. 2014; Guo et al. 2013), and show limited *in vitro* insulin secretion in response to glucose. Furthermore, these cells resemble transient endocrine cells found in human foetal pancreases (Bruin et al. 2014; D'Amour et al. 2006).

In 2014, Rezania et al. (2014) generated insulin expressing β-like cells from hPSCs, cells capable of secreting insulin in response to glucose and reversing diabetes *in vivo* restoring the blood glucose levels of STZ-induced diabetic mice. According the authors (Rezania et al. 2014), the differentiation process occurs in seven stages which are defined by specific markers. The key stages are: development of the definitive endoderm (stage 1), primitive gut tube (stage 2), posterior foregut (stage 3), pancreatic progenitor (stage 4), endocrine progenitor (stage 5), immature β-cells (stage 6) and mature cells (stage 7). In stage 4, PDX1 and NKX6.1 are co-expressed and are needed for the generation of glucose-responsive and mono-hormonal β-cells (Rezania et al. 2014). From this stage the cells can differentiate *in vitro* into mature β-cells and can be transplanted into mice for further *in vivo* maturation. Pagliuca et al. also developed a differentiation protocol to generate β-like cells from hPSC. The cells were responsive to glucose *in vitro* and functionally resembled adult cells (Pagliuca et al. 2014). In 2015, Russ et al. published a

differentiation protocol without using bone morphogenic protein (BMP) inhibitors during pancreatic specification to avoid formation of non-functional polyhormonal cells. This represented an improvement in the protocol, generating pancreatic progenitors that were then differentiated into glucose responsive cells *in vitro* (Russ et al. 2015).

More recently, Aigha et al. developed a protocol to generate a population of pancreatic progenitor population expressing NKX6.1 in the absence of PDX1 from hPSCs. These cells are potentially able to generate endocrine islet cells (Aigha et al. 2018). Some authors have used hPSC-derived pancreatic progenitor cells and have observed that when transplanted into mice with T1DM, the cells are able to differentiate and mature into glucose-sensitive insulin cells and may even reverse DM (Rezania et al. 2012, 2014; Bruin et al. 2013).

Thus, optimizing protocols to generate β-like cells from hPSC is a challenge, though great progress has been made in recent years and many research groups are capable of producing pancreatic progenitor and immature islet-like cells. Nevertheless, work still needs to be done in the process of obtaining mature cells capable of secreting insulin, *in vivo,* in response to glucose (Balboa et al. 2019*;* Shahjalal et al. 2018*;* Abdelalim and Memon 2020*).*

2.1.4 Organoid Cultures

In recent years, modelling diseases *in vitro* has bloomed with the generation of three-dimensional (3D) cell culture systems, which resemble the diseased organ architecture better than traditional 2D cultures. Among the 3D cell structures, cell aggregates or spheroids, cysts and true organoids can be distinguished. Spheroids are solid cell aggregates without a central lumen, cysts are spheres of polarised epithelial cells with a central lumen, while true organoids are complex, polarised structures with a central lumen (Bakhti et al. 2019). An organoid can be defined as a 3D structure derived from either pluripotent stem cells (PSCs), neonatal tissue stem cells or adult-derived stem/progenitor cells (AdSCs), in which cells spontaneously self-organise into structures that resemble the *in vivo* tissue in terms of cellular composition and tissue function (Hindley and Cordero-Espinoza 2016). These organoids can be used to model diseases *in vitro* and as a source for cell therapy or organ transplant.

The ultimate goal of organoid biology for regenerative medicine is to faithfully generate *in vitro* functional organs using the patient's own cells for cell therapy, organ transplant or replacement. To this end, the best option is to generate the organoid using induced pluripotent stem cells (iPSCs) derived from the patient's fibroblasts or peripheral blood mononuclear cells (see above). To accomplish this, a detailed knowledge of the organ embryonic development, function and cell composition is required. The organ development will inform about signals and gene activity that will be required to efficiently direct iPSCs differentiation into the cells present in the organ. The detailed organ function is needed to test how faithfully the organoid recapitulates the organ. Finally, organ cell composition knowledge is required to ensure that all the needed cell types for organ function are present in the organoid. Ideally, the progenitor population that allows for the homeostasis of the organ should also be identified to facilitate the organoid generation from the adult organ.

Pancreatic cysts and organoids can be derived from mouse foetal tissues (Greggio et al. 2013; Sugiyama et al. 2013; Bonfanti et al. 2015). These organoids and cysts are composed by acinar, ductal, endocrine and exocrine cells, hence faithfully representing the pancreatic cell composition. Given the poor regenerative potential of the pancreas, it is controversial whether an established progenitor population (AdSCs) or rather transdifferentiation from one pancreatic cell type into another is responsible for pancreas homeostasis (Kopp et al. 2016). Regardless, pancreatic cysts and organoids have been generated from adult mice using different starting cell populations, indicating that a clear pancreatic progenitor population is elusive (Huch et al. 2013; Jin et al. 2013, 2014). If Lgr5+ cells are used, organoids composed by duct cells are obtained, that only upon transplantation *in vivo* can differentiate into endocrine cells (exocrine and acinar fates were

not tested) (Huch et al. 2013). However, if CD133 + Sox9+, are used, cysts composed by endocrine and acinar fates are obtained (no transplantation tests were done) (Jin et al. 2013, 2014). In summary, all these studies using mouse samples help to understand the mechanisms of pancreas development. Hence, they can be used to model pancreatic diseases like DM, though their suitability for cell therapy is still to be tested.

The generation of human pancreatic spheres from adult samples was initially achieved upon cell reprogramming with islet developmental regulators (Lee et al. 2013). These spheres can differentiate into endocrine cells *in vitro*. More recently, applying adult mouse organoid generation conditions to human foetus samples has allowed to generate human pancreatic cysts with limited differentiation success (Bonfanti et al. 2015; Loomans et al. 2018).

Several groups have targeted their efforts into generating islet-like spheroids using cell lines, hESCs or hiPSCs rather than pancreatic organoids. The cells EndoC-βH1 (Ravassard et al. 2011), EndoC-βH2 (Scharfmann et al. 2014) and EndoC-βH3 can be cultured as 3D pseudo-islets *in vitro* (Benazra et al. 2015). Other cells, such as 1.1 B4, form pseudo-islets spontaneously and show higher resistance to toxicity and DNA damage if grown as pseudo-islets than in monolayers (Green et al. 2015). The first advantage of using pseudo-islets instead of pancreatic islets is their availability. Furthermore they are similar to primary islets and they present an increase in insulin production in response to glucose (Rogal et al. 2019). Indeed, interaction between cells increases the response to glucose (Kojima 2014). Furthermore, pseudo-islets can be modified genetically, accordingly to the research goal. However, they neither have vascularization, nor an intrinsic structure. Given the scarcity of human donor, islet-like spheroids generated from hESCs or hiPSCs could be a potential source for transplantation into diabetic patients. The first protocols using hESCs or hIPSCs only produced immature β-cells (D'Amour et al. 2006; Hrvatin et al. 2014). Later protocols have achieved mature β-cells from hESCs or hiPSCs (Rezania et al. 2014; Pagliuca et al. 2014; Russ et al. 2015; Kim et al. 2016b; Shim et al. 2015). Importantly, the islet-like spheroids improve hyperglycaemia in diabetic mice. The improvement and efficiency vary depending on the protocol used for islet-like spheroid generation. Only 2 protocols report an improvement after 3–4 days that only lasts for a short period of time (Russ et al. 2015; Kim et al. 2016b). The other protocols only show improvement weeks after transplantation (Rezania et al. 2014; Pagliuca et al. 2014; Shim et al. 2015). These limited results in reversing hyperglycaemia are likely due to their limited functionality, which might include poor tissue engraftment, lack of revascularization of the transplanted tissue or absence of a niche.

The improvement of organoid functionality can be achieved by increasing its complexity applying bioengineering approaches like co-cultures and biomimetic scaffolds (Yin et al. 2016). Co-cultures of islet-like cells with mesenchymal stem cells (Shin et al. 2015; Takebe et al. 2015) and human amniotic epithelial cells (Lebreton et al. 2019) enhance engraftment, viability and function in transplant experiments by increasing vascularisation. The co-cultures can also be done using cell lines like MIN6 (Takahashi et al. 2018). The aim of using biomimetic scaffolds is to provide an extrinsic microenvironment that supplies biochemical and biophysical signals, including structural support, to the growing organoid. For example, islet-like organoids from hESCs using Matrigel and collagen as scaffold secrete insulin in response to glucose (Wang et al. 2017). Finally, both co-cultures together with biomimetic scaffolds can be used (Candiello et al. 2018). In this case hESCs together with endothelial cells and a novel engineered hydrogel are used, which also secrete insulin in response to glucose.

In summary, multiple protocols and approaches have been developed to generate pancreatic or islet-like organoids that harbour the potential to be used for transplantation in diabetic patients. However, their efficiency is not always comparable among them as not all test their *in vivo* functionality in diabetic mice.

2.2 *In Vitro* Models of Diabetes in Pregnancy

The human placenta is the interface between the mother and the foetus. During pregnancy, the placenta is exposed to morphological and functional changes at the cellular and tissue level (Desoye and Mouzon 2007). The foetal-maternal interface is formed by a heterogeneous group of trophoblast cells with a wide range of functions.

There are several models and cell lines available to investigate the effect of DM on the placenta.

2.2.1 Primary Cell Lines

These cell lines are of placental origin from early gestation or at term. Some have been used to study different aspects of trophoblast function, such as invasion, migration and immunology.

Primary term trophoblast cells have been used to study the association between maternal lipid metabolism and GDM (Stirm et al. 2018). The human first trimester trophoblast cell line Sw.71 has been used to study the effects of high concentrations of glucose on trophoblasts and the effect of metformin (Han et al. 2015) and to understand how hyperglycaemia increases the risk of preeclampsia (Heim et al. 2018).

Primary human villous trophoblasts have been also used in culture to study the effect of free fatty acids (palmitate and oleate) on cell viability and function (Colvin et al. 2017). Specifically, to understand the effect of maternal obesity before pregnancy on GDM, and the latter on preeclampsia and complications in the foetus. Similar studies investigate the effect of IL-6 and TNF-α (elevated in GDM and obesity) on fatty acid accumulation in human primary trophoblast cells culture (Lager et al. 2011).

Primary cells have some limitations, such as relatively low number of isolated cells, short lifespan and lack of proliferation *in vitro*. To overcome these limitations, several trophoblastic cell lines have been established, using two methods: establishment of human choriocarcinoma cell lines and introduction of the gene encoding simian virus 40 large T (SV40T) antigen (Graham et al. 1993).

2.2.2 Choriocarcinoma Cells

Despite being a cancer cell model, choriocarcinoma cells are widely used to study the function of the placenta. These cells are easy to culture and propagate. They present barrier capacity, are able to express glucose transporters (GLUT-1, GLUT-3) and release hormones (Schmitz et al. 1999; Nusrat et al. 2001; Brown et al. 2011; Saleh et al. 2007). Nevertheless, only some clones are available, including: BeWo (Heaton et al. 2008), JAR (Azizkhan et al. 1979) and Jeg-3 (Frank et al. 2000). In addition, ACH-3P (Hiden et al. 2007; Fröhlich et al. 2015; Weiss et al. 2014) and AC1-M59 are AC-1 choriocarcinoma cells fused with first and third trimester trophoblast cells.

These cells have been broadly used as *in vitro* models. However, they show relevant differences with respect to primary trophoblasts (Poaty et al. 2012). For example, the HLA expression of these cells is distinct. Furthermore, studies in DNA methylation show high variability producing differential expression profiles (Apps et al. 2011). Hence, to interpret the results obtained using choriocarcinoma cells it is necessary to compare them with those obtained using primary cells.

In DM research, the BeWo choriocarcinoma cell line can be exposed to high glucose levels to identify changes in transcripts and metabolites (Hulme et al. 2018). It has also been used to assess the effect of choline and betaine on the placental transport, the role of miR-130b-3p in regulating oxidative stress during GDM and to test the effects of hyperglycaemia on endoplasmic reticulum stress (Nanobashvili et al. 2018; Jiang et al. 2017; Yung et al. 2016).

2.2.3 Immortalized Cells

The human, first trimester, extravillous trophoblast cell line (HTR-8/SVneo) was developed using first trimester extravillous trophoblast infected with SV40 T-antigen. It contains two populations of cells suggesting the presence of trophoblast and stromal/mesenchymal cells (Abou-Kheir et al. 2017). HTR-8/SVneo cells are largely used to study trophoblast functions including cell fusion, migration and invasion during hyperglycaemia (Wu et al. 2018).

HTR-8/SVneo cells are also used to study microRNA expression profiles under high glucose conditions. They have been used, for example, to assess the influence of miR-137 on trophoblast viability and migration under high glucose conditions, to evaluate the combined effect of glucose and fatty acids on early placentation and to study the effects of hypoxia on placentation and the role of glucose and its transporters (Peng et al. 2018; Basak et al. 2015, 2019; Bermejo-Alvarez et al. 2012a).

2.2.4 Human Trophoblast Stem Cells

There are three main trophoblast populations in the human placenta: cytotrophoblast (CT), extravillous cytotrophoblast and syncytiotrophoblast (Okae et al. 2018). Recently, a culture system has been developed to generate trophoblast stem cells (Okae et al. 2018). The authors derived human syncytiotrophoblast from cytotrophoblast and from blastocysts. These cells are genetically stable and can be potentially used to study growth, trophoblast defects and preeclampsia (Okae et al. 2018). They seem promising to evaluate the influence of DM on trophoblast development and function. However, further studies are needed to fully characterise the model.

2.2.5 Placental Organoids

Recently, trophoblast organoids that model maternal-foetal interactions have been developed (Haider et al. 2018; Turco et al. 2018). The authors from both studies successfully generate the trophoblast organoids using first trimester placentas, from either 6th–9th (Turco et al. 2018) or 6th–7th weeks, but not from 10th–11th weeks of pregnancy (Haider et al. 2018). Moreover, decidual glandular organoids can also be obtained to model the placenta (Turco et al. 2018). Using similar culture conditions, both studies rely on the long-term culture capabilities of the organoids (over a year versus 5 months) and the starting material (individual patient versus pooled samples) in (Turco et al. 2018) versus (Haider et al. 2018). Moreover, the main focus of both studies varies, being in (Haider et al. 2018) to model the development of the placenta understanding the signalling pathways involved. While in (Turco et al. 2018), the authors focus on fully characterising the organoids, including cell origin (foetal), transcriptomic and methylation profile, structural, secretome and invasive capabilities.

It is also possible to generate extravillous trophoblast spheroids (Nandi et al. 2018), which can be obtained by culturing HTR8/SVneo EVT cells in ultralow attachment plates and be used as a model for placental extravillous trophoblast invasion (Wong et al. 2019).

The new trophoblast organoids derived from human samples opens new avenues to model maternal-foetal interactions that will be of interest to further progress in how placentas develop in women with DM. However, these models present with some limitations, as they only represent the trophoblast component of the placenta (Turco and Moffett 2019). In this sense, new organoid models mimicking diabetic microenvironments are being developed, and by the use co-culture techniques, this may provide more complex models also under diabetic conditions (Tsakmaki et al. 2020). Further studies, maybe including bioengineering approaches, will be necessary before true placental organoids can be generated.

2.2.6 Embryo Cultures

Maternal DM is associated with retarded preimplantation embryo development in mouse models (Moley et al. 1991; Beebe and Kaye 1991), due to apoptosis (Moley et al. 1998) and changes in their metabolic state (Moley et al. 1996). Preimplantation development comprises the stage of development from fertilization till embryo implantation in the uterus. During this period, two sequential cell fate decisions occur that result in three cell populations. Upon the first decision, cells become either trophectoderm (TE) or inner cell mass (ICM) cells. Descendants of TE cells form the foetal portion of the placenta, while the ICM cells make a further decision: they differentiate either into Epiblast (Epi) or into Primitive Endoderm (PrE). Epi cells predominantly give rise to the embryo proper while PrE cell descendants generate the endodermal part of the yolk sac (Bassalert et al. 2018).

To assess the effect of intrauterine conditions in diabetic mothers during preimplantation development, embryos can be cultured under high glucose concentrations. This approach allows investigating early developmental defects without inducing DM in the mothers. Therefore, this approach can be considered a refinement method following the 3R's principles. Under these culture conditions, embryos exhibit higher intracellular concentration of glucose (Moley et al. 1996). There is controversy about the glucose concentration present in the reproductive tract milieu where embryos develop and the concentration that provides optimal development when embryos are cultured *in vitro* (Biggers and McGinnis 2001). Hence, different studies use increasing concentrations of glucose in their embryo culture medium to understand the underlying cause of poor embryo development in diabetic mothers. While control conditions use a 0.2 mM concentration of glucose, experimental conditions use up to 52 mM. However most studies use 15–27 mM, that is 2–3 times that of serum of non-diabetic mice (Bermejo-Alvarez et al. 2012b). Summarising, *in vitro* culture of mouse embryos in the presence of glucose reduces total and TE cell numbers at the blastocyst stage (Bermejo-Alvarez et al. 2012b) and also cell allocation to the ICM (Fraser et al. 2007).

An alternative model to study the effect of high glucose during early embryonic development is the use of blastoids and ICM organoids (Rivron et al. 2018; Mathew et al. 2019). Blastoids are blastocyst-like structures obtained from mouse trophoblast and embryonic stem cells, which morphologically and transcriptionally resemble blastocysts. ICM organoids are three-dimensional spheroids obtained from modified mouse embryonic stem cells that recapitulate Epi and PrE differentiation. In this context, these models could serve as an approach to replace the use of mice.

Altogether, the use of cultured embryos (blastoids or ICM organoids) in the presence of high glucose levels allows characterising the defects and causes of poor embryo quality obtained by diabetic mothers without inducing DM in the females. However, the results are limited and more studies to address the molecular mechanisms responsible of the embryonic defects will be needed in the future.

2.3 Recreation of the Diabetic *Milieu*

In vitro models are composed, not only by the cells themselves, but also by the conditions under which they are grown. To study the effect of DM on the β-cells, pancreatic islets etc. and even the effect on the development and physiology of the placenta, it is crucial to select a good cell model, but also to imitate the diabetic environment as closely as possible.

DM is defined by fasting plasma glucose concentrations above 7.0 mmol/L (126 mg/dL) or random glucose concentrations above 11.1 mmol/L (200 mg/dl) (American Diabetes Association 2013). For GDM, the cut-offs are even lower. However, concentrations used to mimic diabetes *in vitro* are not always consistent with this.

To recreate a non-diabetic milieu *in vitro* most authors agree with the concentrations to mimic normoglycemia, using 5.5 mM of glucose (Han et al. 2015; Heim et al. 2018; Yung et al. 2016; Peng et al. 2018; Basak et al. 2015), whereas other authors use 7 mM (Li et al. 2019), 10 mM (Jiang et al. 2017) or even 11 mM of glucose (Basak et al. 2019).

To simulate diabetic conditions, different concentrations are used: 20 mM (Yung et al. 2016), 22 mM (Triñanes et al. 2017), but 25 mM is the concentration of glucose most frequently used (Han et al. 2015; Hulme et al. 2018; Peng et al. 2018; Basak et al. 2015, 2019; Li et al. 2019), although 35.5 mM is also employed (Nanobashvili et al. 2018). Regarding prediabetic conditions, 10 mM (Basak et al. 2015) and 11 mM of glucose are the concentrations chosen (Han et al. 2015; Heim et al. 2018; Yung et al. 2016).

On the other hand, to simulate high fatty acids concentrations, authors employ the two most common dietary fatty acids, palmitate and oleate. Since it has been shown that palmitate is toxic to human trophoblast but oleate is not toxic (Colvin

et al. 2017), the first is mainly used to understand the effect of fatty acids on the developing placenta and foetus. It is also the most frequently employed to study the effects of fatty acids on the β-cells and pancreas physiology. Most of the authors apply a concentration of 100 μM (Stirm et al. 2018; Colvin et al. 2017; Triñanes et al. 2017), but 500 μM palmitate has also been used (Hong et al. 2018).

To summarize, in recent years there has been important progress in the development of *in vitro* models to study DM. The *in vitro* models derived from animal cells have allowed to study DM physiology and test drugs. However, the advance in human *in vitro* models should lead to important progress in the understanding of the disease and the applications in medicine. Significant advances have been made in the field. For example, in the differentiation of human pluripotent stem cells into pancreatic β-like cells, in pancreatic islet research and in the development of 3D cultures (Tsakmaki et al. 2020). Development of molecular techniques have also improved that allow the modification of the *in vitro* models according to the goal. Regarding the placenta, it is still not very a well-known organ and much research is needed to understand its development and functions in humans. However, recent progress such as new human cell lines, human trophoblast stem cells, human embryo culture and trophoblast organoids, should allow improved understanding of the effect of DM and other diseases on placental and foetal development.

3 Potential Translation, Research Gaps and Future Perspectives

The translation of research from the experimental frame to the patient, usually lacks of direct transmission of the result success from the first scenario to the latter. This fact has driven research organizations to claim and establish common criteria for adequate methodology and reporting of the results, as this could be one of the main factors affecting replication and translation (Jastreboff 2014; Starling 2019; Nakao 2019; Kilkenny et al. 2010).

In this regard, several aspects can be highlighted regarding the DM models described in the present review. Criteria for animal model definition and selection are not uniform, and methods to induce and test the models are also varied, even when similar aims are pursued. The type of DM targeted in the animal model is commonly not well established, or disagrees with the actual definitions of the disease. Regarding *in vitro* modelling, there are also important variations amongst authors in the definition of hyper- and normo-glycaemia. Therefore, starting a new study can be challenging if the protocol is to be based on published evidence. Common criteria need to be established for methodological aspects, both *in vivo* and *in vitro*. This will improve reproducibility of the results, as well as potential translation. The recent organoid and stem cell based strategies, and initiatives like the standards established by the ICRCC, will probably improve research translation.

Furthermore, models that adequately match the specific phenotype of GDM and pre-gestational DM or their complications are also scarce and necessary for this translation. In this sense, genetic models may also help, and recent advances in genetic engineering will boost the available options, given the growing list of candidate genes for GDM (Moon et al. 2019; Li et al. 2020; Lin et al. 2020; Thong et al. 2020).

Nevertheless, an immediate interesting strategy to improve these options could be a thorough evaluation of DM around pregnancy, in previously known diabetic models, and especially in the genetically modified. A previous example is available, where a macrosomic phenotype associated with impaired glucose metabolism was identified during routine rodent management, in a well-characterized *Socs2* null mouse model (Lau et al. 1993). Therefore, approaches to evaluate DM in pregnancy in previously known genetic models should be considered, as they are especially necessary in the assessment of such important areas like intrauterine programming, placentation and perinatal complications.

4 Summary and Recommendations

Maternal diabetes is associated with reduced fertility (Fraser et al. 2007) and an increased risk of poor pregnancy outcomes, both for the mother and her offspring (Hjort et al. 2019). Although clinical and epidemiological studies are invaluable to assess these outcomes and the effectiveness of potential treatments, there are certain ethical and practical limitations to what can be assessed in human studies. Thus, both *in vivo* and *in vitro* models can aid us in the understanding of the mechanisms behind these complications and, in the long run, towards their prevention and treatment. However, some important issues should be considered in the design and performance of the studies.

1. The aim of the study should be clearly defined: what type of DM are we focusing on? Is it pregestational or gestational? In the former case, is it T1DM or T2DM we want to assess?
2. The model should be selected in accordance with the aim of the study. In the case of animal studies, this includes the species, strain and mode and timing of DM induction.
3. The experimental (and control) milieu should mimic DM (and healthy control) as closely as possible, i.e. mildly hyperglycaemic for GDM and T2DM and more overtly so for T1DM.

Increasing progress in the development of *in vitro* models, as well as standardisation of methods and reporting should improve translation of experimental research in diabetic pregnancy to human health.

5 Funding

JLG is supported by the pre-doctoral program from the Universidad de Las Palmas de Gran Canaria (ULPGC) (2017), CVT is supported by the Postdoctoral Program from the ULPGC (2018). SMD is supported by the 'Viera y Clavijo' Program from the Agencia Canaria de Investigación Innovación y Sociedad de la Información (ACIISI)CIISI and the ULPGC. This manuscript is linked to the project PI16/00587 from the National Institute of Health Carlos III from the Spanish Government (ISCIII), cofounded by the European Funding for Regional Development (FEDER).

References

Abdelalim E, Memon B (2020) Stem cell therapy for diabetes: beta cells versus pancreatic progenitors. Cell 9(2):pii: E283

Abou-Kheir W, Barrak J, Hadadeh O, Daoud G (2017) HTR-8/SVneo cell line contains a mixed population of cells. Placenta 50:1–7

Acar N, Korgun ET, Cayli S, Sahin Z, Demir R, Ustunel I (2008) Is there a relationship between PCNA expression and diabetic placental development during pregnancy? Acta Histochem [Internet] 110(5):408–417. [cited 2019 Nov 6]. Available from: http://www.ncbi.nlm.nih.gov/pubmed/18377963

Aerts L, Vercruysse L, Van Assche FA (1997) The endocrine pancreas in virgin and pregnant offspring of diabetic pregnant rats. Diabetes Res Clin Pract [Internet] 38(1):9–19. [cited 2019 Nov 5]. Available from: http://www.ncbi.nlm.nih.gov/pubmed/9347241

Aigha II, Memon B, Elsayed AK, Abdelalim EM (2018) Differentiation of human pluripotent stem cells into two distinct NKX6.1 populations of pancreatic progenitors. Stem Cell Res Ther 9(1):83

American Diabetes Association (2013) Diagnosis and classification of diabetes mellitus, ADA clinical practice recommendations. Diabetes Care 36(Suppl 1): S67–S74

American Diabetes Association (2019) 2.Classification and diagnosis of diabetes: standards of medical care in diabetes 2019. Diabetes Care 42:S13–S28

Amirruddin NS, Low BSJ, Lee KO, Tai ES, Teo AKK (2019) New insights into human beta cell biology using human pluripotent stem cells. Semin Cell Dev Biol. pii: S1084-9521(18)30308-2

Amorim EMP, Damasceno DC, Perobelli JE, Spadotto R, Fernandez CDB, Volpato GT et al (2011) Short- and long-term reproductive effects of prenatal and lactational growth restriction caused by maternal diabetes in male rats. Reprod Biol Endocrinol 9:154

Andersson LE, Valtat B, Bagge A, Sharoyko VV, Nicholls DG, Ravassard P et al (2015) Characterization of stimulus-secretion coupling in the human pancreatic EndoC-βH1 beta cell line. PLoS One 10(3):e0120879

Apps R, Sharkey A, Gardner L, Male V, Trotter M, Miller N et al (2011) Genome-wide expression profile of first trimester villous and extravillous human trophoblast cells. Placenta 32(1):33–43

Araujo Júnior E, Peixoto AB, Zamarian ACP, Elito Júnior J, Tonni G (2017) Macrosomia. In: Best practice

and research: clinical obstetrics and gynaecology, vol 38. Bailliere Tindall Ltd, pp 83–96

Asfari M, Janjic D, Meda P, Li G, Halban PA, Wollheim CB (1992) Establishment of 2-mercaptoethanol-dependent differentiated insulin secreting cell lines. Endocrinology 130:167–178

Azizkhan JC, Speeg KV, Stromberg K, Goode D (1979) Stimulation of human chorionic gonadotropin by JAr line choriocarcinoma after inhibition of DNA synthesis. Cancer Res 39(6 Pt 1):1952–1959

Bakhti M, Böttcher A, Lickert H (2019) Modelling the endocrine pancreas in health and disease. Nat Rev Endocrinol 15(3):155–171

Balboa D, Saarimäki-Vire J, Otonkoski T (2019) Concise review: human pluripotent stem cells for the modeling of pancreatic β-cell pathology. Stem Cells 37(1):33–41

Barbe A, Bongrani A, Mellouk N, Estienne A, Kurowska P, Grandhaye J et al (2019) Mechanisms of adiponectin action in fertility: An overview from gametogenesis to gestation in humans and animal models in normal and pathological conditions. Int J Mol Sci [Internet] 20(7). [cited 2019 Oct 29]. Available from: http://www.ncbi.nlm.nih.gov/pubmed/30934676

Basak S, Das MK, Srinivas V, Duttaroy AK (2015) The interplay between glucose and fatty acids on tube formation and fatty acid uptake in the first trimester trophoblast cells, HTR8/SVneo. Mol Cell Biochem 401 (1–2):11–19

Basak S, Vilasagaram S, Naidu K, Duttaroy AK (2019) Insulin-dependent, glucose transporter 1 mediated glucose uptake and tube formation in the human placental first trimester trophoblast cells. Mol Cell Biochem 451 (1–2):91–106

Bassalert C, Valverde-Estrella L, Chazaud C (2018) Primitive endoderm differentiation: from specification to epithelialization. Curr Top Dev Biol [Internet] 128:81–104. Available from: http://linkinghub.elsevier.com/retrieve/pii/S0070215317300716

Beebe LF, Kaye PL (1991) Maternal diabetes and retarded preimplantation development of mice. Diabetes 40 (4):457–461

Benazra M, Lecomte M-J, Colace C, Müller A, Machado C, Pechberty S et al (2015) A human beta cell line with drug inducible excision of immortalizing transgenes. Mol Metab 4(12):916–925

Bermejo-Alvarez P, Rosenfeld CS, Roberts RM (2012a) Effect of maternal obesity on estrous cyclicity, embryo development and blastocyst gene expression in a mouse model. Hum Reprod [Internet] 27 (12):3513–3522. Available from: https://academic.oup.com/humrep/article-lookup/doi/10.1093/humrep/des327

Bermejo-Alvarez P, Roberts RM, Rosenfeld CS (2012b) Effect of glucose concentration during in vitro culture of mouse embryos on development to blastocyst, success of embryo transfer, and litter sex ratio. Mol Reprod Dev 79(5):329–336

Biggers JD, McGinnis LK (2001) Evidence that glucose is not always an inhibitor of mouse preimplantation development in vitro. Hum Reprod 16(1):153–163

Bonfanti P, Nobecourt E, Oshima M, Albagli-Curiel O, Laurysens V, Stangé G et al (2015) Ex vivo expansion and differentiation of human and mouse fetal pancreatic progenitors are modulated by epidermal growth factor. Stem Cells Dev 24(15):1766–1778

Brito-Casillas Y, Melián C, Wägner AM (2016) Study of the pathogenesis and treatment of diabetes mellitus through animal models. Endocrinol Nutr [Internet] 63 (7):345–353. Available from: http://linkinghub.elsevier.com/retrieve/pii/S1575092216300481

Brito-Casillas Y, Aranda-Tavío H, Rodrigo-González L, Expósito-Montesdeoca AB, Martín-Rodríguez P, Guerra B, Wägner AM, Fernández-Pérez L (2019) SOCS2$^{-/-}$ mouse as a potential model of macrosomia and gestational diabetes. Eur Med J [Internet]. [cited 2019 Dec 20]. Available from: https://www.emjreviews.com/diabetes/abstract/socs2-mouse-as-a-potential-model-of-macrosomia-and-gestational-diabetes/

Brown K, Heller DS, Zamudio S, Illsley NP (2011) Glucose transporter 3 (GLUT3) protein expression in human placenta across gestation. Placenta 32 (12):1041–1049

Brown HM, Green ES, Tan TCY, Gonzalez MB, Rumbold AR, Hull ML et al (2018) Periconception onset diabetes is associated with embryopathy and fetal growth retardation, reproductive tract hyperglycosylation and impaired immune adaptation to pregnancy. Sci Rep 8 (1):2114

Bruin JE, Rezania A, Xu J, Narayan K, Fox JK, O'Neil JJ et al (2013) Maturation and function of human embryonic stem cell-derived pancreatic progenitors in macroencapsulation devices following transplant into mice. Diabetologia 56(9):1987–1998

Bruin JE, Erener S, Vela J, Hu X, Johnson JD, Kurata HT et al (2014) Characterization of polyhormonal insulin-producing cells derived in vitro from human embryonic stem cells. Stem Cell Res 12(1):194–208

Burke SD, Dong H, Hazan AD, Croy BA (2007) Aberrant endometrial features of pregnancy in diabetic NOD mice. Diabetes 56(12):2919–2926

Candiello J, Grandhi TSP, Goh SK, Vaidya V, Lemmon-Kishi M, Eliato KR et al (2018) 3D heterogeneous islet organoid generation from human embryonic stem cells using a novel engineered hydrogel platform. Biomaterials 177:27–39

Capobianco E, Jawerbaum A, Romanini MC, White V, Pustovrh C, Higa R et al (2005) 15-Deoxy-Delta12,14-prostaglandin J2 and peroxisome proliferator-activated receptor gamma (PPARgamma) levels in term placental tissues from control and diabetic rats: modulatory effects of a PPARgamma agonist on nitridergic and lipid placental metabolism. Reprod Fertil Dev [Internet] 17(4):423–433. [cited 2019 Nov 6]. Available from: http://www.ncbi.nlm.nih.gov/pubmed/15899154

Carlson AJ, Drennan FM (1911) The control of pancreatic diabetes in pregnancy by the passage of the internal secretion of the pancreas of the fetus to the blood of the mother. Am J Physiol Content 28(7):391–395

Chang AS, Dale AN, Moley KH (2005) Maternal diabetes adversely affects Preovulatory oocyte maturation, development, and granulosa cell apoptosis. Endocrinology [Internet] 146(5):2445–2453. [cited 2019 Nov 29]. Available from: https://academic.oup.com/endo/article-lookup/doi/10.1210/en.2004-1472

Chaudhry ZZ, Morris DL, Moss DR, Sims EK, Chiong Y, Kono T et al (2013) Streptozotocin is equally diabetogenic whether administered to fed or fasted mice. Lab Anim 47(4):257–265

Chen Z, Canet MJ, Sheng L, Jiang L, Xiong Y, Yin L et al (2015) Hepatocyte TRAF3 promotes insulin resistance and type 2 diabetes in mice with obesity. Mol Metab 4 (12):951–960

Chi MMY, Pingsterhaus J, Carayannopoulos M, Moley KH (2000) Decreased glucose transporter expression triggers BAX-dependent apoptosis in the murine blastocyst. J Biol Chem 275(51):40252–40257

Chick WL, Warren S, Chute RN, Like AA, Lauris V, Kitchen KC (1977) A transplantable insulinoma in the rat. Proc Natl Acad Sci U S A 74:628–632

Colvin BN, Longtine MS, Chen B, Costa ML, Nelson DM (2017) Oleate attenuates palmitate-induced endoplasmic reticulum stress and apoptosis in placental trophoblasts. Reproduction 153(4):369–380

D'Amour KA, Bang AG, Eliazer S, Kelly OG, Agulnick AD, Smart NG et al (2006) Production of pancreatic hormone–expressing endocrine cells from human embryonic stem cells. Nat Biotechnol 24 (11):1392–1401

Desoye G, Mouzon SH (2007) The human placenta in gestational diabetes mellitus. Diabetes Care 30(Supplement 2):S120–S126

Dickinson JE, Meyer BA, Brath PC, Chmielowiec S, Walsh SW, Parisi VM et al (1990) Placental thromboxane and prostacyclin production in an ovine diabetic model. Am J Obstet Gynecol [Internet] 163(6 Pt 1):1831–1835. [cited 2019 Oct 30]. Available from: http://www.ncbi.nlm.nih.gov/pubmed/2147814

Ding R, Liu XM, Xiang YQ, Zhang Y, Zhang JY, Guo F et al (2018) Altered matrix metalloproteinases expression in placenta from patients with gestational diabetes mellitus. Chin Med J 131:1255–1258

Dontas IA, Marinou KA, Karatzas T (2012) Research in diabetes using animal models. Br J Pharmacol 166 (3):877–894

Dowling D, Corrigan N, Horgan S, Watson CJ, Baugh J, Downey P et al (2014) Cardiomyopathy in offspring of pregestational diabetic mouse pregnancy. J Diabetes Res 2014:624939

Elumalai S, Karunakaran U, Lee IK, Moon JS, Won KC (2017) Rac1-NADPH oxidase signaling promotes CD36 activation under glucotoxic conditions in pancreatic beta cells. Redox Biol 11:126–134

Eriksson UJ, Bone AJ, Turnbull DM, Baird JD (1989) Timed interruption of insulin therapy in diabetic BB/E rat pregnancy: effect on maternal metabolism and fetal outcome. Acta Endocrinol (Copenh) [Internet] 120(6):800–810. [cited 2019 Nov 5]. Available from: http://www.ncbi.nlm.nih.gov/pubmed/2658457

Esakoff TF, Cheng YW, Sparks TN, Caughey AB (2009) The association between birthweight 4000 g or greater and perinatal outcomes in patients with and without gestational diabetes mellitus. Am J Obstet Gynecol 200 (6):672.e1–672.e4

Ezekwe MO, Ezekwe EI, Sen DK, Ogolla F (1984) Effects of maternal streptozotocin-diabetes on fetal growth, energy reserves and body composition of newborn pigs. J Anim Sci [Internet] 59(4):974–980. [cited 2019 Oct 30]. Available from: http://www.ncbi.nlm.nih.gov/pubmed/6239852

Favaro RR, Salgado RM, Covarrubias AC, Bruni F, Lima C, Fortes ZB et al (2013) Long-term type 1 diabetes impairs decidualization and extracellular matrix remodeling during early embryonic development in mice on occasion of the 30th anniversary of the Laboratory of Reproductive and Extracellular Matrix Biology we dedicate this article to its founder, Professor Paulo Abrahamsohn. Placenta 34(12):1128–1135

Feige JN, Lagouge M, Auwerx J, Feige JN, Lagouge M, Auwerx J (2008) Dietary manipulation of mouse metabolism. In: Current protocols in molecular biology [Internet]. Wiley, Hoboken, pp 29B.5.1–29B.5.12. Available from: http://doi.wiley.com/10.1002/0471142727.mb29b05s84

Frank HG, Gunawan B, Ebeling-Stark I, Schulten HJ, Funayama H, Cremer U et al (2000) Cytogenetic and DNA-fingerprint characterization of choriocarcinoma cell lines and a trophoblast/choriocarcinoma cell hybrid. Cancer Genet Cytogenet 116(1):16–22

Fraser RB, Waite SL, Wood KA, Martin KL (2007) Impact of hyperglycemia on early embryo development and embryopathy: in vitro experiments using a mouse model. Hum Reprod 22(12):3059–3068

Fröhlich JD, Desoye G, König J, Huppertz B (2015) Oxygen and glucose dependent viability of HLA-G positive and negative trophoblasts using ACH-3P cells as first trimester trophoblast-derived cell model. J Reprod Heal Med 1(1):4–9

Gauguier D, Bihoreau MT, Ktorza A, Berthault MF, Picon L (1990) Inheritance of diabetes mellitus as consequence of gestational hyperglycemia in rats. Diabetes [Internet] 39(6):734–739. [cited 2019 Oct 30]. Available from: http://www.ncbi.nlm.nih.gov/pubmed/2189765

Ge ZJ, Liang QX, Hou Y, Han ZM, Schatten H, Sun QY et al (2014) Maternal obesity and diabetes may cause DNA methylation alteration in the spermatozoa of offspring in mice. Reprod Biol Endocrinol 12(1):29

Gonzalez E, Jawerbaum A (2006) Diabetic pregnancies: the challenge of developing in a pro-inflammatory environment. Curr Med Chem 13(18):2127–2138

Graham CH, Hawley TS, Hawley RC, MacDougall JR, Kerbel RS, Khoo N et al (1993) Establishment and characterization of first trimester human trophoblast cells with extended lifespan. Exp Cell Res 206 (2):204–211

Green AD, Vasu S, McClenaghan NH, Flatt PR (2015) Pseudoislet formation enhances gene expression, insulin secretion and cytoprotective mechanisms of clonal human insulin-secreting 1.1B4 cells. Pflügers Arch – Eur J Physiol 467(10):2219–2228

Greggio C, De Franceschi F, Figueiredo-Larsen M, Gobaa S, Ranga A, Semb H et al (2013) Artificial three-dimensional niches deconstruct pancreas development in vitro. Development 140(21):4452–4462

Grieco FA, Moore F, Vigneron F, Santin I, Villate O, Marselli L et al (2014) IL-17A increases the expression of proinflammatory chemokines in human pancreatic islets. Diabetologia 57(3):502–511

Guo S, Dai C, Guo M, Taylor B, Harmon JS, Sander M et al (2013) Inactivation of specific β cell transcription factors in type 2 diabetes. J Clin Invest 123 (8):3305–3316

Gurgul-Convey E, Kaminski MT, Lenzen S (2015) Physiological characterization of the human EndoC-βH1 β-cell line. Biochem Biophys Res Commun 464 (1):13–19

Haider S, Meinhardt G, Saleh L, Kunihs V, Gamperl M, Kaindl U et al (2018) Self-renewing trophoblast organoids recapitulate the developmental program of the early human placenta. Stem Cell Rep 11 (2):537–551

Han CS, Herrin MA, Pitruzzello MC, Mulla MJ, Werner EF, Pettker CM et al (2015) Glucose and metformin modulate human first trimester trophoblast function: a model and potential therapy for diabetes-associated Uteroplacental insufficiency. Am J Reprod Immunol 73(4):362–371

Hanafusa T, Miyagawa J, Nakajima H, Tomita K, Kuwajima M, Matsuzawa Y et al (1994) The NOD mouse. Diabetes Res Clin Pract [Internet] 24:S307–S311. [cited 2019 Nov 15]. Available from: https://linkinghub.elsevier.com/retrieve/pii/0168822794902674

Hart NJ, Powers AC (2019) Use of human islets to understand islet biology and diabetes: progress, challenges and suggestions. Diabetologia 62(2):212–222

Heaton SJ, Eady JJ, Parker ML, Gotts KL, Dainty JR, Fairweather-Tait SJ et al (2008) The use of BeWo cells as an in vitro model for placental iron transport. Am J Physiol Cell Physiol 295(5):C1445–C1453

Heim KR, Mulla MJ, Potter JA, Han CS, Guller S, Abrahams VM (2018) Excess glucose induce trophoblast inflammation and limit cell migration through HMGB1 activation of Toll-Like receptor 4. Am J Reprod Immunol 80(5):e13044

Herberg L, Coleman DL (1977) Laboratory animals exhibiting obesity and diabetes syndromes. Metabolism 26(1):59–99

Hiden U, Wadsack C, Prutsch N, Gauster M, Weiss U, Frank H-G et al (2007) The first trimester human trophoblast cell line ACH-3P: a novel tool to study autocrine/paracrine regulatory loops of human trophoblast subpopulations – TNF-α stimulates MMP15 expression. BMC Dev Biol 7(1):137

Hindley CJ, Cordero-Espinoza L (2016) Organoids from adult liver and pancreas: stem cell biology and biomedical utility. Dev Biol 420(2):251–261

Hjort L, Novakovic B, Grunnet LG, Maple-Brown L, Damm P, Desoye G et al (2019) Diabetes in pregnancy and epigenetic mechanisms—how the first 9 months from conception might affect the child's epigenome and later risk of disease. Lancet Diabetes Endocrinol (Lancet Publishing Group) 7:796–806

Holemans K, Caluwaerts S, Poston L, Van Assche FA (2004) Diet-induced obesity in the rat: a model for gestational diabetes mellitus. Am J Obstet Gynecol 190(3):858–865

Hong Y, Ahn H-J, Shin J, Lee JH, Kim J-H, Park H-W et al (2018) Unsaturated fatty acids protect trophoblast cells from saturated fatty acid-induced autophagy defects. J Reprod Immunol 125:56–63

Hrvatin S, O'Donnell CW, Deng F, Millman JR, Pagliuca FW, DiIorio P et al (2014) Differentiated human stem cells resemble fetal, not adult, β cells. Proc Natl Acad Sci U S A 111(8):3038–3043

Huang C, Snider F, Cross JC (2009) Prolactin receptor is required for normal glucose homeostasis and modulation of beta-cell mass during pregnancy. Endocrinology [Internet] 150(4):1618–1626. [cited 2019 Nov 5]. Available from: http://www.ncbi.nlm.nih.gov/pubmed/19036882

Huch M, Bonfanti P, Boj SF, Sato T, Loomans CJM, van de Wetering M et al (2013) Unlimited in vitro expansion of adult bi-potent pancreas progenitors through the Lgr5/R-spondin axis. EMBO J 32(20):2708–2721

Hulme CH, Stevens A, Dunn W, Heazell AEP, Hollywood K, Begley P et al (2018) Identification of the functional pathways altered by placental cell exposure to high glucose: lessons from the transcript and metabolite interactome. Sci Rep 8(1):5270

Illsley NP, Baumann MU (1866) Human placental glucose transport in fetoplacental growth and metabolism. Biochim Biophys Acta Mol basis Dis 2020(2):165359

Jacob HJ, Pettersson A, Wilson D, Mao Y, Lernmark Å, Lander ES (1992a) Genetic dissection of autoimmune type I diabetes in the BB rat. Nat Genet 2(1):56–60

Jacob HJ, Pettersson A, Wilson D, Mao Y, Lernmark Å, Lander ES (1992b) Differential effects of fat and sucrose on the development of obesity and diabetes in C57BL/6J and A/J mice. Nat Genet 2(1):56–60

Jansson T, Wennergren M, Powell TL (1999) Placental glucose transport and GLUT 1 expression in insulin-dependent diabetes. Am J Obstet Gynecol 180 (1 I):163–168

Jansson T, Cetin I, Powell TL, Desoye G, Radaelli T, Ericsson A et al (2006) Placental transport and

metabolism in fetal overgrowth – a workshop report. Placenta 27(SUPPL):109–113

Jastreboff AM (2014) Giving leptin a second chance. Sci Transl Med 6(220):220ec14

Jawerbaum A, White V (2010) Animal models in diabetes and pregnancy. Endocr Rev [Internet] 31(5):680–701. [cited 2019 Nov 1].. Available from: http://www.ncbi.nlm.nih.gov/pubmed/20534704

Jawerbaum A, Gonzalez ET, Catafau JR, Rodriguez RR, Gomez G, Gimeno AL et al (1993) Glucose, glycogen and triglyceride metabolism, as well as prostaglandin production in uterine strips and in embryos from diabetic pregnant rats. Influences of the presence of substrate in the incubation medium. Prostaglandins [Internet] 46(5):417–431. [cited 2019 Oct 31] Available from: http://www.ncbi.nlm.nih.gov/pubmed/8278619

Jiang S, Teague AM, Tryggestad JB, Chernausek SD (2017) Role of microRNA-130b in placental PGC-1α/TFAM mitochondrial biogenesis pathway. Biochem Biophys Res Commun 487(3):607–612

Jin L, Feng T, Shih HP, Zerda R, Luo A, Hsu J et al (2013) Colony-forming cells in the adult mouse pancreas are expandable in Matrigel and form endocrine/acinar colonies in laminin hydrogel. Proc Natl Acad Sci U S A 110(10):3907–3912

Jin L, Feng T, Zerda R, Chen C-C, Riggs AD, Ku HT (2014) In vitro multilineage differentiation and self-renewal of single pancreatic colony-forming cells from adult C57BL/6 mice. Stem Cells Dev 23 (8):899–909

Kaddis JS, Olack BJ, Sowinski J, Cravens J, Contreras JL, Niland JC (2009) Human pancreatic islets and diabetes research. JAMA 301(15):1580–1587

Kaiser N, Nesher R, Donath MY, Fraenkel M, Behar V, Magnan C et al (2005) Psammomys obesus, a model for environment-gene interactions in type 2 diabetes. Diabetes 54(SUPPL. 2):S137–S144

Kataoka M, Kawamuro Y, Shiraki N, Miki R, Sakano D, Yoshida T et al (2013) Recovery from diabetes in neonatal mice after a low-dose streptozotocin treatment. Biochem Biophys Res Commun 430 (3):1103–1108

Kaufmann RC, Amankwah KS, Dunaway G, Maroun L, Arbuthnot J, Roddick JW (1981) An animal model of gestational diabetes. Am J Obstet Gynecol 141 (5):479–482

Kilkenny C, Browne WJ, Cuthill IC, Emerson M, Altman DG (2010) Improving bioscience research reporting: the ARRIVE guidelines for reporting animal research. PLoS Biol [Internet] 8(6):e1000412. Available from: https://dx.plos.org/10.1371/journal.pbio.1000412

Kim JH, Pan JH, Cho HT, Kim YJ (2016a) Black ginseng extract counteracts Streptozotocin-induced diabetes in mice. Irwin N, editor. PLoS One [Internet] 11(1): e0146843. [cited 2019 Nov 29]. Available from: http://dx.plos.org/10.1371/journal.pone.0146843

Kim Y, Kim H, Ko UH, Oh Y, Lim A, Sohn J-W et al (2016b) Islet-like organoids derived from human pluripotent stem cells efficiently function in the glucose responsiveness in vitro and in vivo. Sci Rep 6 (1):35145

Kojima N (2014) In vitro reconstitution of pancreatic islets. Organogenesis 10(2):225–230

Kopp JL, Grompe M, Sander M (2016) Stem cells versus plasticity in liver and pancreas regeneration. Nat Cell Biol 18(3):238–245

Krause M, Keane K, Rodrigues-Krause J, Crognale D, Egan B, De Vito G et al (2014) Elevated levels of extracellular heat-shock protein 72 (eHSP72) are positively correlated with insulin resistance in vivo and cause pancreatic β-cell dysfunction and death in vitro. Clin Sci 126(10):739–752

Krishnan K, Ma Z, Björklund A, Islam MS (2015) Calcium signaling in a genetically engineered human pancreatic β-cell line. Pancreas 44(5):773–777

Kurlawalla-Martinez C, Stiles B, Wang Y, Devaskar SU, Kahn BB, Wu H (2005) Insulin hypersensitivity and resistance to streptozotocin-induced diabetes in mice lacking PTEN in adipose tissue. Mol Cell Biol [Internet] 25(6):2498–2510. [cited 2019 Nov 29]. Available from: http://www.ncbi.nlm.nih.gov/pubmed/15743841

Lager S, Jansson N, Olsson AL, Wennergren M, Jansson T, Powell TL (2011) Effect of IL-6 and TNF-α on fatty acid uptake in cultured human primary trophoblast cells. Placenta 32(2):121–127

Lappas M, Hiden U, Desoye G, Froehlich J, De Mouzon SH, Jawerbaum A (2011) The role of oxidative stress in the pathophysiology of gestational diabetes mellitus. Antioxid Redox Signal 15:3061–3100

Lau C, Sullivan MK, Hazelwood RL (1993) Effects of diabetes mellitus on lactation in the rat. Proc Soc Exp Biol Med 204(1):81–89

Lebreton F, Lavallard V, Bellofatto K, Bonnet R, Wassmer CH, Perez L et al (2019) Insulin-producing organoids engineered from islet and amniotic epithelial cells to treat diabetes. Nat Commun 10(1):4491

Lee J, Sugiyama T, Liu Y, Wang J, Gu X, Lei J et al (2013) Expansion and conversion of human pancreatic ductal cells into insulin-secreting endocrine cells. elife 2: e00940

Lee J, Lee HC, Kim SY, Cho GJ, Woodruff TK (2019) Poorly-controlled type 1 diabetes mellitus impairs LH-LHCGR signaling in the ovaries and decreases female fertility in mice. Yonsei Med J 60(7):667–678

Li G, Lin L, Wang Y, Yang H (2019) 1,25(OH)2D3 protects trophoblasts against insulin resistance and inflammation via suppressing mTOR signaling. Reprod Sci 26(2):223–232

Li M, Rahman ML, Wu J, DIng M, Chavarro JE, Lin Y et al (2020) Genetic factors and risk of type 2 diabetes among women with a history of gestational diabetes: findings from two independent populations. BMJ Open Diabetes Res Care 8(1):e000850

Liao Z, Wang J, Tan H, Wei L (2017) Cinnamon extracts exert intrapancreatic cytoprotection against streptozotocin in vivo. Gene 627:519–523

Lin R, Yuan Z, Zhang C, Ju H, Sun Y, Huang N et al (2020) Common genetic variants in ADCY5 and gestational glycemic traits. Petry CJ, editor. PLoS One [Internet] 15(3):e0230032. [cited 2020 Apr 12]. Available from: https://dx.plos.org/10.1371/journal.pone.0230032

Loomans CJM, Williams Giuliani N, Balak J, Ringnalda F, van Gurp L, Huch M et al (2018) Expansion of adult human pancreatic tissue yields organoids harboring progenitor cells with endocrine differentiation potential. Stem Cell Rep 10(3):712–724

López-Soldado I, Herrera E (2003) Different diabetogenic response to moderate doses of streptozotocin in pregnant rats, and its long-term consequences in the offspring. Exp Diabesity Res 4(2):107–118

Lozano I, Van Der Werf R, Bietiger W, Seyfritz E, Peronet C, Pinget M et al (2016) High-fructose and high-fat diet-induced disorders in rats: impact on diabetes risk, hepatic and vascular complications. Nutr Metab 13:15

Luo H, Chen C, Guo L, Xu Z, Peng X, Wang X et al (2018) Exposure to maternal diabetes mellitus causes renal dopamine D1 receptor dysfunction and hypertension in adult rat offspring. Hypertension 72 (4):962–970

Mage RG, Esteves PJ, Rader C (2019) Rabbit models of human diseases for diagnostics and therapeutics development. Dev Comp Immunol (Elsevier Ltd) 92:99–104

Marchetti P, Schulte AM, Marselli L, Schoniger E, Bugliani M, Kramer W et al (2019) Fostering improved human islet research: a European perspective. Diabetologia 62(8):1514–1516

Markowitz J, Soskin S (1927) Pancreatic diabetes and pregnancy. Am J Physiol Content 79(3):553–558

Martin ME, Garcia AM, Blanco L, Herrera E, Salinas M (1995) Effect of streptozotocin diabetes on polysomal aggregation and protein synthesis rate in the liver of pregnant rats and their offspring. Biosci Rep 15 (1):15–20

Martínez N, Capobianco E, White V, Pustovrh MC, Higa R, Jawerbaum A (2008) Peroxisome proliferator-activated receptor α activation regulates lipid metabolism in the feto-placental unit from diabetic rats. Reproduction 136(1):95–103

Mathew B, Muñoz-Descalzo S, Corujo-Simon E, Schröter C, Stelzer EHK, Fischer SC (2019) Mouse ICM organoids reveal three-dimensional cell fate clustering. Biophys J 116(1):127–141

McClenaghan NH, Barnett CR, Ah-Sing E, Abdel-Wahab YHA, O'Harte FPM, Yoon T-W et al (1996) Characterization of a novel glucose-responsive insulin-secreting cell line, BRIN-BD11, produced by electrofusion. Diabetes 45(8):1132–1140

Miyazaki J-I, Araki K, Yamato E, Ikegami H, ASANO T, Shibasaki Y et al (1990) Establishment of a pancreatic β cell line that retains glucose-inducible insulin secretion: special reference to expression of glucose transporter isoforms∗. Endocrinology 127(1):126–132

Moley KH, Vaughn WK, DeCherney AH, Diamond MP (1991) Effect of diabetes mellitus on mouse pre-implantation embryo development. J Reprod Fertil [Internet] 93(2):325–332. Available from: http://www.ncbi.nlm.nih.gov/pubmed/1787451

Moley KH, M-Y Chi M, Manchester JK, McDougal DB, Lowry OH (1996) Alterations of intraembryonic metabolites in preimplantation mouse embryos exposed to elevated concentrations of glucose: a metabolic explanation for the developmental retardation seen in preimplantation embryos from diabetic Animals1. Biol Reprod 54(6):1209–1216

Moley KH, Chi MM-Y, Knudson CM, Korsmeyer SJ, Mueckler MM (1998) Hyperglycemia induces apoptosis in pre-implantation embryos through cell death effector pathways. Nat Med [Internet] 4 (12):1421–1424. Available from: http://www.nature.com/articles/nm1298_1421

Moon S, Bin KDY, Ko JH, Kim YS (2019) Recent advances in the CRISPR genome editing tool set. Exp Mol Med (NLM Medline) 51:130

Moshref M, Tangey B, Gilor C, Papas KK, Williamson P, Loomba-Albrecht L et al (2019) Concise review: canine diabetes mellitus as a translational model for innovative regenerative medicine approaches. Stem Cells Transl Med (Wiley) 8:450–455

Nakao K (2019) Translational science: newly emerging science in biology and medicine – lessons from translational research on the natriuretic peptide family and leptin. Proc Jpn Acad Ser B Phys Biol Sci 95 (9):538–567

Nandi P, Lim H, Torres-Garcia EJ, Lala PK (2018) Human trophoblast stem cell self-renewal and differentiation: role of decorin. Sci Rep 8(1):8977

Nanobashvili K, Jack-Roberts C, Bretter R, Jones N, Axen K, Saxena A et al (2018) Maternal choline and betaine supplementation modifies the placental response to hyperglycemia in mice and human trophoblasts. Nutrients 10(10):1507

Narushima M, Kobayashi N, Okitsu T, Tanaka Y, Li S-A, Chen Y et al (2005) A human β-cell line for transplantation therapy to control type 1 diabetes. Nat Biotechnol 23(10):1274–1282

Niland JC, Stiller T, Cravens J, Sowinski J, Kaddis J, Qian D (2010) Effectiveness of a web-based automated cell distribution system. Cell Transplant 19(9):1133–1142

Novaro V, Jawerbaum A, Faletti A, Gimeno MA, González ET (1998) Uterine nitric oxide and prostaglandin E during embryonic implantation in non-insulin-dependent diabetic rats. Reprod Fertil Dev [Internet] 10(3):217–223.[cited 2019 Nov 7]. Available from: http://www.ncbi.nlm.nih.gov/pubmed/11596867

Nusrat A, von Eichel-Streiber C, Turner JR, Verkade P, Madara JL, Parkos CA (2001) Clostridium difficile toxins disrupt epithelial barrier function by altering membrane microdomain localization of tight junction proteins. Infect Immun 69(3):1329–1336

Okae H, Toh H, Sato T, Hiura H, Takahashi S, Shirane K et al (2018) Derivation of human trophoblast stem cells. Cell Stem Cell 22(1):50–63.e6

Ota H, Itaya-Hironaka A, Yamauchi A, Sakuramoto-Tsuchida S, Miyaoka T, Fujimura T et al (2013) Pancreatic β cell proliferation by intermittent hypoxia via up-regulation of Reg family genes and HGF gene. Life Sci 93(18–19):664–672

Pagliuca FW, Millman JR, Gürtler M, Segel M, Van Dervort A, Ryu JH et al (2014) Generation of functional human pancreatic β cells in vitro. Cell 159 (2):428–439

Pasek RC, Gannon M (2013) Advancements and challenges in generating accurate animal models of gestational diabetes mellitus. Am J Physiol Endocrinol Metab 305:1327–1338

Pearson JA, Wong FS, Wen L (2016) The importance of the Non Obese Diabetic (NOD) mouse model in autoimmune diabetes. J Autoimmun (Academic Press) 66:76–88

Peng HY, Li MQ, Li HP (2018) High glucose suppresses the viability and proliferation of HTR-8/SVneo cells through regulation of the miR-137/PRKAA1/IL-6 axis. Int J Mol Med 42(2):799–810

Pérez-López L, Boronat M, Melián C, Saavedra P, Brito-Casillas Y, Wägner AM (2019) Assessment of the association between diabetes mellitus and chronic kidney disease in adult cats. J Vet Intern Med 33 (5):1921–1925

Phillips MS, Liu Q, Hammond HA, Dugan V, Hey PJ, Caskey CT et al (1996) Leptin receptor missense mutation in the fatty Zucker rat. Nat Genet 13(1):18–19

Plows JF, Stanley JL, Baker PN, Reynolds CM, Vickers MH (2018a) Molecular sciences the pathophysiology of gestational diabetes mellitus. Int J Mol Sci 19(11): pii: E3342. [cited 2019 Oct 29] Available from: www.mdpi.com/journal/ijms

Plows J, Stanley J, Baker P, Reynolds C, Vickers M (2018b) The pathophysiology of gestational diabetes mellitus. Int J Mol Sci [Internet] 19(11):3342. [cited 2019 Nov 11]. Available from: http://www.mdpi.com/1422-0067/19/11/3342

Poaty H, Coullin P, Peko JF, Dessen P, Diatta AL, Valent A et al (2012) Genome-wide high-resolution aCGH analysis of gestational Choriocarcinomas. Krahe R, editor. PLoS One 7(1):e29426

Priel T, Aricha-Tamir B, Sekler I (2007) Clioquinol attenuates zinc-dependent β-cell death and the onset of insulitis and hyperglycemia associated with experimental type I diabetes in mice. Eur J Pharmacol 565 (1–3):232–239

Ravassard P, Hazhouz Y, Pechberty S, Bricout-Neveu E, Armanet M, Czernichow P et al (2011) A genetically engineered human pancreatic β cell line exhibiting glucose-inducible insulin secretion. J Clin Invest 121 (9):3589–3597

Rezania A, Bruin JE, Riedel MJ, Mojibian M, Asadi A, Xu J et al (2012) Maturation of human embryonic stem cell-derived pancreatic progenitors into functional islets capable of treating pre-existing diabetes in mice. Diabetes 61(554722):1–14

Rezania A, Bruin JE, Arora P, Rubin A, Batushansky I, Asadi A et al (2014) Reversal of diabetes with insulin-producing cells derived in vitro from human pluripotent stem cells. Nat Biotechnol 32(11):1121–1133

Rivron NC, Frias-Aldeguer J, Vrij EJ, Boisset J-C, Korving J, Vivié J et al (2018) Blastocyst-like structures generated solely from stem cells. Nature [Internet] 557(7703):106–111. Available from: http://www.nature.com/articles/s41586-018-0051-0

Rogal J, Zbinden A, Schenke-Layland K, Loskill P (2019) Stem-cell based organ-on-a-chip models for diabetes research. Adv Drug Deliv Rev 140:101–128

Rousseau-Ralliard D, Couturier-Tarrade A, Thieme R, Brat R, Rolland A, Boileau P et al (2019) A short periconceptional exposure to maternal type-1 diabetes is sufficient to disrupt the feto-placental phenotype in a rabbit model. Mol Cell Endocrinol [Internet] 480:42–53. [cited 2019 Mar 29]. Available from: https://www.sciencedirect.com/science/article/pii/S0303720718302910?via%3Dihub#

Russ HA, Parent AV, Ringler JJ, Hennings TG, Nair GG, Shveygert M et al (2015) Controlled induction of human pancreatic progenitors produces functional beta-like cells in vitro. EMBO J 34(13):1759–1772

Saleh L, Prast J, Haslinger P, Husslein P, Helmer H, Knöfler M (2007) Effects of different human chorionic gonadotrophin preparations on trophoblast differentiation. Placenta 28(2–3):199–203

Scharfmann R, Pechberty S, Hazhouz Y, von Bülow M, Bricout-Neveu E, Grenier-Godard M et al (2014) Development of a conditionally immortalized human pancreatic β cell line. J Clin Invest 124(5):2087–2098

Scharfmann R, Didiesheim M, Richards P, Chandra V, Oshima M, Albagli O (2016) Mass production of functional human pancreatic β-cells: why and how? Diabetes Obes Metab 18(Suppl 1):128–136

Schmied BM, Ulrich A, Matsuzaki H, Batra SK, Pour PM, Schmied BM et al (2000) Maintenance of human islets in long term culture. Differentiation 66(4–5):173–180

Schmitz H, Barmeyer C, Fromm M, Runkel N, Foss H-D, Bentzel CJ et al (1999) Altered tight junction structure contributes to the impaired epithelial barrier function in ulcerative colitis. Gastroenterology 116(2):301–309

Schwartz R, Gruppuso PA, Petzold K, Brambilla D, Hiilesmaa V, Teramo KA (1994) Hyperinsulinemia and macrosomia in the fetus of the diabetic mother. Diabetes Care 17(7):640–648

Šeda O, Vieira AR, Proshchina A, Molina-Hernández A, Márquez-Valadez B, Valle-Bautista R et al (2018) Maternal diabetes and fetal programming toward neurological diseases: beyond neural tube defects. Front Endocrinol [Internet] 9:664. [cited 2019 Nov 28]. Available from: www.frontiersin.org

Shahjalal HM, Abdal Dayem A, Lim KM, Jeon T-l, Cho SG (2018) Generation of pancreatic β cells for treatment of diabetes: advances and challenges. Stem Cell Res Ther 9(1):1–19

Sharma A, Zangen DH, Reitz P, Taneja M, Lissauer ME, Miller CP et al (1999) The homeodomain protein IDX-1 increases after an early burst of proliferation during pancreatic regeneration. Diabetes [Internet] 48 (3):507–513. [cited 2019 Oct 30]. Available from: http://www.ncbi.nlm.nih.gov/pubmed/10078550

Shim J-H, Kim J, Han J, An SY, Jang YJ, Son J et al (2015) Pancreatic islet-Like three-dimensional aggregates derived from human embryonic stem cells ameliorate hyperglycemia in Streptozotocin-induced diabetic mice. Cell Transplant 24(10):2155–2168

Shimizu R, Sakazaki F, Okuno T, Nakamuro K, Ueno H (2012) Difference in glucose intolerance between C57BL/6J and ICR strain mice with streptozotocin/nicotinamide-induced diabetes. Biomed Res 33:63–66

Shin J-Y, Jeong J-H, Han J, Bhang SH, Jeong G-J, Haque MR et al (2015) Transplantation of Heterospheroids of islet cells and mesenchymal stem cells for effective angiogenesis and Antiapoptosis. Tissue Eng Part A 21(5–6):1024

Song B, Scheuner D, Ron D, Pennathur S, Kaufman RJ (2008) Chop deletion reduces oxidative stress, improves β cell function, and promotes cell survival in multiple mouse models of diabetes. J Clin Invest 118 (10):3378–3389

Starling S (2019) New therapeutic promise for leptin. Nat Rev Endocrinol (Nature Publishing Group) 15:625

Stirm L, Kovářová M, Perschbacher S, Michlmaier R, Fritsche L, Siegel-Axel D et al (2018) BMI-independent effects of gestational diabetes on human placenta. J Clin Endocrinol Metab 103 (9):3299–3309

Sugimura Y, Murase T, Oyama K, Uchida A, Sato N, Hayasaka S et al (2009) Prevention of neural tube defects by loss of function of inducible nitric oxide synthase in fetuses of a mouse model of streptozotocin-induced diabetes. Diabetologia 52(5):962–971

Sugiyama T, Benitez CM, Ghodasara A, Liu L, McLean GW, Lee J et al (2013) Reconstituting pancreas development from purified progenitor cells reveals genes essential for islet differentiation. Proc Natl Acad Sci 110(31):12691–12696

Surwit RS, Kuhn CM, Cochrane C, McCubbin JA, Feinglos MN (1988) Diet-induced type II diabetes in C57BL/6J mice. Diabetes [Internet] 37(9):1163–1167. Available from: http://www.ncbi.nlm.nih.gov/pubmed/3044882

Suwaki N, Masuyama H, Masumoto A, Takamoto N, Hiramatsu Y (2007) Expression and potential role of peroxisome proliferator-activated receptor gamma in the placenta of diabetic pregnancy. Placenta [Internet] 28(4):315–323. [cited 2019 Nov 6]. Available from: http://www.ncbi.nlm.nih.gov/pubmed/16753211

Takahashi Y, Takebe T, Taniguchi H (2018) Methods for generating vascularized islet-Like organoids via self-condensation. Curr Protoc Stem Cell Biol 45(1):e49

Takebe T, Enomura M, Yoshizawa E, Kimura M, Koike H, Ueno Y et al (2015) Vascularized and complex organ buds from diverse tissues via mesenchymal cell-driven condensation. Cell Stem Cell 16 (5):556–565

Thong EP, Codner E, Laven JSE, Teede H (2020) Diabetes: a metabolic and reproductive disorder in women. Lancet Diabetes Endocrinol 8(2):134–149

Triñanes J, Rodriguez-Rodriguez AE, Brito-Casillas Y, Wagner A, De Vries APJ, Cuesto G et al (2017) Deciphering tacrolimus-induced toxicity in pancreatic β cells. Am J Transplant [Internet] 17(11):2829–2840. Available from: http://www.ncbi.nlm.nih.gov/pubmed/28432716

Tsakmaki A, Fonseca Pedro P, Bewick GA (2020) Diabetes through a 3D lens: organoid models. Diabetologia 27:1–10

Tsonkova VG, Sand FW, Wolf XA, Grunnet LG, Kirstine Ringgaard A, Ingvorsen C et al (2018) The EndoC-βH1 cell line is a valid model of human beta cells and applicable for screenings to identify novel drug target candidates. Mol Metab 8:144–157

Turco MY, Moffett A (2019) Development of the human placenta. Development 146(22):pii: dev163428

Turco MY, Gardner L, Kay RG, Hamilton RS, Prater M, Hollinshead MS et al (2018) Trophoblast organoids as a model for maternal–fetal interactions during human placentation. Nature 564(7735):263–267

Türk G, Rişvanlı A, Çeribaşı AO, Sönmez M, Yüce A, Güvenç M et al (2018) Effect of gestational diabetes mellitus on testis and pancreatic tissues of male offspring. Andrologia [Internet] 50(4):e12976. [cited 2019 Nov 29] Available from: http://doi.wiley.com/10.1111/and.12976

Uchida S, Watanabe S, Aizawa T, Furuno A, Muto T (1979) Polyoncogenicity and insulinoma-inducing ability of BK Virus, a human Papovavirus, in Syrian golden hamsters. J Natl Cancer Inst 63(1):119–126

Van Assche FA, Holemans K, Aerts L (2001) Long-term consequences for offspring of diabetes during pregnancy. Br Med Bull 60:173–182

Vasu S, McClenaghan NH, McCluskey JT, Flatt PR (2013) Cellular responses of novel human pancreatic β-cell line, 1.1B4 to hyperglycemia. Islets 5 (4):170–177

Vaxillaire M, Froguel P (2006) Genetic basis of maturity-onset diabetes of the young [Internet]. Endocrinol Metab Clin N Am 35:371–384. Available from: https://linkinghub.elsevier.com/retrieve/pii/S0889852906000107. [cited 2020 Mar 24]

Vercheval M, De Hertogh R, Pampfer S, Vanderheyden I, Michiels B, De Bernardi P et al (1990) Experimental diabetes impairs rat embryo development during the preimplantation period. Diabetologia [Internet] 33 (4):187–191. [cited 2019 Nov 1]. Available from: http://www.ncbi.nlm.nih.gov/pubmed/2347432

Wang Q, Moley KH (2010) Maternal diabetes and oocyte quality. Mitochondrion 10:403–410

Wang W, Jin S, Ye K (2017) Development of islet organoids from H9 human embryonic stem cells in biomimetic 3D scaffolds. Stem Cells Dev 26 (6):394–404

Wang G, Liang J, Gao LR, Si ZP, Zhang XT, Liang G et al (2018) Baicalin administration attenuates hyperglycemia-induced malformation of cardiovascular system article. Cell Death Dis 9(2):234

Weiss G, Huppertz B, Lang I, Siwetz M, Moser G (2014) First trimester trophoblast cell line ACH-3P as model to study invasion into arteries vs. veins. Placenta 35(9): A99–A100

Wong MK, Wahed M, Shawky SA, Dvorkin-Gheva A, Raha S (2019) Transcriptomic and functional analyses of 3D placental extravillous trophoblast spheroids. Sci Rep 9(1):1–13

Wu L, Song W, Xie Y, Hu L, Hou X, Wang R et al (2018) miR-181a-5p suppresses invasion and migration of HTR-8/SVneo cells by directly targeting IGF2BP2. Cell Death Dis 9(2):16

Wyman A, Pinto AB, Sheridan R, Moley KH (2008) One-cell zygote transfer from diabetic to nondiabetic mouse results in congenital malformations and growth retardation in offspring. Endocrinology 149 (2):466–469

Yamashita H, Shao J, Ishizuka T, Klepcyk PJ, Muhlenkamp P, Qiao L et al (2001) Leptin administration prevents spontaneous gestational diabetes in heterozygous Lepr(db/+) mice: effects on placental leptin and fetal growth. Endocrinology [Internet] 142 (7):2888–2897. [cited 2019 Nov 5]. Available from: http://www.ncbi.nlm.nih.gov/pubmed/11416008

Yamashita H, Shao J, Qiao L, Pagliassotti M, Friedman JE (2003) Effect of spontaneous gestational diabetes on fetal and postnatal hepatic insulin resistance in Leprdb/+ mice. Pediatr Res 53(3):411–418

Yang S-C, Tseng H-L, Shieh K-R (2013) Circadian-clock system in mouse liver affected by insulin resistance. Chronobiol Int [Internet] 30(6):796–810. [cited 2019 Nov 29]. Available from: http://www.tandfonline.com/doi/full/10.3109/07420528.2013.766204

Yin X, Mead BE, Safaee H, Langer R, Karp JM, Levy O (2016) Engineering stem cell organoids. Cell Stem Cell 18(1):25–38

Yu Y, Singh U, Shi W, Konno T, Soares MJ, Geyer R et al (2008) Influence of murine maternal diabetes on placental morphology, gene expression, and function. Arch Physiol Biochem 114(2):99–110

Yung H, Alnæs-Katjavivi P, Jones CJP, El-Bacha T, Golic M, Staff A-C et al (2016) Placental endoplasmic reticulum stress in gestational diabetes: the potential for therapeutic intervention with chemical chaperones and antioxidants. Diabetologia 59(10):2240–2250

Zamudio S, Torricos T, Fik E, Oyala M, Echalar L, Pullockaran J et al (2010) Hypoglycemia and the origin of hypoxia-induced reduction in human fetal growth. PLoS One 5(1):e8551

Zhou Q, Melton DA (2018) Pancreas regeneration. Nature (Nature Publishing Group) 557:351–358

2. The transition from local to global patterns governs the differentiation of mouse blastocysts

PLOS ONE

RESEARCH ARTICLE

The transition from local to global patterns governs the differentiation of mouse blastocysts

Sabine C. Fischer[1¤a], Elena Corujo-Simon[2¤b], Joaquin Lilao-Garzon[2,3], Ernst H. K. Stelzer[1‡*], Silvia Muñoz-Descalzo[2,3‡*]

1 Physikalische Biologie, Buchmann Institute for Molecular Life Sciences, Goethe-Universität Frankfurt am Main, Frankfurt am Main, Germany, **2** Department of Biology and Biochemistry, University of Bath, Bath, England, United Kingdom, **3** Instituto Universitario de Investigaciones Biomédicas y Sanitarias, Universidad Las Palmas de Gran Canaria, Las Palmas de Gran Canaria, Las Palmas de Gran Canaria, Spain

¤a Current address: Center for Computational and Theoretical Biology, Department of Biology, Universität Würzburg, Würzburg, Germany
¤b Current address: Wellcome-MRC Cambridge Stem Cell Institute, Jeffrey Cheah Biomedical Centre Cambridge Biomedical Campus, University of Cambridge, Cambridge, England, United Kingdom
‡ These authors are joint senior authors on this work.
* ernst.stelzer@physikalischebiologie.de (EHKS); silvia.munoz@ulpgc.es (SMD)

Citation: Fischer SC, Corujo-Simon E, Lilao-Garzon J, Stelzer EHK, Muñoz-Descalzo S (2020) The transition from local to global patterns governs the differentiation of mouse blastocysts. PLoS ONE 15 (5): e0233030. https://doi.org/10.1371/journal.pone.0233030

Editor: Gregory M. Kelly, Western University, CANADA

Received: January 21, 2020

Accepted: April 27, 2020

Published: May 15, 2020

Data Availability Statement: For the segmentation and the Delaunay cell graph calculations, we used previously published tools, which can be obtained from the respective references [33,34]. The code for the neighbourhood analyses is available as a Supporting Information file. This further includes the data for data I, III and IV obtained from MINS as .csv files, as well as the processes data as .json files. Data II as well as V-VIII from MINS has previously been published and is available from [22]. The processed data as .json files is included in the Supporting Information files. The minimal

Abstract

During mammalian blastocyst development, inner cell mass (ICM) cells differentiate into epiblast (Epi) or primitive endoderm (PrE). These two fates are characterized by the expression of the transcription factors NANOG and GATA6, respectively. Here, we investigate the spatio-temporal distribution of NANOG and GATA6 expressing cells in the ICM of the mouse blastocysts with quantitative three-dimensional single cell-based neighbourhood analyses. We define the cell neighbourhood by local features, which include the expression levels of both fate markers expressed in each cell and its neighbours, and the number of neighbouring cells. We further include the position of a cell relative to the centre of the ICM as a global positional feature. Our analyses reveal a local three-dimensional pattern that is already present in early blastocysts: 1) Cells expressing the highest NANOG levels are surrounded by approximately nine neighbours, while 2) cells expressing GATA6 cluster according to their GATA6 levels. This local pattern evolves into a global pattern in the ICM that starts to emerge in mid blastocysts. We show that FGF/MAPK signalling is involved in the three-dimensional distribution of the cells and, using a mutant background, we further show that the GATA6 neighbourhood is regulated by NANOG. Our quantitative study suggests that the three-dimensional cell neighbourhood plays a role in Epi and PrE precursor specification. Our results highlight the importance of analysing the three-dimensional cell neighbourhood while investigating cell fate decisions during early mouse embryonic development.

dataset is available at: https://github.com/scfischer/fischer-et-al-2020.git.

Funding: Research in the AK Stelzer is supported by the Deutsche Forschungsgemeinschaft (DFG, CEF-MC II, EXC-115). Research in the Muñoz-Descalzo lab (in Bath) was supported by the University of Bath and a Wellcome Trust Seed Award (109589/Z/15/Z). Research in the Muñoz-Descalzo lab (in Las Palmas) is supported by the ´Viera y Clavijo´ Program from the ACIISI and the ULPGC. JL (in Las Palmas) is supported by the Cabildo de Gran Canaria and the ULPGC. SCF and SMD acknowledge the support by an International Exchanges Grant from The Royal Society (IE141022). The funders had no role in study design, data collection and analysis, decision to publish, or preparation of the manuscript.

Competing interests: The authors have declared that no competing interests exist.

Introduction

During mammalian preimplantation development, two sequential cell fate decisions occur that result in three cell populations (reviewed in [1]). Upon the first decision, cells become either trophectoderm (TE) or inner cell mass (ICM) cells. Descendants of TE cells form the foetal portion of the placenta. The ICM cells make a further decision: they differentiate either into Epiblast (Epi) or into Primitive Endoderm (PrE). Epi cells predominantly give rise to the embryo proper while PrE cell descendants mainly generate the endodermal part of the yolk sac. In mice, three major processes have been proposed for ICM cell differentiation into Epi or PrE [2,3]. In early blastocysts, ICM cells co-express Epi and PrE markers such as NANOG and GATA6, respectively. As time progresses, Epi and PrE progenitors arise. Epi progenitors express high levels of NANOG, and almost no GATA6, while PrE progenitors express high levels of GATA6, and almost no NANOG [3–5]. FGF/MAPK signalling reinforces PrE commitment: Epi progenitors secrete FGF4, which binds to FGFR1 on Epi, and FGFR1 and FGFR2 on PrE biased cells [4,6–11]. This results in a distribution of Epi and PrE progenitors in the ICM without an obvious spatial pattern [3,12,13]. As development progresses, PrE progenitors migrate to occupy their position before the embryo implants. This results in the spatial segregation of the two lineages. PrE progenitors are polarized and positioned at the surface of the ICM, where they form an epithelium in contact with the blastocyst cavity or blastocoele [14–16]. The Epi progenitors occupy a central position between TE and PrE.

Epi versus PrE differentiation has been extensively studied in the context of marker expression dynamics and the involved signalling pathways (reviewed in [1]). Technical developments have made it possible to study cell fate decisions during preimplantation mouse development at single-cell resolution (reviewed in [17]). Invasive studies based on single cell transcriptomics have been used. However, transcriptomic techniques disrupt the cell positional information within the ICM [8,9,11,18,19]. A complementary approach is single cell resolution imaging based on immunofluorescence stainings [4–6,9,13,20–22] or fluorescent reporters [10,23–32]. Combined with quantitative image analysis, the immunofluorescence approach provides protein expression levels together with cell positional information. Applying this technique in our recent study in mouse embryos and ICM organoids has revealed a local cell fate clustering during PrE differentiation [12].

Here, we broaden the three-dimensional analysis of the spatial distribution of NANOG and GATA6 expressing cells in the ICMs of mouse embryos at different stages. We combine the positional information of a cell and its expression levels of NANOG and GATA6 with information of its neighbouring cells to obtain the local cell neighbourhood features and a global positional feature (see Terminology Box). We find a complex pattern in the three-dimensional cell neighbourhood in the ICM of early blastocysts, characterized by local positional features and expression level clusters (see Terminology Box). Highest NANOG expression levels are found in cells with a specific number of neighbours. The GATA6 level of a cell correlates with the levels of GATA6 in its neighbours, resulting in GATA6 expression level clusters. We apply a rule-based computer simulation to show that these two local cell neighbourhood features are sufficient to describe the complex population distribution found in early embryos. We further demonstrate that the simulations are also applicable in a *Nanog* mutant background. As potential regulators of the expression level clustering, we identify NANOG and FGF/MAPK signalling. Patterns in the global positional features start in mid blastocyst and are obvious in late blastocysts with *Nanog* regulating this feature in GATA6 expressing cells.

In summary, we present three-dimensional cell neighbourhood analyses that allow a novel approach in the study of Epi versus PrE differentiation in relation to nearby cells and fate

Terminology box.

General terms	
Cell neighbourhood	Cell vicinity as determined by the Delaunay Cell Graph, this implies that cells in direct contact or at close distance are neighbours (max. 30 μm)
Feature	Measurement used to describe a specific trait (e.g.: the expression level of a fate marker in a cell)
Pattern	Non-random spatial distribution
Measurements to describe the expression pattern in ICM	
Expression levels	NANOG or GATA6 mean fluorescence intensity per nucleus; results in continuous values
Cell state	N+, N-, G+, G- as discrete categories
Population type	Double negative (DN), double positive (DP), NANOG positive and GATA6 negative (N+G-), NANOG negative and GATA6 positive (N-G+), as discrete categories
Cell fate	Epi or PrE
Local cell features	Measurements for an individual cell related to: Positional information (cell nucleus centroid) Continuous expression levels of NANOG and GATA6 Discrete population type Number of neighbours
Local cell neighbourhood	Cells and neighbouring cells (determined by DCG) with all their features
Local positional feature	Fate marker expression levels in a cell vs number of its neighbours
Local expression level feature	Fate marker expression levels in a cell vs fate marker expression levels of its neighbours
Population cluster	Group of neighbouring cells of the same population (discrete clustering, e. g. N+G6- cells in early embryos)
Expression level cluster	Group of neighbouring cells with correlated levels of a fate marker (continuous clustering; e.g. DP cells according to their GATA6 expression levels)
Local cell neighbourhood features	Description of the local cell neighbourhood including: - Local positional feature - Local expression level feature - Population cluster - Expression level cluster
Global positional feature	Expression levels of a cell relative to its distance from the centroid of the ICM

https://doi.org/10.1371/journal.pone.0233030.t001

marker expression levels. Our results point at NANOG and FGF/MAPK-dependent mechanisms as responsible for the spatial arrangement of NANOG and GATA6 expressing cells in the ICM. These mechanisms become obvious in local cell neighbourhood features. Importantly, we present for the first time a signature that correlates with Epi precursor specification.

Materials and methods

Ethics statement

Mouse work was approved by the University of Bath Animal Welfare and Ethical Review Body (AWERB) and undertaken under UK Home Office license PPL 30/3219 in accordance with the Animals (Scientific Procedures) Act incorporating EU Directive 2010/63/EU. Additional mouse work was approved by the Consejería de Agricultura, Ganadería, Pesca y Aguas of the Gobierno de Canarias (CEEA-ULPGC 08/2018).

Mice, embryos and immunohistochemistry

Wild-type CD1 and *Nanog*$^{+/+}$, *Nanog*$^{+/-}$ and *Nanog*$^{-/-}$ embryos were generated by in-house breeding and natural mating. Detection of copulation plug confirmed successful mating; the resulting embryos were then considered embryonic day (E) 0.5. Embryos were isolated in M2

medium (Millipore). Embryos were prepared for immunofluorescence as previously described (89). Primary antibodies used were: anti-NANOG (eBiosciences 14–5761, 1:100), anti-GATA6 (R&D, AF1700, 1:200). Nuclei were stained using DAPI or Hoechst (1:1000, Invitrogen). Embryos were mounted on microscopy slides with Vaseline bridges to prevent their crushing. Three independent immunofluorescence stainings, each with E3.5 and E4.5 embryos from 7 litters, were performed for the first wild-type data set.

Nanog mutant embryos were obtained as previously described [4] and genotyped by NANOG antibody staining.

Imaging and automated image analysis

For the first wild-type data set (S1 and S2 Tables, data I) a total of 45 embryos was imaged in four batches of 19, 15, 2 and 9 embryos. Images were acquired using a Zeiss LSM 510-META and a Plan-Apochromat 63x/1.4 Oil Ph3 objective, with optical section thickness of 1 μm. *Nanog* wild-type, heterozygous and mutant embryos (S1 and S2 Tables, data III and IV) were similarly imaged in 5 confocal sessions using a Zeiss LSM700 and a Plan-Apochromat 40x/1.3 Oil DIC (UV) VIS-IR M27 objective. All images in each imaging session were obtained using the sequential scanning mode, with the same conditions of laser intensity, gain, and pinhole, and were processed in exactly the same way. The range indicator palette option (Zeiss AIM/ZEN software) was used to ensure that no oversaturated images were taken. For a schematic representation of the image and data pre-processing and further analysis, see also S1 Fig. The three-dimensional image stacks were segmented using MINS [33], cells were automatically assigned to ICM or TE, the features of the cell nuclei were extracted including the nuclear centroid and volume, together with the mean intensity of NANOG and GATA6 for each nucleus. The automatically assigned TE or ICM fate was manually checked (S1 Fig Step1). Given the extension of the analysed data sets (over 27.000 cells) a manual correction of the segmentation results was not performed. Extreme errors (over-segmentation and pyknotic nuclei) in the segmentation were removed manually when correcting the classification of TE versus ICM.

Data analysis

The calculations were performed with *Mathematica* 11.1 (Wolfram Research). Details on the total number of embryos and cells in each population type analysed are shown in S1 and S2 Tables. For further details, see S1 Text and S1 Fig.

Pre-processing and staging of data from [22] (data II)

We used the embryos labelled as "littermate", available from GitHub [22]. This resulted in 147 additional data sets (S1 and S2 Tables, data II). Compared to data I, the experimental setup was slightly different. Specifically, a different NANOG antibody was used and the embryos were imaged without being mounted. Given the extra thickness of the samples, the correction of fluorescent decay along the z-axis was required. Furthermore, while the same algorithm was used for the segmentation, a different thresholding method was applied to obtain the four populations (k-means clustering). We used the same cell number-based staging method as the one used for our data set, which resulted in 64 early, 34 mid and 49 late blastocysts. We excluded all NANOG and GATA6 levels from the distribution that were two standard deviations away from the respective mean as we noticed that there were some oversaturated nuclei images. The calculations were performed with *Mathematica* 11.1 (Wolfram Research). For further details, see S1 Text.

Cell graph generation and neighbourhood analyses

We derived a cell graph representation to characterize the spatial distribution of the cells in each embryo in our wild-type data set (data I), 73 *Nanog*$^{+/+}$ or *Nanog*$^{+/-}$ embryos (data III) and 19 *Nanog*$^{-/-}$ (data IV), and the data set from [22] (data II) (S1 Fig, Step 3(ii)).

The calculations were performed with *Mathematica* 11.1 (Wolfram Research). For further details, see S1 Text.

Correlation analyses

The Spearman's correlation analysis and bootstrapping were performed in Matlab R2012b (MathWorks). The simulations of the null model were performed with *Mathematica* 11.1 (Wolfram Research).

To classify the strength of the correlations we used the criteria by Evans [34]:

0.00–0.19: 'very weak'

0.20–0.39: 'weak'

0.40–0.59: 'moderate'

0.60–0.79: 'strong'

0.80–1.0: 'very strong'.

For further details, see S1 Text.

Analyses of global positional feature

We aimed to investigate global patterns within the ICM at all three blastocysts stages. To this end, a reference point is needed. The one that immediately springs to mind is the embryo centroid. However, distributions of cells with respect to the embryo centroid would mainly highlight effects from the sorting process in mid and late embryos. Therefore, we decided to use the ICM centroid as reference point and analysed the expression levels of NANOG and GATA6 with respect to a cell's distance to the ICM centroid. The ICM centroid was determined as the mean of the positions of all ICM cells. For the graphs, the distance in μm was binned into 5 μm intervals, which is the typical radius of an ICM cell.

Rule-based simulations of population composition in ICM of early blastocysts

The calculations were performed with *Mathematica* 11.1 (Wolfram Research). For further details, see S1 Text.

For the simulations shown in Fig 7D (*Nanog* mutant embryos), we use the cell positions, cells proportions from early *Nanog*$^{+/+}$ or *Nanog*$^{+/-}$ embryos (44 embryos; p_{GATA6} = 94% and p_{NANOG} = 78%) and *startNumNeigh* = 9 to simulate the wild-type situation. For the *Nanog* mutants, we set the proportion of N+ cells (p_{NANOG}) to 0.

Statistics

For the comparison of expression levels, Mann-Whitney tests were applied as the distribution do not follow a Gaussian (performed in Matlab [35]). To compare populations proportions, z-tests with Bonferroni corrections were applied. The used statistical test is indicated in the figure legends.

Data accessibility

For the segmentation and the Delaunay cell graph calculations, we used previously published tools, which can be obtained from the respective references [33,36]. The code for the neighbourhood analyses is available as part of the electronic supplementary material. This further includes the data for data I, III and IV obtained from MINS as.csv files, as well as the processes data as.json files. Data II as well as V-VIII from MINS has previously been published and is available from [22]. The processed data as.json files, codes and S1 Video can be found at: https://github.com/scfischer/fischer-et-al-2020.

Results

Pipeline for quantitative three-dimensional neighbourhood analyses of mouse preimplantation development

In this study, we quantitatively analyse the three-dimensional spatial distribution of cell fate markers, taking into account the single cell levels as well as the levels of the neighbouring cells (Figs 1 and S1). The quantitative immunofluorescence (QIF) analysis of NANOG and GATA6 at the single cell level in mouse preimplantation embryos at different stages of development using MINS (Modular Interactive Nuclear Segmentation) provides the cell position within the embryo, the mean expression level per nucleus and the distinction between ICM and TE (Fig 1A(I-II) and 1B, S1 Fig Step1 [33]). Our data set consists of 45 embryos from three independent experimental replicas, imaged in four confocal sessions, and staged based on the total cell number (early: 32–64, mid: 65–90, late: >90 cells; S1 and S2 Tables, data I). Due to variability in the experimental and imaging setup, we observe quantitative differences between replicas (S1 Fig Step 2). To correct this, we align the data according to NANOG and GATA6 threshold values for each experiment (see S1 Text). Based on the common thresholds, we identify four discrete cell populations: double positive (DP: N+ and G6+), double negative (DN: N- and G6-), NANOG+/GATA6- (Epi progenitor) and NANOG-/GATA6+ (PrE progenitor). The proportions of the populations in the ICM at the different developmental stages show similar trends as previously published data (S2A Fig, [22]). In particular, the proportion of DP cells decreases from early to mid to late blastocysts, and the proportion of PrE progenitor cells increases more than the proportion of Epi progenitor cells.

To investigate the three-dimensional distribution of cells, we use the Delaunay Cell Graph (DCG) to approximate the nearest neighbours of each cell (Fig 1A (III), S1 Step 3, see also S1 Text and [12,36]. The population analyses of TE cells neighbouring ICM cells and all TE cells shows that in early and mid embryos, the TE contains a large proportion of cells that is not DN and hence can provide FGF signalling to the ICM cells (S2B and S2C Fig). Therefore, for our analysis, we consider all ICM cells and those TE cells that are neighbouring at least one ICM cell (S1 Fig Step 4).

Consistent with the presence of the blastocoele, we observe a higher number of neighbours, i.e. a higher cell density, close to the ICM centroid compared to the edge of the ICM irrespective of developmental stage and cell population type, except for DN cells in early and mid blastocysts (Figs 1C and S3A). We also find that for all developmental stages, the cells of the different population types have comparable numbers of neighbours (S3B Fig). Altogether, our data processing allows us to obtain for each ICM cell and its neighbours their position, the expression levels for NANOG and GATA6, the population type and the number of neighbours, resulting in a description of the local cell neighbourhood (see Terminology Box) (Fig 1 (IV)).

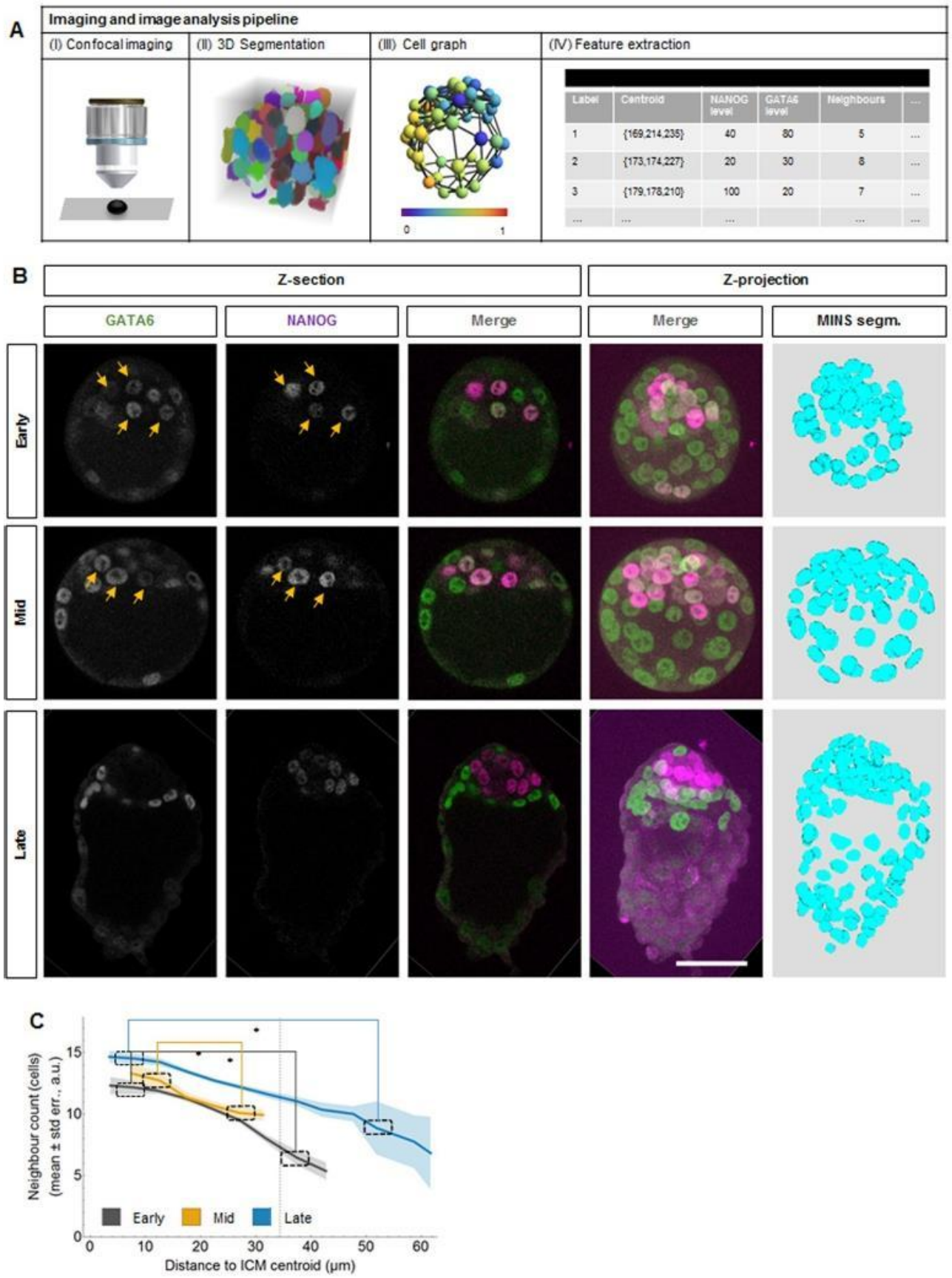

Fig 1. Three-dimensional imaging-based quantitative cell neighbourhood analysis of Epiblast vs Primitive Endoderm fate differentiation in preimplantation mouse embryos (data I). (A) Image analysis pipeline for quantitative characterization of mouse embryos. (I) Imaging with confocal laser scanning fluorescence microscope using sequential scan mode. (II) Segmentation with MINS. (III) A graphical representation of the Delaunay Cell Graph. (IV) Feature extraction for individual cells. See also S1 Fig. **(B)** Representative confocal images of mouse preimplantation embryos immunostained for GATA6 (green) and NANOG (magenta) at the indicated developmental stages. Yellow arrows point to cells co-expressing NANOG and GATA6. All embryos shown were immunostained, imaged and processed together. The first three columns are single confocal z-sections, the last columns show the maximum z-projection of the merged confocal and the segmented images. Scale bar: 50 μm. **(C)** Mean number of neighbouring cells (vertical axis) versus the distance to the centre of the ICM (horizontal axis) in early (grey), mid (yellow) and late (blue) embryos for data I. The shaded regions display the standard errors of the means. Mann-Whitney test with Bonferroni correction; *: $p<0.05$. Details on the number of embryos and cells analysed are in S1 and S2 Tables.

https://doi.org/10.1371/journal.pone.0233030.g001

Similar to previous work, the population analyses further show the presence of DN cells in the ICM already in early blastocysts with proportions increasing as development progresses (S2A Fig; [4,9,20,22]). It has been proposed that these cells might correspond to Epi cells that have downregulated NANOG expression [22]. In order to assess if this cell population has any identifiable pattern of neighbour number or location within the ICM, we analysed their distribution and neighbour number (S3A and S3B Fig). While the other three cell population types have more neighbours closer to the ICM centroid, consistent with a higher cell density, we only find this pattern in the DN cell population in late embryos. This indicates that at the late stage, the DN cells could indeed be Epi cells that have downregulated NANOG. In early embryos, there is no clear pattern and the cell density around DN is comparable at any position within the ICM at this stage. Further studies will be needed to characterize the nature, origin and fate of these DN cells.

In summary, we integrate QIF measurements with an approximation for the nearest neighbours of a cell to obtain a data set that enables studying three-dimensional local cell neighbourhoods in the ICM of early, mid and late mouse blastocysts.

Clustering of population types is observed in the ICM of early embryos

We have recently shown that ICM organoids and mid/late embryos show local clustering of cells with the same population type [12]. Here, we extend this analysis to include early embryos (Figs 2 and S4 for statistical analyses). In the early blastocysts, around 40% of the neighbouring cells of an ICM cell are TE. Surprisingly, we already observe a pattern: the ICM neighbours of DP cells are mostly DP cells and the ICM neighbours of Epi progenitor are either TE or mostly Epi progenitor cells. In mid embryos, the clustering of DP cells and Epi progenitor cells remains, as previously observed [12]. For late blastocysts, we observe the expected pattern. Epi cells have a large proportion of Epi neighbours and the lowest proportion of TE neighbours, as they occupy the internal positions. PrE cells have a larger proportion of TE neighbours and a

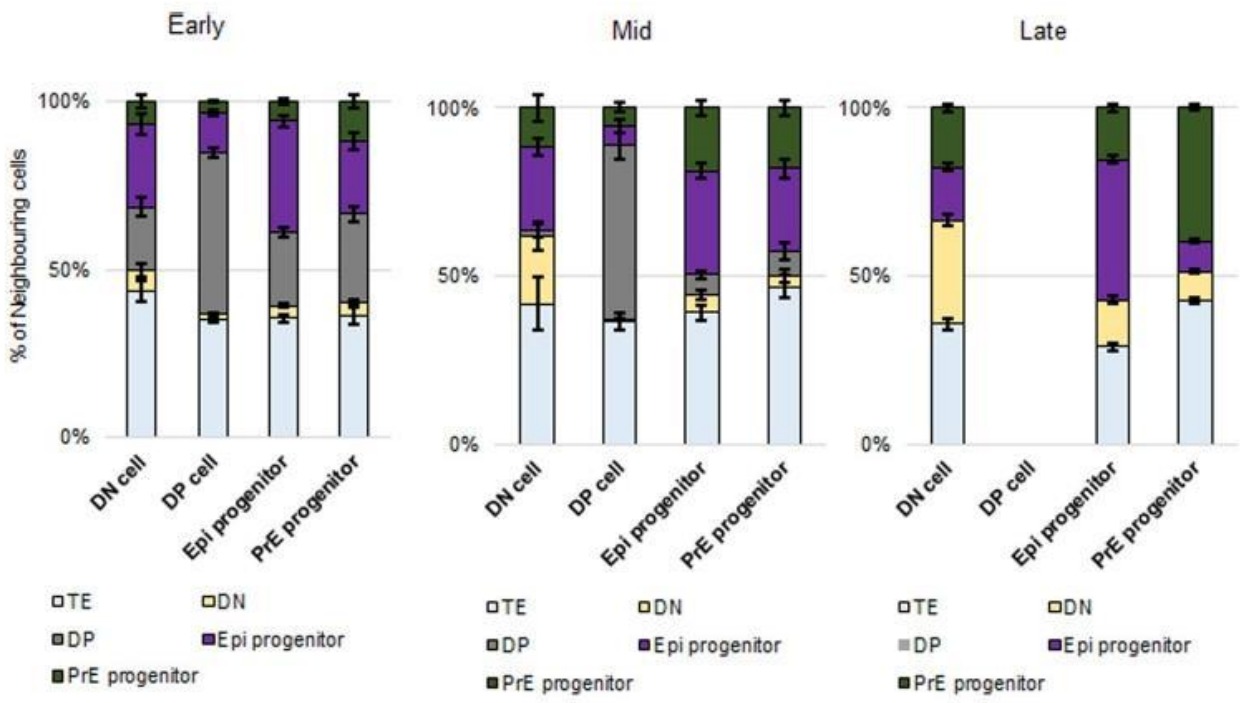

Fig 2. Neighbour composition analysis indicates clustering of Epi progenitor cells and DP cells (data I). The proportion of neighbouring cells of one of the five populations TE, DN, DP, Epi progenitor and PrE progenitor are displayed for DN, DP, Epi progenitor and PrE progenitor cells in in early (left panel), mid (centre) and late (right) embryos for data I. Error bars indicate the standard errors of the means. See S4 Fig for the statistical z-test results. Details on the number of embryos and cells analysed are in S1 and S2 Tables.

https://doi.org/10.1371/journal.pone.0233030.g002

large proportion of PrE neighbours. This is consistent with PrE cells forming an epithelium between the blastocoele and the Epi cells at this late stage with some of them already migrating (see late embryo in Fig 1B, and [37]). Finally, the proportion of PrE neighbours increases for all four populations from early to mid blastocysts, consistent with the increase of PrE cells in the population distribution of the ICM (S2A Fig).

In summary, our results indicate population clustering of DP and Epi progenitor cells, which is already present in early embryos.

DP cells in early blastocysts exhibit GATA6 expression level clusters

Our analyses show a novel population clustering of DP and Epi progenitor cells in early blastocysts. To investigate this further, we step back from the discrete categorisation of the cells and their neighbours into population types based on high or low expression of NANOG and GATA6. Instead, we consider NANOG and GATA6 expression levels as continuous parameters. This approach allows us to measure the correlation strength of the levels of NANOG or GATA6 in a cell with the NANOG or GATA6 levels of its neighbours, respectively. We chose to use Spearman's correlation coefficient as it requires less assumptions, i.e. it does not require bivariate normal data and it measures monotonic, not just linear relationships like the Pearson´s correlation coefficient does (Fig 3 and S5 Fig, [35], see Material and Methods for the classification of correlation strengths, and also S1 Text for further details on the analysis).

Given the dependence of the validity of a correlation analysis on cell number and the typically low number of cells present in mouse preimplantation embryos, we perform a correlation sensitivity analysis (S1 Text). This sensitivity analysis shows that more than 108 cells per cell population are required to obtain robust results with less than 3% variability. For completeness, we included all results in the following plots. However, those that are obtained from less than 108 cells are marked with stripes and should not be relied upon.

The correlation analysis of the GATA6 level in a cell and the median GATA6 level of its neighbours indicates strong positive correlations in DP cells in early and moderate in PrE progenitor cells in late blastocysts (Fig 3A and S5C Fig). The neighbourhood correlation analyses of NANOG result in no correlation, very weak or weak correlations for all populations in early and late blastocysts (Fig 3B and S5D Fig).

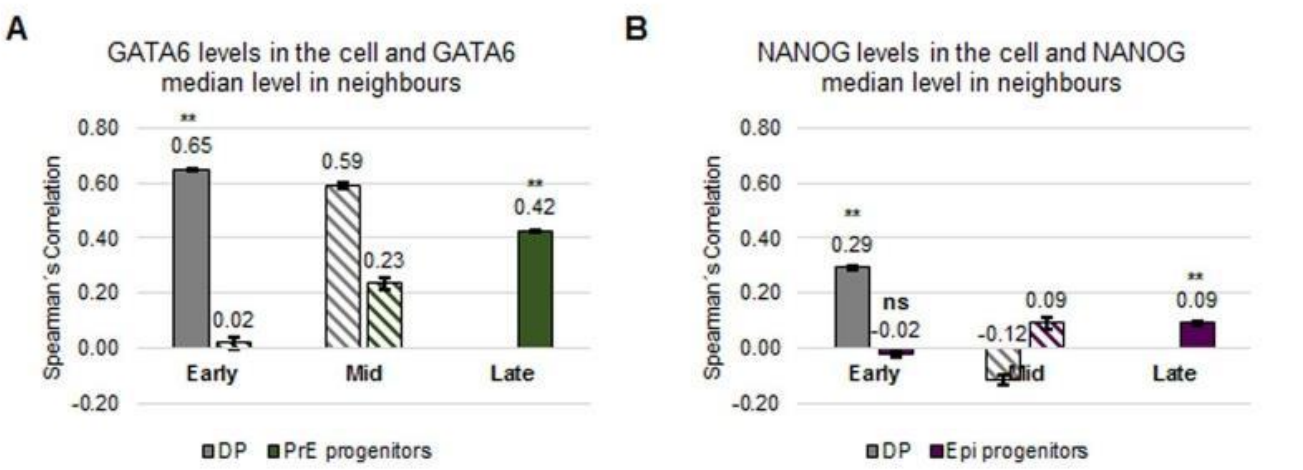

Fig 3. DP cells in early blastocysts cluster together according to their GATA6 levels (data I). (A-B) Spearman's correlation coefficients of GATA6 levels of a cell and median GATA6 levels of its neighbours (A) or of NANOG levels of a cell and median NANOG levels of its neighbours (B) in the indicated populations in the ICM at the indicated embryonic developmental stages for data I. The error bars represent the standard errors calculated by bootstrap sampling the experimental data 100 times. **: $p<0.01$; Mann-Whitney test with Bonferroni correction for the null model; ns: not significant. See also S5 Fig and S1 Text for further details. Striped boxes indicate those populations composed of less than 108 cells. In those cases, no statistical analysis was performed. Details on the number of embryos and cells analysed are in S1 and S2 Tables.

https://doi.org/10.1371/journal.pone.0233030.g003

To ensure that the positive correlation results do not arise randomly or are affected by specific constraints on NANOG/GATA6 distributions, we also investigated whether the correlation values are significantly different from those of a null model (see S1 Text for further details about the null models tested and used). We find that the neighbourhood correlations in the null model are significantly lower than those found for DP cells in early blastocysts and Epi progenitor as well as PrE progenitor cells in late blastocysts. Hence, the correlation values observed for GATA6 do not arise randomly. This is the first time that local correlations of GATA6 levels have been documented for early blastocysts.

It has been proposed that Epi fate reinforces PrE fate in neighbouring cells via FGF4 [4,6–8,11]. This hypothesis would predict a positive correlation of NANOG levels of a cell with GATA6 levels in its neighbouring cells and GATA6 levels of a cell and NANOG levels in its neighbours. However, this hypothesis cannot be tested in this data set as all cell populations in mid blastocysts contain less than 108 cells (S2 Table, S5 Fig; see below and S8C and S8D Fig for more on this issue).

These results suggest that DP cells in the ICM form GATA6 expression level clusters. This local distribution of DP is first present in the early blastocysts. Furthermore, NANOG expressing cells do not cluster according to their expression levels.

NANOG expression levels correlate with the number of neighbours in early blastocysts

We next test whether Epi progenitor clustering is related to positional information within the ICM. To do this, we tested whether there are local or global positional features related to NANOG and GATA6 expression levels (Fig 4).

To investigate the local positional features, we analysed the relation between expression levels and total number of neighbours (Fig 4A and 4B). We observe, particularly in early blastocysts, a peak in NANOG expression in cells with 7 to 14 neighbours, with the maximal level in cells with 9 neighbours (Fig 4A). Three-dimensional illustrations of the number of neighbours and the NANOG levels in the ICMs of the individual early blastocysts support this finding (S6 Fig). Performing the same analyses for GATA6 expression levels, we detected no clear relation at any stage (Fig 4B).

The number of neighbours favouring higher NANOG expression levels in a cell might be an artefact of our DCG approach. To assess this, we performed a sensitivity analysis of the DCG (see S1 Text for further details). It demonstrates that the DCG does not favour a 9 neighbour topology for the ICMs. In early embryos, the DCG favours 2–4 neighbours, which is lower than what we observe in our results for the NANOG analysis.

To investigate further the robustness of our results, we analysed whether there was a specific effect from the particular geometry of the embryos. Therefore, we compared the results for expression level versus number of neighbours with those for the null model, introduced for the correlation analysis (S7A Fig, and see S1 Text for further details). We find that in the null model, the expression levels of NANOG or GATA6 do not correlate with the number of neighbouring cells at any stage.

For the global positional features, we investigate the relation between expression levels and the position of a cell relative to the centroid of the ICM (Fig 4C and 4D, S7B Fig for the null model results, S7C for the statistical analysis of the experimental data, and Materials and Methods). Only in late blastocysts, we observe statistically significant higher NANOG levels closer to the centroid and lower levels away from it (Fig 4C and S7C Fig). This is consistent with Epi cells being located at the centre. The equivalent analysis for GATA6 expressing cells also shows a global positional effect: the highest GATA6 expressing cells are located distally from the ICM

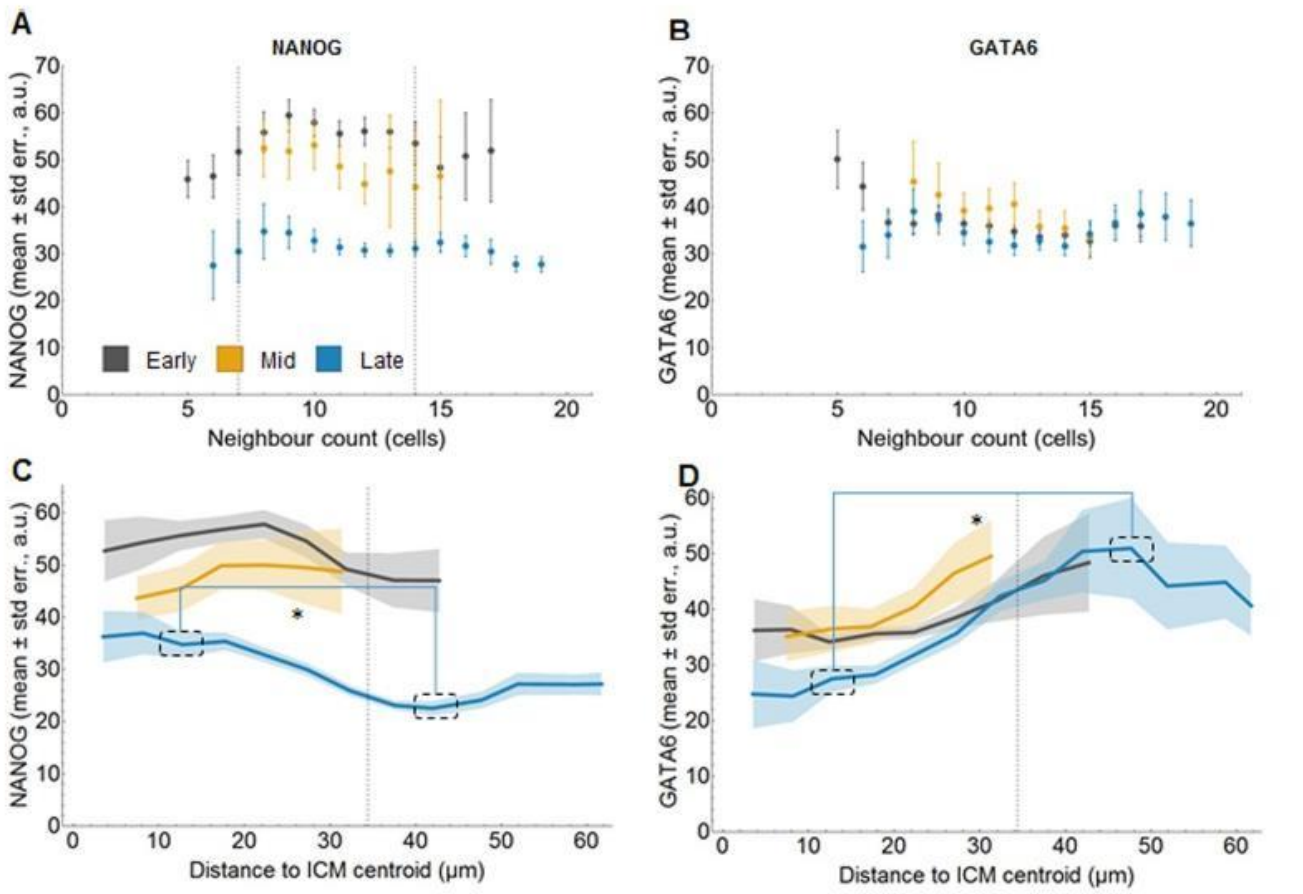

Fig 4. Cells with nine neighbours express highest NANOG levels in early and mid blastocysts (data I). (A-B) Mean level of NANOG (A) or GATA6 (B) (vertical axis) versus the number of neighbours (horizontal axis) for ICM cells in early (grey), mid (yellow) and late (blue) blastocysts for data I. The error bars display the standard errors of the means. See also S7A Fig. **(C-D)** Mean level of NANOG (C) or GATA6 (D) (vertical axis) versus the distance to the ICM centroid (horizontal axis, binned in 5 μm groups) for ICM cells in in early (grey), mid (yellow) and late (blue) blastocysts for data I. Mann-Whitney test with Bonferroni correction; *: $p<0.05$. See also S7B Fig. For simplicity, only selected significant results are indicated for NANOG levels in late embryos, for full statistical results see S7C Fig. Shaded regions display the standard errors of the means. Details on the number of embryos and cells analysed are in S1 and S2 Tables.

https://doi.org/10.1371/journal.pone.0233030.g004

centroid in late blastocysts, consistent with their final position facing the blastocoele (Fig 4D and S7C Fig).

In summary, these results show that there is a clear interrelation between the number of neighbouring cells and NANOG expression levels in early blastocysts. Conversely, the number of neighbours does not correlate with GATA6 expression levels. A global pattern is only present in the ICM of late embryos, likely coincident with the resolution of the sorting process.

GATA6 level clusters arise in DP and PrE progenitor cells in early and mid blastocysts

In the next step, we extend our analysis to a larger data set ([22], S1 and S2 Tables, data II). This allows us to ensure the robustness of our observation. Furthermore, we are able to extend the correlation analysis to the populations for which our initial data (data I) did not include enough cells. The larger data set was generated in a different laboratory with a slightly different experimental set up (see Material and Methods for details). Factors like the variability of the data or the presence of outliers affect the value of a correlation coefficient ([35,38], see also Sup. Info for further details). Therefore, we expect qualitative but not quantitative agreement between the results for data I and data II.

We find that the main conclusions from our previous observations also hold in this second data set: in early blastocysts, we obtain GATA6 expression level clusters in DP cells (Fig 5A)

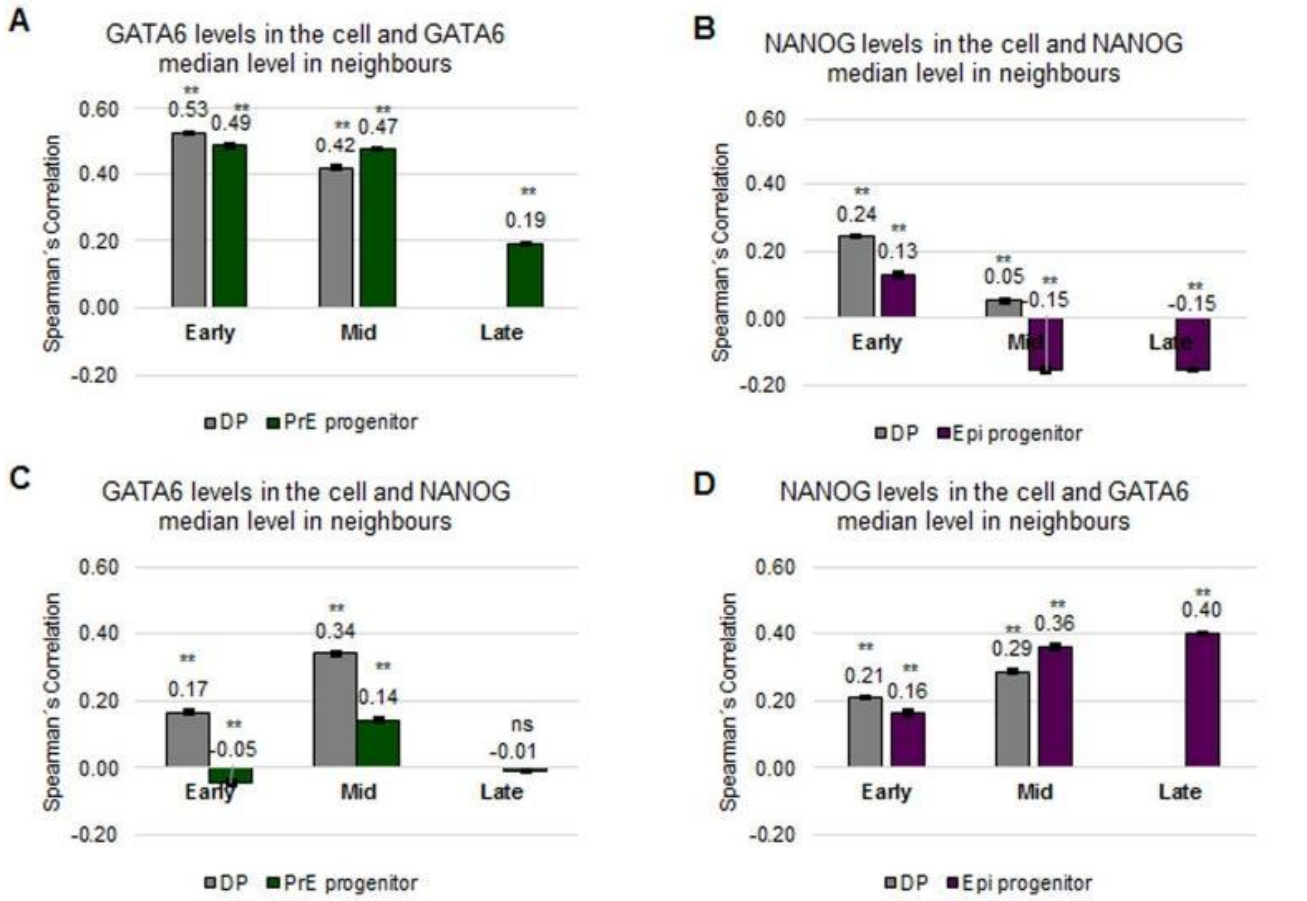

Fig 5. DP as well as PrE progenitor cells in early and blastocysts cluster together according to their GATA6 levels (data II). **(A)** Spearman's correlation coefficients of GATA6 levels of a cell and the median GATA6 levels of its neighbours in the indicated populations in the ICM and embryonic developmental stages (). **": $p<0.01$ Mann-Whitney test with Bonferroni correction for comparison with the null model. The error bars represent the standard errors calculated by bootstrap sampling the experimental data 100 times, here and in B, C and D. See S1 Text for further details. **(B)** Spearman's correlation coefficients of NANOG levels of a cell and the median NANOG levels of its neighbours in the indicated populations in the ICM and embryonic developmental stages. **(C)** Spearman's correlation coefficients of GATA6 levels of a cell and the median NANOG levels of its neighbours in the indicated populations in the ICM and developmental stages. **(D)** Spearman's correlation coefficients of NANOG levels of a cell and the median GATA6 levels of its neighbours in the indicated populations in the ICM and embryonic developmental stages. Details on the number of embryos and cells analysed are in S1 and S2 Tables.

https://doi.org/10.1371/journal.pone.0233030.g005

and NANOG levels are highest in cells with nine neighbours (S8A Fig). NANOG expression level clusters and a correlation between number of neighbours and GATA6 levels was not observed (Fig 5B and S8B Fig). Interestingly, in this second data set, we further find moderate positive correlations for GATA6 in DP cells in mid blastocysts as well as PrE progenitor cells in early and mid blastocysts. These correlations do not arise randomly (Fig 5A, comparison with null model) nor are they an artefact of inter-embryo variability (S8C–S8F Fig).

In addition, we could test the hypothesis of Epi fate reinforcing PrE fate in neighbouring cells [4,6–8,11]. The correlation between GATA6 levels in a cell and NANOG levels in its neighbours is very weak (or weak in the DP cells, S5C Fig) and between NANOG levels in a cell and GATA6 in its neighbours is weak (Fig 5D) or moderate (S5B Fig). Hence Epi fate reinforcing PrE fate in neighbouring cells is still an outstanding question. These results indicate that even if Epi cells can promote PrE fate in the neighbours, the mechanism does not rely on a direct translation of the levels of NANOG in a cell to the GATA6 levels expressed in its neighbours. Furthermore, we observe a global pattern for NANOG expression in mid and late embryos (S8G Fig). In mid embryos, cells at the edge of the ICM have the highest expression of NANOG. In late embryos, we get a pattern with NANOG expression highest in the centre of the ICM and GATA6 expression highest in cells at the edge of the ICM (S8G and S8H Fig and S9 Fig for statistical analysis). Taken together with the results from data I (Fig 4), we conclude that a clear global pattern starts to arise in mid blastocysts.

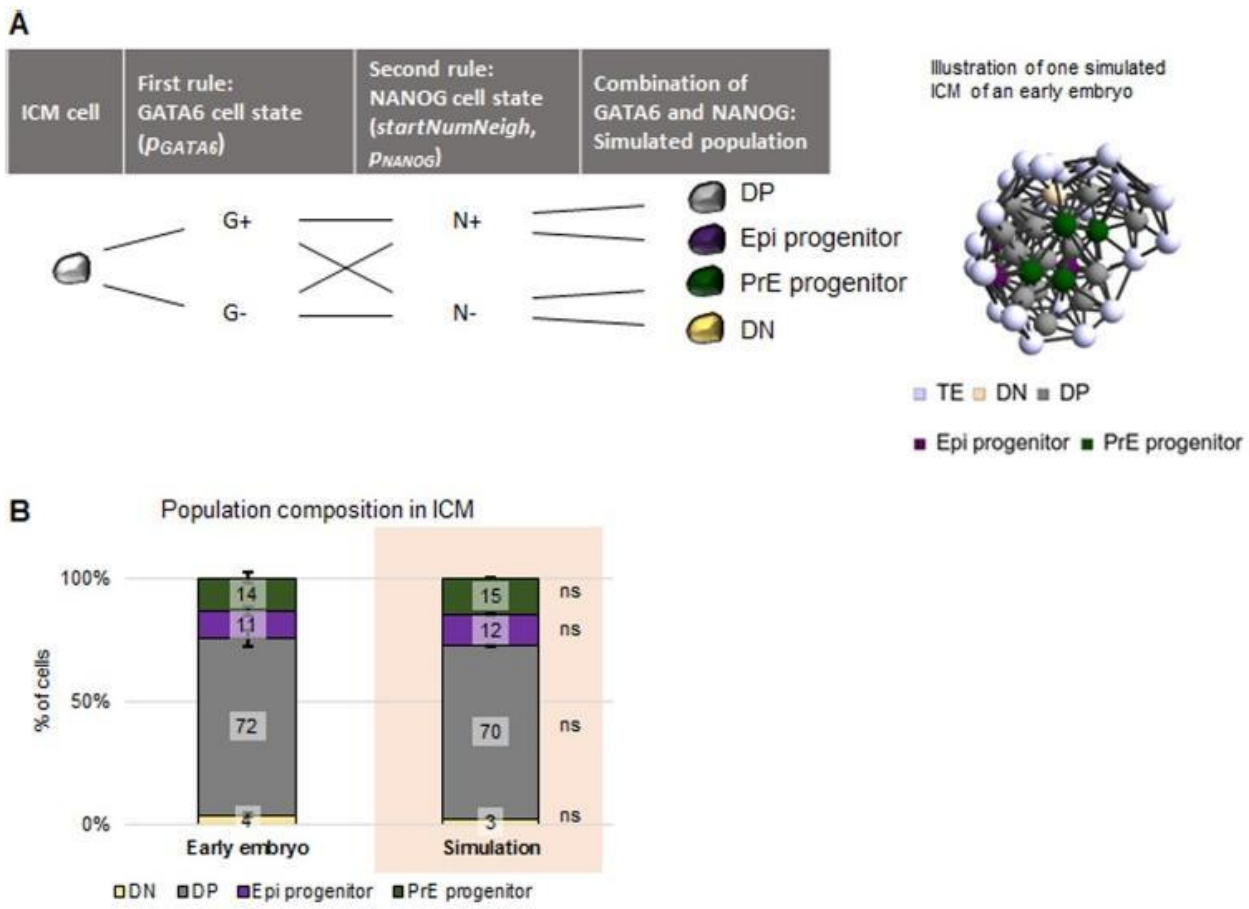

Fig 6. Simulation of two rules recapitulates population composition in early blastocysts. (A) Diagram depicting the population type assignment to the cells in the simulations (left) and an example of a simulated three-dimensional cell distribution (right). See main text and S1 Text for further details on the two rules and parameters. **(B)** Proportion of DN, DP, Epi progenitor and PrE progenitor ICM cells in early blastocysts in data II (first bar) and upon simulating the model (pink background) presented in (A). For the parameters used, see the main text and S1 Text. z-test; *: $p<0.05$. The error bars indicate the standard errors of the means.

https://doi.org/10.1371/journal.pone.0233030.g006

Altogether, our results reveal a novel three-dimensional pattern in the distribution of the population types in ICM cells in early blastocysts. Local positional features and local expression level features characterize this pattern (Figs 3–5 and S5–S9 Figs).

Two simple rules can generate the population composition observed in early blastocysts

Our results indicate that the complex three-dimensional distribution of the population types can be broken down into GATA6 level clustering and NANOG level dependence on number of neighbours. To test this, we implemented a computer simulation based on these two rules and compared the results to the population composition of the experimental data. Different to traditional rule-based models [39], we do not aim at modelling cellular mechanisms. Our approach aims at validating the simple rules that we identified to describe the population type pattern (Fig 6, [12]).

As geometrical basis for the simulations, we used the measured cell centroid positions. To obtain the four populations, we assigned each cell a G6+ or G6- and N+ or N- cell state (see Terminology Box), respectively, according to the following two rules with three parameters (Fig 6A):

1. G6+ cells are clustered according to their GATA6 levels; in the model, this is achieved by randomly assigning the cell state G6+ to a cell with a probability of 85% ($p_{GATA6} = 85\%$), otherwise the cell is G6-;

2. N+ cell state correlates with the number of neighbours; in the model, this is achieved by setting N+ cells as those with nine or close to nine neighbours (*startNumNeigh* = 9) up to 82% (p_{NANOG} = 82%), otherwise the cell is N-.

Hence, we input expression levels for GATA6 and NANOG separately and as output we obtain the four populations as combinations of the two expression levels.

The values for all three parameters are obtained from the experimental data II [22]. The parameters p_{GATA6} and p_{NANOG} are the proportions of ICM cells positive for GATA6 or NANOG expression, respectively. Hence, p_{GATA6} is the proportion of DP and PrE progenitor cells and p_{NANOG} is the proportion of DP and Epi progenitor cells. Combining this information and rules for each cell, we determine its simulated population type. The results of the simulations for these parameter values are comparable to the experimental data, indicating that implementing these two rules allows the generation of the embryos with the observed population composition in early blastocysts (Fig 6B).

To assess the robustness of the model, we perform a parameter sensitivity analysis (see S1 Text). This analysis shows that the simulation results are very robust with respect to the starting number of neighbours. Hence, within the observed range, cell density is not determinant for the proportion of cell fate allocation. The sensitivity analysis further shows that the model is sensitive to changes in the proportion of G6+ and N+ cells. Altogether, this indicates that the main parameter affecting the cell population composition in early embryos is the proportion of cells in a particular cell state.

In summary, these results show that two simple rules for assigning cell state are capable of representing, to a very good approximation, the population composition observed in the ICM of early blastocysts.

NANOG promotes GATA6 expression level clusters

Previous studies indicate that NANOG represses GATA6 during Epi versus PrE differentiation [4]. To analyse if NANOG also regulates GATA6 neighbourhood features, we performed our neighbourhood analyses in *Nanog* mutant embryos (Fig 7).

We analyse and compare *Nanog*$^{+/+}$ or *Nanog*$^{+/-}$ (73 embryos; S1 Table, data III) with *Nanog*$^{-/-}$ (19 embryos; S2 Table, data IV) results. In this case, we pool together *Nanog*$^{+/+}$ and *Nanog*$^{+/-}$ as there is no dosage effect [4,40]. As previously shown, early and mid *Nanog* mutant blastocysts do not show any phenotypic defects until late stages (Fig 7A; [4,7]). The detailed single cell quantitative analysis of GATA6 expression in the absence of *Nanog* shows decreased values in mid and late embryos (S1A Fig), consistent with previous reports indicating PrE specification defects in the mutants [4,7,41].

We start by analysing the clustering of cells according to their GATA6 expression levels (Fig 7B). In the absence of *Nanog*, we still observe clusters of GATA6 expressing cells, reflected in the strong correlation found in GATA6 levels in a cell and median levels in the neighbours in early embryos. However, in the absence of *Nanog*, the correlation decreases from moderate to weak in mid blastocysts. Finally, in the late mutant blastocysts, there are fewer than 108 N-G6+ cells, hence the observed weak anti-correlation cannot be relied upon (see S1 Text). This low cell number probably results from the apoptosis of ICM cells at this stage in *Nanog* mutants [7].

We next analyse the global positional feature (see Terminology Box; Fig 7C). This analysis shows that the distribution of GATA6 expressing cells is altered in the absence of *Nanog* (Fig 7C and S10B Fig for statistical analysis): the clear distribution of highest GATA6 expressing cells located away from the ICM centroid due to cell sorting disappears and cells express similar GATA6 levels independently of their position in late blastocysts.

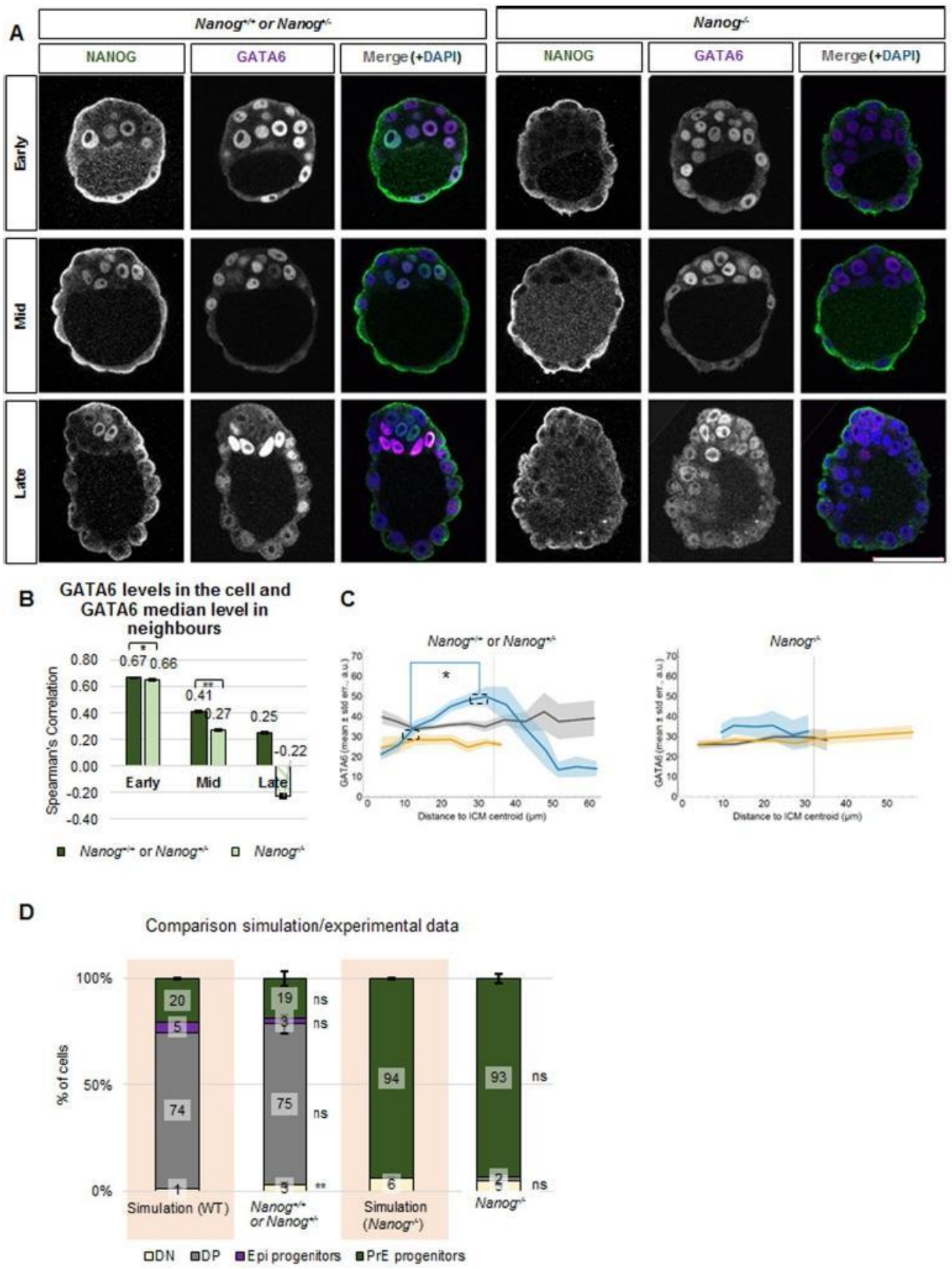

Fig 7. NANOG regulates GATA6 neighbourhood patterning (data III-IV). (A) Representative confocal z-sections of *Nanog*$^{+/+}$ or *Nanog*$^{+/-}$ (left) and *Nanog*$^{-/-}$ (right) embryos immunostained for GATA6 (green) and NANOG (magenta) at the indicated developmental stages. Embryos from the same developmental stage were immunostained, imaged and processed together. Scale bar: 50 μm. **(B)** Spearman's correlation coefficients of the GATA6 level of a cell and the median GATA6 level of its neighbours in G+ populations (DP and PrE progenitor) in the ICM at different embryonic developmental stages in *Nanog*$^{+/+}$ or *Nanog*$^{+/-}$ and *Nanog*$^{-/-}$ embryos for data III and IV. Mann-Whitney test with Bonferroni correction between genotypes; *: $p<0.0.5$. The Mann-Whitney test with Bonferroni correction for the comparison with the null model results in statistically significant differences in all cases (**: $p<0.01$; not shown in the figure). The error bars represent the standard errors calculated by bootstrap sampling the experimental data 100 times. Note that in some cases they are so small that they cannot be appreciated in the figure. DP and PrE progenitor cells in the *Nanog*$^{+/+}$ or *Nanog*$^{+/-}$ were pooled together to simplify the analysis and to increase the total analysed cell number. Striped boxes indicate those populations composed of less than 108 cells. In those cases, no statistical analysis was performed. Details on the number of embryos and cells analysed are in S1 and S2 Tables. **(C)** Mean level of GATA6 (vertical axis) versus the distance to ICM centroid (horizontal axis) for ICM cells in *Nanog*$^{+/+}$ or *Nanog*$^{+/-}$

(left) and *Nanog*$^{-/-}$ (right) early (grey), mid (yellow) and late (blue) blastocysts for data III and IV. Mann-Whitney test with Bonferroni correction; *: $p<0.05$. For simplicity, only selected significant results are indicated, for GATA6 expression levels. For full statistical results, see S9 Fig. Shaded regions indicate the standard errors of the means. Details on the number of embryos and cells analysed are in S1 and S2 Tables. **(D)** Proportion of simulated DN, DP, Epi progenitor and PrE progenitor ICM cells in wild-type or *Nanog*$^{-/-}$ early blastocysts (left, pink background) and proportions obtained in the experimental data (right, data III and IV). Error bars indicate the standard errors of the mean. z-test; **: $p<0.01$. Note: the DP population present in the *Nanog*$^{-/-}$ mutant embryos corresponds to five cells, which lie above the calculated threshold. Details on the number of embryos and cells analysed are in S1 and S2 Tables.

https://doi.org/10.1371/journal.pone.0233030.g007

Finally, we were interested in testing whether our simulations can generate the population composition in *Nanog* mutants (Fig 7D). To simulate the wild-type situation, we use data from early *Nanog*$^{+/+}$ or *Nanog*$^{+/-}$ embryos (44 embryos; see Material and Methods). In the *Nanog* mutant simulations, we set the proportion of N+ cells to 0. We did not detect any statistically significant differences between simulations and experimental results both in *Nanog*$^{+/+}$ or *Nanog*$^{+/-}$ and *Nanog*$^{-/-}$ embryos. Hence, our model is also capable of reproducing the mutant phenotype.

Note: we also had access to quantitative single cell data from a previously published data set composed of 19 *Gata6*$^{+/+}$, 28 *Gata6*$^{+/-}$, and 15 *Gata6*$^{-/-}$ embryos (5). However, we decided not to perform an analysis, since in most cases, the number of cells per population type was below 108 cells.

Altogether, these results suggest NANOG is involved in the neighbourhood regulation of GATA6 expressing cells, coordinating GATA6 expression levels to form the observed clusters and their global position in late embryos.

FGF/ERK signalling promotes GATA6 expression level clusters and inhibits NANOG expression level clusters

As NANOG and GATA6 expression is affected by FGF/ERK signalling (reviewed in [42]), we next investigated if this signalling pathway is involved in the regulation of the local three-dimensional cell neighbourhood features (see Terminology Box). We used the available data sets (Fig 8; [22]; S1 and S2 Tables, data V-VIII). We focused our three-dimensional analyses on mid blastocysts treated for 24 h or 20 h with PD03, an inhibitor of FGF/ERK signalling. This regime promotes NANOG upregulation, without completely abolishing GATA6 expression (S1A and S1B Fig). The data set also includes the use of an FGFRi, however in most cases, the number of cells per population type was below 108 cells. Hence, an analysis of this data would not yield reliable results. The data set further includes FGF4 treatments, which result in almost entirely PrE progenitor cells and therefore do not allow investigating the effect on NANOG or GATA6 neighbourhood features.

We first analyse the effect of the decreased FGF/ERK signalling on GATA6 expression level clustering. This shows decreased GATA6 correlation between PrE progenitor cells and their neighbours (Fig 8A). These results indicate that active FGF/ERK signalling is required to coordinate GATA6 expression levels between neighbouring cells to form the clusters. Concomitantly, we also observe an increased NANOG correlation between Epi progenitor cells and their neighbours, which reflects a NANOG expression level clustering for this population (Fig 8B).

The analysis of the local positional features (see Terminology Box) gives inconclusive results, as the control-cultured embryos did not show the clear pattern observed in the freshly flushed embryos (S12A and S12B Fig). The same applies for the global positional features related to GATA6 expression levels and cell position within the ICM (S12C and S12D Fig). Regarding global positional features related to the NANOG expression levels, there are no

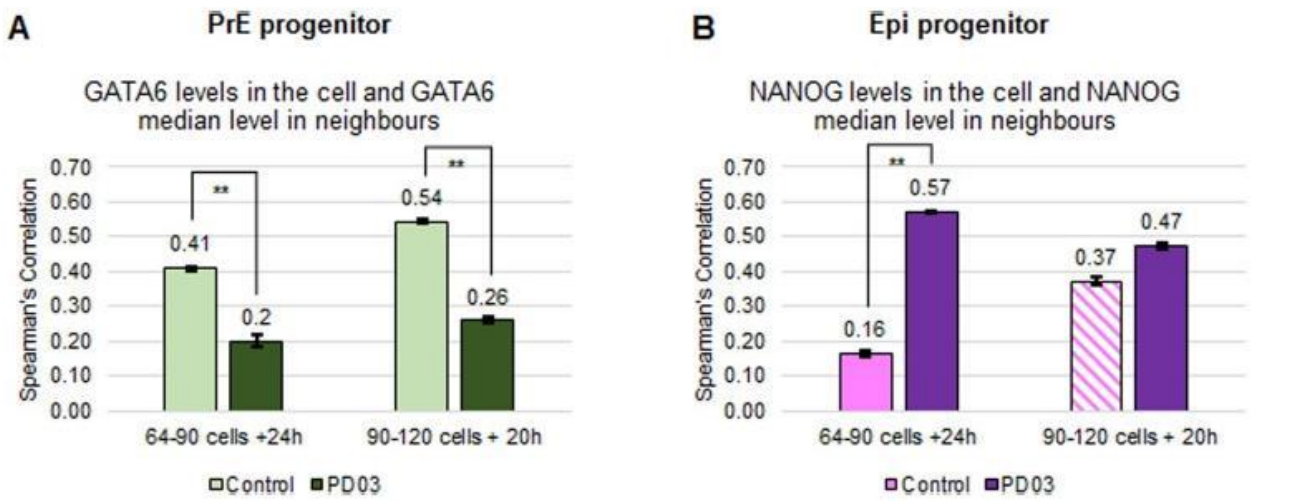

Fig 8. Inhibition of FGF/MAPK signalling inhibits GATA6 clusters and promotes NANOG clusters (data V-VIII). **(A-B)** Spearman's correlation coefficients of GATA6 levels of a cell and the median GATA6 levels of its neighbours in PrE progenitor cells (A) or NANOG levels of a cell and the median levels of its neighbours in Epi progenitor cells (B) in control (light green or magenta, respectively; data V and VI) and PD03 treated embryos for 24 h or 20 h (dark green or magenta, respectively; data VII and VIII). The error bars represent the standard errors calculated by bootstrap sampling the experimental data 100 times The Mann-Whitney test with Bonferroni correction for the comparison with the null model results in statistically significant differences in all cases (**: $p<0.01$; not shown in the figure). Striped boxes indicate those populations composed of less than 108 cells. In those cases, no statistical analysis was performed. Details on the number of embryos and cells analysed are in S1 and S2 Tables 1. See also S11 and S12 Figs.

https://doi.org/10.1371/journal.pone.0233030.g008

differences between control and treated embryos, albeit the absolute levels: highest NANOG expressing cells are closest to the centroid, consistent with these embryos being in late stages (S12E and S12F Fig).

These results, together with previously published results, are consistent with a scenario in which active FGF/ERK signalling is required for regulating NANOG expression in neighbouring cells, and for generating GATA6 expression level clusters.

Discussion

In this study, we present a single cell quantification study, which includes three-dimensional neighbourhood analyses to evaluate how NANOG and GATA6 expressing cells are positioned within the ICM with respect to local and global features during cell fate decisions in mouse embryos. The cell neighbourhood is defined by the levels of fate markers expressed by the cell and its neighbours, the number of neighbouring cells and the population type of the cell and its neighbours. We also study a global positional feature by calculating the position of the cell relative to the ICM centroid. These novel three-dimensional analyses allow us to propose a model of how Epi and PrE fates arise from the early blastocyst based on cell neighbourhood descriptors and relative cell position dependant on FGF/MAPK signalling (Fig 9).

Three-dimensional cell graphs provide local cell neighbourhood

Cell fate decisions rely on groups (communities) of cells showing a coordinated and collective behaviour to achieve the determined fate [43]. Hence, the features of an individual cell have to be put into context of the cell neighbourhood. This need for investigating small groups of cells has also been identified in other developmental contexts [44]. Despite advancements in three-dimensional imaging of developing tissues, investigating the local cell neighbourhood features remains challenging. Even high-end imaging and image analysis protocols focus on the nucleus [45] and rarely include the cell membrane [46], because the number of markers is restricted and the segmentation methods of three-dimensional membrane structures are only slowly evolving [47]. We have shown that the Delaunay Cell Graph (DCG) allows the

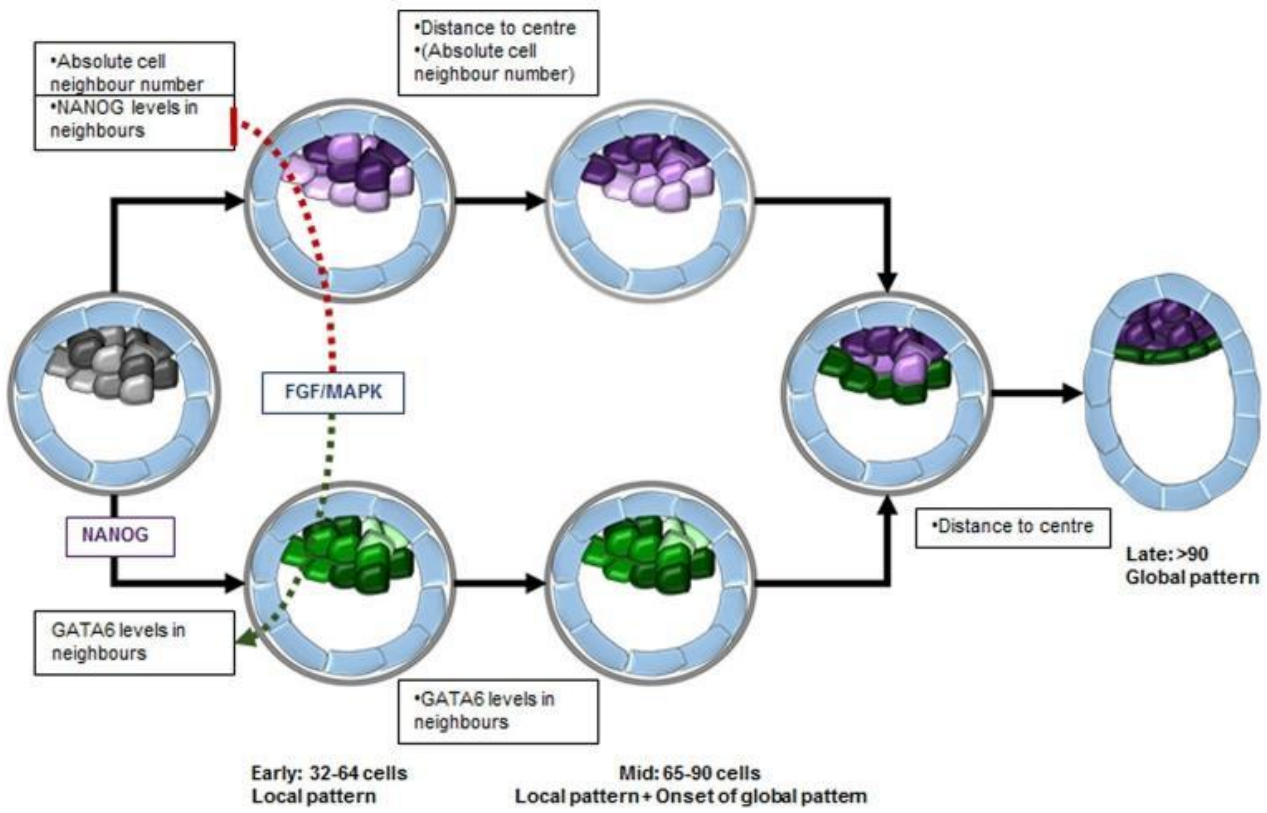

Fig 9. Model for transition from local to global patterns during cell fate decision in the ICM from early to late blastocysts. In early blastocysts, the majority of the ICM cells co-express NANOG and GATA6 but at different levels following a three-dimensional local pattern. NANOG levels in a cell correlate with the absolute cell neighbour number: cells with nine neighbours express the highest NANOG levels. GATA6 levels in a cell correlate with the average level expressed in its neighbours, resulting in clusters of cells with similar levels. FGF/MAPK signalling inhibits NANOG expression level clusters, which in turn, likely via NANOG inhibition on GATA6, promote GATA6 clusters. In mid blastocysts, the local patterns are comparable to those in early blastocysts and a global pattern starts to arise in NANOG expressing cells. In late blastocysts, the cells are segregated into two distinct cell groups and show a clear global pattern: NANOG expressing cells are located closest to the ICM centroid, while GATA6 expressing cells are away from the centroid. Hence, expression patterns occur already in early blastocysts, evolve in mid blastocysts and resolve in late blastocysts before the embryo implants. Grey represents NANOG-GATA6 co-expressing cells, purple represents NANOG expression in cells, and green represents GATA6 expression in cells.

https://doi.org/10.1371/journal.pone.0233030.g009

approximation of the cell neighbourhood from image data for nuclei. Our analysis combines local cell features, providing a good description of the individual cells and the structure of the tissue [12,22,33,36], with correlation analyses, enabling the identification of relationships between two variables [35]. Extending the correlation analysis by the rule-based computer simulation provides a means to describe quantitatively complex three-dimensional population distributions during cell fate decision that is readily applicable to other systems.

To perform a reliable analysis, sufficient amounts of data are required. For the mouse embryos, a robust correlation analysis requires at least 108 cells per measurement. Therefore, a good strategy for future analyses of different signalling pathways might be to first test their features in *in vitro* cultures such as ICM organoids [12] or blastoids [48] and only after a thorough analysis, transfer the results back into mouse embryos.

Here, we obtain the spatial distribution of NANOG and GATA6 expressing cells. To our knowledge, these patterns have not been quantified before. However, we believe they are key to advancing in our understanding of cell differentiation in the preimplantation embryos. There are currently two main models for PrE differentiation [49,50]. The main conceptual difference between them is that the model by Schroter et al. suggests that a bistable system for the NANOG-GATA6 interaction is sufficient, while the second work claims that a tristable system is required. While the model by Schroter et al. focuses on the ratio between Epi and PrE cells [49], the model by Tosenberger et al. has been fitted to the prevailing notion of the expression pattern, i.e. PrE progenitor cells are mainly surrounded by Epi progenitor cells (see Fig 3D in

[50]). Our results differ from this proposed pattern. The interesting question is whether a parameter regime exists, for which either of the two models can reproduce the patterns of the three-dimensional local cell neighbourhood.

Early blastocysts exhibit patterns in local positional features and expression level clustering

Our neighbourhood analyses reveal a pattern in the ICM cells of early blastocysts based on NANOG and GATA6 expression levels. Although most of the ICM cells co-express both markers, the levels of each vary among the different cells. This is reflected in patterns of the local positional features and expression level clustering (Fig 9).

NANOG expression levels in the ICM cells correlate with the cellular arrangement. In early embryos, cells with 8 to 10 neighbouring cells display highest NANOG levels. Several mechanisms could link the positional information to NANOG expression levels. Our results are consistent with previous results of mechanical cues inducing high expression of NANOG in the central cells and their differentiation into Epi cells [51]. Furthermore, it has been shown that the spatial confinement of cells in a three-dimensional microenvironment results in the maintenance of pluripotency even in the absence of LIF [52]. In the early mouse embryo, we might observe a similar effect. The mechanical cues might be sensed via Hippo signalling which has been involved in interpreting positional information (reviewed in [53]). Hippo signalling is clearly determining the first fate choice (TE versus ICM) in the mouse embryos [54,55] and the second fate choice (Epi versus PrE) is linked to the first one [56]. What we observe here might be a reflection of this: first and second cell fate decisions being entwined and Hippo signalling being involved in Epi formation as recently shown [57]. In this study, the authors show attenuation of Hippo signalling promoting nuclear accumulation of YAP in the forming epiblast. In the light of our results, it is plausible that the attenuation of the Hippo signalling might start in those cells having high NANOG levels and around 9 neighbours, and hence contribute to epiblast differentiation.

For GATA6, expression level clustering is observed. The expression levels are independent of the cell localization within the ICM. The functional relevance of the clustering effect might be to ensure an early coordinated PrE cell behaviour during their migration in later stages to occupy their final position at the blastocoele. Recent modelling results for cell population development in ICM organoids show that clonal expansion can play a role in clustering [58]. In addition, the substantial cellular rearrangements taking place during preimplantation development [28,59] might have a positive effect on cell fate clustering. Our results using *Nanog* mutant embryos further indicate a direct or indirect regulation of GATA6 expression level clustering by NANOG. Since PrE fate is regulated through FGF/MAPK signalling (reviewed in [60]), this pathway might also be involved in regulating the spatial distribution of GATA6 and NANOG expressing cells (see below).

The three-dimensional analyses of two independent data sets show a qualitative agreement between the results. The quantitative disagreement between the correlation values obtained are due to the mathematical properties of the correlation coefficient [35,38] and not uncommon in the literature [61]. We have previously used correlations between NANOG and OCT4 levels in individual cells as a pluripotency measurement of mouse embryonic stem cell (mESC) populations. The correlation values decrease as cells differentiate. In this scenario, there are quantitative differences between different wild-type cell lines (Tg2A vs $Tcf3^{+/+}$) cultured under the same conditions, which coincided with them having different pluripotency potential. Given the embryonic origin of the mESCs, one can envisage a similar situation in the mouse early embryos. The quantitative differences found in the correlation values between the data

sets might be due to differences in the variability of the measurements related to the experimental setups or embryos being in slightly different developmental stage. All data sets were staged according to total cell number, the usual method to stage preimplantation embryos. However, this method might not be a reliable timing mechanism and variations can have a quantitative effect on accuracy similar to what we observe here [62]. Indeed alternative ways of measuring developmental timing have been proposed, like the number of DP cells we proposed in ICM organoids, (continuous staging; [12]), or morphogenetic events in rabbit embryos [63].

The theoretical model allows us to break down the complex three-dimensional population pattern into two simple rules with three parameters. Eliminating one of the rules reproduces the *Nanog* mutant situation and the experimental results agree with the simulation. Hence, the population composition in ICMs of early embryos can be derived from the local neighbourhood features.

Altogether, our results are consistent with positional information impinging on cell fate decision in early blastocysts. This, together with previous results, suggests that very early in development, when ICM cells are co-expressing NANOG and GATA6, the two transcription factors as well as FGF/MAPK signalling impact on their expression levels and that the cells are already deciding about their fate.

A global pattern of NANOG and GATA6 expression in the ICM starts arising in mid blastocysts

Our results show that the global positional features (see Terminology Box) of NANOG and GATA6 in early blastocysts do not show a pattern. This lack of a pattern might allow for the previously observed plasticity during the cell fate decision process [22,28,64,65].

Starting in mid and fully established in late blastocysts, once the decision has been made and fate reversal does no longer occur, we see the expected distribution. Higher NANOG level expressing cells are located at the centre of the ICM and higher GATA6 level expressing cells are at the edge. Hence, our results indicate that the cell fate specification does not correlate with the global position of a cell in the ICM. Only once the cell fate is specified, the cells arrange in a global pattern.

Our results show that *Nanog* is involved in the evolvement of the global pattern in late blastocysts as in its absence the GATA6 pattern disappears. A previous study has shown that differential adhesion between ICM cells and directional movement, together with differential adhesion between ICM and TE cells or forces pushing from the blastocoele are responsible for the final distribution of Epi and PrE cells in late blastocysts [59,66]. According to the Krupinski study, Epi cells would have stronger adhesion between them than with other cell types, while PrE cells would show a directed movement towards the blastocoele. In this context, the absence of *Nanog* would be interpreted as absence of differential adhesion. This scenario would result in a lack of global pattern, which is in agreement with our data.

FGF/MAPK signalling affects NANOG and GATA6 expression level clustering

It has been shown that FGF/MAPK signalling is the main signalling pathway involved in Epi versus PrE differentiation (reviewed in [60]). Our three-dimensional analyses of FGF/MAPK signalling inhibitor treated embryos also implicates this pathway in the regulation of the three-dimensional local clustering of NANOG and GATA6 expressing cells. We did not obtain a clear effect of this pathway on the local or global positional features. There are several explanations for this: FGF/ERK signalling is not involved in establishing the global pattern, the long-

term culture of embryos affects their global pattern, or the embryos analysed here are in a different stage from the freshly flushed ones (more than 150 cells *versus* less, respectively). We favour the explanation of an issue with the long-term culture of embryos since cultured embryos until E4.5 stage clearly do not have the same shape (spherical) as freshly flushed E4.5 embryos (prolate; compare embryos shown in Fig 1B stages 120–150 and >150 to those shown in Fig 2C in [22]). Furthermore, it has been shown that embryo culture delays their development [67,68]. The change in the overall shape of the cultured embryos together with their delay are key differences that should not be overlooked as they will affect the global pattern and we believe both differences are at the core of the results obtained.

Our results, together with previous work, allow us to suggest the following series of events during cell fate decision making in early embryos. *Fgf4* expression is directly regulated by the OCT4-SOX2 dimer (as is *Nanog*, [69,70]), and it is expressed in a subpopulation of ICM cells [8,9,11]. We hypothesize that the secretion of FGF4 starts, or is higher, in the subpopulation of NANOG positive cells with 8 to 10 neighbours. Binding to (mainly) FGFR1 presented in the cells activates the signalling pathway [9,10]. Activation of the pathway has opposite effects: it promotes autocrine NANOG degradation via ERK1 phosphorylation and paracrine GATA6 upregulation via ERK1/2 phosphorylation [10,23,71,72]. Autocrine NANOG inhibition might result in the low correlation found in NANOG levels between neighbouring cells. Upregulation of GATA6 will result in the upregulation of FGFR2 expression in those cells as suggested by ChIP-seq experiments [73]. GATA6 expression level clusters might be due to neighbouring cells receiving similar levels of FGF4, hence activating the downstream effectors to a similar extend. The clusters might also be related to directed active movement of the cells at this stage towards the cavity [3]. The effect of FGF/MAPK signalling on the GATA6 clustering could be related to both, as signal inhibition results in decreased correlations and reduced cell movement of ICM cells [28].

As *Fgf4* expression depends on NANOG [4], the decrease in GATA6 expression level clustering observed in the absence of NANOG reinforces the idea that the three-dimensional cell neighbourhood features are regulated by FGF/MAPK signalling. However, this poses the question of how FGF4 is propagated extracellularly once secreted and how its activity is inhibited in the direct neighbours. One possibility is that it is via differential expression of heparan sulfate (HS) chains, which has been associated with heterogeneous di-phosphorylated Erk at this embryonic stage [74]. Another alternative is changes in the internalization and spreading related to endocytosis rates as shown for FGF8 in zebrafish embryos [75].

In summary, we propose that the coordinating mechanism behind the three-dimensional distribution of NANOG and GATA6 expressing cells in early blastocysts is FGF/MAPK signalling. However, we cannot rule out that other major signalling pathways involved in patterning fields or groups of cells, such as Notch, Wnt, BMP, Hippo or EGF might also have an input [76]. In support of this, there are reports of Notch signalling involved in early mouse development [29,77,78], as well as Wnt signalling [79,80], BMP signalling [81,82], p38/MAPK signalling [83] and EGF signalling [84]. In the light of our results, it will be important to revisit how these signalling pathways might be involved in cell fate decisions in early blastocysts, investigating how they affect the local cell neighbourhood features and the global positional feature within the ICM.

Supporting information

S1 Text. Full description of the data analysis.
(PDF)

S1 Fig. Schematic diagram of the image analysis and data pre-processing (data I). Step 1: The confocal images of the fixed embryos are segmented with MINS to obtain the centroid, the cell type (ICM or TE) and the mean NANOG and GATA6 expression levels of a nucleus. Subsequently, the cell fate assignment to TE or ICM is manually checked. **Step 2:** Data I, provided in four different independently imaged batches, are aligned according to their thresholds for high NANOG and high GATA6 expression levels. Top: Scatter plots showing the raw values for NANOG (horizontal axis) and GATA6 (vertical axis) levels in ICM cells in early, mid and late blastocysts (left, centre and right, respectively) in arbitrary units (a.u.). Each dot represents the levels in a single cell from 26 early, 4 mid and 15 late blastocysts. Further details on the number of embryos and cells analysed are in S1 and S2 Tables. Bottom: Scatter plots showing NANOG (horizontal axis) and GATA6 (vertical axis) levels in ICM cells in early, mid and late blastocysts (left, centre and right, respectively) after aligning the data sets. Dashed lines represent the threshold levels for NANOG and GATA6. **Step 3: (i)** Illustration of the cell position rescaling for one embryo to account for slight squeezing along the z-axis due to the mounting. **(ii)** Illustration of the Delaunay Cell Graph (DCG) for this embryo. Lines represent neighbourhood relationship between cells. **Step 4:** Selecting the cells that are relevant for the analyses. We analyse the features of the ICM cells and as neighbours we include the ICM cells and the TE cells that are neighbouring at least one ICM cell. Illustration of the selected cells and the DCG (left), and of the table containing the relevant data (right). See S1 Sup. Info. text for further details.
(PDF)

S2 Fig. Population analyses (data I). (A-C) Population analysis of individual embryos staged by total cell number (early: 32–64 cells, mid: 65–90 cells, late >90) of all ICM cells (A), TE cells with ICM neighbouring cells (included in subsequent analyses, B) and all TE cells (C). Error bars indicate the standard errors of the means. Details on the number of embryos and cells analysed are in S1 and S2 Tables.
(PDF)

S3 Fig. Local and global positional features of ICM cells according to their population type (data I). (A) Mean number of neighbouring cells (vertical axis) versus the distance to the ICM centroid (horizontal axis) of the indicated cell populations in ICMs of early (grey), mid (yellow) and late (blue) blastocysts. Shaded regions indicate the standard errors of the means. **(B)** Scatter dot plot showing the total number of neighbouring cells of DN, DP, Epi progenitor and PrE progenitor cells in ICMs of early (left panel), mid (centre) and late (right) embryos. Mann-Whitney test with Bonferroni correction gives no statistically significant results in all the comparisons ($p<0.05$). The red horizontal line indicates the mean values. Details on the number of embryos and cells analysed are in S1 and S2 Tables.
(PDF)

S4 Fig. Neighbour composition statistical analyses (data I). Tables showing the statistical test results (z-test) for a pairwise comparison of cell neighbour type for each cell population type in the different developmental stages for data set I. *: $p<0.05$ (with Bonferroni correction); ns: not significant. E.g. a DN cell has significantly more TE neighbours than DN neighbours. Details on the number of embryos and cells analysed are in S1 and S2 Tables.
(PDF)

S5 Fig. Extended correlation analysis (data I). (A-B) Spearman's correlation coefficients for GATA6 levels of a cell and the median NANOG levels of its neighbours **(A)** and NANOG levels of a cell and the median GATA6 levels of its neighbours **(B)** at different embryonic developmental stages. **: $p<0.01$ Mann-Whitney test with Bonferroni correction for comparison with

the null model (see S1 Text for further details). The error bars represent the standard errors calculated by bootstrap sampling the experimental data 100 times. Striped boxes indicate populations composed by less than 108 cells. In those cases, no statistical analysis was performed. **(C-F)** Scatter dot plots of the expression levels of the indicated fate markers in individual cells (horizontal axis) and the indicated median fate marker levels of their neighbours (vertical axis) in the specified cell population types and developmental stages in arbitrary units (a.u.). Each dot represents a cell. Only those populations composed of more than 108 cells are shown. The Spearman's correlation coefficients are shown (r). Details on the number of embryos and cells analysed are in S1 and S2 Tables.
(PDF)

S6 Fig. Visualisation of relation of number of neighbours of a cell to its NANOG levels in data I. Three-dimensional Illustrations for number of neighbours and NANOG level for all ICM cells in all early blastocysts of data I. For each embryo two illustrations are shown: the normalised absolute difference of the number of neighbours of a cell to nine (left) and the normalised expression level of NANOG (right). Both values are normalised to the maximum in each embryo. I.e. Cells with nine neighbours and maximum NANOG level are shown in red in both images.
(PDF)

S7 Fig. Extended positional features (data I). (A) Mean level of NANOG (left) or GATA6 (right) (vertical axis) versus the number of neighbours (horizontal axis) for the null model simulation of ICM cells of data I in early (grey), mid (yellow) and late (blue) blastocysts. Error bars indicate the standard errors of the means. **(B)** Mean level of NANOG (left) or GATA6 (right) (vertical axis) versus the distance to the ICM centroid (horizontal axis, binned in 5 μm groups) for the null model simulation of ICM cells of data I in early (grey), mid (yellow) and late (blue) blastocysts. Shaded regions indicate the standard errors of the means. **(C)** Tables summarizing the statistically significant results of the Mann-Whitney statistical tests with Bonferroni correction comparing NANOG or GATA6 levels at the indicated positions relative to the ICM centroid; *: $p<0.05$. Related to Fig 4C and 4D.
(PDF)

S8 Fig. Local neighbourhood features for the [22] data set (data II). (A, B) Mean level of NANOG (A) or GATA6 (B) (vertical axis) versus the number of neighbours (horizontal axis) for ICM cells in early (grey), mid (yellow) and late (blue) blastocysts. The tail of the graph for early embryos in (A) is due to DP cells with high NANGOG levels and a large number of neighbours. The error bars indicate the standard errors of the means. **(C-F)** Scatter dot plots of the expression levels of the indicated fate markers in individual cells (horizontal axis) and the indicated median fate marker levels of their neighbours (vertical axis) in the specified cell population types and developmental stages in arbitrary units (a.u.). Each dot represents a cell. The colours represent different embryos. Only those populations with at least a moderate correlation strength, i.e. correlation coefficient greater than 0.4, are shown. **(G, H)** Mean level of NANOG (G) or GATA6 (H) (vertical axis) versus the distance to the ICM centroid (horizontal axis) for ICM cells in early, mid and late blastocysts. Mann-Whitney test between the indicated levels; **: $p<0.05$. For simplicity, only selected significant results are indicated for NANOG levels in mid and late embryos, GATA6 levels in late embryos, full statistical results are shown in S9 Fig. The shaded regions indicate the standard errors of the means. Details on the number of embryos and cells analysed are in S1 and S2 Tables.
(PDF)

S9 Fig. Statistical analysis of marker expression levels versus distance to the ICM centroid for the [22] data set (data II). Tables summarizing the results of the Mann-Whitney statistical tests with Bonferroni correction comparing NANOG (A-B) and GATA6 (C) levels at the indicated positions relative to the ICM centroid in mid (A) and/or late blastocysts (B-C); *: $p<0.05$, ns: not significant. Related to S8G and S8H Fig. Details on the number of embryos and cells analysed are in S1 and S2 Tables.
(PDF)

S10 Fig. Extended results of *Nanog* mutant analysis (data III and IV). (A) Scatter dot plot showing GATA6 expression levels in the indicated cell populations and developmental stages in $Nanog^{+/+}$ or $Nanog^{+/-}$ and $Nanog^{-/-}$; **: $p<0.01$ Mann-Whitney test with Bonferroni correction. The red horizontal line indicates the mean values. **(B)** Table summarizing the results of the Mann-Whitney statistical tests with Bonferroni correction comparing GATA6 levels at the indicated positions relative to the ICM centroid in $Nanog^{+/+}$ or $Nanog^{+/-}$ embryos at the indicated positions; *: $p<0.05$, ns: not significant. Details on the number of embryos and cells analysed are in S1 and S2 Tables.
(PDF)

S11 Fig. NANOG and GATA6 expression levels upon PD03 treatment for 24 h or 20 h from [22] (data V-VIII). (A-B) Scatter dot plots showing the expression levels of NANOG in Epi progenitor cells of embryos cultured for 24 h (A) or 20 h (B) with control (grey) or PD03-containing (red) media; **: $p<0.01$ Mann-Whitney test with Bonferroni correction. **(C-D)** Scatter dot plots showing the expression levels of GATA6 in PrE progenitor cells of embryos treated for 24 h (C) or 20 h (D) with PD03; **: $p<0.01$ Mann-Whitney test with Bonferroni correction; ns: not significant. In all plots, the red horizontal line indicates the mean values. Details on the number of embryos and cells analysed are in S1 and S2 Tables.
(PDF)

S12 Fig. Local and global positional features upon PD03 treatment for 24 h or 20 h from [22] (data V-VIII). (A-B) Mean level of NANOG (vertical axis) versus the number of neighbours (horizontal axis) for ICM cells in embryos cultured for 24 h (A) or 20 h (B) with control (grey) or PD03-containing (red) media. **(C-D)** Mean level of GATA6 (vertical axis) versus the distance to the centre of the ICM (horizontal axis) for ICM cells in embryos treated for 24 h (C) or 20 h (D) with PD03. **(E-F)** Mean level of NANOG (vertical axis) versus the distance to the centre of the ICM (horizontal axis) for ICM cells in embryos treated for 24 h (E) or 20 h (F) with PD03. In all plots, error bars or shaded regions indicate the standard errors of the means, respectively. Details on the number of embryos and cells analysed are in S1 and S2 Tables.
(PDF)

S1 Video. z-stack of early (1), mid (2) and late (3) embryos comparing DGC neighbour assignment and fluorescent immunostaining. The left panels show membrane and/or nuclear staining. The yellow dots indicate DCG calculated neighbouring cells of the cell with an encircled number, that number indicates its number of neighbours; numbers in other cells indicate the number of neighbouring cells of that cell. The right panels show the original confocal images of the embryos shown, stained for NANOG (magenta), GATA6 (green), DAPI (blue) and β-catenin (membrane, red).
(7Z)

S1 Dataset.
(7Z)

S1 Table. Numbers of analysed embryos.
(PDF)

S2 Table. Numbers of analysed cells.
(PDF)

Acknowledgments

We thank Christian Schröter, Jennifer Nichols, Joaquín de Navascués and Alfonso Martínez-Arias for helpful comments and Carl-Magnus Svensson for critical reading of the manuscript. We also want to thank Néstor Sáiz and Kat Hadjantonakis for their comments, sharing their quantitative data through GitHub as well as through personal communication. We also want to thank Claire Chazaud for kindly sharing *Nanog* heterozygous mice. The funders had no role in study design, data collection and analysis, decision to publish, or preparation of the manuscript.

Author Contributions

Conceptualization: Sabine C. Fischer, Ernst H. K. Stelzer, Silvia Muñoz-Descalzo.

Data curation: Elena Corujo-Simon, Joaquin Lilao-Garzon, Silvia Muñoz-Descalzo.

Formal analysis: Sabine C. Fischer.

Funding acquisition: Sabine C. Fischer, Ernst H. K. Stelzer, Silvia Muñoz-Descalzo.

Investigation: Sabine C. Fischer, Ernst H. K. Stelzer, Silvia Muñoz-Descalzo.

Methodology: Sabine C. Fischer, Joaquin Lilao-Garzon, Silvia Muñoz-Descalzo.

Project administration: Sabine C. Fischer, Ernst H. K. Stelzer, Silvia Muñoz-Descalzo.

Resources: Sabine C. Fischer.

Software: Sabine C. Fischer.

Supervision: Sabine C. Fischer, Ernst H. K. Stelzer, Silvia Muñoz-Descalzo.

Validation: Sabine C. Fischer, Silvia Muñoz-Descalzo.

Visualization: Sabine C. Fischer, Silvia Muñoz-Descalzo.

Writing – original draft: Sabine C. Fischer, Silvia Muñoz-Descalzo.

Writing – review & editing: Sabine C. Fischer, Ernst H. K. Stelzer, Silvia Muñoz-Descalzo.

References

1. Bassalert C, Valverde-Estrella L, Chazaud C. Primitive Endoderm Differentiation: From Specification to Epithelialization. Curr Top Dev Biol. 2018; 128: 81–104. https://doi.org/10.1016/bs.ctdb.2017.12.001 PMID: 29477172
2. Lavial F, Bessonnard S, Ohnishi Y, Tsumura A, Chandrashekran A, Fenwick MA, et al. Bmi1 facilitates primitive endoderm formation by stabilizing Gata6 during early mouse development. Genes Dev. 2012; 26: 1445–1458. https://doi.org/10.1101/gad.188193.112 PMID: 22713603
3. Plusa B, Piliszek A, Frankenberg S, Artus J, Hadjantonakis A-K. Distinct sequential cell behaviours direct primitive endoderm formation in the mouse blastocyst. Development. 2008; 135: 3081–3091. https://doi.org/10.1242/dev.021519 PMID: 18725515
4. Frankenberg S, Gerbe F, Bessonnard S, Belville C, Pouchin P, Bardot O, et al. Primitive Endoderm Differentiates via a Three-Step Mechanism Involving Nanog and RTK Signaling. Dev Cell. 2011; 21: 1005–1013. https://doi.org/10.1016/j.devcel.2011.10.019 PMID: 22172669

5. Schrode N, Saiz N, Di Talia S, Hadjantonakis A-K. GATA6 Levels Modulate Primitive Endoderm Cell Fate Choice and Timing in the Mouse Blastocyst. Nih. 2015; 29. https://doi.org/10.1016/j.devcel.2014.04.011

6. Kang M, Piliszek A, Artus J, Hadjantonakis A-K. FGF4 is required for lineage restriction and salt-and-pepper distribution of primitive endoderm factors but not their initial expression in the mouse. Development. 2013; 140: 267–279. https://doi.org/10.1242/dev.084996 PMID: 23193166

7. Messerschmidt DM, Kemler R. Nanog is required for primitive endoderm formation through a non-cell autonomous mechanism. Dev Biol. 2010; 344: 129–137. https://doi.org/10.1016/j.ydbio.2010.04.020 PMID: 20435031

8. Guo G, Huss M, Tong GQ, Wang C, Li Sun L, Clarke ND, et al. Resolution of Cell Fate Decisions Revealed by Single-Cell Gene Expression Analysis from Zygote to Blastocyst. Dev Cell. 2010; 18: 675–685. https://doi.org/10.1016/j.devcel.2010.02.012 PMID: 20412781

9. Kang M, Garg V, Hadjantonakis AK. Lineage Establishment and Progression within the Inner Cell Mass of the Mouse Blastocyst Requires FGFR1 and FGFR2. Dev Cell. 2017; 41: 496–510.e5. https://doi.org/10.1016/j.devcel.2017.05.003 PMID: 28552559

10. Molotkov A, Mazot P, Brewer JR, Cinalli RM, Soriano P. Distinct Requirements for FGFR1 and FGFR2 in Primitive Endoderm Development and Exit from Pluripotency. Dev Cell. 2017; 41: 511–526.e4. https://doi.org/10.1016/j.devcel.2017.05.004 PMID: 28552557

11. Ohnishi Y, Huber W, Tsumura A, Kang M, Xenopoulos P, Kurimoto K, et al. Cell-to-cell expression variability followed by signal reinforcement progressively segregates early mouse lineages. Nat Cell Biol. 2013; 16: 27–37. https://doi.org/10.1038/ncb2881 PMID: 24292013

12. Mathew B, Muñoz-Descalzo S, Corujo-Simon E, Schröter C, Stelzer EHK, Fischer SC. Mouse ICM Organoids Reveal Three-Dimensional Cell Fate Clustering. Biophys J. 2019; 116: 127–141. https://doi.org/10.1016/j.bpj.2018.11.011 PMID: 30514631

13. Chazaud C, Yamanaka Y, Pawson T, Rossant J. Early Lineage Segregation between Epiblast and Primitive Endoderm in Mouse Blastocysts through the Grb2-MAPK Pathway. Dev Cell. 2006; 10: 615–624. https://doi.org/10.1016/j.devcel.2006.02.020 PMID: 16678776

14. Gerbe F, Cox B, Rossant J, Chazaud C. Dynamic expression of Lrp2 pathway members reveals progressive epithelial differentiation of primitive endoderm in mouse blastocyst. Dev Biol. 2008; 313: 594–602. https://doi.org/10.1016/j.ydbio.2007.10.048 PMID: 18083160

15. Saiz N, Grabarek JB, Sabherwal N, Papalopulu N, Plusa B. Atypical protein kinase C couples cell sorting with primitive endoderm maturation in the mouse blastocyst. Development. 2013; 140: 4311–4322. https://doi.org/10.1242/dev.093922 PMID: 24067354

16. Yang D-H, Smith ER, Roland IH, Sheng Z, He J, Martin WD, et al. Disabled-2 is essential for endodermal cell positioning and structure formation during mouse embryogenesis. Dev Biol. 2002; 251: 27–44. Available: https://doi.org/10.1006/dbio.2002.0810 PMID: 12413896

17. Saiz N, Plusa B, Hadjantonakis A-K. Single cells get together: High-resolution approaches to study the dynamics of early mouse development. Semin Cell Dev Biol. 2015; 47–48: 92–100. https://doi.org/10.1016/j.semcdb.2015.06.004 PMID: 26183190

18. Mohammed H, Hernando-Herraez I, Savino A, Scialdone A, Macaulay I, Mulas C, et al. Single-Cell Landscape of Transcriptional Heterogeneity and Cell Fate Decisions during Mouse Early Gastrulation. Cell Rep. 2017; 20: 1215–1228. https://doi.org/10.1016/j.celrep.2017.07.009 PMID: 28768204

19. Boroviak T, Loos R, Bertone P, Smith A, Nichols J. The ability of inner-cell-mass cells to self-renew as embryonic stem cells is acquired following epiblast specification. Nat Cell Biol. 2014; 16: 516–528. https://doi.org/10.1038/ncb2965 PMID: 24859004

20. Bessonnard S, De Mot L, Gonze D, Barriol M, Dennis C, Goldbeter A, et al. Gata6, Nanog and Erk signaling control cell fate in the inner cell mass through a tristable regulatory network. Development. 2014; 141: 3637–3648. https://doi.org/10.1242/dev.109678 PMID: 25209243

21. Le Bin GC, Muñoz-Descalzo S, Kurowski A, Leitch H, Lou X, Mansfield W, et al. Oct4 is required for lineage priming in the developing inner cell mass of the mouse blastocyst. Development. 2014; 141: 1001–1010. https://doi.org/10.1242/dev.096875 PMID: 24504341

22. Saiz N, Williams KM, Seshan VE, Hadjantonakis A-K. Asynchronous fate decisions by single cells collectively ensure consistent lineage composition in the mouse blastocyst. Nat Commun. 2016; 7: 13463. https://doi.org/10.1038/ncomms13463 PMID: 27857135

23. Meng Y, Moore R, Tao W, Smith ER, Tse JD, Caslini C, et al. GATA6 phosphorylation by Erk1/2 propels exit from pluripotency and commitment to primitive endoderm. Dev Biol. 2018; 436: 55–65. https://doi.org/10.1016/j.ydbio.2018.02.007 PMID: 29454706

24. Morgani SM, Saiz N, Garg V, Raina D, Simon CS, Kang M, et al. A Sprouty4 reporter to monitor FGF/ERK signaling activity in ESCs and mice. Dev Biol. 2018; 441: 104–126. https://doi.org/10.1016/j.ydbio.2018.06.017 PMID: 29964027

25. Dietrich J-E, Panavaite L, Gunther S, Wennekamp S, Groner AC, Pigge A, et al. Venus trap in the mouse embryo reveals distinct molecular dynamics underlying specification of first embryonic lineages. EMBO Rep. 2015; 16: 1005–1021. https://doi.org/10.15252/embr.201540162 PMID: 26142281

26. Freyer L, Schröter C, Saiz N, Schrode N, Nowotschin S, Martinez-Arias A, et al. A loss-of-function and H2B-Venus transcriptional reporter allele for Gata6 in mice. BMC Dev Biol. 2015; 15: 38. https://doi.org/10.1186/s12861-015-0086-5 PMID: 26498761

27. Kang M, Xenopoulos P, Muñoz-Descalzo S, Lou X, Hadjantonakis AK. Live imaging, identifying, and tracking single cells in complex populations in vivo and ex vivo. Methods Mol Biol. 2013; 1052: 109–123. https://doi.org/10.1007/7651_2013_19 PMID: 23640250

28. Xenopoulos P, Kang M, Puliafito A, DiTalia S, Hadjantonakis AK. Heterogeneities in nanog expression drive stable commitment to pluripotency in the mouse blastocyst. Cell Rep. 2015; 10: 1508–01520. https://doi.org/10.1016/j.celrep.2015.02.010 PMID: 25753417

29. Rayon T, Menchero S, Nieto A, Xenopoulos P, Crespo M, Cockburn K, et al. Notch and Hippo Converge on Cdx2 to Specify the Trophectoderm Lineage in the Mouse Blastocyst. Dev Cell. 2014; 30: 410–422. https://doi.org/10.1016/j.devcel.2014.06.019 PMID: 25127056

30. Simon CS, Zhang L, Wu T, Cai W, Saiz N, Nowotschin S, et al. A Gata4 nuclear GFP transcriptional reporter to study endoderm and cardiac development in the mouse. Biol Open. 2018; 7: bio036517. https://doi.org/10.1242/bio.036517 PMID: 30530745

31. Posfai E, Petropoulos S, de Barros FRO, Schell JP, Jurisica I, Sandberg R, et al. Position- and hippo signaling-dependent plasticity during lineage segregation in the early mouse embryo. Elife. 2017; 6: 1–24. https://doi.org/10.7554/eLife.22906

32. Kiyonari H, Kaneko M, Abe T, Shioi G, Aizawa S, Furuta Y, et al. Dynamic organelle localization and cytoskeletal reorganization during preimplantation mouse embryo development revealed by live imaging of genetically encoded fluorescent fusion proteins. genesis. 2019; e23277. https://doi.org/10.1002/dvg.23277 PMID: 30597711

33. Lou X, Kang M, Xenopoulos P, Muñoz-Descalzo S, Hadjantonakis AK. A rapid and efficient 2D/3D nuclear segmentation method for analysis of early mouse embryo and stem cell image data. Stem Cell Reports. 2014; 2: 382–397. https://doi.org/10.1016/j.stemcr.2014.01.010 PMID: 24672759

34. Evans JD. Straightforward statistics for the behavioral sciences. Pacific Grove: Brooks/Cole Pub. Co; 1996. Available: http://www.worldcat.org/title/straightforward-statistics-for-the-behavioral-sciences/oclc/32465263

35. Quinn GP, Keough MJ. Experimental Design and Data Analysis for Biologists. 2002 [cited 13 Apr 2018]. Available: http://www.cambridge.org

36. Schmitz A, Fischer SC, Mattheyer C, Pampaloni F, Stelzer EHK. Multiscale image analysis reveals structural heterogeneity of the cell microenvironment in homotypic spheroids. Sci Rep. 2017; 7: 43693. https://doi.org/10.1038/srep43693 PMID: 28255161

37. Chambers I, Colby D, Robertson M, Nichols J, Lee S, Tweedie S, et al. Functional expression cloning of Nanog, a pluripotency sustaining factor in embryonic stem cells. Cell. 2003; 113: 643–655. https://doi.org/10.1016/s0092-8674(03)00392-1 PMID: 12787505

38. Goodwin LD, Leech NL. Understanding Correlation: Factors That Affect the Size of r. J Exp Educ. 2006; 74: 249–266. https://doi.org/10.3200/JEXE.74.3.249–266

39. Sharpe J. Computer modeling in developmental biology: growing today, essential tomorrow. Development. 2017; 144: 4214–4225. https://doi.org/10.1242/dev.151274 PMID: 29183935

40. Miyanari Y, Torres-Padilla M-E. Control of ground-state pluripotency by allelic regulation of Nanog. Nature. 2012; 483: 470–473. https://doi.org/10.1038/nature10807 PMID: 22327294

41. Silva J, Nichols J, Theunissen TW, Guo G, van Oosten AL, Barrandon O, et al. Nanog Is the Gateway to the Pluripotent Ground State. Cell. 2009; 138: 722–737. https://doi.org/10.1016/j.cell.2009.07.039 PMID: 19703398

42. Simon CS, Hadjantonakis A-K, Schröter C. Making lineage decisions with biological noise: Lessons from the early mouse embryo. Wiley Interdiscip Rev Dev Biol. 2018; 7: e319. https://doi.org/10.1002/wdev.319 PMID: 29709110

43. Gurdon JB. A community effect in animal development. Nature. 1988; 336: 772–774. https://doi.org/10.1038/336772a0 PMID: 3205305

44. Blanchard GB, Fletcher AG, Schumacher LJ. The devil is in the mesoscale: Mechanical and behavioural heterogeneity in collective cell movement. Semin Cell Dev Biol. 2018 [cited 15 Feb 2019]. https://doi.org/10.1016/J.SEMCDB.2018.06.003

45. McDole K, Guignard L, Amat F, Berger A, Malandain G, Royer LA, et al. In Toto Imaging and Reconstruction of Post-Implantation Mouse Development at the Single-Cell Level. Cell. 2018; 175: 859–876. e33. https://doi.org/10.1016/j.cell.2018.09.031 PMID: 30318151

46. Guignard L, Fiuza U-M, Leggio B, Faure E, Laussu J, Hufnagel L, et al. Contact-dependent cell-cell communications drive morphological invariance during ascidian embryogenesis. bioRxiv. 2017; 1–20. https://doi.org/10.1101/238741

47. McQuin C, Goodman A, Chernyshev V, Kamentsky L, Cimini BA, Karhohs KW, et al. CellProfiler 3.0: Next-generation image processing for biology. Misteli T, editor. PLOS Biol. 2018; 16: e2005970. https://doi.org/10.1371/journal.pbio.2005970 PMID: 29969450

48. Rivron NC, Frias-Aldeguer J, Vrij EJ, Boisset J-C, Korving J, Vivié J, et al. Blastocyst-like structures generated solely from stem cells. Nature. 2018; 557: 106–111. https://doi.org/10.1038/s41586-018-0051-0 PMID: 29720634

49. Schroter C, Rue P, Mackenzie JP, Martinez Arias A. FGF/MAPK signaling sets the switching threshold of a bistable circuit controlling cell fate decisions in embryonic stem cells. Development. 2015; 142: 4205–4216. https://doi.org/10.1242/dev.127530 PMID: 26511924

50. Tosenberger A, Gonze D, Bessonnard S, Cohen-Tannoudji M, Chazaud C, Dupont G. A multiscale model of early cell lineage specification including cell division. npj Syst Biol Appl. 2017; 3: 16. https://doi.org/10.1038/s41540-017-0017-0 PMID: 28649443

51. Lian I, Kim J, Okazawa H, Zhao J, Zhao B, Yu J, et al. The role of YAP transcription coactivator in regulating stem cell self-renewal and differentiation. Genes Dev. 2010; 24: 1106–1118. https://doi.org/10.1101/gad.1903310 PMID: 20516196

52. Caiazzo M, Okawa Y, Ranga A, Piersigilli A, Tabata Y, Lutolf MP. Defined three-dimensional microenvironments boost induction of pluripotency. Nat Mater. 2016; 15: 344–352. https://doi.org/10.1038/nmat4536 PMID: 26752655

53. Lorthongpanich C, Issaragrisil S. Emerging Role of the Hippo Signaling Pathway in Position Sensing and Lineage Specification in Mammalian Preimplantation Embryos1. Biol Reprod. 2015; 92: 143. https://doi.org/10.1095/biolreprod.114.127803 PMID: 25947059

54. Yagi R, Kohn MJ, Karavanova I, Kaneko KJ, Vullhorst D, DePamphilis ML, et al. Transcription factor TEAD4 specifies the trophectoderm lineage at the beginning of mammalian development. Development. 2007; 134: 3827–3836. https://doi.org/10.1242/dev.010223 PMID: 17913785

55. Nishioka N, Yamamoto S, Kiyonari H, Sato H, Sawada A, Ota M, et al. Tead4 is required for specification of trophectoderm in pre-implantation mouse embryos. Mech Dev. 2008; 125: 270–283. https://doi.org/10.1016/j.mod.2007.11.002 PMID: 18083014

56. Mihajlović AI, Thamodaran V, Bruce AW. The first two cell-fate decisions of preimplantation mouse embryo development are not functionally independent. Sci Rep. 2015; 5: 15034. https://doi.org/10.1038/srep15034 PMID: 26461180

57. Hashimoto M, Sasaki H. Epiblast Formation by TEAD-YAP-Dependent Expression of Pluripotency Factors and Competitive Elimination of Unspecified Cells. Dev Cell. 2019; 50: 139–154.e5. https://doi.org/10.1016/j.devcel.2019.05.024 PMID: 31204175

58. Liebisch T, Drusko A, Mathew B, Stelzer EHK, Fischer SC, Matthäus F. Cell Fate Clusters in ICM Organoids Arise from Cell Fate Heredity & Division–a Modelling Approach. bioRxiv. 2019; 698928. https://doi.org/10.1101/698928

59. Meilhac SM, Adams RJ, Morris SA, Danckaert A, Le Garrec J-F, Zernicka-Goetz M. Active cell movements coupled to positional induction are involved in lineage segregation in the mouse blastocyst. Dev Biol. 2009; 331: 210–221. https://doi.org/10.1016/j.ydbio.2009.04.036 PMID: 19422818

60. Simon CS, Hadjantonakis A-K, Schröter C. Making lineage decisions with biological noise: Lessons from the early mouse embryo. Wiley Interdiscip Rev Dev Biol. 2018; 7: e319. https://doi.org/10.1002/wdev.319 PMID: 29709110

61. Muñoz-Descalzo S, RuE P, Garcia-Ojalvo J, Arias AM. Correlations Between the Levels of Oct4 and Nanog as a Signature for Naïve Pluripotency in Mouse Embryonic Stem Cells. Stem Cells. 2012; 30: 2683–2691. https://doi.org/10.1002/stem.1230 PMID: 22969005

62. Ebisuya M, Briscoe J. What does time mean in development? Development. 2018; 145: dev164368. https://doi.org/10.1242/dev.164368 PMID: 29945985

63. Fabrèges D, Daniel N, Duranthon V, Peyriéras N. Control of inner cells' proportion by asymmetric divisions and ensuing resilience of cloned rabbit embryos. [cited 23 Mar 2018]. https://doi.org/10.1242/dev.152041

64. Grabarek JB, Zyzynska K, Saiz N, Piliszek A, Frankenberg S, Nichols J, et al. Differential plasticity of epiblast and primitive endoderm precursors within the ICM of the early mouse embryo. Development. 2012; 139: 129–139. https://doi.org/10.1242/dev.067702 PMID: 22096072

65. Wigger M, Kisielewska K, Filimonow K, Plusa B, Maleszewski M, Suwińska A. Plasticity of the inner cell mass in mouse blastocyst is restricted by the activity of FGF/MAPK pathway. Sci Rep. 2017; 7: 15136. https://doi.org/10.1038/s41598-017-15427-0 PMID: 29123210

66. Krupinski P, Chickarmane V, Peterson C. Simulating the Mammalian Blastocyst—Molecular and Mechanical Interactions Pattern the Embryo. Thieffry D, editor. PLoS Comput Biol. 2011; 7: e1001128. https://doi.org/10.1371/journal.pcbi.1001128 PMID: 21573197

67. Frum T, Ralston A. Visualizing HIPPO Signaling Components in Mouse Early Embryonic Development. Humana Press, New York, NY; 2019. pp. 335–352. https://doi.org/10.1007/978-1-4939-8910-2_25

68. Morgani SM, Canham MA, Nichols J, Sharov AA, Migueles R, Ko MSH, et al. Totipotent Embryonic Stem Cells Arise in Ground-State Culture Conditions. Cell Rep. 2013; 3: 1945–1957. https://doi.org/10.1016/j.celrep.2013.04.034

69. Rodda DJ, Chew J-L, Lim L-H, Loh Y-H, Wang B, Ng H-H, et al. Transcriptional regulation of nanog by OCT4 and SOX2. J Biol Chem. 2005; 280: 24731–7. https://doi.org/10.1074/jbc.M502573200 PMID: 15860457

70. Yuan H, Corbi N, Basilico C, Dailey L. Developmental-specific activity of the FGF-4 enhancer requires the synergistic action of Sox2 and Oct-3. Genes Dev. 1995; 9: 2635–45. Available: https://doi.org/10.1101/gad.9.21.2635 PMID: 7590241

71. Kim S-H, Kim MO, Cho Y-Y, Yao K, Kim DJ, Jeong C-H, et al. ERK1 phosphorylates Nanog to regulate protein stability and stem cell self-renewal. Stem Cell Res. 2014; 13: 1–11. https://doi.org/10.1016/j.scr.2014.04.001 PMID: 24793005

72. Adachi Y, Shibai Y, Mitsushita J, Shang WH, Hirose K, Kamata T. Oncogenic Ras upregulates NADPH oxidase 1 gene expression through MEK-ERK-dependent phosphorylation of GATA-6. Oncogene. 2008; 27: 4921–4932. https://doi.org/10.1038/onc.2008.133 PMID: 18454176

73. Wamaitha SE, del Valle I, Cho LTY, Wei Y, Fogarty NME, Blakeley P, et al. Gata6 potently initiates reprograming of pluripotent and differentiated cells to extraembryonic endoderm stem cells. Genes Dev. 2015; 29: 1239–1255. https://doi.org/10.1101/gad.257071.114 PMID: 26109048

74. Shimokawa K, Kimura-Yoshida C, Nagai N, Mukai K, Matsubara K, Watanabe H, et al. Cell Surface Heparan Sulfate Chains Regulate Local Reception of FGF Signaling in the Mouse Embryo. Dev Cell. 2011; 21: 257–272. https://doi.org/10.1016/j.devcel.2011.06.027 PMID: 21839920

75. Scholpp S, Brand M. Endocytosis Controls Spreading and Effective Signaling Range of Fgf8 Protein. Curr Biol. 2004; 14: 1834–1841. https://doi.org/10.1016/j.cub.2004.09.084 PMID: 15498491

76. Perrimon N, Pitsouli C, Shilo B-Z. Signaling mechanisms controlling cell fate and embryonic patterning. Cold Spring Harb Perspect Biol. 2012; 4: a005975. https://doi.org/10.1101/cshperspect.a005975 PMID: 22855721

77. Cormier S, Le Bras S, Souilhol C, Vandormael-Pournin S, Durand B, Babinet C, et al. The murine ortholog of notchless, a direct regulator of the notch pathway in Drosophila melanogaster, is essential for survival of inner cell mass cells. Mol Cell Biol. 2006; 26: 3541–9. https://doi.org/10.1128/MCB.26.9.3541-3549.2006 PMID: 16611995

78. Cormier S, Vandormael-Pournin S, Babinet C, Cohen-Tannoudji M. Developmental expression of the Notch signaling pathway genes during mouse preimplantation development. Gene Expr Patterns. 2004; 4: 713–717. https://doi.org/10.1016/j.modgep.2004.04.003 PMID: 15465494

79. Messerschmidt D, de Vries WN, Lorthongpanich C, Balu S, Solter D, Knowles BB. B-Catenin-Mediated Adhesion Is Required for Successful Preimplantation Mouse Embryo Development. Development. 2016; 143: 1993–1999. https://doi.org/10.1242/dev.133439 PMID: 27246714

80. Muñoz-Descalzo S, Martinez Arias A. The structure of Wntch signalling and the resolution of transition states in development. Semin Cell Dev Biol. 2012; 23: 443–449. https://doi.org/10.1016/j.semcdb.2012.01.012 PMID: 22326376

81. Graham SJL, Wicher KB, Jedrusik A, Guo G, Herath W, Robson P, et al. BMP signalling regulates the pre-implantation development of extra-embryonic cell lineages in the mouse embryo. Nat Commun. 2014; 5: 5667. https://doi.org/10.1038/ncomms6667 PMID: 25514175

82. Reyes de Mochel NS, Luong M, Chiang M, Javier AL, Luu E, Toshihiko F, et al. BMP signaling is required for cell cleavage in preimplantation-mouse embryos. Dev Biol. 2015; 397: 45–55. https://doi.org/10.1016/j.ydbio.2014.10.001 PMID: 25446538

83. Sozen B, Ozturk S, Yaba A, Demir N. The p38 MAPK signalling pathway is required for glucose metabolism, lineage specification and embryo survival during mouse preimplantation development. Mech Dev. 2015; 138: 375–398. https://doi.org/10.1016/j.mod.2015.05.002 PMID: 26025760

84. Threadgill DW, Dlugosz AA, Hansen LA, Tennenbaum T, Lichti U, Yee D, et al. Targeted disruption of mouse EGF receptor: effect of genetic background on mutant phenotype. Science. 1995; 269: 230–4. Available: https://doi.org/10.1126/science.7618084 PMID: 7618084

S1 Supplementary Information text: Full description of the data analysis

In this supplementary information, we provide a full description of the different steps of our data analysis. This includes the arguments for the choice of a particular approach as well as the sensitivity of the output of each approach to its input parameters. Investigating the sensitivity of a method increases our understanding of the relationship between input and output variables. Furthermore, it provides information on the robustness of the approach.

In the following, we consider the four main parts of our analyses:

1. Normalization of expression values and classification of cell populations
2. Determining cell neighbours with the Delaunay Cell Graph (DCG)
3. Correlations of expression levels of neighbouring cells
4. Rule-based simulations of population composition in ICM of early blastocysts

1. Normalization of expression values and classification of cell populations

The imaging data for the embryos was generated in four batches corresponding to different imaging sessions and/or stainings. The mounting of the embryos for imaging resulted in a slight squeezing along the z-axis of the image and hence extension along x and y (Fig S1, Step 3(i)). We checked for fluorescence intensity decay along the z-axis for each batch. As this decay was minimal due to the mounting of the embryos, intensity adjustment along z was not performed (Fig 1).

We assumed that the embryos that do not have fully segregated epiblast and primitive endoderm should be spherical (early and mid blastocysts). Based on this assumption, we calculated the deviation from sphericity for each of these embryos and rescaled the coordinates of the cell nuclei to obtain spherical embryos. Embryos with segregated epiblast and primitive endoderm have hatched from the zona and are elongated (late blastocysts). To rescale the coordinates of these late stage

25 embryos, we calculated for each batch the median rescaling factors for x, y and z of the early and mid
26 blastocysts and applied these to the late blastocysts.
27

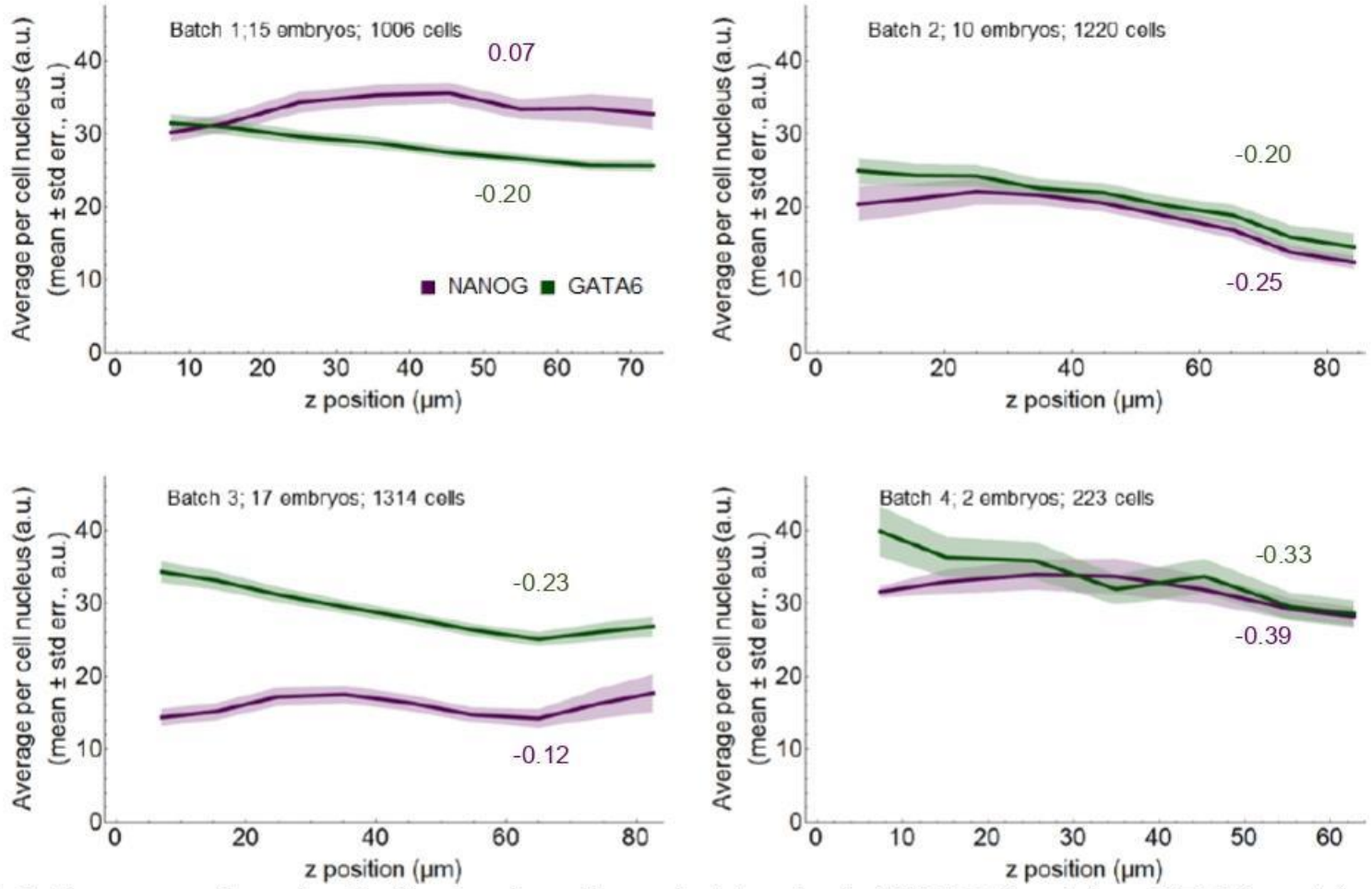

28 **Fig 1: Fluorescence intensity distribution along the z-axis.** Mean level of NANOG (purple) or GATA6 (green) (y-
29 axis) fluorescence intensity in each cell (ICM and TE) versus its z position within the imaged z-stack in each of the
30 four imaged embryo batches. The z position data are binned in 10 µm intervals. The shaded regions display the
31 standard error of the mean. Batch, embryo and total cell numbers are indicated. Coloured numbers indicate the
32 Spearman correlation values between NANOG (purple) and GATA6 (green) levels. Note that all values show a
33 very weak or weak correlation indicating no evident decay of fluorescence intensity in deeper z positions.
34

35 Plotting the mean GATA6 expression levels versus the mean NANOG expression levels for all
36 nuclei in the four imaging batches, we observed a shift in the data related to the batch number (Fig S1,
37 Step 2). To align the data obtained from the four independent sessions, we established thresholds for
38 NANOG and GATA6 expression for each batch, based on the data distribution in late stage embryos,
39 where Epiblast (Epi) and Primitive Endoderm (PrE) are completely separated and no double positive
40 (DP) cells occur. The thresholds were manually adjusted. The criterion was to determine the minimal

NANOG and GATA6 value, respectively, such that there are no double positive cells in late blastocysts (see Fig 3).

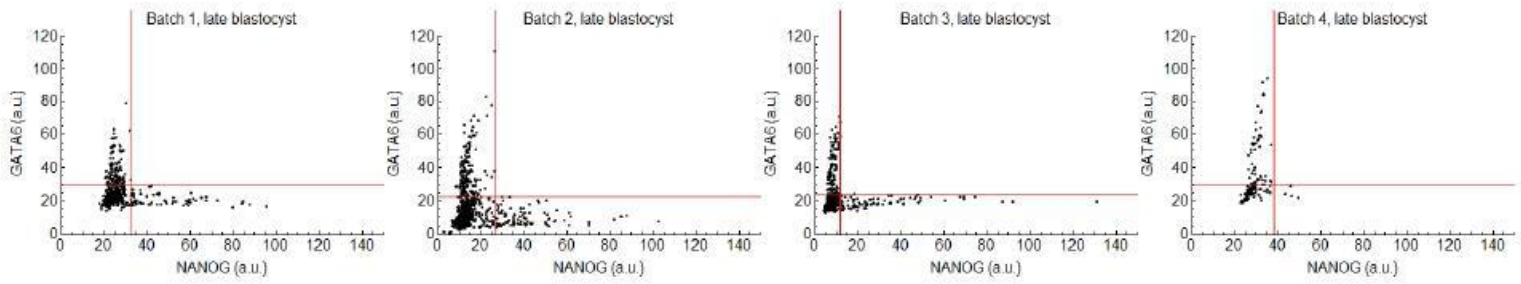

Fig 3: Population thresholds. Raw data for NANOG and GATA6 expression in single cells in arbitrary units (a.u.) in late embryos for the four batches (black) and the manually set thresholds to determine the four populations (red).

Based on the thresholds, we linearly shifted the data of all batches and all stages, such that all thresholds fall on top of each other. Since the range of the data does not vary much between batches, we consider such a linear transformation most appropriate. This changes the absolute intensity levels for each embryo but it does not change the relative intensity values in an embryo, which is the value that is relevant for our analysis. Based on the thresholds for GATA6 and NANOG, all cells were classified as double negative (DN: N- and G-), NANOG+/GATA6- (N+G-), NANOG-/GATA6+ (N-G+) and double positive (DP: N+, G6+). We applied the same method to the *Nanog* mutant data set to align the thresholds obtained from the data obtained in the five imaging sessions.

We also tested the k-means clustering used in [1] to determine the thresholds for our WT embryo data set as well as for the *Nanog* mutant data sets. Unfortunately, for the mutant data set, the clustering approach gave unreasonable results, including a large proportion of DN cells. Therefore, we decided to use the manually adjusted approach that works for both cases.

For the [1] data set, the imaging was performed in small dishes that didn´t require the mounting of the embryos, hence a rescaling was not required. Instead, the data set was corrected for the decrease in intensity along z. Furthermore, Saiz et al. employed a k-means clustering for the population assignment of their data. We took the corrected data set and population assignment from

[1] to perform our neighbourhood analyses. We noticed that there were some oversaturated nuclei images and hence excluded all NANOG and GATA6 levels from the distribution that were two standard deviations away from the respective mean. The remaining analysis was analogous to our data.

2. Determining cell neighbours with the Delaunay Cell Graph (DCG)

We recently proposed two approaches to model the cell neighbourhood [2]: the Proximity Cell Graph (PCG), which provides a purely distance-based description of the cell neighbourhood and the Delaunay Cell Graph (DCG), in which neighbourhood is determined by the Delaunay triangulation. The Delaunay triangulation and its dual, the Voronoi tessellation, are routinely used to approximate the nearest neighbours of a cell [2–4]. The Delaunay cell graph (DCG) is given by $DCG(V, E)$ where V is the vertex set and E is the edge set of the graph. An edge $(u, w) \in E$ exists between two vertices $u \in V$ and $w \in V$ if the corresponding points are connected by a line in the Delaunay triangulation and the Euclidean distance between u and w is less than a given threshold, which we chose as 30 µm (three times the average diameter of a cell nucleus). To validate that the distance between the centroids of two neighbouring cells is at least 10 µm, we calculated this distance between all neighbouring cells in the ICM (and their TE neighbours) for all embryos in data set I and II (Fig 3). These values fall within the reported segmentation errors obtained with MINS [5], increasing in later embryos.

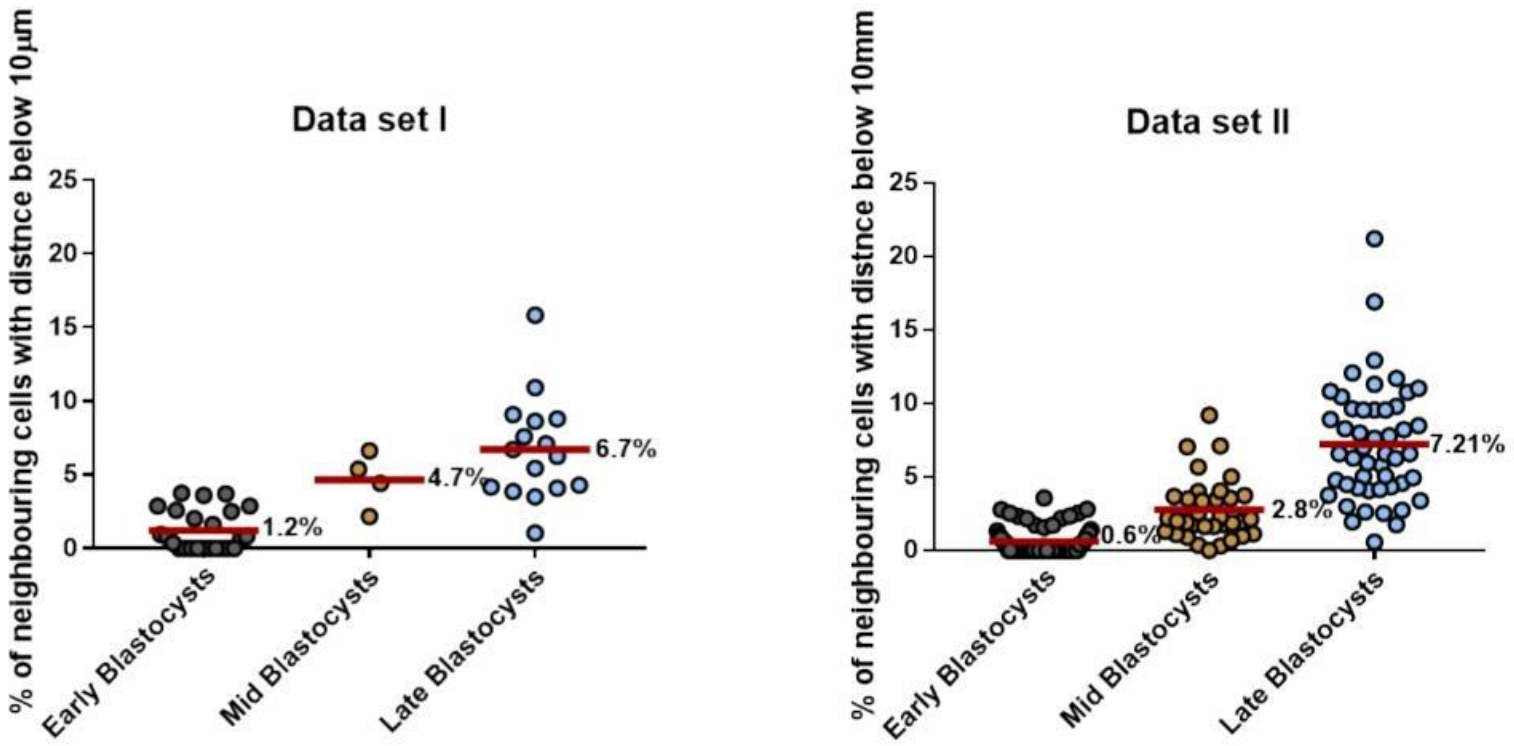

Fig 3: Percentage of cells with a distance below 10 µm in data set I and II. Each dot represents the percentage of distances of a cell to all its neighbours that fall below 10 µm in one embryo. The horizontal red line represents the average percentage within each developmental stage (numerical value is also shown).

In a preliminary study to decide whether to use the Proximity Cell Graph (PCG) and/or the Delaunay Cell Graph (DCG) in mouse embryos, we generated a number of artificial shapes (ball, oblate spheroid, prolate spheroid, cuboid and box) and analysed the number of edges versus the number of vertices. As expected, we found that the number of edges in the PCG increases unreasonably with increasing number of vertices [2]. Furthermore, by definition, the PCG is completely dependent on the cut off length. PCG approximation was used in a recent study on a model for early cell lineage specification in mouse embryos with neighbour type simulations [6]. The authors assume in their simulations that the cells are non-overlapping spheres with a certain radius and a cut off length 1.2 times the sum of the radii of the two cells. This is essentially if the spheres touch or almost touch. For a tissue with polygonal cells of different sizes like the ones found in mouse embryos, it is not trivial to determine an appropriate cut off length to obtain the nearest neighbours. The DCG is less sensitive to the cut off length and for cells in the centre of the embryo like in the ICM, the cut off length is irrelevant unless it is unreasonably small. Therefore, we decided to analyse the embryo data using the DCG.

We employed the DCG on the pre-processed nuclei centre of mass. For a given cell (vertex in the cell graph), the neighbouring cells are represented by the vertices that are connected through edges. In all our analyses, the set of neighbouring cells consists of all ICM cells and the TE cells that are neighbours to at least one ICM cell (Fig S1, Step4).

To evaluate the neighbour assignment of the DCG in the mouse embryos, we compared the results for the ICM cells of four early, three mid and two late embryos to a manual assignment included in our data set (Fig 4, and see Sup. Videos 1-3). For the manual assignment, we considered cells as neighbours if they are touching, identified by the membrane staining. The manual assignment only provides an indication. Judging the three-dimensional neighbourhood of the cells from slices of two-dimensional images is very difficult and gets even more challenging as the cell density and the irregularity of the cellular geometry increase with stage. We find that the accuracy of DCG compared to the manual assignment is 91 % (early), 82% (mid) and 83% (late) (see Table 1). We also found that 0 (early), 3 (mid) and 13 (late) cells were not detected as neighbours by the automatic assignment compared to the manual assignment due to errors in the segmentation method used (MINS). Hence, if the cells were segmented correctly, the DCG did not miss a neighbourhood relationship. We conclude that for all stages, the DCG provides a robust description of the local cell neighbourhood in the ICM and a satisfactory approximation of which cells are touching.

Table 1: Comparison of DCG neighbours to manual assignment of touching cells

	Early (n=4)	Mid (n=3)	Late (n=2)
ICM cells	50	67	79
DCG neighbours	543	751	1031
Manual neighbours (touching)	495	617	851
Accuracy: Manual/DCG neighbours	0.91	0.82	0.83

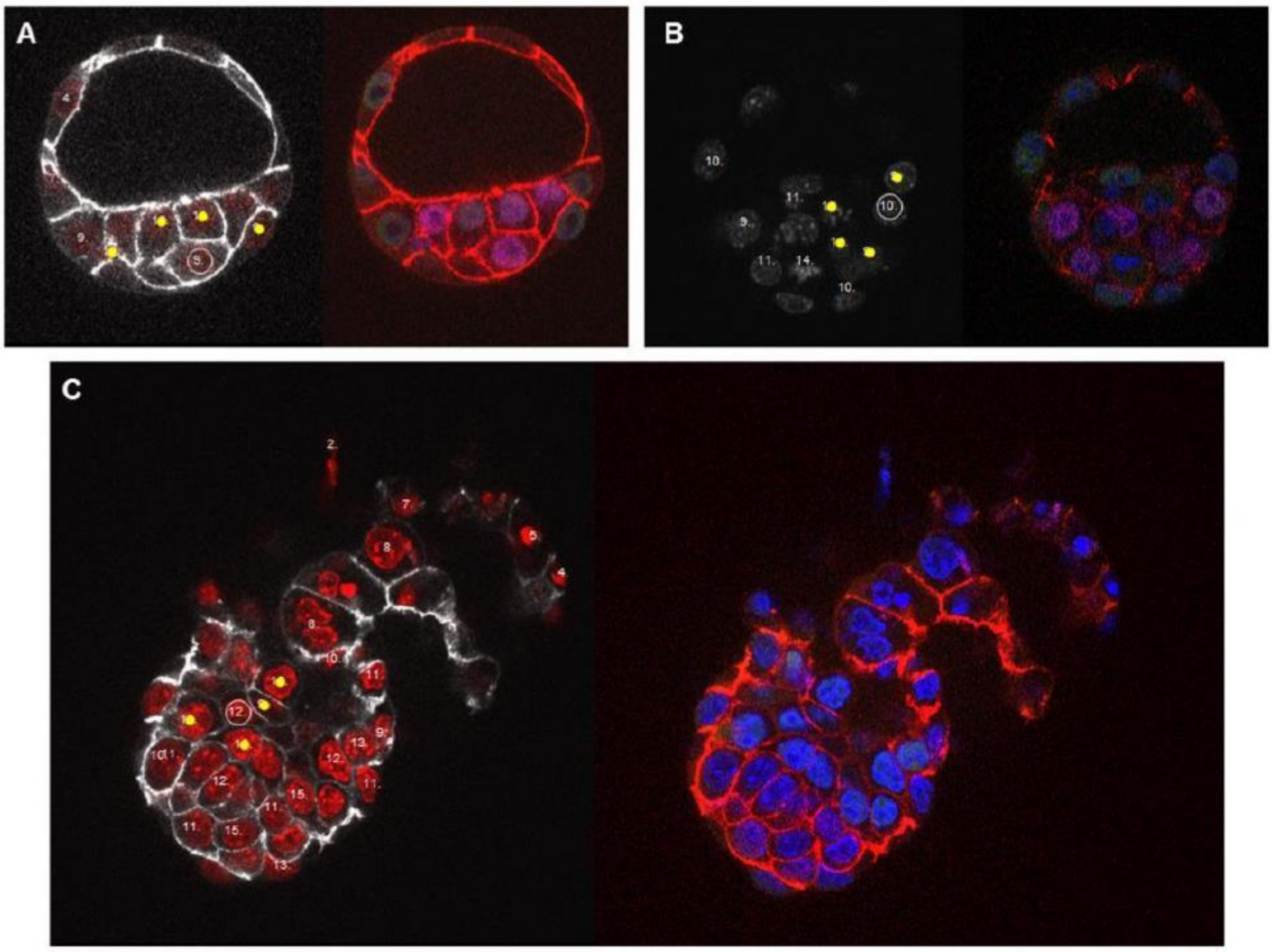

Fig 4: z Sections of early (A), mid (B) and late (C) embryos comparing DGC neighbour assignment and fluorescent immunostaining. The left panels show membrane and/or nuclear staining. The yellow dots indicate DCG calculated neighbouring cells of the cell with an encircled number, that number indicates its number of neighbours; numbers in other cells indicate the number of neighbouring cells of that cell. The right panels show the original confocal images of the embryos shown, stained for NANOG (magenta), GATA6 (green), DAPI (blue) and β-catenin (membrane, red). Note that the embryos are upside down and not all the neighbours of the indicated cell are located in the same z section. See Sup. Videos 1-3 for the complete z-stack.

Sensitivity of the DCG

We investigated the sensitivity of the number of neighbours provided by the DCG with respect to cell density. We considered a ball of radius 50 µm and randomly filled it with non-overlapping spheres of radius 5µm to represent the cells. For these simulated cells, we generated the DCG. The procedure was repeated ten times for cell numbers ranging from 10 to 400 in steps of 10, resulting in

cell densities ranging from $1.9x10^{-5}$ cells/µm³ to $76.43x10^{-5}$ cells/µm³. For comparison, manual inspection of the ICM cells resulted in a cell density of $4x10^{-5}$ cells/µm³ in early embryos and $20x10^{-5}$ cells/µm³ in mid embryos.

For the simulated DCGs, we find that for increasing cell density the average number of neighbours increases and plateaus at around 13 neighbours (Fig 5).

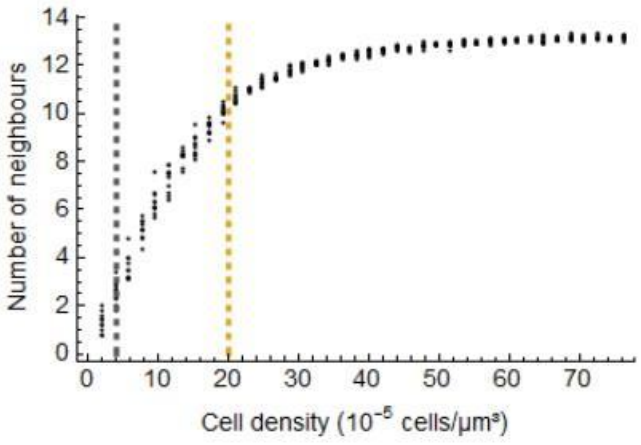

Fig 5: The mean number of neighbours derived from the DCG plateaus for high cell densities. Each dot represents the mean number of neighbours of one simulated DCG. The vertical lines indicate the manually obtained cell densities in ICM of early (grey) and mid (yellow) blastocysts.

3. Correlations of expression levels of neighbouring cells

To relate the expression levels of a given cell to the expression levels of all its neighbours (both TE and ICM), we calculated Spearman's correlation coefficient of the expression levels of a cell and the median expression levels of its neighbours. We chose to use median level in the neighbours in combination with Spearman's correlation coefficient as we reasoned that this measurement was the variable, which made the least assumptions about the type of signals that might be regulating the observed correlations. Furthermore, the median provides a more robust measure than the sum of all signals as the median goes up slower and is also less sensitive to outliers than the sum. Spearman's correlation coefficient does not require normally distributed data.

To determine whether the obtained correlations are statistically significant, we performed a bootstrap resampling of the correlation coefficients of our data and compared the result with

correlation coefficients of a null model. For the bootstrapping, we resampled the experimental data to create 100 different data sets.

Sensitivity of the correlation analysis:

Spearman's rank correlation coefficient is the Pearson correlation coefficient after the two variables have been separately transformed to ranks while retaining their pairing [7]. The value of the correlation coefficient is affected by a number of factors, in particular the sample size [8]. Therefore, we explored the sensitivity of the correlation value to the number of cells analysed. We know that for a random distribution, the correlation value is zero. To test whether this analysis might be affected by the topological properties of small DCG given the specific constraints on cell number, we used 100 artificially generated DCGs. These artificial DCGs consisted of cell numbers 10 to 400 in steps of 10 and randomly assigned expression levels to each cell based on the uniform distribution over [0,1]. For each DCG, we then calculated the correlation value and determined the mean correlation value for DCGs with the same cell number. We find that if the number of cells analysed increases, the mean correlation coefficient approaches zero (Fig 6). Hence, if the number of cells is large enough, the correlation analysis is consistent.

Next, we investigated how the number of cells in the analysis is linked to the deviation of the mean correlation from zero. Fitting the function $f(x) = -\frac{a}{x} - b$ resulted in a=2.19 and b=0.0098. Based on $f(x)$, we estimated that on average, we need at least 108 cells in the analysis to obtain at most 3% deviation (Fig 6). Less cells will lead to more noise in the correlation analysis, while more cells will increase the precision. We chose 3 % as the threshold, since this is the point where the functions levels off.

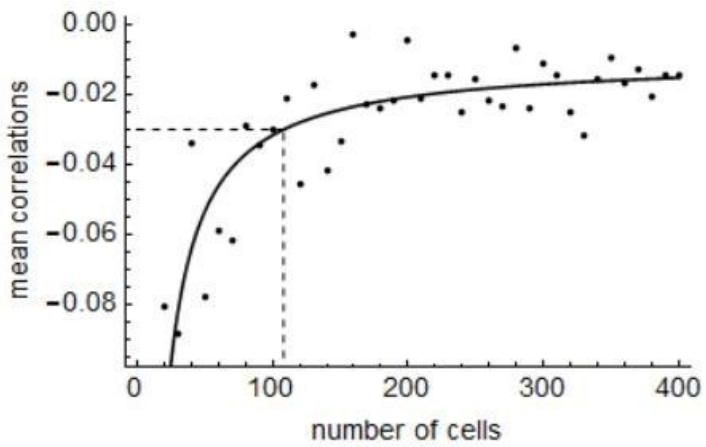

Fig 6: More than 108 analysed cells results in an average deviation of less than 3%. Mean correlation coefficients for 100 artificially generated DCGs of 10 to 400 cells in steps of 10 with expression levels drawn from the uniform distribution over [0,1] (dots). The continuous line indicates the fitted curve $f(x) = -\frac{2.19}{x} - 0.0098$ and the intersection of $f(x)$.The 3% threshold is marked by the dashed line.

The ICM has 20 ± 1 cells in early, 24 ± 1 cells in mid, and 45 ± 4 cells in late embryos. Due to these small numbers, analysing the correlations individually in each embryo does not provide reliable results. Hence, we pooled the data for all cells, expecting a reliable result if the number of pooled cells is at least 108.

<u>Null model for correlations:</u>

The correlation analysis for the experimental data results in non-zero values. To test whether these results might be affected by specific constraints on NANOG/GATA6 distributions, we investigated whether the correlation values are significantly different from those of a null model. For the null model, we assumed the embryo geometry is given by the experimental data, hence we used the measured coordinates of the cells. The expression levels of the TE cells were also based on the experimental data. To assess the effect of NANOG/GATA6 distribution, we generated several different models using different assignment rules for the NANOG and GATA6 values of the ICM cells:

- Random model 1: The NANOG and GATA6 values of the ICM cells are randomly drawn from the uniform distribution over [0,1].
- Random model 2: The values of the ICM of each embryo are shuffled randomly.

• Random model 3: We generate the distributions for NANOG and GATA6 from all ICM cells of all embryos at all stages. The values of an ICM cell are randomly drawn from these distributions.

• Random model 4: We generate the distributions for NANOG and GATA6 from all ICM cells of all embryos of a given stage. This results in six distributions one for each stage for NANOG and GATA6, respectively. For a cell in the ICM of a given embryo, the values for NANOG and GATA6 are randomly drawn from the corresponding distribution depending on the stage of the embryo.

• Random model 5: The values of the ICM cells of all embryos in each stage are randomly shuffled.

We generated each model for all the embryos in our data set, pooled all the cells in the ICM from one stage and calculated the correlations of these cells with their neighbours both for NANOG (Table 2) and GATA6 (Table 3). This procedure was repeated 100 times. We expect very low correlation values for the random models.

Table 2: Correlation values for different random assignments of NANOG expression (mean ± standard deviation)

Model	Early	Mid	Late
Random model 1	-0.0006 ± 0.04	0.15 ± 0.01	0.25 ± 0.003
Random model 2	0.2 ± 0.04	0.04 ± 0.08	0.3 ± 0.05
Random model 3	-0.005 ± 0.05	-0.02 ± 0.1	-0.004 ± 0.04
Random model 4	-0.009 ± 0.04	-0.02 ± 0.1	-0.02 ± 0.04
Random model 5	0.003 ± 0.06	0.002 ± 0.1	-0.01 ± 0.04

Table 3: Correlation values for different random assignments of GATA6 expression (mean ± standard deviation)

Model	Early	Mid	Late
Random model 1 (identical to above)	-0.0006 ± 0.04	0.14 ± 0.01	0.25 ± 0.003
Random model 2	0.6 ± 0.01	0.4 ± 0.07	0.4 ± 0.04
Random model 3	-0.005 ± 0.05	0.0003 ± 0.1	-0.0001 ± 0.04
Random model 4	-0.001 ± 0.05	-0.02 ± 0.1	0.002 ± 0.04
Random model 5	-0.004 ± 0.05	0.004 ± 0.1	0.006 ± 0.04

We find that Random model 2 exhibits larger correlation values than the other models. This indicates that reshuffling the values of the ICM cell in each embryo individually does not introduce a sufficient randomization, due to the small number of cells in the ICM.

All the other models show similar results with values close to zero as expected from a random model. For all subsequent analyses shown in the main text, we used the method of Random model 3 to calculate the null models for the neighbour correlations, rather than models 1, 4 or 5. The main reasons for this are that Random model 3 relies on the original data (unlike Random model 1) and its calculation is more straightforward, because we only need to consider two distributions for the data (one for NANOG and one for GATA6) rather than six as for Random models 4 and 5.

The correlation values for Random model 3 for the different experimental conditions are summarised in Tables 4 and 5.

238 **Table 4: Correlation values for Random model 3 for wild-type and NANOG mutant analyses (mean ± standard**

239 **deviation)**

	Correlations		
Experimental condition	**Early**	**Mid**	**Late**
Our data (NANOG cell, NANOG neighbours)	-0.005 ± 0.05	-0.02 ± 0.1	0.004 ± 0.04
Our data (GATA6 cell, GATA6 neighbours)	-0.005 ± 0.05	0.0003 ± 0.1	-0.0001 ± 0.04
Our data (NANOG cell, GATA6 neighbours)	-0.003 ± 0.04	-0.005 ± 0.1	0.006 ± 0.04
Our data (GATA6 cell, NANOG neighbours)	-0.002 ± 0.05	-0.02 ± 0.1	-0.0004 ± 0.04
Saiz data (NANOG cell, NANOG neighbours)	-0.0005 ± 0.03	0.001 ±0.04	-0.0008 ± 0.03
Saiz data (GATA6 cell, GATA6 neighbours)	-0.002 ± 0.03	-0.008 ± 0.03	0.0001 ± 0.03
Saiz data (NANOG cell, GATA6 neighbours)	-0.004 ± 0.03	-0.002 ± 0.04	-0.0006 ± 0.03
Saiz data (GATA6 cell, NANOG neighbours)	-0.004 ± 0.03	-0.0009 ± 0.03	-0.003 ± 0.03
NANOG mutant analysis, WT and heterozygotes (GATA6 cell, GATA6 neighbours)	-0.0008 ± 0.04	-0.02 ± 0.07	0.2 ± 0.03
NANOG mutant analysis, mutants (GATA6 cell, GATA6 neighbours)	-0.003 ± 0.08	-0.03 ± 0.09	-0.1 ± 0.04

240

241

Table 5: Correlation values for Random model 3 for treated embryos (mean ± standard deviation)

Experimental condition	Correlation (no staging)
Treatment analysis, control (NANOG cell, NANOG neighbours)	-0.003 ± 0.03
Treatment analysis, control (GATA6 cell, GATA6 neighbours)	-0.001 ± 0.04
Treatment analysis, PD03 (NANOG cell, NANOG neighbours)	-0.003 ± 0.04
Treatment analysis, PD03 (GATA6 cell, GATA6 neighbours)	-0.005 ± 0.04

4. Rule-based simulations of population composition in ICM of early blastocysts

To generate the simulations of the four populations, we used the 64 early embryo data sets from Saiz et al. For each ICM cell, we determined the simulated cell population type based on two rules and kept the cell centroid and neighbours as obtained from the experimental data. We included the TE cells that are neighbouring at least one ICM cell with their features obtained from the experimental data. To obtain the population type for an ICM cell, we assigned it N+ or N- and G6+ or G6- expression according to these two rules:

1) G6+ cells are clustered; the clustering is achieved by randomly setting the percentage of being G6+ to 85 % and the rest to G6- ($p_{GATA6} = 0.85$);

2) cells with nine or close to nine neighbours are N+ up to 82 % ($p_{NANOG} = 0.82$), the rest N-.

The values for p_{GATA6} and p_{NANOG} are obtained from the experimental data and are the proportion of ICM cells positive for GATA6 or NANOG expression, respectively. Hence, p_{GATA6} is the proportion of DP and N-G+ cells and p_{NANOG} is the proportion of DP and N+G- cells. Combining this information for each cell, we determined its simulated population type.

Sensitivity of the four populations model:

The four populations model relies on three parameters:

1. $p_{GATA6,}$ the proportion of GATA6 positive cells, i.e DP and N-G+ cells
2. p_{NANOG}, the proportion of NANOG positive cells, i.e DP and N+G- cells
3. $\mathrm{startNumNeigh}$, the number of neighbours at which we start assigning NANOG positive fate to the cells

We analysed the sensitivity of the model to the values of these three parameters. We varied p_{NANOG} and p_{GATA6} between 0 and 1 in steps of 0.2 and $\mathrm{startNumNeigh}$ between 7 and 14 in steps of 1. For each parameter value combination, we performed 100 simulations. For each embryo, we calculated the mean distribution of populations of the 100 simulations. The mean population distributions are then summed up to obtain the total overall population distribution. This simulated total population distribution is then compared to the total population distribution from the experimental data. To assess the goodness of fit, we employed the mean squared error $MSE = Mean((\mathrm{popDist}_{Sim} - \mathrm{popDist}_{Exp})^2)$, where $\mathrm{popDist}_{Sim}$ is the population distribution of the simulations and $\mathrm{popDist}_{Exp}$ the population distribution obtained from the experiments. For a better visualisation, we rescale the MSE and obtain the simulation match $1 - \frac{MSE - Min(MSE)}{Max(MSE) - Min(MSE)}$. Hence, a simulation match of 0 corresponds to the parameter values with the worst match and a simulation match of 1 to the best match (Fig 7)

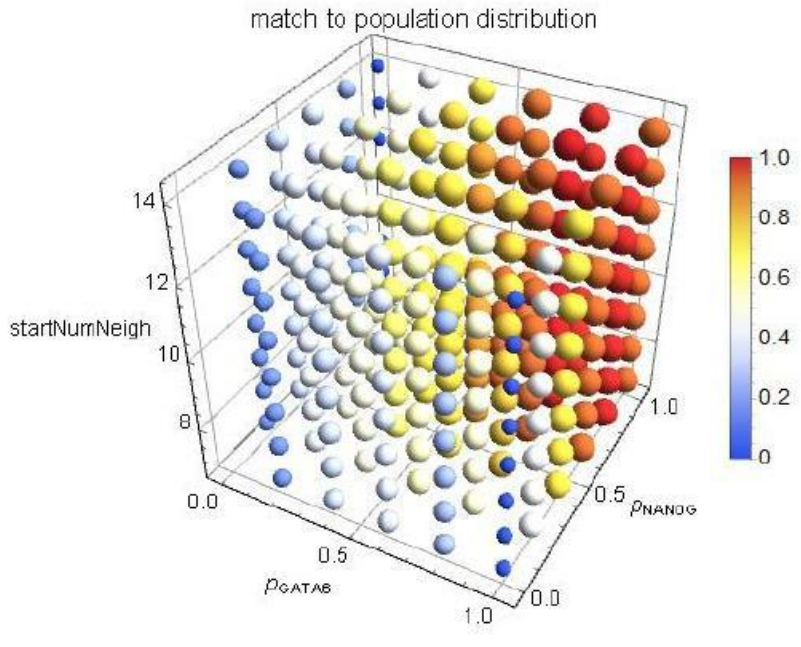

Fig 7: Higher values of p_{NANOG} and p_{GATA6} provide a better match of the simulations to the experimental data. Simulation match to experimental data from early embryos (normalized to [0,1]) for the four populations model, varying p_{NANOG} and p_{GATA6} between 0 and 1 and startNumNeigh between 7 and 14.

Varying startNumNeigh independently showed the best match for 14, followed by 9 (Fig 8A). Plotting the population distributions however showed that the differences between the simulations are negligible (Fig 8B).

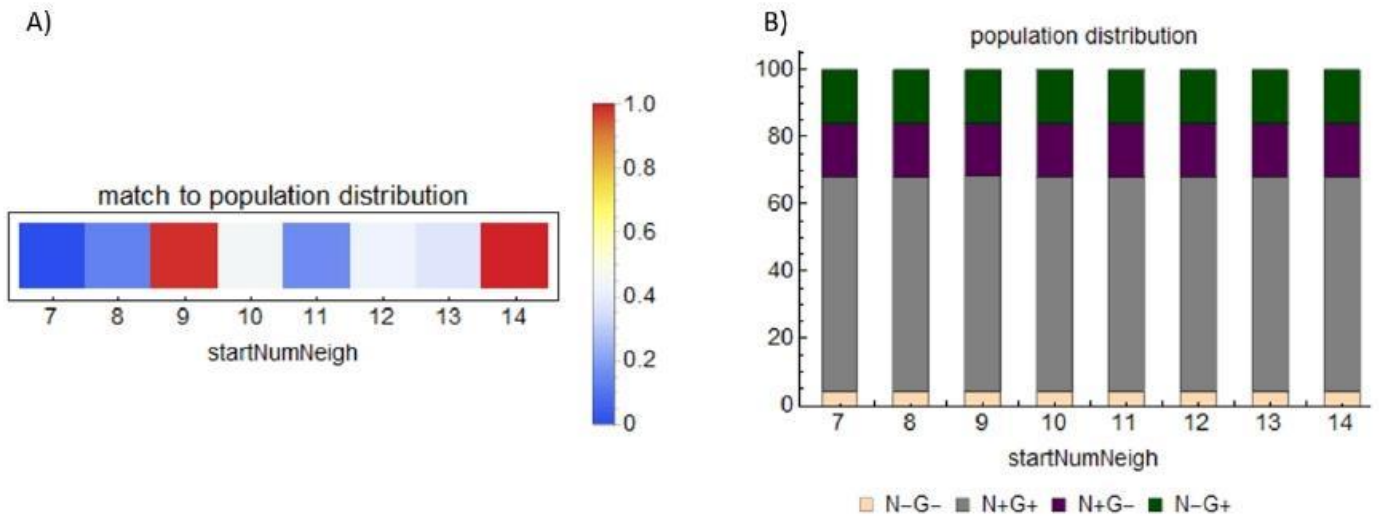

Fig 8: The four populations model is robust with respect to the parameter startNumNeigh. Simulation match to experimental data from early embryos (normalized to [0,1]) (A) and population distributions (B) for the four populations model for $p_{NANOG} = 0.8$ and $p_{GATA6} = 0.8$ and startNumNeigh varying between 7 and 14.

Varying p_{NANOG} and p_{GATA6} shows that for values between 0.6 and 1 for both parameters, we obtain a reasonable fit, with the best fit for $p_{NANOG} = 0.8$ and $p_{GATA6} = 0.8$ (Fig 9A). Plotting the population distribution for the simulations of these nine parameter combinations, shows that increasing the values for p_{NANOG} or p_{GATA6} changes the composition of the populations in the simulated ICMs (Fig 9B). If p_{NANOG} or p_{GATA6} is one, only up to two populations arise. For values below one for p_{NANOG} and p_{GATA6}, the four populations arise and become more evenly distributed the smaller the values are.

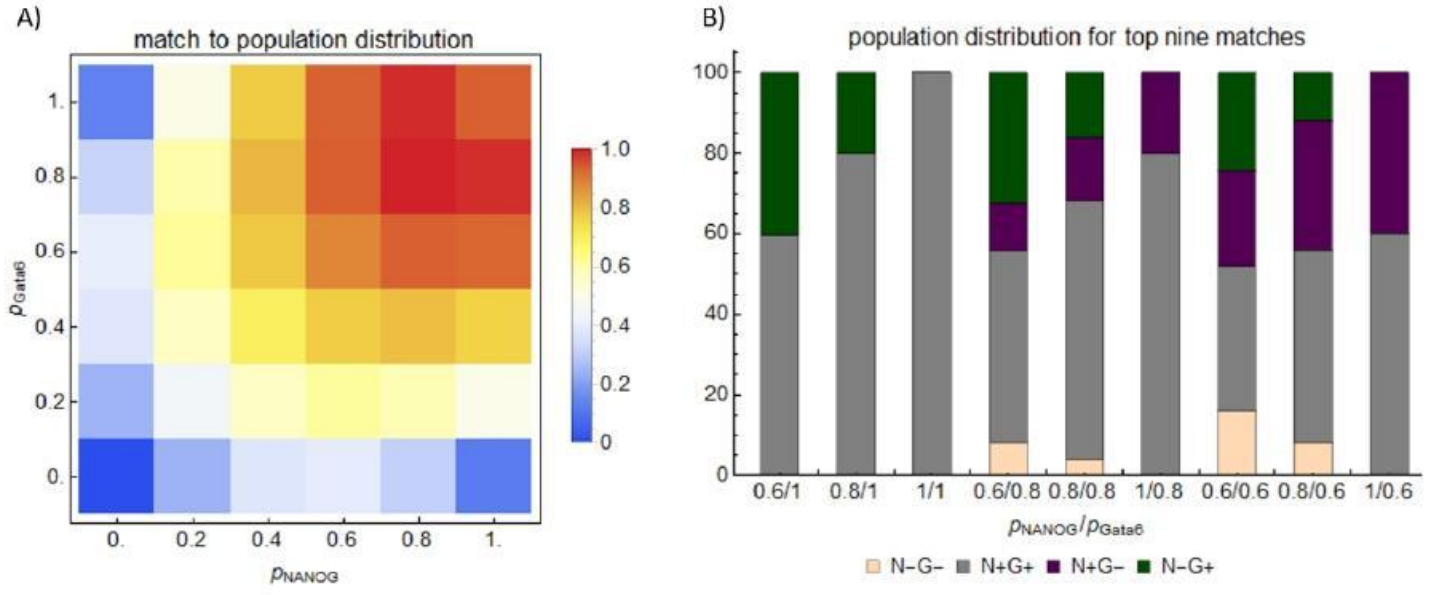

Fig 9: The values of p_{NANOG} and p_{GATA6} determine the population distributions in the simulated ICMs. Simulation match to experimental data from early embryos (normalized to [0,1]) (A) and population distributions for the top nine matches (B) for the four populations model for $\mathrm{startNumNeigh} = 9$ and p_{NANOG} and p_{GATA6} varying between 0 and 1.

References:

1. Saiz N, Williams KM, Seshan VE, Hadjantonakis A-K. Asynchronous fate decisions by single cells collectively ensure consistent lineage composition in the mouse blastocyst. Nat Commun. 2016;7: 13463. doi:10.1038/ncomms13463
2. Schmitz A, Fischer SC, Mattheyer C, Pampaloni F, Stelzer EHK. Multiscale image analysis reveals structural heterogeneity of the cell microenvironment in homotypic spheroids. Sci Rep. 2017;7: 43693. doi:10.1038/srep43693

3. Kaliman S, Jayachandran C, Rehfeldt F, Smith A-S. Limits of Applicability of the Voronoi Tessellation Determined by Centers of Cell Nuclei to Epithelium Morphology. Front Physiol. 2016;7: 551. doi:10.3389/fphys.2016.00551

4. Schaller G, Meyer-Hermann M. Multicellular tumor spheroid in an off-lattice Voronoi-Delaunay cell model. Phys Rev E. 2005;71: 051910. doi:10.1103/PhysRevE.71.051910

5. Lou X, Kang M, Xenopoulos P, Muñoz-Descalzo S, Hadjantonakis AK. A rapid and efficient 2D/3D nuclear segmentation method for analysis of early mouse embryo and stem cell image data. Stem Cell Reports. 2014;2: 382–397. doi:10.1016/j.stemcr.2014.01.010

6. Tosenberger A, Gonze D, Bessonnard S, Cohen-Tannoudji M, Chazaud C, Dupont G. A multiscale model of early cell lineage specification including cell division. npj Syst Biol Appl. 2017;3: 16. doi:10.1038/s41540-017-0017-0

7. Quinn GP, Keough MJ. Experimental Design and Data Analysis for Biologists. 2002 [cited 13 Feb 2018]. Available: http://www.cambridge.org

8. Goodwin LD, Leech NL. Understanding Correlation: Factors That Affect the Size of r. J Exp Educ. 2006;74: 249–266. doi:10.3200/JEXE.74.3.249-266

3. Maternal age, obesity and hyperglycaemia are associated with a delay in preimplantation embryo development in mouse

Reproduction

Maternal age, obesity and hyperglycaemia are associated with a delay in preimplantation embryo development in mouse

Journal:	*Reproduction*
Manuscript ID	REP-23-0024
mstype:	Research paper
Date Submitted by the Author:	24-Jan-2023
Complete List of Authors:	Lilao-Garzón, Joaquín; University of Las Palmas de Gran Canaria, University Institute of Biomedical and Healthcare Research Brito-Casillas, Yeray; University of Las Palmas de Gran Canaria, University Institute of Biomedical and Healthcare Research Quesada-Canales, Oscar; University of Las Palmas de Gran Canaria Faculty of Veterinary, Veterinary Histology and Pathology Wägner, Ana; University of Las Palmas de Gran Canaria, University Institute of Biomedical and Healthcare Research; Complejo Hospitalario Materno-Insular, Servicio Endocrinología y Nutrición Munoz-Descalzo, Silvia; University of Las Palmas de Gran Canaria, University Institute of Biomedical and Healthcare Research
Keywords:	obesity, metabolic syndrome, Cell fate, Quantitative immunofluorescence, Embryo development

Maternal age, obesity and hyperglycaemia are associated with a delay in preimplantation embryo development in mouse

Joaquín Lilao-Garzón[1], Yeray Brito-Casillas[1], Oscar Quesada-Canales[2], Ana M Wägner[1,3,*] and Silvia Muñoz-Descalzo[1,*]

1: Instituto Universitario de Investigaciones Biomédicas y Sanitarias (IUIBS), University of Las Palmas de Gran Canaria (ULPGC), Spain.

2: Veterinary Histology and Pathology, Veterinary School, Institute of Animal Health, University of Las Palmas de Gran Canaria, Spain.

3: Servicio Endocrinología y Nutrición. Complejo Hospitalario Universitario Insular Materno-Infantil de Gran Canaria, Spain.

Orcid:

JLG: Joaquin.lilao@ulpgc.es; https://orcid.org/0000-0002-9971-2459

YBC: Yeray.brito@ulpgc.es; https://orcid.org/0000-0002-0707-7444

OQC: Oscar.quesada@ulpgc.es; https://orcid.org/0000-0002-2365-351X

AMW: Ana.wagner@ulpgc.es; https://orcid.org/0000-0002-7663-9308

SMD: Silvia.munoz@ulpgc.es; https://orcid.org/0000-0003-0939-7721

***Corresponding authors:** SMD silvia.munoz@ulpgc.es (+34 928453473) and AMW ana.wagner@ulpgc.es (+34 928453431)

Keywords: High fat diet, obesity, metabolic syndrome, pregnancy, Fertility, Embryo, Blastocyst, Cell fate, Quantitative immunofluorescence.

Word count: 3505

Main Figures: 7

Abstract

Delayed maternal age, obesity and diabetes are associated with reduced fertility. We investigated how age and obesity/metabolic syndrome impact fertility and hypothesized that its decrease is due to defects in preimplantation embryo development.

Three groups of female C57Bl6 mice (12 weeks, 9 months and 1 year old) were fed either a high fat diet for 8 weeks, to induce obesity and the metabolic syndrome, or a control chow diet. Body weight and composition, glucose tolerance and insulin resistance were assessed. Fecundity was evaluated by mating and pregnancy rates, as well as number of embryos. Embryo quality was assessed morphologically, and cell fate composition was analysed in preimplantation embryos by state-of-the-art single cell quantitative confocal image analysis.

The high fat diet was associated with increased adiposity, glucose intolerance and insulin resistance, especially in the older mice. Fecundity was affected by age, more than by the diet. Both age and high fat diet were associated with reduced cell fate allocation, indicating a delay in preimplantation embryo development, and with increased expression of GATA3, an inhibitor of placentation.

These results support that age and the metabolic syndrome reduce fertility through mechanisms which are present at conception very early in pregnancy.

Introduction:

Lifestyle changes have led to an epidemic increase in obesity and type 2 diabetes, both of which have a negative impact on fertility [1] and offspring health [2]. Intrauterine exposure to diabetes and obesity is associated with short and long-term health risks, such as congenital anomalies and stillbirth, neurodevelopmental disorders, obesity, heart disease and type 2 diabetes [3–5].

Furthermore, the age at first pregnancy has been delayed in Europe to 29.4 years in 2019 [6] with consequences on reproductive capacity, embryo quality and even offspring's overall health [7].

Fecundity is defined by the physiological potential to bear offspring while fertility is the actual number of offspring produced [8]. Obesity and glucose dysregulation lead to altered puberty, ovulation and fertility in women [9]. Therefore, women with obesity and/or diabetes have worse outcomes following fertility treatments, usually due to poorer response to gonadotropins and lower yields in harvested oocytes [10]. Moreover, live birth rates can increase up to 9% for every unit decrease in BMI [11].

The aim of this study was to assess the effect of age and obesity/metabolic syndrome on different aspects related to fertility: fecundability, embryo number and quality and embryo cell type composition. To do this, an established murine model of the metabolic syndrome was used, which underwent further characterisation.

Materials and Methods

C57Bl/6J mice were bred in house at the Universidad de Las Palmas de Gran Canaria (ULPGC) at the Institute for Biomedical and Healthcare Research

(IUIBS) animal facility. All mice were housed with controlled room temperature (20-24ºC) and relative humidity (55-72%), and a 12-h light-darkness cycle. All animal studies were conducted following National and European regulations (RD 1201/2005, Law 32/2007, EU Directive 2010/63/EU), were approved by the Animal Ethics Committee of the ULPGC and were authorised by the competent authority of the Canary Islands Government (reference number: OEBA-ULPGC_10/2019R1).

On average, female mammals cease to exhibit reproductive cycles by middle age, around 15 months in mouse or 51 years in humans, while reproductive maturity is reached at 42 days in mice and 11.5 years in humans [12]. Female mice were divided into three age groups: young adults at the beginning of their reproductive life (Y:12 weeks old), mature adults (M: 9 months old) and middle-late age adults when they were close to reproductive senescence (O: 1 year old). Animals from different cages but with the same date of birth were grouped together and then randomly assigned to one of two diets following ARRIVE guidelines [13]. High fat diet (HFD) in rodents is an established model for the induction of obesity and the metabolic syndrome [14–16]. Half of the animals were fed a standard diet (ND) (Envigo, Global Diet 2014) and the other half a HFD (60% energy from fat, D12492; Research Diets, Brogaarden, Lynge, Denmark) for 8 weeks prior to the target age (Fig. 1). Body weight was measured weekly. At the time of the study, morphometry was performed (head, body and tail length), body mass index (BMI) was calculated [17] and body composition measured, by Time Domain Nuclear Magnetic Resonance using a Minispec lean fat analyzer (Bruker Optics, Inc., The Woodlands, TX). Healthy males of up to 6 months of age, from the same colony, were used for breeding purposes.

Oral Glucose Tolerance Test and Intraperitoneal Insulin Tolerance Test

For the Oral Glucose Tolerance test (OGTT), on the eighth week of diet, mice were fasted for 6h and a 2 g/Kg dose of glucose (G7528, Sigma-Aldrich Chemie GmbH, Steinheim, Germany) was administered by oral gavage. Blood was sampled from the tip of the tail every 15 minutes up to 1 hour and glucose concentrations were measured and recorded (Glucomen Areo, Menarini Diagnostics). An insulin tolerance test (ITT) was performed by intraperitoneal administration of 0.5 U/Kg of insulin (Actrapid, Novo Nordisk, Copenhagen, Denmark), two days after the OGTT following the same protocol [18].

Postmortem Analysis

Animals were killed by isoflurane overdose and bled out from the inferior vena cava. Serum was obtained and a full biochemistry panel comprising albumin, alkaline phosphatase, alanine aminotransferase, amylase, blood urea nitrogen, creatinine, globulin, glucose, phosphorus, total bilirubin, total protein, cholesterol and creatine kinase, was performed (PointCare V2 Biochemistry Analyzer, RAL SA, Barcelona).

Liver, pancreas, heart, spleen, reproductive system, white and brown fat, kidneys, and gastrocnemius muscle were dissected during the necropsy. The tissues were weighed and preserved in 4% neutral buffered formalin (Applichem-Panreac, Barcelona), processed routinely, and embedded in paraffin-wax. Sections (5 µm-thick) were stained with haematoxylin-eosin. All histological sections were randomly and blindly evaluated by a board-certified veterinary pathologist (OQC).

Pancreatic insulin content was evaluated by immunofluorescence. After permeabilization with Triton X-100 0.05%, pancreas sections were incubated with anti-insulin (Santa Cruz, Dallas, TX, USA, sc-9168; 1:80) and anti-Glucagon antibodies (Sigma-Aldrich, G2654, St. Louis, MO, USA, 1:100). Alexa Fluor 488 Tyramide Superboost kit (Invitrogen/Thermo Fisher Scientific, Waltham, MA, USA, B40943) was used to increase insulin fluorescent signal following the manufacturer's instructions.

Fecundity Analysis

Animals were mated for up to eight days to allow two consecutive oestrus cycles and pregnancy was confirmed by the presence of a vaginal plug. The ability to mate and get pregnant and the number of embryos per female were used as fecundity indicators. Mating rate was calculated as the proportion of females with a vaginal plug, as an indirect measure of oestrus cycle. Fertilization rate was calculated as the percentage of females with a plug which had embryos in their uteri. Preimplantation embryo quality was assessed by morphological features and classified into 4 categories (A-D) [19].

Preimplantation embryo analysis

Before implantation, the mammalian embryo develops into a structure known as blastocyst in which three cell types can be identified [20]. The outer cells, the trophectoderm (TE), become the foetal portion of the placenta. The compact inner cells form the inner cell mass (ICM), which will differentiate into Epiblast (Epi) or Primitive Endoderm (PrE). PrE cells generate the endodermal part of the yolk sac while Epi cells form the proper embryo. TE cells are characterized by the expression of markers like GATA3 or CDX2 while in early embryos ICM cells co-

express both NANOG and GATA6. During differentiation of the ICM in mid blastocysts, cells asynchronously downregulate one of these markers so that Epi progenitors express NANOG, while PrE progenitors express GATA6 [21] followed by other markers such as SOX17, GATA4, or SOX7 [20]. In late blastocysts, PrE cells migrate to form an epithelial layer of cells next to the blastocoele, leaving the Epi cells in an internal localization. These differentiation processes, occurring prior to implantation, can be assessed using quantitative immunofluorescence analysis (QIF) [22]. After 3.5 days of embryonic development, females were killed and preimplantation embryos were flushed from dissected uteri in M2 medium (Embryomax®; Millipore, Ref. MR-015-D, Burlington, MA, EE. UU) and prepared for immunofluorescence as previously described [23]. Primary antibodies were anti-NANOG raised in rat (eBioscience, San Diego, CA, USA, Ref.14–5761; 1:200), anti-GATA6 raised in goat (R&D Systems, Minneapolis, MN, USA, AF1700; 1:200), anti-GATA4 raised in rabbit (Santa Cruz, Dallas, TX, USA, sc-9053; 1:200) and anti-GATA3 raised in rabbit (eBioscience, San Diego, CA, USA, Ref. MA1-028; 1:200). DAPI (Invitrogen/Thermo Fisher Scientific, Waltham, MA, USA, D1306; 1:1000) was used to stain the nuclei.

Microscopy and Image Analysis

Both Islets of Langerhans and embryos were imaged using a Zeiss LSM Zeiss LSM700 and a Plan-Apochromat 40x/1.3 Oil DIC (UV) VIS-IR M27 objective, with optical section thickness of 1 µm.

Embryo images were processed and analysed as previously described [22] including the fluorescence decay along the Z axis correction [24]. Briefly, using image analysis tools (MINS) [25], after immunostaining and confocal imaging,

NANOG and GATA6 (GATA4 and/or GATA3) expression levels can be quantified in single cells allowing to monitor the ICM cells differentiation process by custom-made data analyses codes in Mathematica described in [22]. Embryos were classified, according to their total cell number, into early (up to 64 cells), mid (65-90 cells) and late (from 91 cells). Cells were then manually classified into TE and ICM. Cells in the ICM were classified using mixture analysis as positive or negative: double negative (DN, negative expression for NANOG and GATA6), Epi progenitors (positive for NANOG and negative for GATA6), PrE progenitors (negative for NANOG and positive for GATA6), and double positive (DP) for uncommitted ICM cells positive for both, NANOG and GATA6. The same classification was based on GATA4 staining instead of GATA6.

Statistics

Data are presented as mean ± standard error (SEM). Anova with Tukey's multiple comparisons test was used for comparisons between groups and Z-test for frequencies, followed by the Bonferroni correction for multiple comparisons. Values of $p < 0.05$ were considered statistically significant.

Results

Eight weeks of HFD are associated with altered body composition and glucose metabolism, especially in older animals. Rapid weight gain was observed in the mature and old groups on HFD, whereas no significant effect on body weight or BMI was seen in young animals (Fig. 2a, b). HFD was consistently associated with increased total body fat and reduced lean mass (Fig. 2c).

OGTTs and ITTs were performed in the last week of diet to evaluate the effect of both age and HFD on glucose metabolism (Fig. 1, 2). The mice fed with the HFD

showed higher glucose concentrations during the OGTT than those fed with ND, and this was especially evident in the older mice (Fig. 2d). HFD was also associated with decreased glucose-lowering after an insulin injection, reflecting increased insulin resistance (Fig. 2e).

HFD results in increased white fat and reduced muscle mass and high cholesterol and glucose, but no major pathological findings.

Post mortem studies confirmed that animals fed with the HFD had more body fat and less muscle mass than those fed with ND (Fig. 3a, b). A weight increase was also observed in the reproductive system, but this increase was due to the increment of periovaric fat (Supp. Fig. 1). Furthermore, high levels of fat in the diet seem to have a weight curbing effect on the liver and pancreas. In the blood biochemistry results, animals were grouped according to their diet to increase statistical power. Animals fed with HFD showed higher glucose and total cholesterol concentrations than those fed with ND (Fig. 3c, d). High glucose concentrations were observed even in the blood from animals fed with the ND obtained post-mortem from the inferior vena cava, in agreement with previous reports [26, 27] and is attributed to isofluorane [28]. No differences were observed in other measurements (Supp. Fig. 2).

Histological findings were consistent with senescence and/or the phenotype of the model (Table 1). In the absence of an infectious agent, the hepatocellular necrosis observed can be considered as background lesion [29–32]. Also, the systemic amyloidosis observed is considered a common age-related change in some mouse strains, such as the C57BL6 [29] and is consistent with the diagnosis of spontaneous systemic amyloidosis [33].

Young groups showed fewer lesions than older groups, but no evident differences were noted between animals fed with ND or with HFD at any age. No qualitative differences were observed in pancreatic insulin or glucagon content comparing age groups or diets (Fig. 3e).

Overall fecundity decreases with age. Mating and fertilization rates were used as descriptive methods to assess fecundity. Old animals fed with HFD showed lower mating and fertilization rates than younger groups (Fig. 4). Only one old ND fed dam had embryos and no embryos were obtained in old HFD fed dams. Hence, the old groups were excluded from further analysis.

Embryo quality was assessed according to morphological features. Young ND fed dams had a higher percentage of high quality (category A) embryos and fewer with the worst features (category D) compared with young HFD fed dams (Fig. 4e). Total cell number together with the classification into TE or ICM cells was done, and the ratio ICM/TE calculated. An age effect was observed in HFD fed groups (see Supp. Table 1), indicating altered patterns in embryo cell fate allocation.

Age and HFD are associated with delayed development in preimplantation embryos. Preimplantation embryos flushed from the uteri were stained for GATA3, NANOG and GATA6 and images were analysed by single-cell quantitative methods (Figs. 5-6). Results for early embryos are shown (see classification details in Methods). In general, embryos from HFD fed females showed an increased proportion of uncommitted cells (DP cells) when compared with their ND fed controls. This is especially noticeable in mature groups where

Epi progenitor proportion diminished upon HFD feeding (Fig. 6a). Comparing embryos from different ages, despite no change in uncommitted cells, those from mature dams showed a defect in PrE cell fate progression.

Although the population analysis showed more Epi progenitors in embryos from young HFD fed animals, NANOG levels were significantly lower both in DP cells (Fig. 6b) and in Epi progenitors (Fig. 6c). The same was observed in embryos from mature dams regardless of the diet: NANOG levels were significantly lower in DP cells (Fig. 6b). Epi progenitors showed higher levels of NANOG in embryos from mature HFD fed females (Fig. 6c).

GATA6 levels were significantly lower in embryos from HFD fed females independently of the age in DP cells (Fig. 6d). Embryos from MND fed females showed higher levels of GATA6 than those from YND fed females (Fig. 6d).

Equivalent results were obtained for the population analysis in mid and late embryos (Supp. Fig. 3) as well as the analysis with the more developmentally advanced PrE marker GATA4 (Supp. Fig. 4).

The higher number of uncommitted cells together with fewer cells fully committed to one cell fate (especially to PrE), and cell fate marker levels indicate that preimplantation embryos developed under an obese environment or from mature females are delayed in their normal development when compare to controls.

Both HFD and advanced maternal age had an increasing effect in the levels of GATA3. GATA3 was analysed in the TE cells where it was almost ubiquitously expressed (Fig. 7a). GATA3 expression increased with age. However, its response to HFD changed in opposite directions in young (increase) and mature (decrease) dams (Fig. 7b).

Discussion

In the present study, we assessed the impact of maternal age and HFD on early embryo development, specifically Epi versus PrE cell fate decision, through state-of-the-art single cell quantitative confocal image analysis [22]. Indeed, HFD led to increased body fat, glucose intolerance and insulin resistance. To our knowledge, this is the first study to report delayed early embryo development, based on Epi versus PrE cell fate specification, associated with both HFD and age. We also describe alterations in GATA3 levels, showing an effect of age and HFD in TE differentiation. This is significant as it allows us to establish embryo development disorders that could be responsible for embryo loss in the first few days after fertilization, leading to the low fertility described in older and overweight women [10].

We first confirmed that 8 weeks of HFD in adulthood induced overweight in female mice as shown in previous studies [34, 35] but not when started before puberty. Despite similar weight and BMI, the young HFD fed animals showed almost twice as much fat mass as their control group. The OGTT and ITT revealed that HFD induces glucose impairment and insulin resistance, especially in the older groups. However, age itself did not have a direct effect on glucose intolerance, in agreement with a previous study [35].

Frequently, when the effects of childhood obesity in adulthood are assessed, only body weight and BMI are used as indicators [36]. Here, we show that in young mice, 8 weeks of HFD did not affect body weight and BMI. However, other parameters that affect overall health such as body composition and glucose metabolism were severely affected.

Furthermore, we validated the 8 weeks HFD in C57Bl6 female mice as a prediabetic mouse model with different levels of obesity and hyperglycaemia depending on age; young adults, mature adults, and middle-late age adults. This strategy allowed us to evaluate how HFD and maternal age affect fecundity.

Selected maternal ages were based on previous studies. Mice are often divided into mature adults (3-6 months), middle aged (10-15 months) and old (18-24 months) [37, 38] with some authors even expanding mouse lifespan up to 36 months [39]. In this context, their reproductive senescence is established between 10 to 15 months. Other authors establish the irregular fertility that precedes reproductive senescence at approximately 8 months of age [40] in accordance with the lower fertility observed in mature groups in the present study.

Infertility (failure to conceive after attempting at least twelve months of natural fertilization) is a rising problem in our society. Life factors such as psychological stress, smoking, drugs or diet and variations in body weight have a substantial effect. Overweight in women is often associated with multiple reproductive disorders such as polycystic ovary syndrome, infertility, increased miscarriage rate, as well as pregnancy complications (gestational diabetes, pre-eclampsia, and macrosomia). Furthermore, overweight (BMI>25 Kg/m^2) and obese (BMI>30 Kg/m^2) women have worse outcomes following fertility treatments than women with normal BMI. They respond poorly to induction of ovulation, require higher doses of gonadotropins and longer treatment courses for follicular development and ovulatory cycles [41]. When focusing on their blastocyst quality, high BMI is not associated with low embryo quality, though the implantation rate is reduced [42–44]. Type 2 diabetes is most frequently associated with obesity. However, in the absence of obesity, type 2 diabetes is also associated with reduced fertility

and more frequent need for assisted reproduction [45]. Implantation rate is indeed reduced in women with type 2 diabetes, regardless of BMI, as shown by a recent study based on the Danish registry of assisted reproductive techniques [44]. Our results showed no significant differences in mating or fertilization rates. However, we did observe reduced embryo quality in YHFD fed females. Surprisingly, no diet effect was observed in embryos from mature females suggesting that age itself has a bigger impact than obesity.

During mammalian preimplantation development, two sequential cell fate decisions occur. The first decision induces TE (precursor of the placenta) versus ICM cells. The ICM cells make a further decision, differentiating either into Epi or into PrE [20]. Evidence suggests that inflammation and oxidative stress can severely affect these cellular events and embryo quality [46]. Moreover, preimplantation embryos cultivated with lipopolysaccharides showed a lower proportion of SOX17 expressing cells, suggesting that the oxidative stress induced by lipopolysaccharides could be impairing the normal development of the embryonic PrE. Furthermore, the correction of the associated oxidative stress, reverted these PrE development impairments [46].

GATA3 is highly expressed in the invasive murine trophoblast giant cells of the blastocyst and its knockdown enhances placental cell invasion [47]. Hence, the high levels of GATA3 associated with HFD we observe here might impair placentation. Similarly, embryos treated with lipopolysaccharides also showed an increased expression of TE markers [46].

A limitation of this study is that we did not measure caspase-3 activity or reactive oxygen species (ROS) in the embryos to assess oxidative stress. However,

previous studies showed that oxidative stress is strongly correlated with the prevalence of type 2 diabetes, obesity and aging through different mechanisms such as high ROS production caused by hyperglycaemia and oxidation of fatty acids or by the decrease in antioxidant capacity [48–51]. Also, while 8 weeks of HFD feeding may be enough to model changes in embryo development, lifelong female obesity may have more drastic effects.

In summary, we demonstrated that 8 weeks of HFD are enough to model obesity and the metabolic syndrome in mice even at young ages when there are no apparent effects on weight. Age seems to be the most important factor determining reduced fecundity, but both HFD and age are associated with delayed preimplantation embryo development that might explain the lower implantation rates observed in women with overweight or type 2 diabetes [42, 44].

Contribution statement

JLG, YBC, AMW and SMD conceived and designed the research; JLG, YBC, OQC and SMD performed the research, acquired the data and analysed the results; JLG, YBC, SMD and AMW analysed and interpreted the data. All authors were involved in drafting and revising the manuscript. SMD is the guarantor of all the data.

Disclosure of interest

The authors declare that there is no conflict of interest that could be perceived as prejudicing the impartiality of the research reported.

Funding

This work was supported at SMD lab by the ACIISI (CEI2019-02), Programa de Ayudas a la Investigación de la ULPGC, and ACIISI co-funded by FEDER Funds (ProID2020010013). Also at AMW lab by Instituto de Salud Carlos III (PI16/00587, PI20/00846, PMP21/00069) and ACIISI (ProID2021010143) co-

funded by European Regional Development Funds, as well as the European Horizon 2020 Programme (101017385) and Fundación Canaria del Instituto de Investigaciones Sanitarias de Canarias (PI19/30, PIFIISC20/16). JLG is supported by the ULPGC predoctoral program. SMD by the “Viera y Clavijo” Program from the Agencia Canaria de Investigación, Innovación y Sociedad de la Información (ACIISI) and the ULPGC.

Acknowledgements

We are grateful to Tina Balayo, Ana Exposito-Montesdeoca and the IUIBS animal facility staff for the technical support. Sabine Fischer for data analysis support.

References

1. Thong EP, Codner E, Laven JSE, Teede H (2020) Diabetes: a metabolic and reproductive disorder in women. Lancet Diabetes Endocrinol 8(2):134–149. https://doi.org/10.1016/S2213-8587(19)30345-6

2. Fleming TP, Watkins AJ, Velazquez MA, et al (2018) Origins of lifetime health around the time of conception: causes and consequences. Lancet (London, England) 391(10132):1842. https://doi.org/10.1016/S0140-6736(18)30312-X

3. Faruque S, Tong J, Lacmanovic V, Agbonghae C, Minaya DM, Czaja K (2019) The Dose Makes the Poison: Sugar and Obesity in the United States – a Review. Polish J Food Nutr Sci 69(3):219

4. Godfrey KM, Reynolds RM, Prescott SL, et al (2017) Influence of maternal obesity on the long-term health of offspring. Lancet Diabetes Endocrinol. 5:53–64

5. Ornoy A, Reece EA, Pavlinkova G, Kappen C, Miller RK (2015) Effect of maternal diabetes on the embryo, fetus, and children: Congenital anomalies, genetic and epigenetic changes and developmental outcomes. Birth Defects Res Part C - Embryo Today Rev 105(1):53–72. https://doi.org/10.1002/bdrc.21090

6. Women in the EU are having their first child later - Products Eurostat News - Eurostat. https://ec.europa.eu/eurostat/web/products-eurostat-news/-/ddn-20210224-1. Accessed 24 Mar 2022

7. Myrskylä M, Fenelon A (2012) Maternal Age and Offspring Adult Health: Evidence From the Health and Retirement Study. Demography 49(4):1231–1257. https://doi.org/10.1007/s13524-012-0132-x

8. Shenk M (2015) Fertility and fecundity. Int. Encycl. Hum. Sex. 369–426

9. Nandi A, Poretsky L (2013) Diabetes and the female reproductive system. Endocrinol Metab Clin North Am 42(4):915–946. https://doi.org/10.1016/J.ECL.2013.07.007

10. Silvestris E, de Pergola G, Rosania R, Loverro G (2018) Obesity as disruptor of the female fertility. 16(1):1–13

11. Grzegorczyk-Martin V, Fréour T, de Bantel Finet A, et al (2020) IVF outcomes in patients with a history of bariatric surgery: a multicenter retrospective cohort study. Hum Reprod 35(12):2755–2762. https://doi.org/10.1093/HUMREP/DEAA208

12. Men and mice: Relating their ages | Elsevier Enhanced Reader. https://reader.elsevier.com/reader/sd/pii/S0024320515300527?token=CE03E74B95ABE77B63A2F62BCA8378DF86349C4B6FF3AAADDAB8F3DD3A6D7D87DE97AAB1B3DFCC2ECD1A6157C30F3BF7&originRegion=eu-west-1&originCreation=20220216110724. Accessed 16 Feb 2022

13. Percie Du Sert N, Hurst V, Ahluwalia A, et al (2020) The ARRIVE guidelines 2.0: Updated guidelines for reporting animal research. BMC Vet Res 16(1):1–7. https://doi.org/10.1186/S12917-020-02451-Y/TABLES/2

14. Chen T, Hill JT, Moore TM, et al (2020) Lack of skeletal muscle liver kinase B1 alters gene expression, mitochondrial content, inflammation and oxidative stress without affecting high-fat diet-induced obesity or insulin resistance. Biochim Biophys Acta - Mol Basis Dis 165805. https://doi.org/10.1016/j.bbadis.2020.165805

15. Igosheva N, Abramov AY, Poston L, et al (2010) Maternal Diet-Induced Obesity Alters Mitochondrial Activity and Redox Status in Mouse Oocytes and Zygotes. PLoS One 5(4):e10074–e10074. https://doi.org/10.1371/journal.pone.0010074

16. Lilao-Garzón J, Valverde-Tercedor C, Muñoz-Descalzo S, Brito-Casillas Y, Wägner AM (2020) In Vivo and In Vitro Models of Diabetes: A Focus on Pregnancy. In: Advances in experimental medicine and biology. Adv Exp Med Biol

17. Gargiulo S, Gramanzini M, Megna R, et al (2014) Evaluation of growth patterns and body composition in c57bl/6j mice using dual energy x-ray absorptiometry. Biomed Res Int 2014.

https://doi.org/10.1155/2014/253067

18. Brito-Casillas Y, Melián C, Wägner AM (2016) Study of the pathogenesis and treatment of diabetes mellitus through animal models. Endocrinol y Nutr 63(7):345–353. https://doi.org/10.1016/j.endonu.2016.03.011

19. Gardner DK, Balaban B (2016) Assessment of human embryo development using morphological criteria in an era of time-lapse, algorithms and "OMICS": is looking good still important? Mol Hum Reprod 22(10):704–718. https://doi.org/10.1093/MOLEHR/GAW057

20. Rossant J (2018) Genetic Control of Early Cell Lineages in the Mammalian Embryo. https://doi.org/101146/annurev-genet-120116-024544 52:185–201. https://doi.org/10.1146/ANNUREV-GENET-120116-024544

21. Saiz N, Williams KM, Seshan VE, Hadjantonakis A-K (2016) Asynchronous fate decisions by single cells collectively ensure consistent lineage composition in the mouse blastocyst. Nat Commun 7:13463. https://doi.org/10.1038/ncomms13463

22. Fischer SC, Corujo-Simon E, Lilao-Garzon J, Stelzer EHK, Muñoz-Descalzo S (2020) The transition from local to global patterns governs the differentiation of mouse blastocysts. PLoS One 15(5). https://doi.org/10.1371/journal.pone.0233030

23. Nichols J, Silva J, Roode M, Smith A (2009) Suppression of Erk signalling promotes ground state pluripotency in the mouse embryo. Development 136(19):3215–3222. https://doi.org/10.1242/dev.038893

24. Saiz N, Mora-Bitrià L, Rahman S, et al (2020) Growth-factor-mediated coupling between lineage size and cell fate choice underlies robustness of mammalian development. Elife 9:1–38. https://doi.org/10.7554/ELIFE.56079

25. Lou X, Kang M, Xenopoulos P, Muñoz-Descalzo S, Hadjantonakis AK (2014) A rapid and efficient 2D/3D nuclear segmentation method for analysis of early mouse embryo and stem cell image data. Stem Cell Reports 2(3):382–397. https://doi.org/10.1016/j.stemcr.2014.01.010

26. Yu Q, Li J, Dai C ling, et al (2020) Anesthesia with sevoflurane or isoflurane induces severe hypoglycemia in neonatal mice. PLoS One 15(4):e0231090. https://doi.org/10.1371/JOURNAL.PONE.0231090

27. Chan YK, Davis PF, Poppitt SD, et al (2012) Influence of tail versus cardiac sampling on blood glucose and lipid profiles in mice. Lab Anim 46:142–147. https://doi.org/10.1258/la.2011.011136

28. Horber FF, Krayer S, Miles J, Cryer P, Rehder K, Haymond MW (1990) Isoflurane and whole body leucine, glucose, and fatty acid metabolism in dogs. Anesthesiology 73(1):82–92. https://doi.org/10.1097/00000542-199007000-00013

29. Thoolen B, Maronpot RR, Harada T, et al (2010) Proliferative and nonproliferative lesions of the rat and mouse hepatobiliary system. Toxicol Pathol 38(7 SUPPL.). https://doi.org/10.1177/0192623310386499

30. Tessitore A, Cicciarelli G, Del Vecchio F, et al (2016) MicroRNA expression analysis in high fat diet-induced NAFLD-NASH-HCC progression: study on C57BL/6J mice. BMC Cancer 16(1). https://doi.org/10.1186/S12885-015-2007-1

31. Hall WC, Ganaway JR, Rao GN, et al (1992) Histopathologic observations in weanling B6C3F1 mice and F344/N rats and their adult parental strains. Toxicol Pathol 20(2):146–154. https://doi.org/10.1177/019262339202000202

32. Percy DH, Barthold SW, Griffey SM Pathology of laboratory rodents and rabbits. 371

33. Willard-Mack CL, Elmore SA, Hall WC, et al (2019) Nonproliferative and Proliferative Lesions of the Rat and Mouse Hematolymphoid System. Toxicol Pathol 47(6):665. https://doi.org/10.1177/0192623319867053

34. Picklo MJ, Idso J, Seeger DR, Aukema HM, Murphy EJ (2017) Comparative effects of high oleic acid vs high mixed saturated fatty acid obesogenic diets upon PUFA metabolism in mice. Prostaglandins, Leukot Essent Fat Acids 119:25–37. https://doi.org/10.1016/J.PLEFA.2017.03.001

521 35. Soleimanzad H, Montaner M, Ternier G, et al (2021) Obesity in Midlife
522 Hampers Resting and Sensory-Evoked Cerebral Blood Flow in Mice.
523 Obesity 29(1):150–158. https://doi.org/10.1002/OBY.23051

524 36. Bentham J, Di Cesare M, Bilano V, et al (2017) Worldwide trends in body-
525 mass index, underweight, overweight, and obesity from 1975 to 2016: a
526 pooled analysis of 2416 population-based measurement studies in 128·9
527 million children, adolescents, and adults. Lancet 390(10113):2627–2642.
528 https://doi.org/10.1016/S0140-6736(17)32129-3

529 37. Life span as a biomarker. https://www.jax.org/research-and-
530 faculty/research-labs/the-harrison-lab/gerontology/life-span-as-a-
531 biomarker. Accessed 31 Mar 2022

532 38. Dutta S, Sengupta P (2016) Men and mice: Relating their ages. Life Sci
533 152:244–248. https://doi.org/10.1016/J.LFS.2015.10.025

534 39. Chaix A, Deota S, Bhardwaj R, Lin T, Panda S (2021) Sex- and age-
535 dependent outcomes of 9-hour time-restricted feeding of a Western high-
536 fat high-sucrose diet in C57BL/6J mice. Cell Rep 36(7):109543.
537 https://doi.org/10.1016/J.CELREP.2021.109543

538 40. Brinton RD (2012) Minireview: Translational animal models of human
539 menopause: Challenges and emerging opportunities. Endocrinology
540 153(8):3571–3578. https://doi.org/10.1210/en.2012-1340

541 41. Ozekinci M, Seven A, Olgan S, et al (2015) Does obesity have
542 detrimental effects on IVF treatment outcomes? BMC Womens Health
543 15(1). https://doi.org/10.1186/S12905-015-0223-0

544 42. Bellver J, Ayllón Y, Ferrando M, et al (2010) Female obesity impairs in
545 vitro fertilization outcome without affecting embryo quality. Fertil Steril
546 93(2):447–454. https://doi.org/10.1016/J.FERTNSTERT.2008.12.032

547 43. Qi L, Liu YP, Wang SM, et al (2022) Abnormal BMI in Male and/or Female
548 Partners Are Deleterious for Embryonic Development and Pregnancy
549 Outcome During ART Process: A Retrospective Study. Front Endocrinol
550 (Lausanne) 13:517. https://doi.org/10.3389/FENDO.2022.856667/BIBTEX

551 44. Larsen MD, Jensen DM, Fedder J, Jølving LR, Nørgård BM (2020) Live-
552 born children after assisted reproduction in women with type 1 diabetes
553 and type 2 diabetes: a nationwide cohort study. Diabetologia 1–9.
554 https://doi.org/10.1007/s00125-020-05193-6

555 45. Mattsson K, Nilsson-Condori E, Elmerstig E, et al (2021) Fertility
556 outcomes in women with pre-existing type 2 diabetes—a prospective
557 cohort study. Fertil Steril 116(2):505–513.
558 https://doi.org/10.1016/j.fertnstert.2021.02.009

559 46. Miao X, Cui W (2022) Berberine alleviates LPS-induced apoptosis,
560 oxidation, and skewed lineages during mouse preimplantation
561 development. Biol Reprod. https://doi.org/10.1093/BIOLRE/IOAC002

562 47. Chiu YH, Chen H (2016) GATA3 inhibits GCM1 activity and trophoblast
563 cell invasion. Sci Rep 6. https://doi.org/10.1038/SREP21630

564 48. Davalli P, Mitic T, Caporali A, Lauriola A, D'Arca D (2016) ROS, Cell
565 Senescence, and Novel Molecular Mechanisms in Aging and Age-Related
566 Diseases. Oxid Med Cell Longev 2016.
567 https://doi.org/10.1155/2016/3565127

568 49. Fernández-Sánchez A, Madrigal-Santillán E, Bautista M, et al (2011)
569 Inflammation, oxidative stress, and obesity. Int J Mol Sci 12(5):3117–
570 3132. https://doi.org/10.3390/IJMS12053117

571 50. Jawerbaum A, White V (2010) Animal models in diabetes and pregnancy.
572 Endocr Rev 31(5):680–701. https://doi.org/10.1210/er.2009-0038

573 51. Rehman K, Akash MSH (2017) Mechanism of Generation of Oxidative
574 Stress and Pathophysiology of Type 2 Diabetes Mellitus: How Are They
575 Interlinked? J Cell Biochem 118(11):3577–3585.
576 https://doi.org/10.1002/JCB.26097

577

578

579

580 Table1: Histopathological features found in the respective group and location
581 (number of individuals/total of individuals per group)

Group	YND	YHFD	MND	MHFD	OND	OHFD
Liver	Mild, diffuse hepatocellular vacuolization (glycogen accumulation) (4/4) Randomly, scattered, small aggregates of lymphocytes and rare neutrophils (2/4)	Mild and diffuse hepatocellular vacuolization (glycogen accumulation) (4/4) Minimal perivascular infiltrate of lymphocytes and neutrophils. (1/4) Randomly, scattered small aggregates of lymphocytes and rare neutrophils (3/4)	Moderate, diffuse hepatocellular vacuolization (glycogen accumulation) (4/4) Moderate, diffuse macrovesicular fatty change, (1/4) Mild to moderate perivascular (centrilobular) infiltrate of lymphocytes with fewer neutrophils, (4/4) Randomly, minimal aggregates of lymphocytes, with rare neutrophils, (4/4)	Moderate, diffuse hepatocellular vacuolization (glycogen accumulation) (4/4) Moderate, diffuse macrovesicular fatty change, (2/4) Mild to moderate perivascular (centrilobular) infiltrate of lymphocytes with fewer neutrophils, (4/4) Randomly, minimal aggregates of lymphocytes, with rare neutrophils, (1/4)	Moderate, diffuse hepatocellular vacuolization (glycogen accumulation), (4/4) Mild to moderate perivascular (centrilobular) infiltrate of lymphocytes with fewer neutrophils (2/4) Multifocal, mild-moderate, perivascular (periportal and centrilobular) amyloidosis extending into and expanding adjacent sinusoids (2/4).	Moderate, diffuse hepatocellular vacuolization (glycogen accumulation) (2/4) Mild, multifocal, macrovesicular fatty change (2/4) Multifocal, mild-moderate, perivascular (periportal and centrilobular) amyloidosis,extending into and expanding adjacent sinusoids (4/4). Mild to moderate perivascular (centrilobular) infiltrate of lymphocytes with fewer neutrophils (4/4) Randomly, minimal aggregates of lymphocytes, with rare neutrophils, (4/4) Randomly, ocasional and discrete foci of hepatocellular necrosis with with cellular debris and rare neutrophils (1/4)
Spleen	NPF	npf	Moderate, multifocally disseminated, golden brown pigment-laden macrophages (4/4) Multifocal lymphoid hyperplasia. (4/4)	Moderate, multifocally disseminated, golden brown pigment-laden macrophage (4/4) Multifocal lymphoid hyperplasia (4/4)	Moderate, multifocally disseminated, golden brown pigment-laden macrophage (2/4) Severe amyloidosis (2/4) Multifocal lymphoid hyperplasia (4/4)	Severe amyloidosis (4/4) Multifocal lymphoid hyperplasia (1/4)
Heart	NPF	NPF	Mild, multifocal amyloidosis (1/4)	NPF	Severe, multifocal amyloidosis (1/4), mild,	Severe, multifocal amyloidosis (2/4)

					multifocal amyloidosis (1/4)	
Kidneys	NPF	NPF	Mild-moderate, locally extensive medullary tubular mineralization (1/4)	Mild-moderate, multifocal perivascular infiltration of lymphocites in the cortex (1/4)	Mild, multifocal, interstitial amyloidosis (1/4) Multifocal, severe, interstitial lymphocytic nephritis (1/4)	Mild, multifocal, interstitial amyloidosis (1/4) Multifocal, severe, interstitial lymphocytic nephritis (2/4) Mild, multifocal perivascular infiltration of lymphocites in the cortex (3/4)
Pancreas	NPF	NPF	NPF	NPF	Moderate, multifocal, perivascular amyloidosis (1/4)	Moderate, multifocal, perivascular amyloidosis (2/4) Mild, multifocal periductal infiltrate of lymphocytes, (1/4)

582

583 Table 1: **Pathology evaluation of tissue samples**. Only tissues with
584 histopathological features are included in this descriptive table; n=24 (4/group).
585 NPF= Non pathological findings; YND= Young Normal Diet, YHFD= Young High
586 Fat Diet, MND= Mature Normal Diet, MHFD= Mature High Fat Diet, OND= Old
587 Normal Diet, OHFD= Old High Fat Diet.

588

589

590

591

592

593

594

595

596

597

598 Figures

599 Fig. 1: **Experiment design**. Female mice of different ages were fed either normal
600 diet (ND) or high fat diet (HFD) and their weight was monitored once a week. On
601 the eighth week, oral glucose tolerance test (OGTT), insulin tolerance test (ITT)
602 and body composition assessment were performed. Then, females were mated
603 with young healthy males for up to 8 days and preimplantation embryos were
604 flushed from the uterus 3.5 days after vaginal plugs were detected. A necropsy
605 was performed in a few animals after the 8 weeks of diet.

606 Fig. 2: **Effect of 8 weeks of high fat diet (HFD) on weight, body composition,**
607 **oral glucose tolerance test (OGTT) and insulin tolerance test (ITT)**
608 **compared to normal diet (ND)**. (a) Weekly body weight and (b) body mass
609 index. n= 14 YND, 20 YHFD, 14 MND, 17 MHFD, 9 OND and 21 OHFD. (c) Body
610 composition by nuclear magnetic resonance. n= 14 YND, 20 YHFD, 14 MND, 17
611 MHFD, 9 OND and 20 OHFD. (d, left) OGTT blood glucose. (d, right) AUC
612 calculated from OGTT. (e, left) ITT blood glucose. (e, right) AUC calculated from
613 ITT. n=12 YND, 17 YHFD, 14 MND, 17 MHFD, 9 OND and 20 OHFD. Data are
614 expressed as mean ± SEM, *p<0.05 comparing each HFD group with its ND
615 control or between age-groups. In (c), ns= Not significant, otherwise significant
616 *p<0.05. YND= Young (12 weeks) Normal Diet (solid blue), YHFD= Young High
617 Fat Diet (patterned blue); MND= Mature (9 months) Normal Diet (solid red),
618 MHFD= Mature High Fat Diet (patterned red); OND= Old (1 year) Normal Diet
619 (solid black), OHFD= Old High Fat Diet (patterned black).

620 Fig. 3: **Mice were killed and dissected after being fed for 8 weeks with normal**
621 **or high-fat diet and their organs were weighed**. (a) White fat as the addition
622 of fat from the paragenital fat pads. (b) Gastrocnemius as the addition of the
623 weight of both gastrocnemius muscles from the hind legs. (c-d) For the
624 biochemistry analysis animals were grouped by diet: (c) blood glucose levels and
625 (d) total cholesterol levels at the moment of death. Data are expressed as
626 median, *p<0.05 either comparing each HFD group with its ND control or between
627 ages; Each point refers to one animal. (e) Pancreas histological sections
628 immunostained for Insulin (green) and Glucagon (red). Representative maximum
629 projection images from Z stacks for each condition are shown. Scale bar: 20 μm.

YHFD= Young High Fat Diet (patterned blue); MND= Mature (9 months) Normal Diet (solid red), MHFD= Mature High Fat Diet (patterned red); OND= Old (1 year) Normal Diet (solid black), OHFD= Old High Fat Diet (patterned black).

Fig. 4: **Effect of 8 weeks of high fat diet on fecundity**. (a) Mating rate. n= 33 YND, 38 YHFD, 41 MND, 48 MHFD, 9 OND, 20 OHFD. (b) Fertilization rate. n= 27 YND, 26 YHFD, 25 MND, 31 MHFD, 5 OND and 1 OHFD. (c) Number of embryos recorded per female. Each dot indicates one litter. No statistical significance was found in any case, *$p<0.05$ either comparing each HFD group with its ND control or between ages. (d) Representative micrographs of embryos from indicated females. (e) Embryos classified according to their morphological features into four categories (A, B, C, and D, from high to low quality) *$p<0.05$; YHFD= Young High Fat Diet (patterned blue); MND= Mature (9 months) Normal Diet (solid red), MHFD= Mature High Fat Diet (patterned red); OND= Old (1 year) Normal Diet (solid black), OHFD= Old High Fat Diet (patterned black).

Fig. 5: **Representative confocal images of mouse preimplantation embryos**. Embryos are immunostained for DAPI (blue), NANOG (green), GATA6 (red) and GATA3 (white) at early stage. Staging criteria: Early (up to 64 cells), Mid (65-90 cells) and Late (from 91 cells). Young Normal Diet (YND); Young High Fat Diet; Mature Normal Diet (MND); and Mature High Fat Diet (MHFD). All embryos shown were immunostained, imaged and processed together. The first four columns are single confocal z-sections; the last column show the merged confocal images. Scale bar: 50 µm.

Fig. 6: **Variations in embryo developmental stage assessed by single cell quantitative immunofluorescence.** (a) Population analysis as the percentage of the total number of cells in the ICM. (b-c) Violin plots showing NANOG expression levels in single DP cells (b) and in Epi progenitors (c). (d-e) Violin plots showing GATA6 levels in single DP cells (d) and in PrE progenitors (e). Data are expressed as mean ± SEM, *$p<0.05$ comparing each HFD group with its ND control or between age-groups. Results showed only for early embryos; YHFD= Young High Fat Diet (patterned blue); MND= Mature (9 months) Normal Diet (solid red), MHFD= Mature High Fat Diet (patterned red).

Fig. 7: **Variations in GATA3 levels in the trophectoderm (TE) assessed by quantitative immunofluorescence.** (a) Population analysis as the percentage of the total number of cells in the TE. (b) Violin plots showing GATA3 expression levels. *p<0.05 either comparing each HFD group with its ND control or between ages. Results showed only for early embryos; YHFD= Young High Fat Diet (patterned blue); MND= Mature (9 months) Normal Diet (solid red), MHFD= Mature High Fat Diet (patterned red).

.

688 Abbreviations

689 BMI: Body Mass Index

690 DN: Double Negative

691 DP: Double Positive

692 Epi: Epiblast

693 HFD: High Fat Diet

694 ICM: Inner Cell Mass

695 ITT: Insulin Tolerance Test

696 MHFD: Mature High Fat Diet

697 MND: Mature Normal Diet

698 ND: Normal Chow Diet

699 OGTT: Oral Glucose Tolerance Test

700 OHFD: Old High Fat Diet

701 OND: Old Normal Diet

702 OQC: Oscar Quesada-Canales

703 PrE: Primitive Endoderm

704 QIF: Quantitative Immunofluorescence Analysis

705 ROS: Reactive Oxygen Species

706 TE: Trophectoderm

707 YHFD: Young High Fat Diet

708 YND: Young Normal Diet

709

710

711

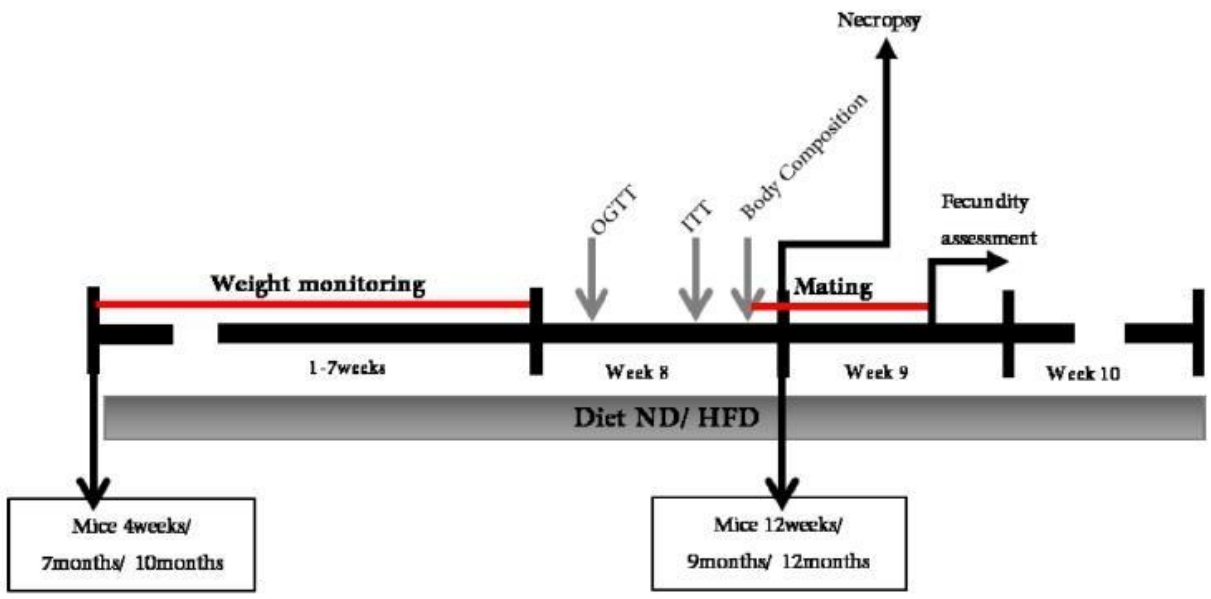

Fig. 1: Experiment design. Female mice of different ages were fed either normal diet (ND) or high fat diet (HFD) and their weight was monitored once a week. On the eighth week, oral glucose tolerance test (OGTT), insulin tolerance test (ITT) and body composition assessment were performed. Then, females were mated with young healthy males for up to 8 days and preimplantation embryos were flushed from the uterus 3.5 days after vaginal plugs were detected. A necropsy was performed in a few animals after the 8 weeks of diet.

96x50mm (300 x 300 DPI)

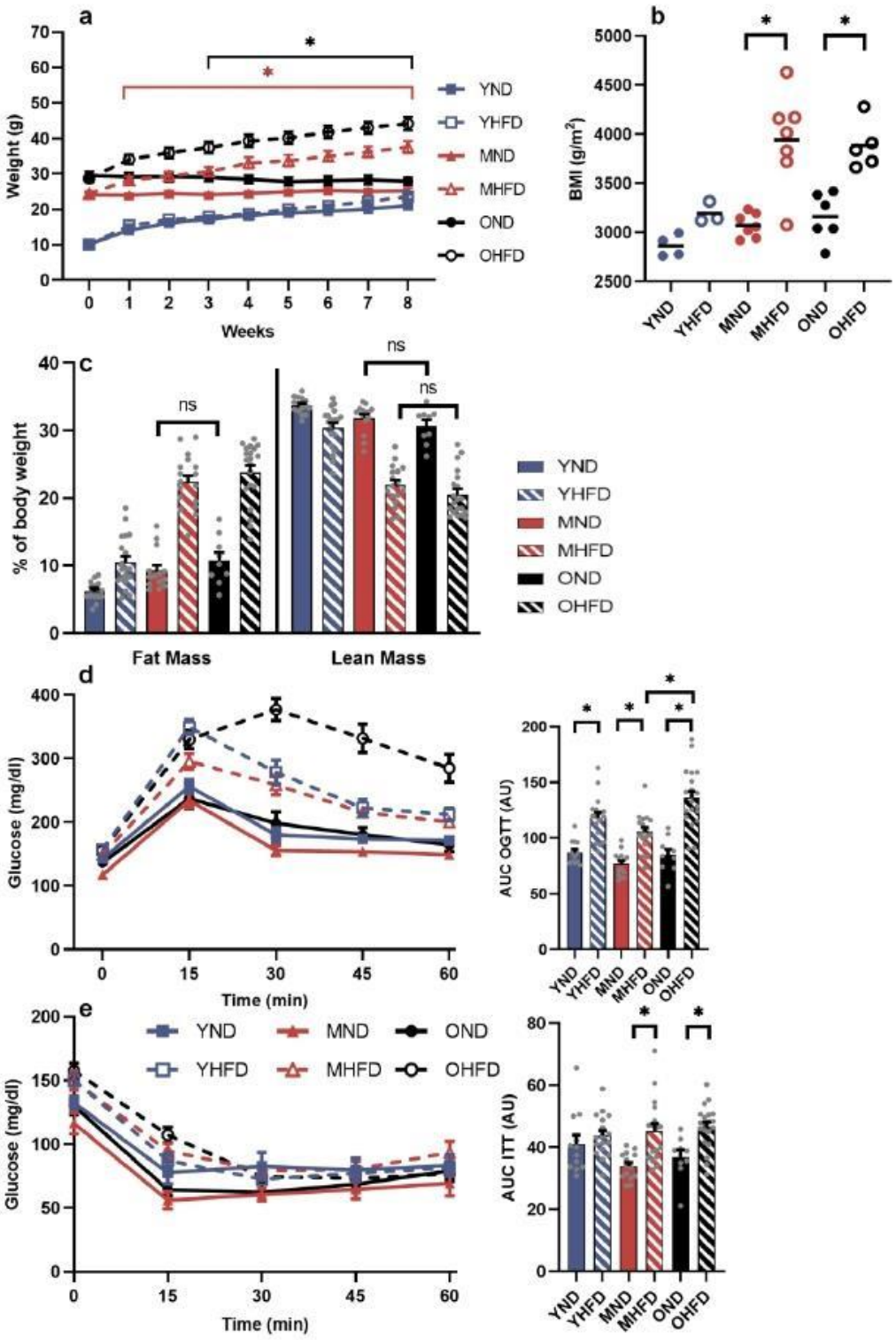

Fig. 2: Effect of 8 weeks of high fat diet (HFD) on weight, body composition, oral glucose tolerance test (OGTT) and insulin tolerance test (ITT) compared to normal diet (ND). (a) Weekly body weight and (b) body mass index. n= 14 YND, 20 YHFD, 14 MND, 17 MHFD, 9 OND and 21 OHFD. (c) Body composition by nuclear magnetic resonance. n= 14 YND, 20 YHFD, 14 MND, 17 MHFD, 9 OND and 20 OHFD. (d, left) OGTT blood glucose. (d, right) AUC calculated from OGTT. (e, left) ITT blood glucose. (e, right) AUC calculated from ITT. n=12 YND, 17 YHFD, 14 MND, 17 MHFD, 9 OND and 20 OHFD. Data are expressed as mean ± SEM, *p<0.05 comparing each HFD group with its ND control or between age-groups. In (c), ns= Not significant, otherwise significant *p<0.05. YND= Young (12 weeks) Normal Diet (solid blue), YHFD= Young High Fat Diet (patterned blue); MND= Mature (9 months) Normal Diet (solid red), MHFD= Mature High Fat Diet (patterned red); OND= Old (1 year) Normal Diet (solid black), OHFD= Old High Fat Diet (patterned black).

185x235mm (300 x 300 DPI)

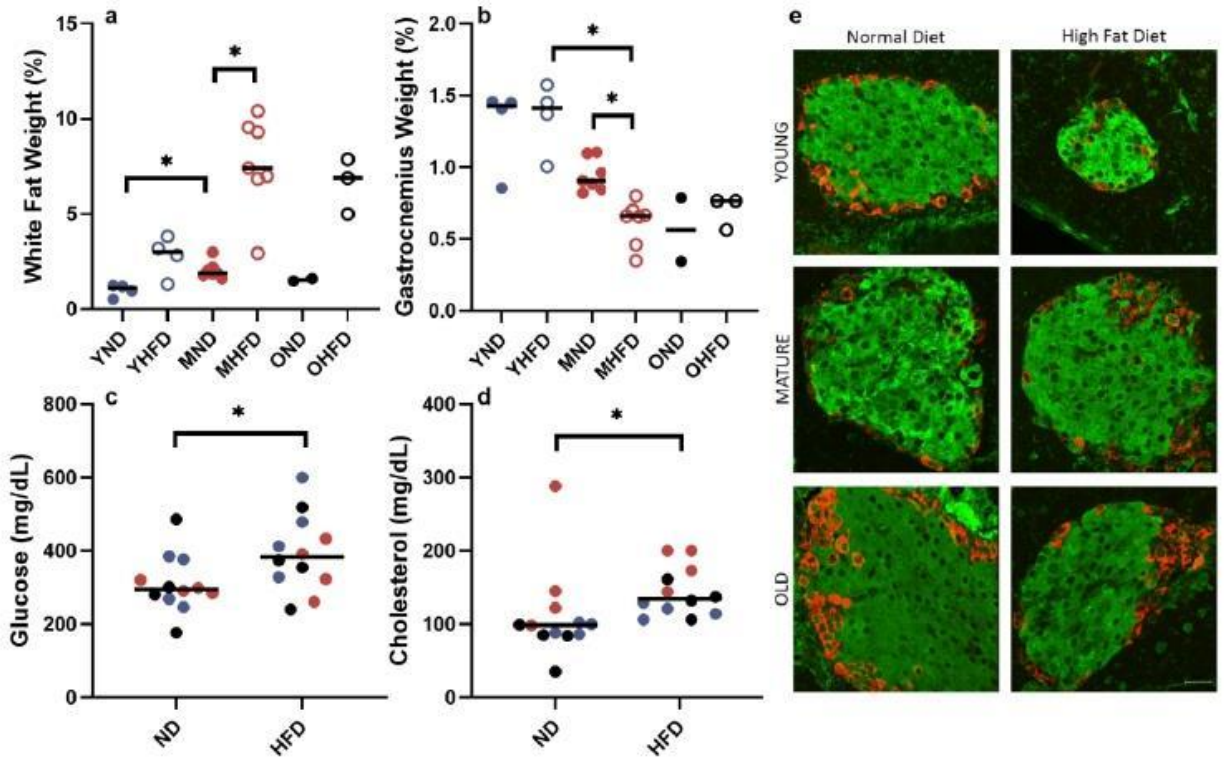

Fig. 3: Mice were killed and dissected after being fed for 8 weeks with normal or high-fat diet and their organs were weighed. (a) White fat as the addition of fat from the paragenital fat pads. (b) Gastrocnemius as the addition of the weight of both gastrocnemius muscles from the hind legs. (c-d) For the biochemistry analysis animals were grouped by diet: (c) blood glucose levels and (d) total cholesterol levels at the moment of death. Data are expressed as median, *$p<0.05$ either comparing each HFD group with its ND control or between ages; Each point refers to one animal. (e) Pancreas histological sections immunostained for Insulin (green) and Glucagon (red). Representative maximum projection images from Z stacks for each condition are shown. Scale bar: 20 μm. YHFD= Young High Fat Diet (patterned blue); MND= Mature (9 months) Normal Diet (solid red), MHFD= Mature High Fat Diet (patterned red); OND= Old (1 year) Normal Diet (solid black), OHFD= Old High Fat Diet (patterned black).

186x114mm (300 x 300 DPI)

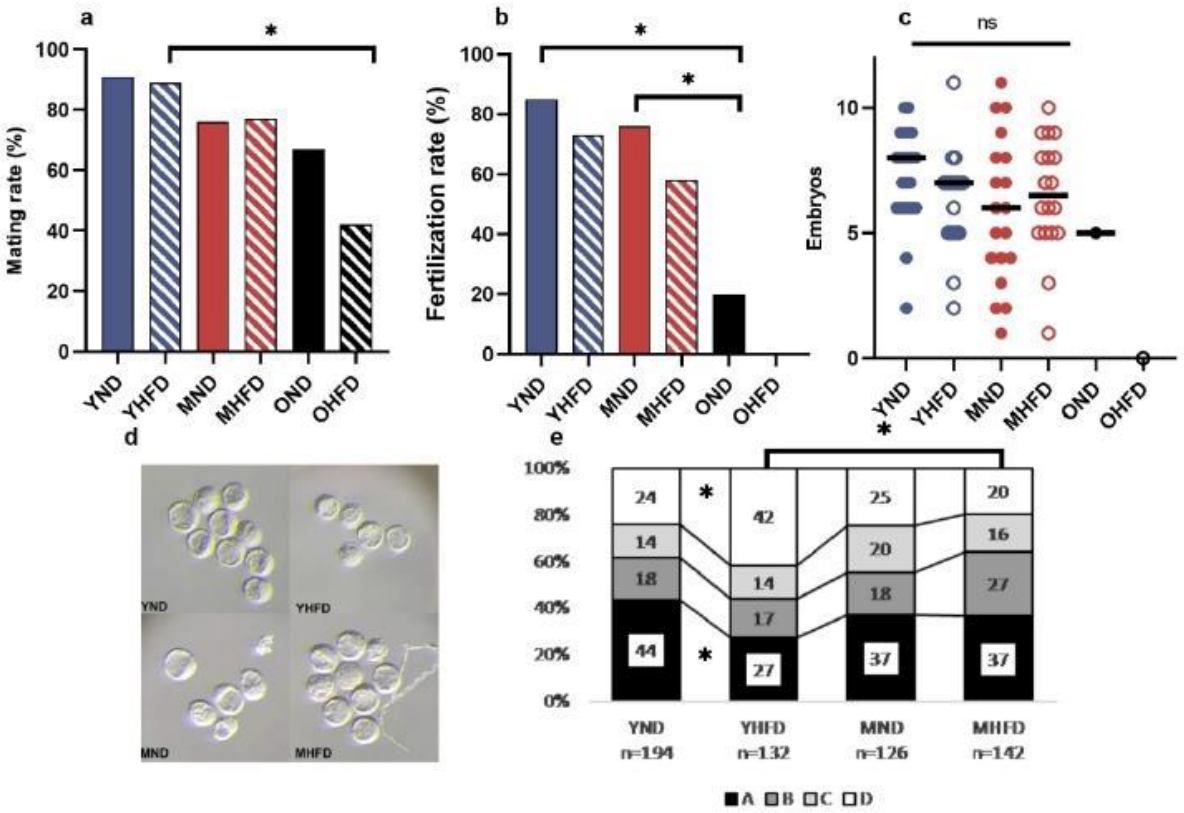

Fig. 4: Effect of 8 weeks of high fat diet on fecundity. (a) Mating rate. n= 33 YND, 38 YHFD, 41 MND, 48 MHFD, 9 OND, 20 OHFD. (b) Fertilization rate. n= 27 YND, 26 YHFD, 25 MND, 31 MHFD, 5 OND and 1 OHFD. (c) Number of embryos recorded per female. Each dot indicates one litter. No statistical significance was found in any case, *p<0.05 either comparing each HFD group with its ND control or between ages. (d) Representative micrographs of embryos from indicated females. (e) Embryos classified according to their morphological features into four categories (A, B, C, and D, from high to low quality) *p<0.05; YHFD= Young High Fat Diet (patterned blue); MND= Mature (9 months) Normal Diet (solid red), MHFD= Mature High Fat Diet (patterned red); OND= Old (1 year) Normal Diet (solid black), OHFD= Old High Fat Diet (patterned black).

185x122mm (300 x 300 DPI)

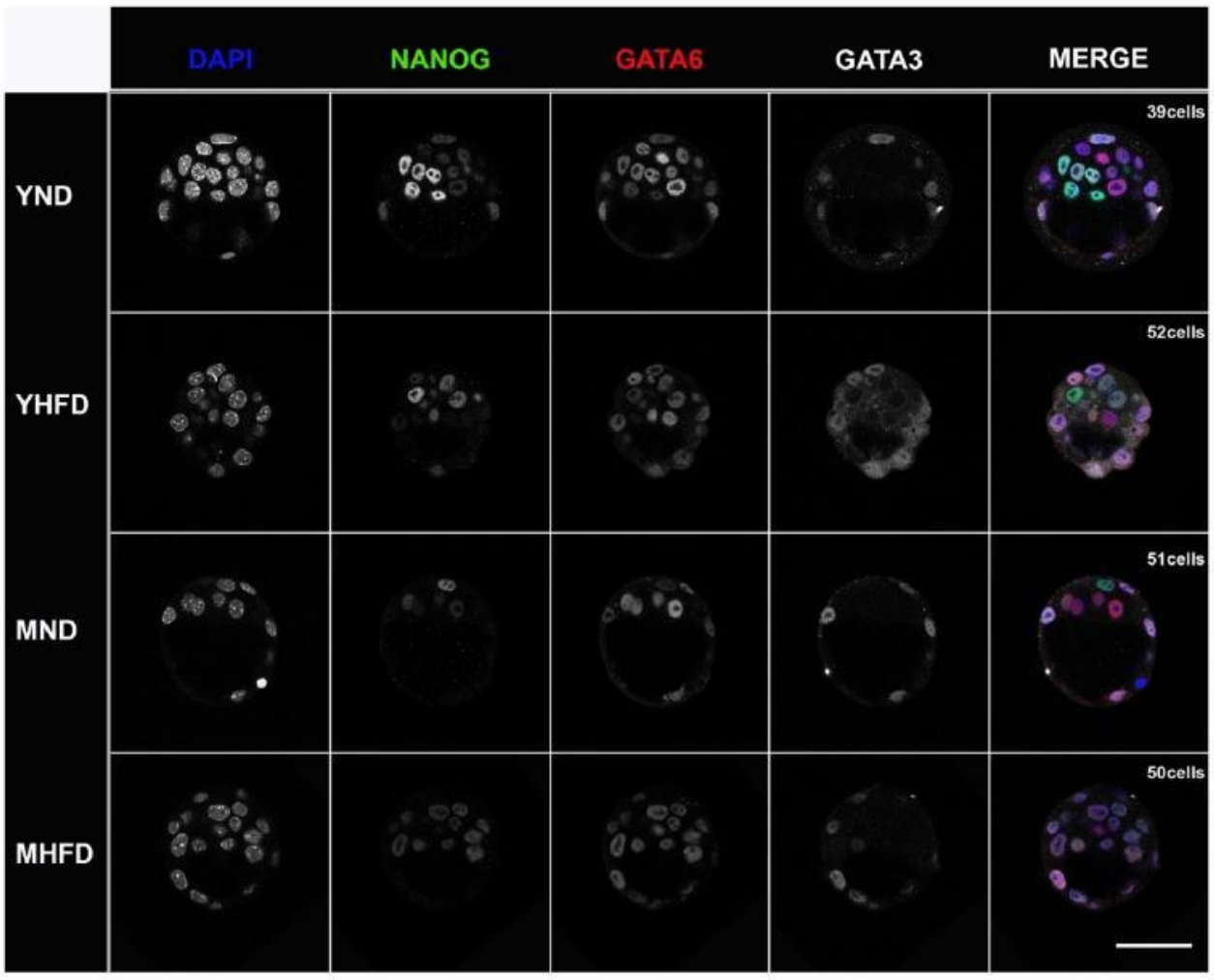

Fig. 5: Representative confocal images of mouse preimplantation embryos. Embryos are immunostained for DAPI (blue), NANOG (green), GATA6 (red) and GATA3 (white) at early stage. Staging criteria: Early (up to 64 cells), Mid (65-90 cells) and Late (from 91 cells). Young Normal Diet (YND); Young High Fat Diet; Mature Normal Diet (MND); and Mature High Fat Diet (MHFD). All embryos shown were immunostained, imaged and processed together. The first four columns are single confocal z-sections; the last column show the merged confocal images. Scale bar: 50 μm.

187x150mm (300 x 300 DPI)

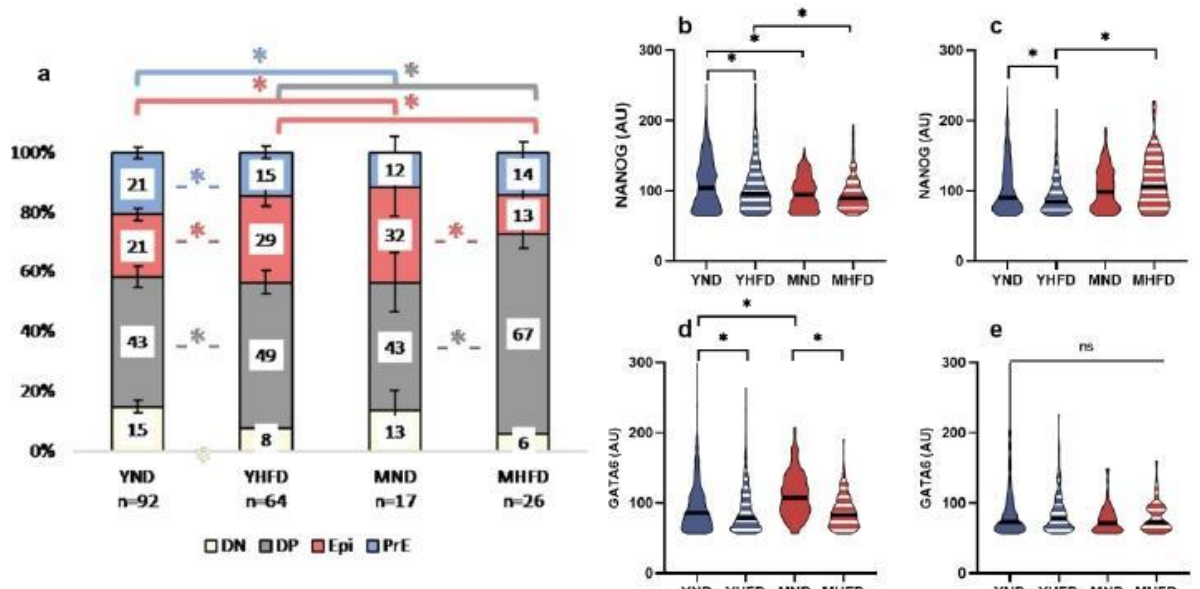

Fig. 6: Variations in embryo developmental stage assessed by single cell quantitative immunofluorescence. (a) Population analysis as the percentage of the total number of cells in the ICM. (b-c) Violin plots showing NANOG expression levels in single DP cells (b) and in Epi progenitors (c). (d-e) Violin plots showing GATA6 levels in single DP cells (d) and in PrE progenitors (e). Data are expressed as mean ± SEM, *p<0.05 comparing each HFD group with its ND control or between age-groups. Results showed only for early embryos; YHFD= Young High Fat Diet (patterned blue); MND= Mature (9 months) Normal Diet (solid red), MHFD= Mature High Fat Diet (patterned red).

186x94mm (300 x 300 DPI)

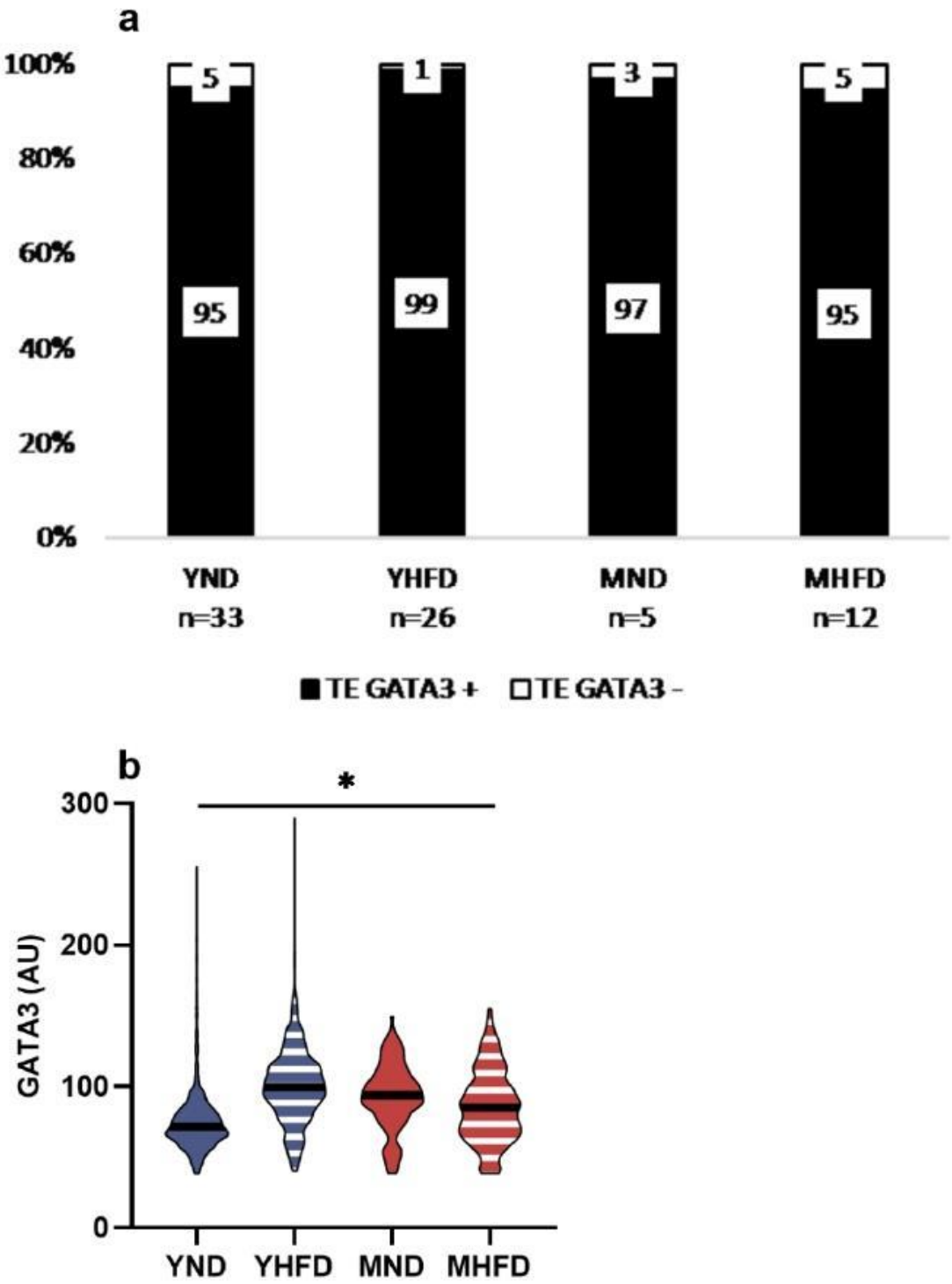

Fig. 7: Variations in GATA3 levels in the trophectoderm (TE) assessed by quantitative immunofluorescence. (a) Population analysis as the percentage of the total number of cells in the TE. (b) Violin plots showing GATA3 expression levels. *p<0.05 either comparing each HFD group with its ND control or between ages. Results showed only for early embryos; YHFD= Young High Fat Diet (patterned blue); MND= Mature (9 months) Normal Diet (solid red), MHFD= Mature High Fat Diet (patterned red).

95x119mm (300 x 300 DPI)

Online Supplemental Materials

reproduction@bioscientifica.com

SuplementaryFigure1

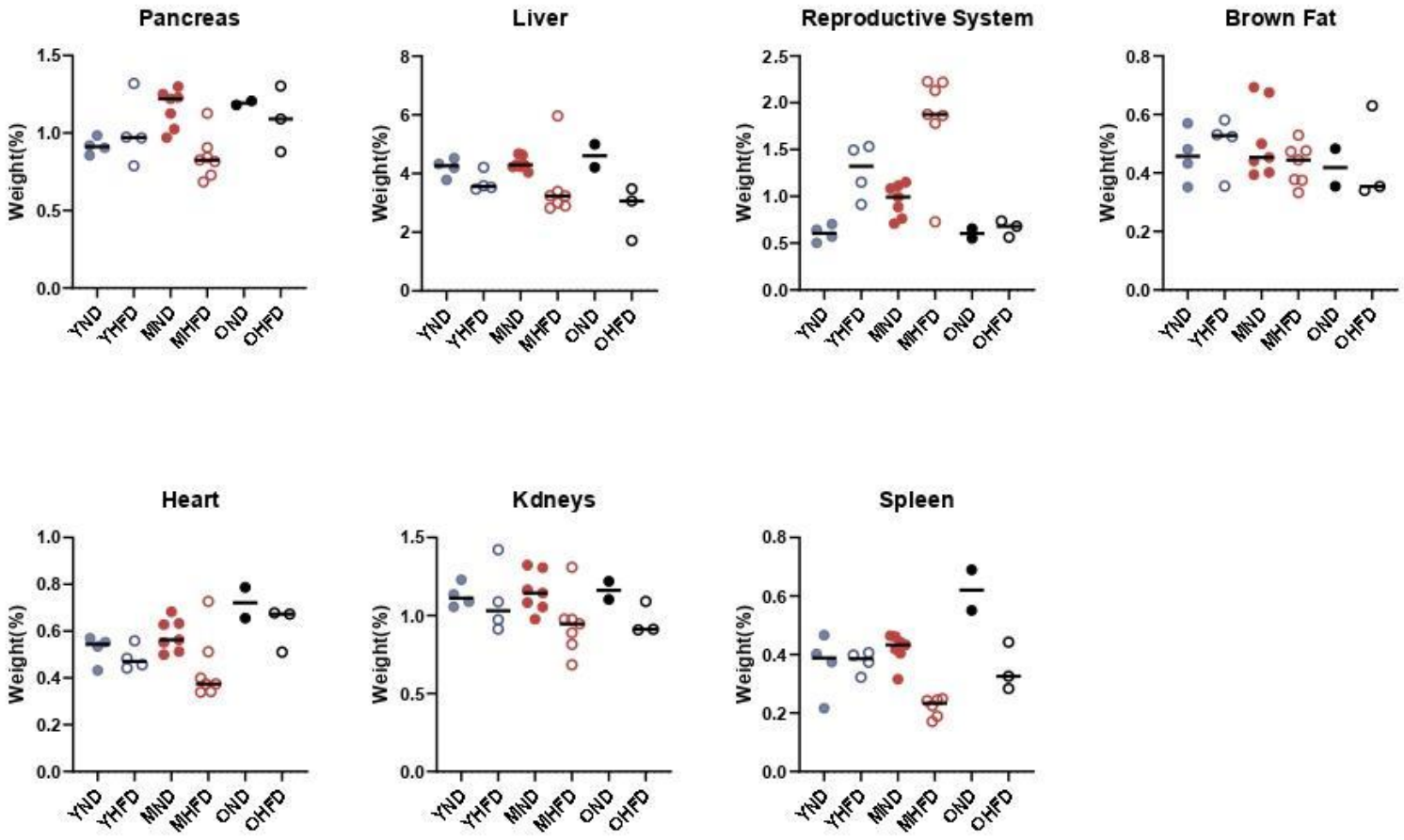

Sup. Fig. 1: Mice were killed and dissected after being fed for 8 weeks with HFD and their organs were weighed. Pancreas, Liver, Reproductive system, Brown fat, Heart, Kidneys and Spleen; Each point refers to one animal; YND= Young Normal Diet, YHFD= Young High Fat Diet, MND= Mature Normal Diet, MHFD= Mature High Fat Diet, OND= Old Normal Diet, OHFD= Old High Fat Diet.

SuplementaryFigure2

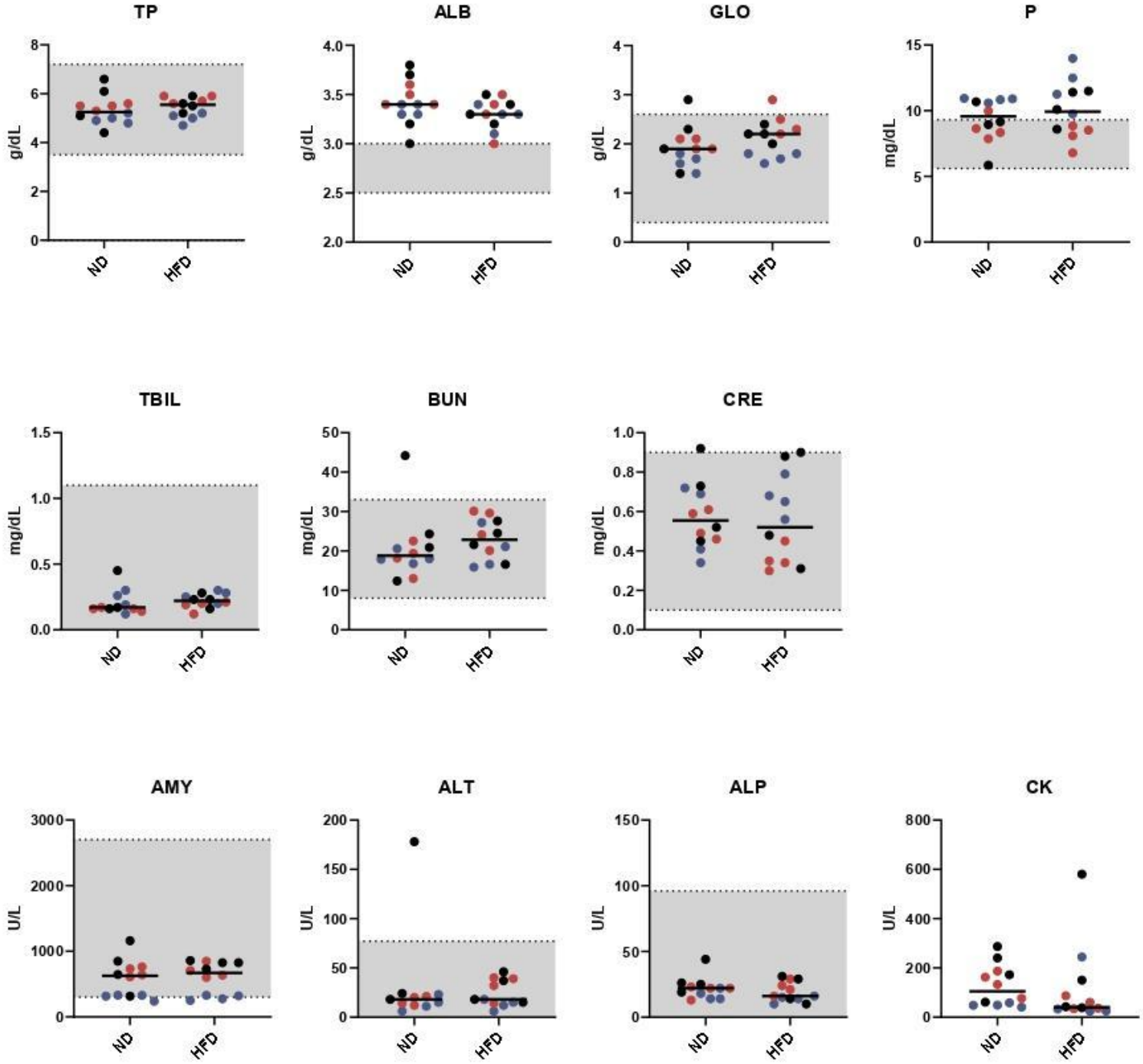

Sup. Fig. 2: Biochemistry analysis. Animals were grouped by diet: total protein (TP), albumin (ALB), globulin (GLOB), phosphorus (P), total bilirubin (TBIL), blood urea nitrogen (BUN), creatinine (CRE), amylase (AMY), alanine aminotransferase (ALT), alkaline phosphatase (ALP), and creatine kinase (CK). Data are expressed as median, *p<0.05 comparing each HFD group with its ND control; Each point refers to one animal; 12 weeks (blue), 9 months (red) and 1 year old (black). YND= Young Normal Diet, YHFD= Young High Fat Diet, MND= Mature Normal Diet, MHFD= Mature High Fat Diet, OND= Old Normal Diet, OHFD= Old High Fat Diet. Gray areas indicate physiological ranges according to the manufacturer.

SuplementaryTable1

			Total cell number		Total TE number		Total ICM		ICM/TE Ratio	
	Stage	N Embryos	Average	SE	Average	SE	Average	SE	Average	SE
YND	Early	92	54.18	1.06	33.93	0.71	20.25	0.56	0.61	0.02
	Mid	33	72.12	1.07	48.82	1.23	23.30	0.68	0.49	0.03
	Late	2	92.00	1.00	68.50	3.50	23.50	2.50	0.35	0.06
YHFD	Early	64	52.47	1.39	32.45	1.02	20.02	0.61	0.64*	0.02
	Mid	7	71.57	2.22	45.86	3.26	25.71	1.60	0.59	0.07
	Late	1	91.00	NA	65.00	NA	26.00	NA	0.40	NA
MND	Early	17	45.35	3.39	28.47	2.19	16.88	1.51	0.60	0.04
	Mid	4	79.00	3.54	53.00	4.02	26.00	1.08	0.50	0.06
	Late	2	93.00	0.00	67.50	0.50	25.50	0.50	0.38	0.01
MHFD	Early	26	44.84	2.61	29.24	1.63	15.60	1.12	0.53*	0.03
	Mid	23	75.09	1.91	48.04	1.82	27.04	0.76	0.58	0.03
	Late	14	97.86	1.62	69.21	1.97	28.57	1.45	0.42	0.03
*p<0.05 only YHFD vs MHFD										

Sup. Table 1: Embryo analysis by quantitative immunofluorescence. Staging criteria: Early (up to 64 cells), Mid (65-90 cells) and Late (from 91 cells). YND= Young Normal Diet, YHFD= Young High Fat Diet, MND= Mature Normal Diet, MHFD= Mature High Fat Diet. TE= trophectoderm cells, ICM= inner cell mass cells.

SuplementaryFigure3

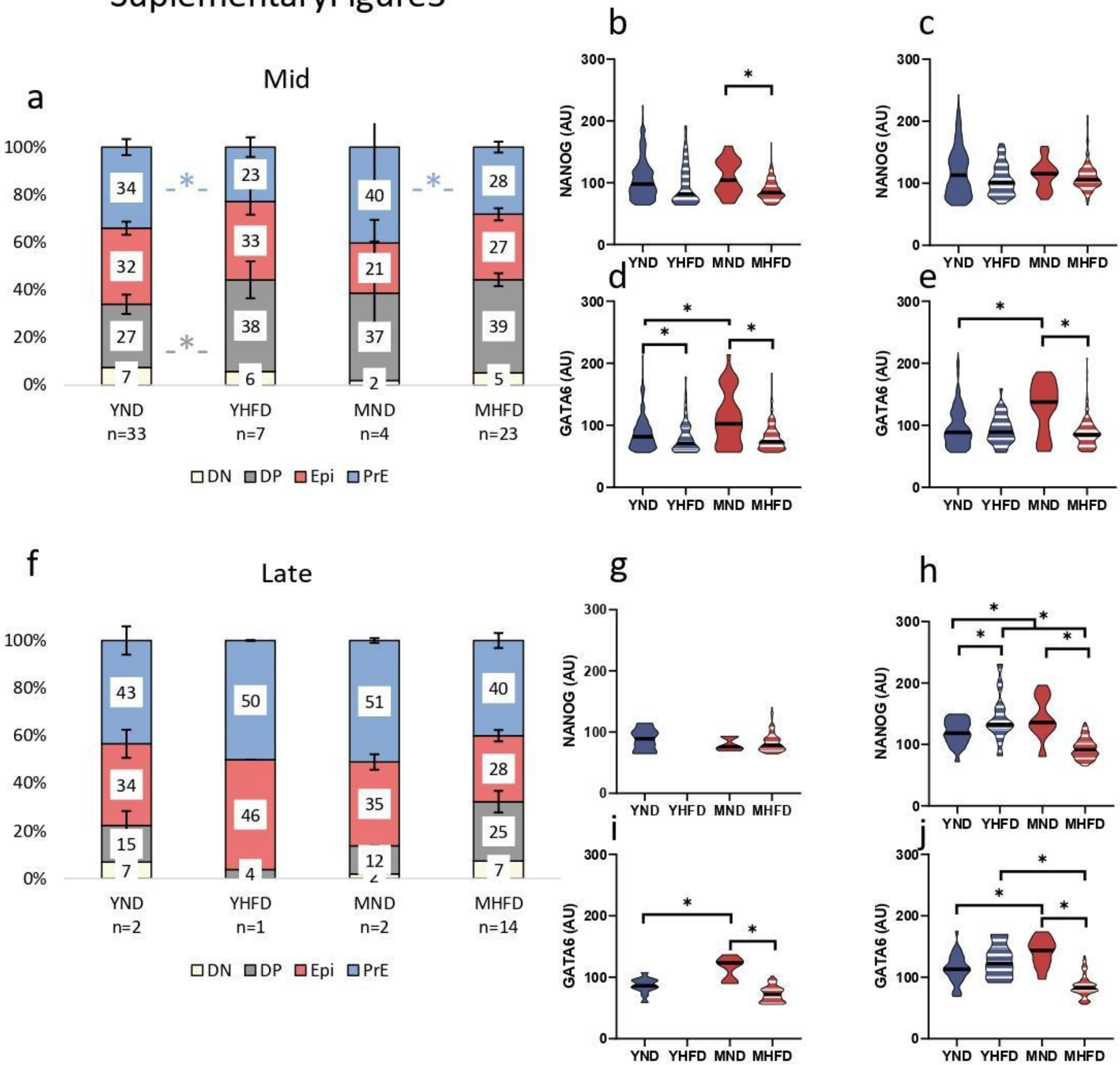

Sup. Fig. 3: Variations in embryo developmental stage assessed by quantitative immunofluorescence. (a, f) Population analysis as the percentage of the total number of cells in the ICM for Mid (a) and late (f) embryos; Violin plots showing fate marker expression levels: (b, g) NANOG levels in single DP cells and (c, h) in Epi progenitors. (d, i) GATA6 levels in single DP cells (e, j) and in PrE progenitors. Data are expressed as mean ± SEM, *p<0.05 comparing each HFD group with its ND control or between age-groups; YND= Young Normal Diet, YHFD= Young High Fat Diet, MND= Mature Normal Diet, MHFD= Mature High Fat Diet, OND= Old Normal Diet, OHFD= Old High Fat Diet.

SuplementaryFigure4

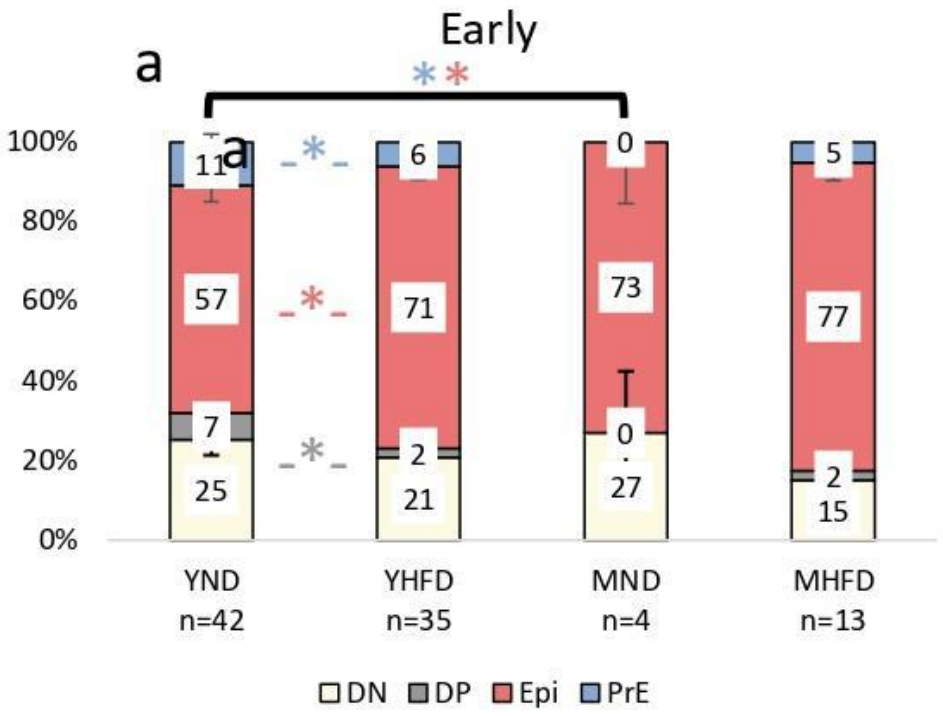

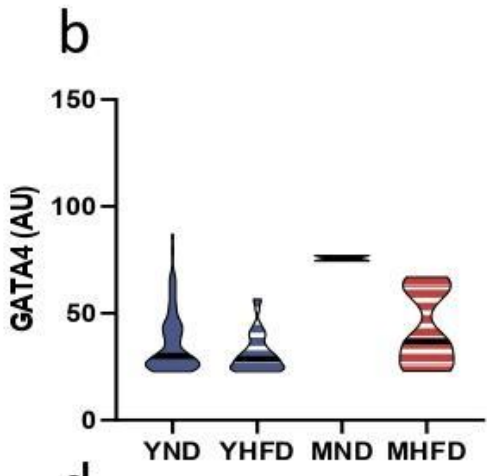

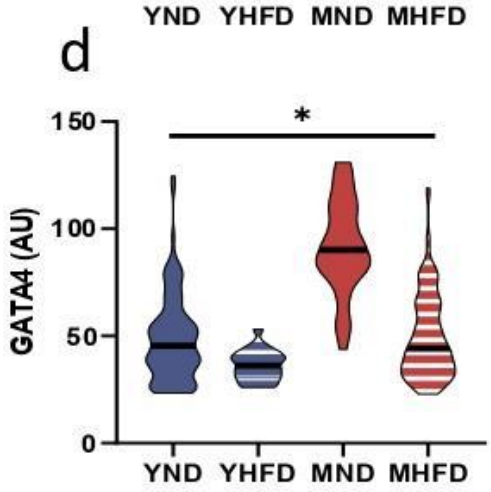

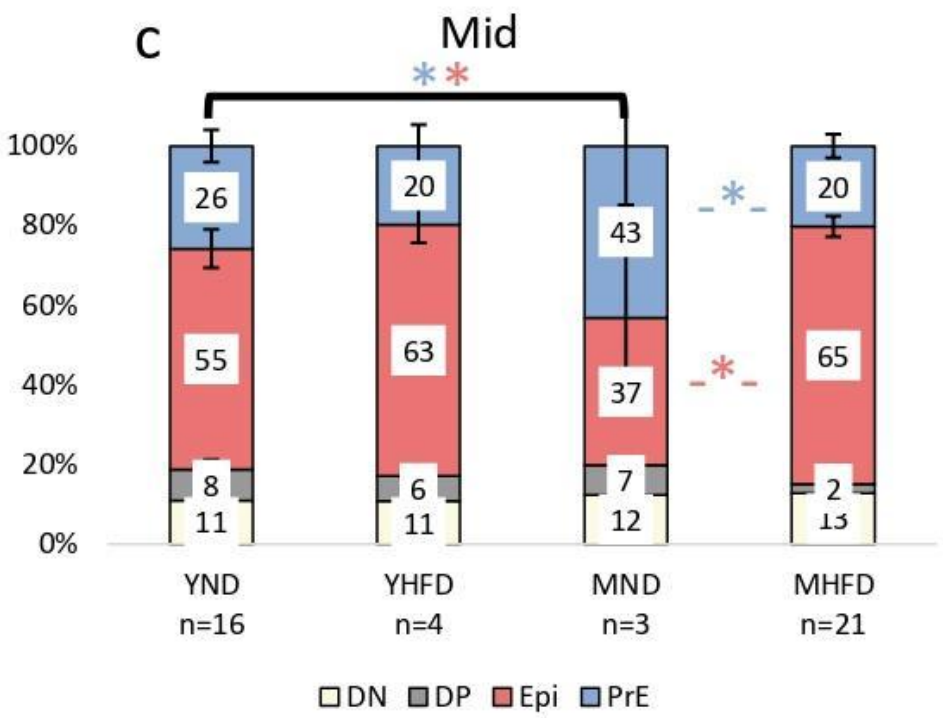

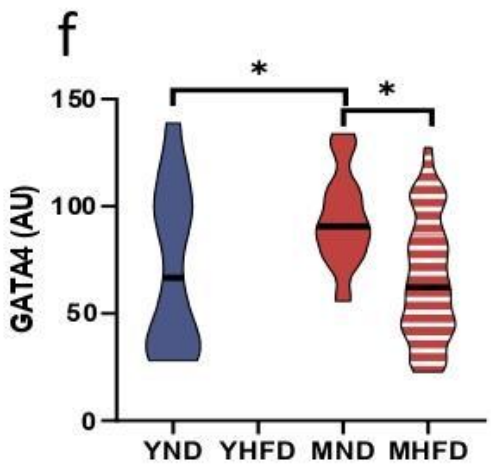

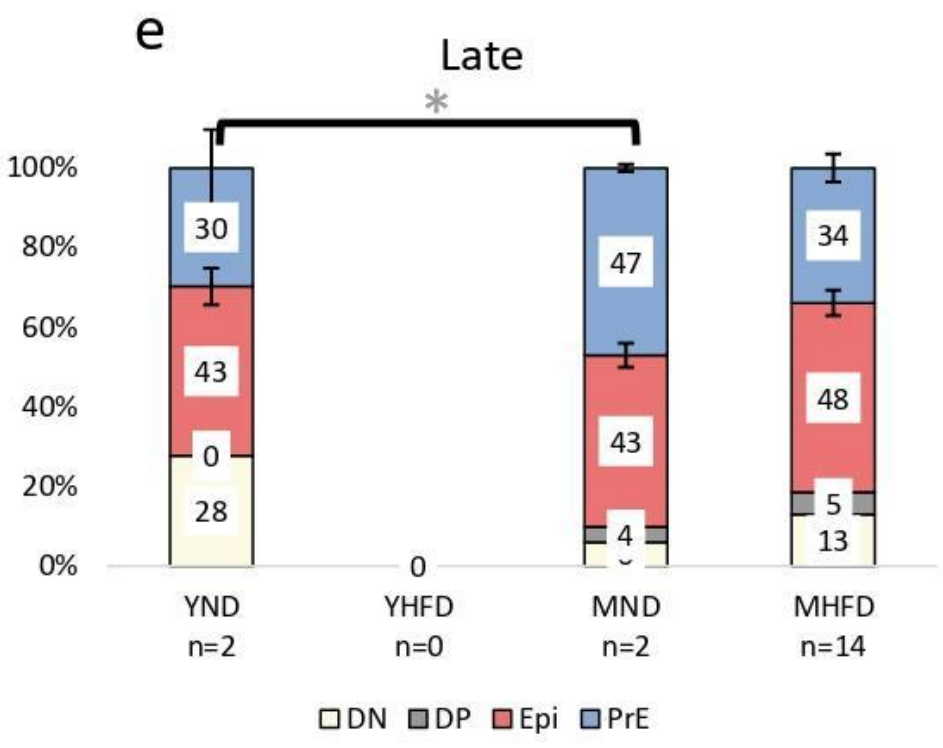

Sup. Fig. 4: Variations in embryo developmental stage assessed by quantitative immunofluorescence. (a, c, e) Population analysis as the percentage of the total number of cells in the ICM for early (a), Mid (c) and Late (e) embryos; Cells positive for GATA4 but negative for NANOG were considered PrE progenitors. Violin plots showing fate marker expression levels: (b, d, e) GATA4 levels in single PrE progenitors. Data are expressed as mean ± SEM, *p<0.05 comparing each HFD group with its ND control or between age-groups; YND= Young Normal Diet, YHFD= Young High Fat Diet, MND= Mature Normal Diet, MHFD= Mature High Fat Diet, OND= Old Normal Diet, OHFD= Old High Fat Diet.

Annex 2

Additional Publications:

1. Exploring the link between Parkinson's disease and Type 2 Diabetes Mellitus in Drosophila; Francisco José Sanz, Cristina Solana-Manrique, **Joaquín Lilao-Garzón**, Yeray Brito-Casillas, Silvia Muñoz-Descalzo and Nuria Paricio; The FASEB Journal. (2022) https://doi.org/10.1096/fj.202200286R

2. Modelos de diabetes inducida. ¿Cómo elegir el modelo correcto?; **Joaquín Lilao-Garzón**, Carmen Valverde-Tercedor, Silvia Muñoz-Descalzo, Ana M. Wägner and Yeray Brito-Casillas; Animales de Laboratorio, SECAL. (2021).

3. Alternativas al uso de animales en el estudio de la diabetes, también durante la gestacional; Carmen Valverde-Tercedor, Silvia Muñoz-Descalzo, **Joaquín Lilao-Garzón**, Yeray Brito-Casillas and Ana M. Wägner; Animales de Laboratorio, SECAL. (2021).

Scientific meetings:

1. Do maternal age and diabetes influence early embryo development?; **Joaquin Lilao-Garzon**, Yeray Brito-Casillas, Ana Wägner and Silvia Muñoz-Descalzo; 19th

International Congress of Developmental Biology; Algarve, Portugal; 2022.

2. Effect of maternal age and metabolic syndrome on early embryo development in a mouse model; **Joaquin Lilao-Garzon**, Yeray Brito-Casillas, Silvia Muñoz-Descalzo and Ana Wägner; 58th EASD Annual Meeting of the European Association for the Study of Diabetes; Stockholm, Sweden; 2022. https://doi.org/10.1007/s00125-022-05755-w

3. Efecto sobre la fecundidad de la edad materna y el síndrome metabólico asociado a dieta grasa en un modelo murino; **Joaquín Lilao-Garzón**, Yeray Brito-Casillas, Silvia Muñoz-Descalzo and Ana M Wägner; XXXIII Congreso Nacional de la Sociedad Española de Diabetes; Las Palmas de Gran Canaria, Spain; 2022.

4. Diabetes pregestacional y programación intrauterina: Estudio funcional in vitro de microARN asociado a diabetes materna; Carmen Valverde-Tercedor, José Ángel Guillén-Salgado, Silvia Muñoz-Descalzo, Miriam Valcárcel-Herrera, **Joaquín Lilao-Garzón**, Luisa Hernández-Baraza, Luisa and Ana Wagner; XXXIII

Congreso Nacional de la Sociedad Española de Diabetes; Las Palmas de Gran Canaria, Spain; 2022.

5. Wnt/β-Catenin signalling cooperates with FGF/MAPK during cell fate decision making in early mouse embryos; **Joaquín Lilao-Garzón**, Tina Balayo, Sabine Fischer and Silvia Muñoz Descalzo; BSDB/Genetics Society Annual Spring Meeting 2021; United Kingdom; 2021.

6. FERTIBETES. A prediabetic mouse model for embryonic development studies; **Joaquín Lilao-Garzón**, Yeray Brito-Casillas, Tina Balayo, Ana Wagner and Silvia Muñoz-Descalzo; 17th Spanish Society for Developmental Biology Meeting; Spain; 2020.

7. Wnt/β-catenin signalling promotes primitive endoderm differentiation in early mouse embryos; **Joaquín Lilao-Garzón**, Tina Balayo, Elena Corujo-Simón and Silvia Muñoz-Descalzo; 17th Spanish Society for Developmental Biology Meeting; Spain; 2020.

8. FERTIBETES: A new mouse model to study fertility in age, obesity and diabetic context; **Joaquín Lilao-Garzón**, Yeray Brito-Casillas, Ana Belén Expósito-Montesdeoca,

Tina Balayo, Ana Wagner and Silvia Muñoz-Descalzo; BSDB/Genetics Society Spring Meeting 2020; Warwick, United Kingdom; 2020.

9. Age influence in high fat diet induced prediabetes in C57Bl/6J female mice; **Joaquín Lilao-Garzón**, Yeray Brito-Casillas, Ana Belén Expósito-Montesdeoca, Tina Balayo, Ana Wagner and Silvia Muñoz-Descalzo; XV Congreso Nacional de la Sociedad Española para las Ciencias del Animal de Laboratorio (SECAL 2019); Sevilla, Spain; 2019.

10. Maternal age, obesity and diabetes in embryonic development. A murine model; **Joaquín Lilao-Garzón**, Yeray Brito-Casillas, Ana Belen Expósito-Montesdeoca, Tina Balayo, Ana Wagner and Silvia Muñoz-Descalzo; European Developmental Biology Congress; Alicante, Spain; 2019.

11. The transition from local to global patterns governs the differentiation of mouse blastocyst; Sabine Fischer, Elena Corujo-Simon, **Joaquín Lilao-Garzón**, Ernst Stelzer and Silvia Munoz Descalzo; European Developmental Biology Congress; Alicante, Spain; 2019.

Acknowledgments

En primer lugar, quiero agradecer a mis directores por su supervisión durante la tesis.

A Ana Wägner, por darme la oportunidad de pedir la beca en la ULPGC y por todas las revisiones y correcciones de abstracts, artículos y la propia tesis. También por todo el apoyo que dado para la organización de seminarios en el IUIBS.

A Yeray Brito, por toda su gestión y trabajo para conseguir un mejor animalario para todos, por su ayuda con todo el trabajo de caracterización del modelo y por tener siempre una broma, un chiste o una rima para sacarte una sonrisa.

A Silvia muñoz, por abrirme la puerta a la biología del desarrollo y por devolverme el interés por el laboratorio y la pasión por la investigación cuando empecé en su laboratorio en Bath. Por toda su ayuda y supervisión durante la tesis, tanto en el laboratorio como en la escritura y en el análisis de datos. También por dejarme hacer cualquier experimento o marcianada que se me ocurriese en el laboratorio y por enseñarme a hablar de ciencia animándome a participar congresos y meetings.

También quiero agradecer a Alfonso Martínez Arias por permitirme realizar la estancia en su laboratorio de Cambridge. Fue una estancia peculiar, realizada en gran medida de forma telemática por la pandemia, pero que me permitió conocer a

grandes investigadores de todo el mundo y aprender sobre novedosas investigaciones dentro del campo.

Gracias a la Universidad de las Palmas de Gran Canaria por la financiación que he recibido estos años de la beca predoctoral y a la ACIISI durante estos últimos meses.

Muchas gracias a José Juan Mateo y Sergi Maicas en la Universitat de València, por ser los primeros en darme la oportunidad de trabajar en un laboratorio de investigación y descubrirme y descubrirme este mundo que me entusiasma.

Durante estos último casi 5 años, han pasado varias personas muy importantes por el laboratorio. En primer lugar, quiero darle las gracias a Tina por su ayuda con todo tanto dentro como fuera del laboratorio. Sus PCRs, cultivos y gestiones dentro del instituto fueron de gran ayuda. También a Michi, que fue el mejor estudiante que puede pasar por el laboratorio. Y finalmente, por estos últimos meses a la compi Cristina, que se ha volcado con el trabajo en el laboratorio siendo un gran apoyo.

A todo el personal del animalario, Merci, Natalia y Pino por cuidar tan bien de los ratones, pero también por su ayuda en partes de los experimentos, los cafés y las charlas mañaneras nada más llegar al instituto. También reconocer todo el trabajo que han tenido que hacer junto con Yeray para trasportar a los

animales y que estuviesen en las mejores condiciones posibles teniendo en cuanta la situación de este último año.

A Haidée, Patri, Marian, Elena, Henoc y Ester por los cafés, las comidas en buena compañía, las risas, las cenas esporádicas y toda vuestra ayuda durante todos estos años. Mención especial para Miguel, compañero de despacho y amigo que nada más llegar a la isla me introdujo en su grupo de amigos como a uno más. Muchas gracias por enseñarme tu isla, sus fiestas y por aguantarme tanto dentro como fuera del instituto.

A toda la gente del IUIBS, los compañeros del grupo de endocrino en la planta 5 y a todos en la planta 2 Norte. Gracias por vuestro apoyo, las charlas, los cafés de la mañana (o la tarde) y los buenos ratos.

De nuevo quiero agradecer a Silvia, junto con Carlos y Raúl por convertirse en mi familia en la isla.

A Felipe, Kevin, Josu, Carla, Patri, Amanda y Alba, que me han acompañado estos últimos años y con los que espero volver a repetir esos buceos, carnavales, romerías, siestas en el cine o cervezas en el Mavericks.

A los amigos de Teruel: Martínez, Marco, María José, Ángel, Eva, Cuis, Alba, Ester, Paula, Irene, Clau, Sara… que siempre están cuando se les necesita, muchas gracias por vuestro apoyo, por

todos estos años de cervezas, cenas, medievales, vaquillas, fiestas de pueblo, viajes…

A ese grupo de canteros, amigos de toda la vida y los que han ido llegando después: Sara, Yaiza, David, Javi, Mike, Jesús, Jorge y Víctor. Con los que he vivido mucho y que, aunque vivamos en ciudades distintas, nunca perdemos el contacto y cuando coincidimos siempre hacemos por vernos todo lo posible.

A los Maigos, compañeros de fatigas durante la carrera, de horas de biblioteca y de cafetería: Marta, Anna, Nerea, Alicia, Sergio, Jesús, María, Maca, Vero, Marce, Pitu, Iván, Elena y Carlos. Porque sin duda hicieron la carrera mucho más divertida y porque después de todos estos años seguimos quedando siempre que podemos.

A mi familia, que siempre me ha apoyado, mis abuelos, mis tías y tíos, Maribel, Piedad, Juan, Bene, Ana y Ángel. Y también a mis primos Lorena, Areli, Lucas y Alan de los que estoy súper orgulloso.

A mis hermanos, Javi y Adrián porque fue una suerte crecer con ellos y porque, aunque eran los pequeños siempre he aprendido y aprendo cosas de ellos. A Javi, darle las gracias también porque junto a Amaya han tenido el mejor niño del mundo Óscar. Un niño tan alegre que nunca me canso de jugar con él.

Y, por último, y las dos personas más importantes, gracias a mis padres. A mi padre, con el que siempre estoy de bronca, pero porque en realidad somos iguales. Gracias por todo lo que me has enseñado. A mi madre por ser mi mayor apoyo en todo y por cuidarme toda la vida, por preocuparse siempre (aunque no haga falta) y por nuestras llamadas diarias a pesar de la distancia. Estoy seguro que sin ella no habría llegado hasta aquí.

A todos los que he nombrado y a los que se me han podido olvidar en este momento pero que han tenido un impacto a lo largo de estos años, MUCHAS GRACIAS.